Université Paris-Sud

ÉCOLE DOCTORALE: Particules, Noyaux et Cosmos (517)
Laboratoire de Physique Théorique d'Orsay

DISCIPLINE Physique Théorique

THÈSE DE DOCTORAT

soutenue le 10/12/2013

par

Pantelis MITROPOULOS

Dark Matter in the Next-to-Minimal Supersymmetric Standard Model

Directeur de thèse:	Ulrich ELLWANGER	Enseignant-chercheur (LPT)
Composition du jury:		
Présidente du jury:	Asmâa ABADA	Enseignant-chercheur (LPT)
Rapporteurs:	Geneviève BÉLANGER	Chercheur (LAPTH)
	Michel TYTGAT	Enseignant-chercheur (Service de Physique Théorique, ULB)
Examinateur:	Aldo DEANDREA	Enseignant-chercheur (IPNL)

ACKNOWLEDGMENTS

I am very grateful to my advisor Ulrich Ellwanger for his priceless support and his patience during all these years. I feel exceptionally lucky having had the opportunity to do research under his guidance.

I would also like to thank all the members of our group for the warm working environment they provided me, but I am especially grateful to Yann Mambrini and Adam Falkowski, the organizers of the journal club of our group, for the inspiration they provided. Of course, I cannot forget to thank my previous colleague but still friend Debottam Das for his warm welcome when I first came to the lab and his help during my work.

Last but not least, I would like to thank Asmaa Abada, Genevieve Belanger, Aldo Deandrea and Michel Tytgat who did me the honor to participate in my jury.

I acknowledge financial support from the Greek State Scholarship Foundation (I.K.Y.).

CONTENTS

INTRODUCTION

One of the current major puzzles of theoretical physics is the explanation of a non-luminous and yet unknown form of matter present throughout the Universe, called Dark Matter (DM). Although the evidence for its existence, originating from various gravitational effects, are so far only implicit observations, they are strong enough to consider with great certainty that more than about 80% of the total matter in the Universe is dark. Moreover, this evidence suggests that DM consists of non-baryonic, massive long-lived particles which interact only through gravity and weak interactions. None of the particles described by the Standard Model (SM) of particle physics do meet the required specifications to account for dark matter. Many models that extend the standard theory have been proposed, in an effort to incorporate particles with the desired characteristics.

Among the numerous possibilities, supersymmetry seems to be quite appealing. Supersymmetry is a symmetry between bosons and fermions, introduced to solve theoretical problems of the Standard Model. In most cases, supersymmetric extensions of the Standard Model also conserve a discrete symmetry, the R-parity, in order to conform with particle physics phenomenology, especially the non-observation of the proton decay. A new possibility appeared in this class of models: one of the new particles is stable and neutral and, in principle, it is possible to be a viable DM candidate with the observed abundance.

Many experiments are running around the world, aiming either at the direct detection of DM particles or at the detection of indirect signals coming from them. The latter originate from dark matter annihilation in regions of the Universe that it is expected to be more condensed. The results of these experiments constitute a test of the various theoretical models proposed to explain the DM problem.

Another puzzling fact is the agreement of the values, at the level of order of magnitude, of the DM abundance and the abundance of baryonic matter. If this is not just a coincidence, these two forms of matter should have something in common. In order to explain this coincidence, the possibility that the DM particles carry a conserved quantum number related to baryon number has recently attracted a lot of attention. Then, it is in principle possible that the DM current abundance is the asymmetry

between DM particles and antiparticles, as it is in the case of baryons. The difference for the two densities comes simply from the difference in their masses.

In the first part of the current dissertation we deal in general with particle Dark Matter. In Chapter 1 we review the DM physics. We give the evidence for the DM existence and explain why particle DM is more favorable among other possibilities. We also describe the common mechanism that determines the DM relic abundance and, finally, we examine the DM detection methods and present the current experimental status. In order to explain the DM, foremost, one needs a theory that describes successfully the known fundamental particles. In Chapter 2 we describe the theory that has been established during the last decades as the Standard Model of particle physics. In the same chapter, we also discuss the theoretical problems from which this model suffers and motivate the supersymmetric extensions of the SM.

In the second part we examine the DM in the context of a specific supersymmetric model, the Next-to-Minimal Supersymmetric Standard Model (NMSSM). There are good theoretical and phenomenological reasons to move from the minimal supersymmetric model to the NMSSM. These are described in Chapter 3. We also describe the Lagrangian of the model and the possible DM candidates this model provides, exploring the general DM characteristics and detection. In the subsequent Chapter 4, we attempt to explain in the NMSSM a possible indirect DM signal, a monochromatic photon excess, that may originate from DM annihilation.

The last, third, part of the thesis is devoted to asymmetric DM. In Chapter 5 we introduce the asymmetric DM and explore the conditions under which the DM current density is determined indeed by its asymmetry. We derive quite severe upper bounds on the DM particle-particle or antiparticle-antiparticle self-annihilation, which constrain the asymmetric DM models. Subsequently, we propose in Chapter 6 a specific asymmetric DM model, obtained by an extension of the NMSSM, which respects the self-annihilation bounds. We investigate, in the same chapter, the properties of the proposed DM and discuss possible bounds coming from collider physics, cosmology and DM detection experiments.

Note: The original work of this thesis is included in the last three chapters (Ch. 4, 5 and 6), which are based on the publications [1–3].

INTRODUCTION

La Matière Noire (MN) est une forme inconnue de matière non-lumineuse et répandue dans toute Univers. L'explication de la MN figure parmi les défis principales de la physique théorique. Bien que les évidences de son existence sont jusqu'à maintenant que des observations implicites, d'origine d'une variété des effets gravitationnelles, ils sont assez robustes pour considérer avec grande certitude que la MN constitue plus que le 80% de la matière totale de l'Univers. En plus, les évidences suggèrent que la MN est constituée par particules massifs, non-baryoniques, à vie longue, lesquels interagissent seulement à travers la gravité et des interactions faibles. Aucun des particules décrites par le Modèle Standard (MS) de la physique des particules ne correspond pas aux spécificités de la MN. Plusieurs modèles ont été proposé en s'étendant la théorie standard et ayant comme but d'inclure les particules présentant les caractéristiques désirés.

Parmi les plusieurs possibilités, la théorie de supersymétrie semble être la plus attirante. La supersymétrie est une symétrie entre les bosons et les fermions, introduite pour résoudre les problèmes théoriques du MS. Dans la majorité de cas, les extensions supersymétriques du MS conservent une symétrie discrète, la R-parité, afin de se conformer avec la phénoménologie de la physique des particules, spécialement en ce qui concerne l'absence d'observation de la désintégration du proton. Une nouvelle possibilité a été apparue dans cette classe des modèles: un de nouveaux particules est stable et neutre et, en principe, il est possible d'être un candidat pour expliquer la MN, viable avec l'abondance observée.

Plusieurs expériences sont effectuées au monde, ayant comme but soit la détection directe des particules de MN, soit la détection de signaux indirects d'origine des particules de MN. Les résultats de ces expériences constituent un test des différents modèles théoriques qui proposent et qui expliquent le problème de la MN.

Un autre problème est l'accord au niveau de l'ordre de magnitude entre les valeurs d'abondance de MN et de l'abondance de matière baryonique. S'il s'agit pas d'une coïncidence, ces deux formes de matières devraient avoir quelque chose en commun. En conséquence, afin d'expliquer cette coïncidence, la possibilité que les particules de MN portent un nombre quantique qui est conservé en relation avec le nombre bary-

onique a récemment attiré beaucoup d'attention. Il est donc possible que l'abondance actuelle de MN est expliquée par l'asymétrie entre les particules de MN et les antiparticules, comme c'est le cas pour les baryons. La différence entre les deux densités vient simplement par la différence entre les masses.

Dans la première partie de cette thèse nous traitons de manière générale les particules de la MN. Dans Chapitre 1 nous effectuons une révision de la physique de MN. Nous fournissons les preuves pour l'existence de la MN et nous expliquons pourquoi les particules de MN sont plus favorable parmi les autres possibilités. Nous décrivons aussi le mécanisme commun qui détermine l'abondance de la MN et, filialement nous examinons les méthodes de détection de MN et présentons l'état de l'art actuel des expériences. Afin d'expliquer la MN, il faut utiliser la théorie qui décrit en succès les particules fondamentales déjà connus. Dans le Chapitre 2 nous décrivons la théorie qui a été établie dans les derniers décennies selon le MS de la physique des particules. Dans le même chapitre, nous discutons aussi les problèmes théoriques du MS et ceux qui motivent les extensions supersymétriques du MS.

Dans la deuxième partie, nous examinons la MN, dans le contexte d'un modèle spécifique de supersymétre, le Next-to-Minimal Supersymmetric Standard Model (NMSSM). Il y a des bonnes raisons théoriques ainsi que phénoménologiques pour passer du modèle supersymétrique minimal au NMSSM. Ces raisons sont décrites dans le Chapitre 3. Nous décrivons aussi le Lagrangien du modèle ainsi que les particules candidat possible de la MN que ce modèle nous offre, en explorant les caractéristiques générales de la MN. Au prochain Chapitre 4, nous tentons à expliquer dans NMSSM un signal de MN indirect, un excès de photons monochromatique, qui peuvent provenir de l'annihilation de la MN.

La dernière partie de cette thèse est dévouée aux asymétries de la MN. Dans le Chapitre 5 nous introduisons la MN asymétrique et nous explorons les conditions sous lesquels la densité actuelle de la MN est en effet déterminée par son asymétrie. Nous trouvons des limites supérieures assez sévères sur l'auto-annihilation de particule-particule ou de antiparticule-antiparticule. En plus, nous proposons dans Chapitre 6 un modèle d'asymétrie spécifique de MN, obtenu par l'extension de NMSSM, qui respect l'auto annihilation des limites. Nous investiguons, dans le même chapitre, les propriétés de la MN telles que proposées et nous discutons les limites possibles de l'origine de physique des collisionneurs, de la cosmologie et des expériences de détection de la MN.

Note: Le travail original de cette thèse est inclue dans les derniers trois chapitres (Ch. 4, 5 et 6), lesquels sont basés sur des publications [1–3].

Part I

Particle Dark Matter

CHAPTER 1

DARK MATTER

The latest results from the Linear Hadron Collider (LHC) and the Planck satellite offered an amazing verification of the Standard Models of both Particle Physics (henceforth, denoted just as SM) and Cosmology. The discovery of the Higgs boson completed the detection of all particles predicted by the SM and put an end to any potential doubts about it. On the other hand, the Cosmic Microwave Background radiation observed by Planck is consistent in high precision with the standard cosmology. But at the same time, Planck confirmed once more the fact that the total matter of the Universe is dominated by one yet unknown form of matter, the so-called Dark Matter (DM). The nature of DM constitutes one of the major puzzles of the theoretical physics today.

The story of DM is not new. In 1970s, it was realized that the measured rotational velocity of isolated stars or gas clouds in the outer parts of galaxies was not as one should expect from the gravitational attraction of the known matter. This fact brought back to light an old idea about a non-luminous form of matter and forced to take it seriously. It was back in 1933 that Zwicky [4,5] observed that the mass of the luminous matter (stars, gas etc.) in the Coma system, a cluster of about one thousand galaxies, was not adequate to explain the motion of cluster member galaxies. The idea, however, of a non-luminous form of matter preexisted [6] and it was actually used one year earlier by Oort [7] to explain his observations, which nevertheless proved erroneous. However, today, the existence of this non-luminous, dark matter is considered unquestionable due to various kinds of evidence, many of them independent of the others. It is almost certain nowadays that DM does not only cluster with stellar matter forming the galactic halos, but it also exists as a background throughout the entire Universe.

The evidence for the DM will be the subject of the next but one section (Sec. 1.2). Meanwhile, we have to give a brief review of the standard cosmological model. In Sec. 1.3 we discuss the possible DM candidates and the reason that a particle DM is most favorable. Subsequently, in Sec. 1.4 we review the standard mechanism that determines the density of the DM particles, a quantity that has been calculated quite accurately by astrophysical observations. We finish this chapter by describing, in the

last two sections 1.5 and 1.6, the detection methods of particle DM and the current experimental status.

1.1 The Standard Big Bang Cosmological Model

In this section we are going to review the standard cosmological model based on the Big Bang theory and on general relativity. However, it is not going to be an introduction to the general theory of relativity, but rather a very brief review of notions and formulas that we need for the description of DM.

A basic characteristic of the standard cosmological model is the evidence that the universe is expanding. The expansion was discovered at the late 1920's [8] by observing the spectra of distant galaxies. A local observer that detects light from a distant object sees a redshift z in the frequency, which corresponds to the motion of the object away from the observer due to the Doppler effect. All of the observed galaxy spectra up to the present time (except of few coming from very nearby galaxies) are red-shifted, a fact stressing the universality of the expansion. The redshift z can be written in power series in terms of the luminosity distance $d_L \equiv \left(\frac{\mathcal{L}}{4\pi\mathcal{F}}\right)^{1/2}$ (where $\mathcal{L}$ is the object's luminosity and $\mathcal{F}$ the measured flux) as

$$z = H_0 d_L + \frac{1}{2}(q_0 - 1)\left(H_0 d_L\right)^2, \tag{1.1}$$

where H_0 is the present expansion rate of the Universe, known as the Hubble constant and q_0 is a parameter that represents the deviation from the linear Hubble law and measures the deceleration of the Universe. Usually, the Hubble parameter is taken to be

$$H_0 = 100h\,\mathrm{km\,s^{-1}\,Mpc^{-1}}, \tag{1.2}$$

with the numerical uncertainties moved to the dimensionless parameter h, which takes the value $h = 0.673 \pm 0.012$ [9].

The expansion of the Universe may originate naturally from an isotropic and homogeneous cosmological model based on general relativity. Although Einstein imposed these two assumptions without any observational evidence, today they are general thought as undeniable. The best evidence for isotropy comes from the observation of the Cosmic Microwave Background (CMB) radiation, which exhibits a temperature uniformity. Testing the homogeneity of the Universe is not so straightforward, but sky surveys have confirmed it with large accuracy [10]. The validity of these assumptions form the modern cosmological principle, which reflects the fact that all spatial positions in the Universe are essentially equivalent.

Isotropy and homogeneity are playing an essential role, since they allow the description of the space-time of the Universe in terms of only two parameters denoted by $R(t)$ and k, accounting, respectively, for its overall expansion (or contraction) and its spatial curvature. The most general expression for a space-time metric, known as Friedmann-Robertson-Walker or FRW metric, can be written as (see, for example, [11])

$$\mathrm{d}s^2 = \mathrm{d}t^2 - R(t)\left[\frac{\mathrm{d}r^2}{1-kr^2} + r^2\left(\mathrm{d}\theta^2 + \sin^2\theta\mathrm{d}\phi^2\right)\right], \tag{1.3}$$

where as usual r, θ, ϕ and t are the spherical and time coordinates, respectively. The curvature constant k takes only the discrete values $+1$, 0, -1, corresponding to closed, (spatially) flat and open geometries. $R(t)$ is the cosmological scale factor and determines proper distances in terms of the comoving coordinates. Usually, it is convenient to define a dimensionless scale factor $a(t) \equiv \frac{R(t)}{R_0}$, where R_0 is the present-day value of R. The Hubble parameter can be defined through the scale factor as

$$H(t) \equiv \frac{\dot{R}(t)}{R(t)} = \frac{\dot{a}(t)}{a(t)}. \tag{1.4}$$

We can use the metric (1.3) in order to show that the cosmological redshift is a direct consequence of the Hubble expansion. The redshift is defined as

$$z = \frac{f_1 - f_2}{f_2}, \tag{1.5}$$

with f_1 the frequency of the emitted light and f_2 the frequency of the observed light. For scales smaller than cosmological, so that the expansion velocity v_{12} (corresponding to the velocity with which the distant object moves away from the observer) is not relativistic, the redshift is approximated as $z \simeq \frac{v_{12}}{c}$. Using the metric (1.3) for a light signal ($\mathrm{d}s^2 = 0$), we eventually arrive at the simple relation $1 + z = \frac{R_2}{R_1}$ between the redshift z and the scale factor R.

The evolution of the Universe can be described by two rather simple equations, known as Friedmann–Lemaître equations. Assuming the matter content of the Universe as a perfect fluid, the *energy–momentum* tensor is written as

$$T_{\mu\nu} = -p g_{\mu\nu} + (p + \rho) u_\mu u_\nu, \tag{1.6}$$

where $g_{\mu\nu}$ is the metric tensor related to the metric (1.3), p the isotropic pressure, ρ the energy density and $u = (1, 0, 0, 0)$ the velocity vector for the isotropic fluid in comoving coordinates. The Einstein's equations lead to the following expressions:

$$H^2 = \frac{8\pi}{3} G_N \rho - \frac{k}{R^2} + \frac{\Lambda}{3} \tag{1.7}$$

and

$$\frac{\ddot{R}}{R} = -\frac{4\pi}{3} G_N (\rho + 3p) + \frac{\Lambda}{3}, \tag{1.8}$$

where G_N is the gravitational constant and Λ the cosmological constant, which can be interpreted to correspond to the energy of the vacuum. (The first of these equations is often called the *Friedmann equation*.) The energy–momentum conservation leads to a third equation:

$$\dot{\rho} = -3H(p + \rho). \tag{1.9}$$

Examining (1.7), we see that in the absence of a cosmological constant ($\Lambda = 0$), the expansion or contraction of the Universe is determined solely by the value of k. For $k = +1$ it will recollapse, while it is going to expand indefinitely if $k = 0$ or $k = -1$.

This way, one can define the following expression that gives the critical density, such that $k = 0$ (when $\Lambda = 0$)

$$\rho_C \equiv \frac{3H^2}{8\pi G_N}. \tag{1.10}$$

Finally, the cosmological density parameter Ω_{tot} is defined as the energy density relative to its critical value

$$\Omega_{tot} \equiv \frac{\rho}{\rho_C}. \tag{1.11}$$

The Friedmann equation can be rewritten in terms of the density parameter as $\frac{k}{R^2} = H^2\left(\Omega_{tot} - 1\right)$. It is often useful to distinguish the origin of the contribution to the total density. In this sense,

$$\Omega_{tot} = \Omega_{mat} + \Omega_{rad} + \Omega_\Lambda, \tag{1.12}$$

where Ω_{mat} is the contribution from pressureless matter, Ω_{rad} comes from relativistic particles (radiation) and Ω_Λ is due to the cosmological constant. The matter density is further divided to the contribution from baryonic matter (Ω_b) and from (non-baryonic) DM (Ω_{DM}).

It is important to note that much of the history of the Universe can be described by assuming that either matter or radiation dominates the total energy density. By defining the parameter $w = \frac{p}{\rho}$, Eq. (1.9) is written in terms of w as $\dot{\rho} = -3(1+w)\rho\frac{\dot{R}}{R}$. After integration, it gives

$$\rho \propto R^{-3(1+w)}. \tag{1.13}$$

In the radiation dominated era of the Universe $w = 1/3$, while during matter domination $w = 0$, so that $\rho \propto R^{-4}$ (radiation dominated) and $\rho \propto R^{-3}$ (matter dominated), respectively.

1.2 Evidence of DM

1.2.1 Galactic rotation velocities

As it was mentioned before, the first strong evidence for the existence of DM were the galactic rotation velocities [12]. The mass distribution of a spiral galaxy can be approximated as spherical or ellipsoidal. Applying the Newton's law, which is sufficient for such large distances, we can see that at a distance r from the galactic center the rotation velocity obeys the equation $\frac{v^2}{r} = \frac{G_N M(r)}{r^2}$, where $M(r)$ is the mass distribution in the galaxy. Taking r much larger than the radius of the luminous mass, so that $M(r)$ corresponds to the total galactic mass, Newton's law implies that $v \propto 1/\sqrt{r}$. However, galaxy observations based on the Doppler effect show that the velocity rises with r towards a constant value $v_{const} \simeq 100 - 200\,\mathrm{km\,s^{-1}}$. The first galaxy in which this behavior observed was Messier 33, a spiral galaxy about 3 million light years (ly) away. Its rotation curve can be seen in Fig. 1.1 (left). Along with the observed curve, the expected rotation velocity due to the luminous mass has also been plotted. The same phenomenon has already been observed for a plethora of galaxies, including our galaxy [13] (see Fig. 1.1 – right).

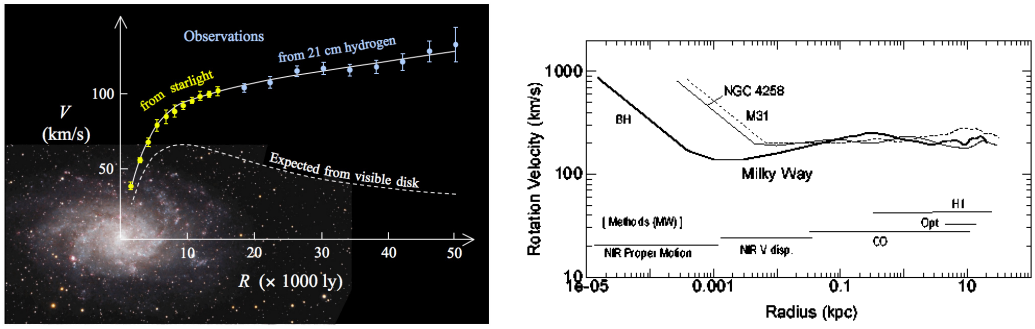

Figure 1.1: *Left:* The rotation curve for the M33 dwarf galaxy, superimposed on its optical image, as observed by starlight and 21 cm hydrogen spectrum lines, and the expected rotation curve due to the luminous amount of mass. From [14,15]. *Right:* The rotation velocities for the Milky Way, the NGC 4258 and M31 galaxies as a function of the distance from the galactic center. From [13].

Returning to the Newton's law, we can easily check that the aforementioned disagreement would have been resolved, if the mass distribution was growing linearly with r, $M(r) \propto r$. Actually, a self-gravitating ball of an ideal gas at a uniform temperature $kT = \frac{1}{2} m_X v_{const}$, with m_X the mass of the particles that constitute the gas and v_{const} the asymptotic value of the rotation velocity, would have exactly this mass profile [16]. Therefore, a simple solution to the missing mass problem is the assumption that the disk galaxies are immersed in extended DM halos. Current analyses of rotation curves imply that $\Omega_{mat} \simeq 0.1$ (see [17] for a review), while observations of the luminous matter constrain its density to only $\Omega_{lum} \lesssim 0.01$. Hence, about 90% of the total mass of the galaxies is dark.

1.2.2 Gravitational lensing

Since DM interacts gravitationally, its mass warps the space-time causing the distortion of a passing beam of light. Hence, although dark, the presence of DM should be visible through the "bending" of the light coming from behind sources. This fact is used in the so-called gravitational lensing: large clusters of galaxies can be used as astrophysical lenses that bend and magnify the light coming from galaxies far behind them. The distorted picture can give an estimate for the mass distribution of the lens. Since lensing does not rely on the dynamics of the observed systems, it is a completely independent method of predicting the DM density.

In contrast to optical lenses, a gravitational lens has no single focal point, but instead a focal line. The maximum bending occurs closest to the center of the lens, and the minimum furthest from it. In the ideal case that the light source (a distant galaxy), the lens (the cluster of galaxies) and the telescope lie in a straight line, the source galaxy would appear as a ring around the lensing object. In fact, partially because of a misalignment of the three objects, but also due to the complex mass

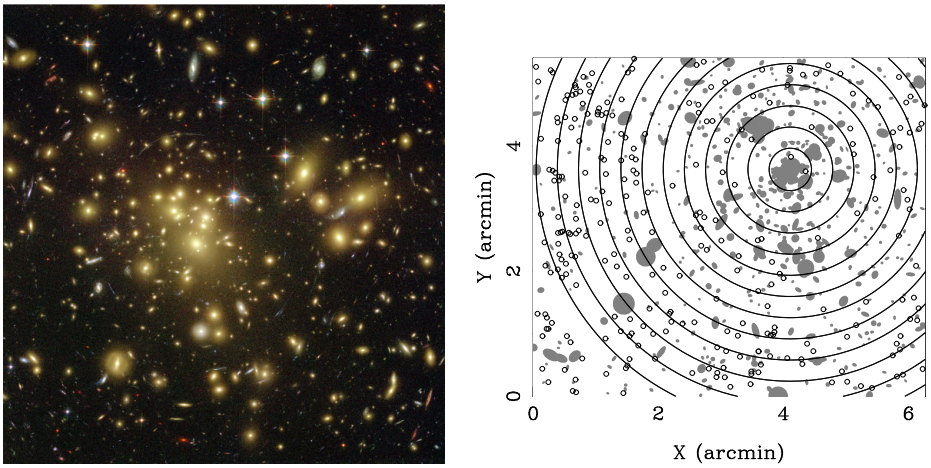

Figure 1.2: *Left:* Abell 1689 acting as gravitational lens that bends and magnifies the light of the galaxies located far behind it. Some of the faintest objects in the picture are probably over 13 billion light-years away (redshift value 6). This color image is a composite of visible-light and near-infrared exposures taken by the Hubble telescope in June 2002. According to NASA, it reveals 10 times more arcs than would be seen by a ground-based telescope. Courtesy of the Space Telescope Science Institute (STScI). *Right:* A masked region of Abell 1689. Cluster members were selected using color information and then masked over, so that these regions do not affect the surface density estimate of background sources. The background galaxies are also shown as open circles. Superimposed are the concentric bins used to calculate the radial profile, centered on the peak in the light distribution. From [18].

distribution of the lensing cluster, the source resembles partial arcs scattered around the lens. Fig. 1.2 is an example of the arcs formed as the light of distant galaxies passed through the cluster Abell 1689, one of the most massive known galaxy clusters, acting as a 2-million-light-year-wide lens in space.

In many cases, the distortion of the light of background sources is too weak to form arcs and can be detected only by analyzing a large number of sources and using statistical methods. This kind of lensing is known as weak lensing. The lensing shows up statistically as a preferred stretching of the distant objects perpendicular to the direction towards the center of the lens. By measuring the shapes and orientations of large numbers of distant galaxies, their orientations can be averaged to measure the shear of the lensing field in any region. For a population of unlensed galaxies, the shear pattern should be, on average, randomly distributed. In the presence of lensing, the shear field is polarized and, since it is related non-locally to the surface mass density, it can be used to estimate the mass distribution.

Perhaps the most compelling evidence for DM came applying these weak lensing techniques on the colliding system of Bullet cluster [19, 20]. The Bullet cluster consists of two primary galaxy concentrations, a less massive subcluster that is currently moving away from a more massive main cluster. The X-ray image reveals the relative motion

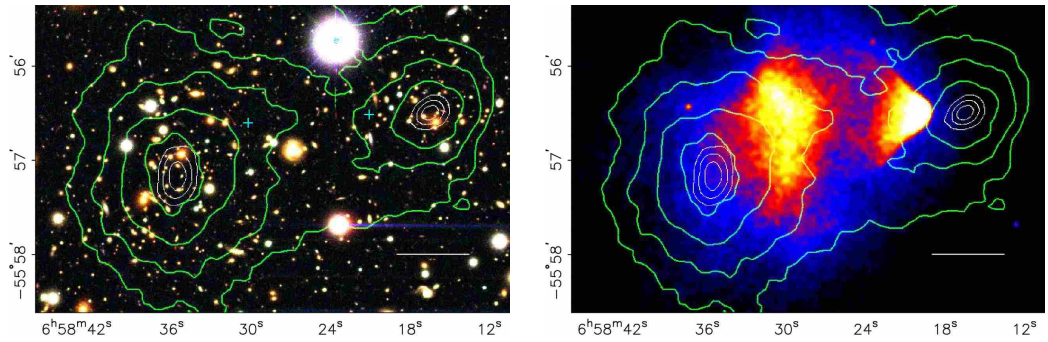

Figure 1.3: The left panel is a color image from the Magellan images of the merging Bullet cluster, with the white bar indicating 200 kpc at the distance of the cluster. The right panel is an X-ray Chandra image of the same cluster. The contours represent the weak lensing mass reconstruction. The separation between the location of the luminous interacting X-ray halo and the location of gravitating matter can be clearly seen. From [20].

of the two systems. Comparing with the line-of-sight velocity differences of the two components, it can be deduced that the two cores passed through each other about 100 million years ago and that the merger is occurring in the plane of the sky.

The cluster observation reveals that its mass is partially made of baryons observable in optical and infrared data, but it is dominated by baryons observable in X-rays. During the merger, the galaxies, which correspond to the small amount of optical baryons, remain collisionless, while the X-ray halo is affected by ram pressure. The mass distribution of the system was reconstructed by means of weak lensing. In the absence of DM, one should expect that the reconstructed mass distribution would exhibit a primary peak coincident with the dominant X-ray gas, which is spatially offset from the galaxy distribution (right panel of Fig. 1.3). However, as it can be seen in the left panel of Fig. 1.3, the mass maps created from weak lensing have the primary mass peaks in good spatial agreement with the galaxies.

The analysis performed in [20] is in agreement with the other astrophysical observations: only 12% of the total mass of the cluster is due to baryons (from which 1% is visible in optical spectrum and the rest is the X-ray halo) and 88% is the DM. Combining all the astrophysical bounds, one can make a rough estimation for the DM density, which lies on the range

$$0.1 \lesssim \Omega_{DM}^{astr}\, h^2 \lesssim 0.3. \tag{1.14}$$

1.2.3 CMB radiation

The most precise prediction of the DM density is coming, however, from analyses of the Cosmic Microwave Background (CMB) spectrum. The most recent observation of CMB by the Planck satellite (which improved previous results [21, 22] by WMAP)

constrained the DM density in the interval [9]

$$\Omega_{DM}h^2 = 0.1199 \pm 0.0027. \tag{1.15}$$

This result plays a key role for testing possible DM candidates and we are going to use it many times throughout this work. In the following, we will describe how DM affects the CMB spectrum. Once again, the detailed analysis leading to the above calculation is complicated and goes well beyond the scope of this thesis. We will rather try to give a qualitative picture of the relation among DM and the shape of the observed spectrum.

The CMB that we observe today consists of photons that have started a free travel through space since their last scattering with matter, early in the history of the Universe (see, for example, [23, 24]). Even earlier, while the Universe was made up from a very hot interacting plasma of photons, electrons and baryons, the large temperature of photons was preventing the electrons to combine with protons to form hydrogen atoms. As the Universe was expanding, the photon temperature was decreasing, and at some point the formation of atoms was possible. This corresponds to the recombination epoch of the Universe. After then, the photons no longer interacted with the neutral plasma and their free propagation started, with a temperature that is redshifting following the expansion of the Universe. The value of this temperature today is $\sim 2.73\,\mathrm{K}$ [25].

Although the CMB radiation is highly isotropic[1], small anisotropies appear if one concentrates on smaller scales, which correspond to smaller angles in the sky, later led to structure formation in the Universe. In order to study these anisotropies (see for example [26,27]), the temperature, which is a function of the polar coordinates defining the direction on the sky, is expanded in spherical harmonics:

$$T(\theta,\phi) = \sum_{l,|m|\leq l} a_{lm} Y_{lm}(\theta,\phi). \tag{1.16}$$

The coefficients a_{lm} describe temperature variations on angular scales $l \sim \pi/\Delta\theta$. The $l = 0$ term is the isotropic temperature, while $l = 1$ is the dipole anisotropy corresponding to the motion of the solar system. The variance of the temperature $\langle \Delta T^2 \rangle \equiv \langle (T - \langle T \rangle)^2 \rangle$ is written, using the orthogonality of the spherical harmonics, as

$$\langle \Delta T^2 \rangle = \frac{1}{4\pi} \sum_{l>1} (2l+1) C_l, \tag{1.17}$$

where we $C_l \equiv \langle |a_{lm}|^2 \rangle_m$ is the average of the coefficients a_{lm} over m. The quantity

$$\mathcal{D}_l^2 \equiv \frac{l(l+1)}{2\pi} C_l \tag{1.18}$$

gives the contribution to the temperature fluctuations per interval of $\ln l$. The CMB power spectrum – the plot of $\mathcal{D}_l$ versus l – as observed by the Planck satellite is shown in Fig. 1.4.

[1] About 1 part in 100,000, after subtracting the uninteresting dipole anisotropy, which is due to the Doppler effect caused by the solar system's motion.

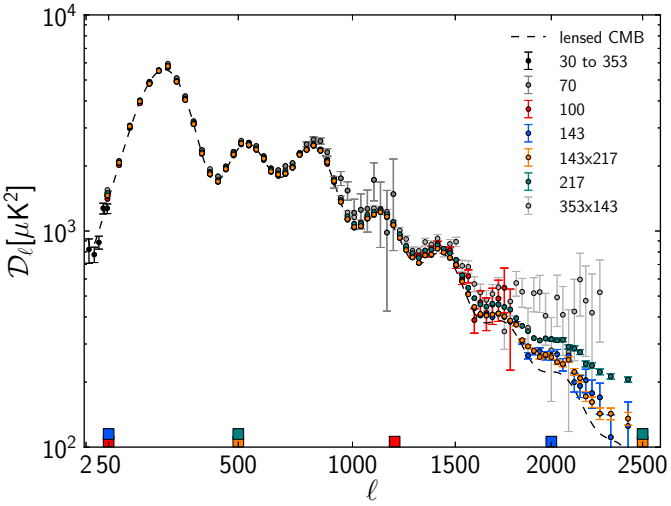

Figure 1.4: The Planck power spectra. The dashed line indicates the best-fit Planck spectrum. From [28].

We are ready to reach the main point of this section, to wit, how these anisotropies were generated and, eventually, why the existence of DM is necessary to explain the observed spectrum. To do so, we have to go back once again to the study of the early Universe. Before recombination, the CMB photons and the baryons acted as a nearly perfect fluid. Gravitational potential wells, caused by random fluctuations, had been stretched to cosmic scales during inflation. The photon-baryon fluid was under the influence of this potential. While gravity was compressing the fluid, its radiation pressure was resisting, resulting in acoustic oscillations. The sound waves were changing the photon temperature; it was rising during compression and it was falling during rarefaction. The oscillations stopped at recombination as the photons were released from the fluid, and what we observe today is actually a frozen picture of this procedure. The peaks are caused by modes that have reached extrema of compression and rarefaction at the time of last scattering. The first peak corresponds to modes that have had enough time to oscillate through exactly one half of a period before last scattering, the second peak is caused by modes oscillated through a full period (half the wavelength of the first mode), and so on.

Much information can be deduced from the CMB power spectrum. For example, without entering into the details, the position of the first peak is related to the spatially geometry of the Universe, whereas the relative height of the second peak, compared to the first one, is related to the baryonic density [29]. Here, we will focus on the effect of DM on the power spectrum.

We start without assuming a priori the existence of DM. When radiation dominated over matter, the density fluctuation stabilizes as the radiation pressure prevents further compression, causing the decay of the gravitational potential. Since the potential well lowers after the compression, the amplitude of the rarefaction will be larger. We note that modes with smaller wavelength (higher multipoles) started oscillating first, so that

it is expected that each even peak would be higher than the successive odd peak. In the presence of a collisionless cold (non-relativistic) fluid, the density fluctuation remains after the compression and the gravitational potential does not decay. Therefore, in the presence of (cold) DM, the third peak is expected to be comparable or higher than the second one[2]. Indeed, this is the case of the observed CMB power spectrum (Fig. 1.4).

In practice, the effect of the various phenomena determining the shape of the power spectrum is more complicated than the above simplified qualitative analysis. One has to apply statistical methods in order to fit a cosmological model to the observed CMB spectrum. The best fit to the power spectrum as observed by Planck [9] is a flat ΛCDM model[3], with baryonic density $\Omega_b h^2 = 0.02205 \pm 0.00028$, dark matter density $\Omega_{DM} h^2 = 0.1199 \pm 0.0027$ and energy density of the cosmological constant (dark energy density) $\Omega_\Lambda = 0.685^{+0.018}_{-0.016}$.

1.2.4 Other evidence

The clues for the existence of DM are not limited to the three aforesaid phenomena. For example, sky surveys of Baryon Acoustic Oscillations (BAO) – periodic fluctuations of the baryonic density caused by acoustic oscillations in the early Universe – are consistent with the results extracted by the CMB spectrum. The velocity dispersion of galaxies in galactic clusters indicate a large mass-to-light ratio, giving another evidence for DM. Furthermore, numerical simulations require a significant amount of cold DM in order to reproduce the large scale structure of the Universe.

1.3 Particle DM

Before we proceed to possible DM candidates, we have to refer to an attempt for an alternative explanation of the above phenomena, without the introduction of DM. Mainly in order to explain the anomalous galactic rotation curves, Milgrom proposed in 1983 [31] a modified version of Newton's law in galactic scales. This theory is known as Modified Newtonian Dynamics (MoND) and it has gained a lot of attention since then (see, for example, [32] for a review). However, MoND seem insufficient to account for the necessity of DM at scales larger than the galactic ones [17,33,34]. Furthermore, weak lensing of the Bullet cluster disfavors these theories [19], since in the case of MoND the X-ray gas would be the dominant component of the total mass and the separation indicated in Fig. 1.3 (right panel) would not have been observed.

One of the first possibilities examined for DM candidates were astrophysical objects that may count for DM. These were collectively called MAssive Compact Halo Objects (MACHOs) and such examples are brown or white dwarfs, neutron stars and stellar black hole remnants. These objects contribute to the density of baryonic DM. However, Big Bang nucleosynthesis and the CMB have set a limit on this density, which is also confirmed by the observation of MACHOs in the Milky Way halo through their

[2]The higher multipoles are affected by a damping effect [30].

[3]The standard cosmological model with a cosmological constant Λ and Cold Dark Matter.

gravitational lensing effect. This limit is far below the required value in order to fit the DM observations. As a consequence, non-baryonic DM is a necessary ingredient of the Universe.

Since the astrophysical objects are not adequate to count for the main component of DM, the attention has focused on possible particles that can play the role of this non-luminous matter. The only known particle that fits the criteria for DM is the neutrino. Although neutrinos are massless in the SM of particle physics, oscillations among their various flavors suggest a small but non-zero mass. However, a universe dominated by particles with such small mass would form large structures first, with the small structures forming later by fragmentation of the larger objects. This time scale, in which the galaxies form last and quite recently, seems incompatible with our current view of galactic evolution.

Nevertheless, extensions of the SM, essential to solve some of its theoretical drawbacks, provide particles that can, in principle, successfully solve the DM problem. In the next section, we will see that favorable candidates are Weakly Interacting Massive Particles (WIMPs). Supersymmetric theories that respect a discrete symmetry, the R-parity, provide a very promising WIMP, the neutralino. We will not extend here, since we are going to discuss neutralinos in more detail in the following chapters. However, WIMPs are also predicted by other, non-supersymmetric theories, such as models with TeV scale extra dimensions.

For completeness, we will finish this section by just mentioning the axions, although we will not deal with them in the rest of this thesis. Axions are neutral scalar hypothetical particles associated with the spontaneous breaking of the global $U(1)$ Peccei-Quinn symmetry [35, 36], introduced to dynamically solve the strong CP problem. Their very small coupling to ordinary matter gives a large lifetime to axions, larger than the age of the Universe. Axions were never in thermal equilibrium and were always non-relativistic. These characteristics allow them to be possible DM candidates.

1.4 The Standard Thermal Mechanism

1.4.1 Relic Abundance, thermal cross section and WIMPs

We shall discuss subsequently the mechanism that is widely considered responsible for the current DM density, in case of particle DM, as well as the requirements in order to fit this density to the observed value. We will also see why WIMPs are favorable DM candidates. This subsection will remain descriptive; a more detailed analysis will follow.

We assume a particle X with mass m_X that is neutral and stable. X would be the DM particle for this analysis. Early in the history of the Universe, when its temperature was much larger than the particle's mass ($T \gg m_X$), Xs were abundant with a density comparable with the photon's density. Due to pair annihilations with their antiparticles, they were rapidly converting to lighter particles and vice versa. The annihilations were in equilibrium, without affecting the density of the X particles. Shortly after T drops below the mass m_X, the number density of X started to drop

very fast, since lighter particles do not have enough energy anymore to produce X particles and pair annihilation continued to destroy them. The equilibrium particle density is given by

$$n_X^{eq} = \frac{g}{(2\pi^3)} \int f(\vec{p})\, \mathrm{d}^3\vec{p}, \tag{1.19}$$

where g is the number of internal (spin) degrees of freedom of the particle and $f(\vec{p})$ is the Bose-Einstein or the Fermi-Dirac distribution function in terms of the momentum $\vec{p}$. We will see[4] that Eq. (1.19) gives (after integration) $n_X^{eq} \propto T^3$, for $T \gg m_X$, whereas for $T \ll m_X$ the particle density is Boltzmann (exponentially) suppressed with $n_X^{eq} \propto \mathrm{e}^{-m_X/T}$.

As the Universe is expanding and the X particle density decreases, the pair annihilations of X particles become more rare, until they eventually stop when their rate Γ drops below the expansion rate, $\Gamma \lesssim H$. The rate of a pair annihilation Γ is proportional to the density of the annihilating particles, more precisely $\Gamma = n\langle\sigma v\rangle$, where $\langle\sigma v\rangle$ is the thermal average of the annihilation cross section σ times the particles relative velocity v (we will return to this in more detail in the following subsection). At the point where the Xs cease to annihilate, they fall out of equilibrium with the thermal plasma and what remains is their relic cosmological abundance, almost constant since then. It is customary to say that the DM density froze-out and call the temperature where this occurred the freeze-out temperature, henceforth T_{fo}.

We can use the freeze-out condition $\Gamma \simeq H$ to approximate the DM relic density in terms of the thermal averaged annihilation cross section (we reproduce the calculation performed originally in [37]). For this purpose, we will need the expressions for the energy and entropy density, which are defined in the App. A and which we rewrite here

$$\rho(T) = \frac{\pi^2}{30}\, g_{\mathrm{eff}}(T)\, T^4 \tag{1.20}$$

and

$$s(T) = \frac{2\pi^2}{45}\, h_{\mathrm{eff}}(T)\, T^3. \tag{1.21}$$

We recall (see App. A, for more details) that g_{eff} and h_{eff} are effective relativistic degrees of freedom. Assuming that there is no significant entropy production since the freeze-out, the entropy per comoving volume remains constant, so that the ratio n_X/s remains also constant (since the freeze-out). Hence, the present-day DM particle density is given by $n_{X_0} = s_0 \left(\frac{n_X}{s}\right)_{fo}$, with $s_0 \simeq 4 \cdot 10^3\,\mathrm{cm}^{-3}$ the current entropy density. Therefore, we have to compute the ratio n_X/s during freeze-out.

The early Universe is radiation dominated, hence Eq. (1.2) reads, after replacing the energy density by Eq. (1.20), as $H = \frac{2\pi}{3}\sqrt{\frac{\pi}{5}G_N}\, g_{\mathrm{eff}}^{1/2}\, T^2$. The freeze-out condition

[4] Number densities will be discussed again much later in this thesis, in Sec. 5.1, in the presence of chemical potentials.

gives, then, $\left(\frac{n_X}{s}\right)_{fo} = \frac{45}{3\pi}\sqrt{\frac{\pi}{5}G_N}\frac{g_{\rm eff}^{1/2}}{h_{\rm eff}}\left(T_{fo}\langle\sigma v\rangle\right)^{-1}$, which evaluates[5] to

$$\left(\frac{n_X}{s}\right)_{fo} \simeq 7\cdot 10^{-9}\,\frac{\rm GeV}{m_X}\,\frac{10^{-27}\,{\rm cm}^3\,{\rm s}^{-1}}{\langle\sigma v\rangle}. \tag{1.22}$$

We remind that $\Omega_X \equiv \frac{\rho_X}{\rho_c} = \frac{m}{\rho_c}\left(\frac{n_X}{s}\right)_{fo} s_0$, where the critical density today is $\rho_c = 10^{-5}h^2\,{\rm GeV\,cm}^{-3}$, so that, finally, the relic density is

$$\Omega_X h^2 \simeq \frac{3\cdot 10^{-27}\,{\rm cm}^3\,{\rm s}^{-1}}{\langle\sigma v\rangle}, \tag{1.23}$$

independently of the DM mass m_X.

In order to reproduce the observed relic density (1.15), the annihilation cross section during the freeze-out has to be

$$\langle\sigma v\rangle_{th} \simeq 3\cdot 10^{-26}\,{\rm cm}^3\,{\rm s}^{-1}. \tag{1.24}$$

This quantity is known as *thermal cross section*. The scale of this value is remarkably close to the cross section of weakly interacting particles, which can be estimated to be $\langle\sigma_{weak}v\rangle \sim \frac{\alpha^2}{m_W^2} \sim 10^{-25}\,{\rm cm}^3\,{\rm s}^{-1}$, with α a generic weak coupling. This fact established the WIMPs as the most favorable DM candidates.

1.4.2 The Boltzmann equation[6]

Although a weakly interacting particle has, in principle, the correct order of magnitude of the annihilation cross section for the correct order of relic density, in practice, the final result may vary over many orders of magnitude. This is the reason that a more detailed analysis is required in order to be able to calculate the precise value of the DM relic density.

The density of a species is governed by the Boltzmann equation, which can be written in compact operator form as

$$L[f] = C[f], \tag{1.25}$$

with L and C the Liouville and collision operators, respectively. $f = f(\vec{p},\vec{x})$ is the phase-space density, which is, in general, a function of the momentum and space-time coordinates and it is defined as

$$f = \frac{(2\pi)^3}{g}\frac{{\rm d}N}{{\rm d}^3p\,{\rm d}^3x}, \tag{1.26}$$

with N the number of particles. It is normalized in such a way that $f = 1$ corresponds to the maximum phase-space density allowed by the Pauli principle for a fermion. In

[5] In this evaluation, we have used the expected relation between the freeze-out temperature and the mass m_X of the particle, $T_{fo} \sim \frac{m_X}{20}$. However, we notice that the exact value of the denominator depends on the annihilation cross section.

[6] In this part, we follow part of the analysis performed in [38].

the special case of the spatially homogeneous and isotropic FRW cosmology, the phase-space density has the same symmetries and depends only on the particle energy E and the time t, i.e. $f = f(E,t)$.

The Liouville operator gives the net rate of change in time of f and the collision operator describes the number of particles per phase-space volume that are lost or gained per unit time due to collisions with other particles. The particle number density $n = \int \frac{\mathrm{d}N}{\mathrm{d}^3x}$ is given through (1.26) by the integral (1.19) of $f(E,t)$ over all momenta and sum over all spin degrees of freedom. We will perform the same integral and sum in the Boltzmann equation (1.25), in order to write it in a more convenient form involving the particle densities.

First, the Liouville term for $f = f(E,T)$ is written as

$$L[f] = \frac{\partial f}{\partial t} - H\,\frac{|p|^2}{E}\frac{\partial f}{\partial E}. \tag{1.27}$$

Integrating it and summing over all the spin degrees of freedom, it becomes

$$\begin{aligned} g_1 \int L[f_1]\frac{\mathrm{d}^3p_1}{(2\pi^3)} &= \frac{\partial}{\partial t}\int f_1\,\frac{g_1\mathrm{d}^3p_1}{(2\pi)^3} - Hg_1\int \frac{|p_1|^2}{E_1}4\pi|p_1|^2\frac{\mathrm{d}p_1}{(2\pi^3)} \\ &= \dot{n} - \frac{Hg_1}{(2\pi)^3}4\pi\int |p_1|^3\frac{\partial f_1}{\partial E_1}\mathrm{d}E_1 \\ &= \dot{n} + 3Hn, \end{aligned} \tag{1.28}$$

where we have used Eq. (1.27) and (1.19), $p\mathrm{d}p = E\mathrm{d}E$ and in the last step we have performed a partial integration.

Now we turn to the collision term, which in integrated form and summed over spins is written, in the case of annihilation of two particles 1 and 2 to two others, 3 and 4, as

$$\begin{aligned} g_1 \int C[f_1]\frac{\mathrm{d}^3p_1}{(2\pi)^3} = \\ -\sum_{spins}\left[f_1f_2(1\pm f_3)(1\pm f_4)\left|\mathcal{M}_{12\to34}\right|^2 - f_3f_4(1\pm f_1)(1\pm f_2)\left|\mathcal{M}_{34\to12}\right|^2\right] \\ \cdot(2\pi)^4\,\delta^4(p_1+p_2-p_3-p_4)\,\frac{\mathrm{d}^3p_1}{(2\pi)^3 2E_1}\,\frac{\mathrm{d}^3p_2}{(2\pi)^3 2E_2}\,\frac{\mathrm{d}^3p_3}{(2\pi)^3 2E_3}\,\frac{\mathrm{d}^3p_4}{(2\pi)^3 2E_4}, \end{aligned} \tag{1.29}$$

where the "+" sign applies for bosons and "−" for fermions. We assume that the annihilation products 3 and 4 go quickly into equilibrium with the thermal plasma, such that the density functions f_3 and f_4 in Eq. (1.29) can be replaced by the equilibrium densities f_3^{eq} and f_4^{eq}, respectively. Furthermore, the δ-function in the integral enforces $E_1 + E_2 = E_3 + E_4$ and, since $f_3^{eq}f_4^{eq} \propto \exp\left(-\frac{E_3+E_4}{T}\right)$, the product $f_3^{eq}f_4^{eq}$ is replaced by the corresponding product of the annihilating particle densities $f_1^{eq}f_2^{eq}$ (*principle of detailed balance*). In order to simplify the expression (1.29), we will apply the unitarity

condition which yields

$$\sum_{spins}\int |\mathcal{M}_{34\to 12}|^2\,(2\pi)^4\,\delta^4(p_1+p_2-p_3-p_4)\,\frac{\mathrm{d}^3p_3}{(2\pi)^3 2E_3}\,\frac{\mathrm{d}^3p_4}{(2\pi)^3 2E_4} = \sum_{spins}\int |\mathcal{M}_{12\to 34}|^2\,(2\pi)^4\,\delta^4(p_1+p_2-p_3-p_4)\,\frac{\mathrm{d}^3p_3}{(2\pi)^3 2E_3}\,\frac{\mathrm{d}^3p_4}{(2\pi)^3 2E_4} \quad (1.30)$$

and also the definition of the unpolarized cross section to write

$$\sum_{spins}\int |\mathcal{M}_{12\to 34}|^2\,(2\pi)^4\,\delta^4(p_1+p_2-p_3-p_4)\,\frac{\mathrm{d}^3p_3}{(2\pi)^3 2E_3}\,\frac{\mathrm{d}^3p_4}{(2\pi)^3 2E_4} = 4F g_1 g_2\,\sigma_{12\to 34}, \quad (1.31)$$

where $F \equiv [(p_1\cdot p_2)^2 - m_1^2 m_2^2]^{1/2}$ and the spin factors g_1, g_2 come from the average over initial spins. This way, the collision term (1.29) is written in a more compact form

$$g_1\int C[f_1]\frac{\mathrm{d}^3p_1}{(2\pi)^3} = -\int \sigma v_{\mathrm{M\o l}}\,(\mathrm{d}n_1\mathrm{d}n_2 - \mathrm{d}n_1^{eq}\mathrm{d}n_2^{eq})\,, \quad (1.32)$$

where $\sigma = \sum_{(\mathrm{all}\ f)}\sigma_{12\to f}$ is the total annihilation cross section summed over all the possible final states and $v_{\mathrm{M\o l}} \equiv \frac{F}{E_1E_2}$. The so called Møller velocity, $v_{\mathrm{M\o l}}$, is defined in such a way that the product $v_{\mathrm{M\o l}}n_1n_2$ is invariant under Lorentz transformations and, in terms of particle velocities $\vec{v}_1$ and $\vec{v}_2$, it is given by the expression

$$v_{\mathrm{M\o l}} = \left[\left|\vec{v}_1^{\,2} - \vec{v}_2^{\,2}\right|^2 - |\vec{v}_1\times\vec{v}_2|^2\right]^{1/2}. \quad (1.33)$$

Due to symmetry considerations, the distributions in kinetic equilibrium are proportional to those in chemical equilibrium, with a proportionality factor independent of the momentum. Therefore, the collision term (1.32), both before and after decoupling, can be written in the form

$$g_1\int C[f_1]\frac{\mathrm{d}^3p_1}{(2\pi)^3} = -\langle\sigma v_{\mathrm{M\o l}}\rangle(n_1n_2 - n_1^{eq}n_2^{eq}), \quad (1.34)$$

where the thermal averaged total annihilation cross section times the Møller velocity has been defined by the expression

$$\langle\sigma v_{\mathrm{M\o l}}\rangle = \frac{\int \sigma v_{\mathrm{M\o l}}\mathrm{d}n_1^{eq}\mathrm{d}n_2^{eq}}{\int \mathrm{d}n_1^{eq}\mathrm{d}n_2^{eq}}. \quad (1.35)$$

We will come back to the thermal averaged cross section in the next subsection.

We are, now, able to write the full integrated Boltzmann equation, using the expressions (1.28), (1.34) that we have derived for the Liouville and the collision term, respectively. In the simplified but interesting case of identical particles 1 and 2, the Boltzmann equation is, finally, written as

$$\dot{n} + 3Hn = -\langle\sigma v_{\mathrm{M\o l}}\rangle(n^2 - n_{eq}^2). \quad (1.36)$$

However, instead of using n, it is more convenient to take the expansion of the universe into account and calculate the number density per comoving volume Y, which can be defined as the ratio of the number and entropy densities: $Y \equiv n/s$. The total entropy density $S = R^3 s$ (R is the scale factor) remains constant, hence we can obtain a differential equation for Y by dividing (1.36) by S. Before we write the final form of the Boltzmann equation that it is used for the relic density calculations, we have to change the variable that parametrizes the comoving density. In practice, the time variable t is not convenient and the temperature of the Universe (actually the photon temperature, since the photons were the last particles that went out of equilibrium) is used instead. However, it proves even more useful to use as time variable the quantity defined by $x \equiv m/T$ with m the DM mass, so that Eq. (1.36) transforms into

$$\frac{\mathrm{d}Y}{\mathrm{d}x} = \frac{1}{3H}\frac{\mathrm{d}s}{\mathrm{d}x}\langle\sigma v_{\mathrm{M\o l}}\rangle\left(Y^2 - Y_{eq}^2\right). \tag{1.37}$$

Last, using the Hubble parameter (1.2) for a radiation dominated Universe and the expressions (1.20), (1.21) for the energy and entropy density, the Boltzmann equation is written in its final form

$$\frac{\mathrm{d}Y}{\mathrm{d}x} = -\sqrt{\frac{45G_N}{\pi}}\frac{g_*^{1/2}m}{x^2}\langle\sigma v_{\mathrm{M\o l}}\rangle\left(Y^2 - Y_{eq}^2\right), \tag{1.38}$$

where the effective degrees of freedom $g_*^{1/2}$ have been defined by

$$g_*^{1/2} \equiv \frac{h_{\mathrm{eff}}}{g_{\mathrm{eff}}^{1/2}}\left(1 + \frac{1}{3}\frac{T}{h_{\mathrm{eff}}}\frac{\mathrm{d}h_{\mathrm{eff}}}{\mathrm{d}T}\right). \tag{1.39}$$

The equilibrium density per comoving volume $Y_{eq} \equiv n_{eq}/s$ can be expressed as

$$Y_{eq}(x) = \frac{45g}{4\pi^4}\frac{x^2\mathrm{K}_2(x)}{h_{\mathrm{eff}}(m/x)}, \tag{1.40}$$

with K_2 the modified Bessel function of second kind.

1.4.3 Thermal average of the annihilation cross section

We are going to derive a simple formula that one can use to calculate the thermal average of the cross section times velocity, based again on the analysis of [38]. We will use the assumption that equilibrium functions follow the Maxwell-Boltzmann distribution, instead of the actual Bose-Einstein or Fermi-Dirac. This is a well established assumption if the freeze out occurs after $T \simeq m/3$ or for $x \gtrsim 3$, which is actually the case for WIMPs. Under this assumption, the expression (1.35) gives, in the cosmic comoving frame,

$$\langle\sigma v_{\mathrm{M\o l}}\rangle = \frac{\int v_{\mathrm{M\o l}}\mathrm{e}^{-E_1/T}\mathrm{e}^{-E_2/T}\mathrm{d}^3p_1\mathrm{d}^3p_2}{\int \mathrm{e}^{-E_1/T}\mathrm{e}^{-E_2/T}\mathrm{d}^3p_1\mathrm{d}^3p_2}. \tag{1.41}$$

The volume element can be written as $\mathrm{d}^3p_1\mathrm{d}^3p_2 = 4\pi p_1\mathrm{d}E_1 4\pi p_2\mathrm{d}E_2\frac{1}{2}\cos\theta$, with θ the angle between $\vec{p}_1$ and $\vec{p}_2$. After changing the integration variables to E_+, E_-, s given by

$$E_+ = E_1 + E_2, \qquad E_- = E_1 - E_2, \qquad s = 2m^2 + 2E_1E_2 - 2p_1p_2\cos\theta, \tag{1.42}$$

(with $s = -(p_1 - p_2)^2$ one of the Mandelstam variables,) the volume element becomes $\mathrm{d}^3p_1\mathrm{d}^3p_2 = 2\pi^2 E_1E_2\mathrm{d}E_+\mathrm{d}E_-\mathrm{d}s$ and the initial integration region

$$\{E_1 > m,\, E_2 > m,\, |\cos\theta| \leq 1\rangle$$

transforms into

$$|E_-| \leq \left(1 - \frac{4m^2}{s}\right)^{1/2}(E_+^2 - s)^{1/2}, \qquad E_+ \geq \sqrt{s}, \qquad s \geq 4m^2. \tag{1.43}$$

After some algebraic calculations, it can be found that the quantity $\langle\sigma v_{\mathrm{M\o l}}\rangle E_1E_2$ depends only on s, specifically $v_{\mathrm{M\o l}}E_1E_2 = \frac{1}{2}\sqrt{s(s-4m^2)}$. Hence, the numerator of the expression (1.41), which after changing the integration variables reads $2\pi^2\int\mathrm{d}E_+\int\mathrm{d}E_-\int\mathrm{d}s\sigma v_{\mathrm{M\o l}}E_1E_2\mathrm{e}^{-E_+/T}$, can be written, eventually, as

$$\int v_{\mathrm{M\o l}}\mathrm{e}^{-E_1/T}\mathrm{e}^{-E_2/T} = 2\pi^2\int_{4m^2}^{\infty}\mathrm{d}s\sigma(s-4m^2)\int\mathrm{d}E_+\mathrm{e}^{-E_+/T}(E_+^2 - s)^{1/2}. \tag{1.44}$$

The integral over E_+ can be written with the help of the modified Bessel function of the first kind K_1 as $\sqrt{s}\,T\,\mathrm{K}_1(\sqrt{s}/T)$. The denominator of (1.41) can be treated in a similar way, so that the thermal average is, finally, given by the expression

$$\langle\sigma v_{\mathrm{M\o l}}\rangle = \frac{1}{8m^4T\mathrm{K}_2^2(x)}\int_{4m^2}^{\infty}\mathrm{d}s\,\sigma(s)(s-4m^2)\sqrt{s}\,\mathrm{K}_1(\sqrt{s}/T). \tag{1.45}$$

Eqs. (1.38)–(1.40) along with this last Eq. (1.45) are all we need in order to calculate the relic density of a WIMP, if its total annihilation cross section in terms of the Mandelstam variable s is known.

In many cases, in order to avoid the numerical integration in Eq. (1.45), an approximation for $\langle\sigma v_{\mathrm{M\o l}}\rangle$ can be used. The thermal average is expanded in powers of x^{-1} (or, equivalently, in powers of the squared WIMP velocity):

$$\langle\sigma v_{\mathrm{M\o l}}\rangle = a + bx^{-1} + \ldots. \tag{1.46}$$

(The coefficient a corresponds to the s-wave contribution to the cross section, the coefficient b to the p-wave contribution, and so on.) This partial wave expansion gives a quite good approximation, provided there are no s-channel resonances and thresholds for the final states [39].

In [40], it was shown that, after expanding the integrands of Eq. (1.41) in powers of x^{-1}, all the integrations can be performed analytically. As we saw, the expression

$v_{\text{Møl}} E_1 E_2$ depends on momenta only through s. Therefore, one can form the Lorentz invariant quantity

$$w(s) \equiv \sigma(s) v_{\text{Møl}} E_1 E_2 = \frac{1}{2}\sigma(s)\sqrt{s(s-4m^2)}. \tag{1.47}$$

The integration involves the Taylor expansion of this quantity w around $s/4m^2 = 1$ and the general formula for the partial wave expansion of the thermal average is [40]

$$\langle \sigma v_{\text{Møl}} \rangle = \frac{1}{m^2}\left[w - \frac{3}{2}(2w - w')x^{-1} + \frac{3}{8}(16w - 8w' + 5w'')x^{-2} \right. \\ \left. - \frac{5}{16}(30w - 15w' + 3w'' - 7x''')x^{-3} + \mathcal{O}(x^{-4}) \right]_{s/4m^2=1}, \tag{1.48}$$

where primes denote derivatives with respect to $s/4m^2$ and all quantities have to be evaluated at $s = 4m^2$.

1.5 Direct Detection of DM

Since the beginning of 1980s, it has been realized that besides the numerous facts showing evidence for the existence of these new dark particles, it is also possible to detect them directly. Already in 1985, two pioneering articles [41, 42] appeared, describing the detection methods for WIMPs. Since WIMPs are expected to cluster gravitationally together with ordinary stars in the Milky Way halo, they would pass also through Earth and, in principle, they can be detected through scattering with the nuclei in a detector's material. In practice, one has to measure the recoil energy deposited by this scattering.

However, although one can deduce from rotation curves that DM dominates the dark halo in the outer parts of our galaxy, it is not so obvious from direct measurements whether there is any substantial amount of DM inside the solar radius $R_0 \simeq 8\,\text{kpc}$. Using indirect methods (involving the determination of the gravitational potential, through the measuring of the kinematics of stars, both near the mid-plane of the galactic disk and at heights several times the disk thickness), it is almost certain that the DM is also present in the solar system, with a local density $\rho_0 = (0.3 \pm 0.1)\,\text{GeV}\,\text{cm}^{-3}$ [43].

This value for the local density implies that for a WIMP mass of order $\sim 100\,\text{GeV}$, the local number density is $n_0 \sim 10^{-3}\,\text{cm}^{-3}$. It is also expected that the WIMPs velocity is similar to the velocity with which the Sun orbits around the galactic center ($v_0 \simeq 220\,\text{km}\,\text{s}^{-1}$), since they are both moving under the same gravitational potential. These two quantities allow to estimate the order of magnitude of the incident flux of WIMPs on the Earth: $J_0 = n_0 v_0 \sim 10^5\,\text{cm}^{-2}\,\text{s}^{-1}$. This value is manifestly large, but the very weak interactions of the DM particles with ordinary matter makes their detection a difficult, although in principle feasible, task. In order to compensate for the very low WIMP-nucleus scattering cross section, very large detectors are required.

1.5.1 Elastic scattering event rate

In the following, we will confine ourselves to the elastic scattering with nuclei. Although inelastic scattering of WIMPs off nuclei in a detector or off orbital electrons producing an excited state is possible, the event rate of these processes is quite suppressed. In contrast, during an elastic scattering the nucleus recoils as a whole.

The direct detection experiments measure the number of events per day and per kilogram of the detector material, as a function of the amount of energy Q deposited in the detector. This event rate would be given by $R = n_{\rm WIMP}\, n_{\rm nuclei}\, \sigma v$ in a simplified model with WIMPs moving with a constant velocity v. The number density of WIMPs is $n_{\rm WIMP} = \rho_0/m_X$ and the number density of nuclei is just the ratio of the detector's mass over the nuclear mass m_N.

For accurate calculations, one should take into account that the WIMPs move in the halo not with a uniform velocity, but rather following a velocity distribution $f(v)$. The Earth's motion in the solar system should be included into this distribution function. The scattering cross section σ also depends on the velocity. Actually, the cross section can be parametrized by a nuclear form factor $F(Q)$ as

$$\mathrm{d}\sigma = \frac{\sigma}{4m_r^2 v^2} F^2(Q) \mathrm{d}|\vec{q}|^2, \tag{1.49}$$

where $|\vec{q}|^2 = 2m_r^2 v^2(1-\cos\theta)$ is the momentum transferred during the scattering, $m_r = \frac{m_X m_N}{m_X + m_N}$ is the reduced mass of the WIMP – nucleus system and θ is the scattering angle in the center of momentum frame. Therefore, one can write a general expression for the differential event rate per unit detector mass as

$$\mathrm{d}R = \frac{\rho_0}{m_X}\frac{1}{m_N}\frac{\sigma F^2(Q)\mathrm{d}|\vec{q}|^2}{4m_r^2 v^2}\, v f(v) \mathrm{d}v. \tag{1.50}$$

The energy deposited in the detector (transferred to the nucleus through one elastic scattering) is

$$Q = \frac{|\vec{q}|^2}{2m_N} = \frac{m_r^2 v^2}{m_N}\left(1-\cos\theta\right). \tag{1.51}$$

Therefore, the differential event rate over deposited energy can be written, using the equations (1.50) and (1.51), as

$$\frac{\mathrm{d}R}{\mathrm{d}Q} = \frac{\sigma\rho_0}{\sqrt{\pi} v_0 m_X m_r^2} F^2(Q) T(Q), \tag{1.52}$$

where, following [37], we have defined the dimensionless quantity $T(Q)$ as

$$T(Q) \equiv \frac{\sqrt{\pi}}{2} v_0 \int_{v_{min}}^{\infty} \frac{f(v)}{v} \mathrm{d}v, \tag{1.53}$$

with the minimum velocity given by $v_{min} = \sqrt{\frac{Qm_N}{2m_r^2}}$, obtained by Eq. (1.51). Finally, the event rate R can be calculated by integrating (1.52) over the energy

$$R = \int_{E_T}^{\infty} \frac{\mathrm{d}R}{\mathrm{d}Q} \mathrm{d}Q. \tag{1.54}$$

The integration is performed for energies larger than the threshold energy E_T of the detector, below which it is insensitive to WIMP-nucleus recoils.

Using Eqs. (1.54) and (1.52), one can derive the scattering cross section from the event rate. The experimental collaborations prefer to give their results already in terms of the scattering cross section as a function of the WIMP mass. To be more precise, the WIMP-nucleus total cross section consists of two parts: the spin-dependent (SD) cross section and the spin-independent (SI) one. The former comes from axial current couplings, whereas the latter comes from scalar-scalar and vector-vector couplings. The SD cross section is much suppressed compared to the SI one in the case of heavy nuclei targets and it vanishes if the nucleus contains an even number of nucleons, since in this case the total nuclear spin is zero.

We see that two uncertainties enter the above calculation: the exact value of the local density ρ_0 and the exact form of the velocity distribution $f(v)$. To these, one has to include one more. The cross section σ that appears in the previous expressions concerns the WIMP-nucleon cross section. The couplings of a WIMP with the various quarks that constitute the nucleon are not the same and the WIMP-nucleon cross section depends strongly on the exact quark content of the nucleon. To be more precise, the largest uncertainty lies on the strange content of the nucleon, but we shall return to this point when we will calculate the cross section in a specific particle theory, the Next-to-Minimal Supersymmetric Standard Model, in Sec. 3.5.1.

1.5.2 Experimental status

The situation of the experimental results from direct DM searches is a bit confusing. The null observations in most of the experiments led them to set upper limits on the WIMP-nucleon cross section. These bounds are quite stringent for the spin-independent cross section[7], especially in the regime of WIMP masses of the order of 100 GeV. However, some collaborations have already reported possible DM signals, mainly in the low mass regime. The preferred regions of these experiments do not coincide, while some of them have been already excluded by other experiments. The present picture, for WIMP masses ranging from 5 to 1000 GeV, is summarized in Fig. 1.5, 1.6.

Fig. 1.5 mainly presents upper bounds coming from XENON100 [44]. XENON100 [46] is an experiment located at the Gran Sasso underground laboratory in Italy. It contains in total 165 kg of liquid Xenon, with 65 kg acting as target mass and the rest shielding the detector from background radiation. For these upper limits, 225 live days of data were used. The minimum value for the predicted upper bounds on the cross section is $2 \cdot 10^{-45}\,\mathrm{cm}^2$ for WIMP mass $\sim 55\,\mathrm{GeV}$ (at 90% confidence level), almost one order of magnitude lower than the previously released limits [47] by the same collaboration, using 100 live days of data.

The stringent upper bounds up-to-date (at least for WIMP mass larger than about 7 GeV) come from the first results of the LUX experiment (see Fig. 1.6), after the first

[7] For the spin-dependent scattering, the exclusion limits are quite relaxed. Hence, we will focus on the SI cross sections.

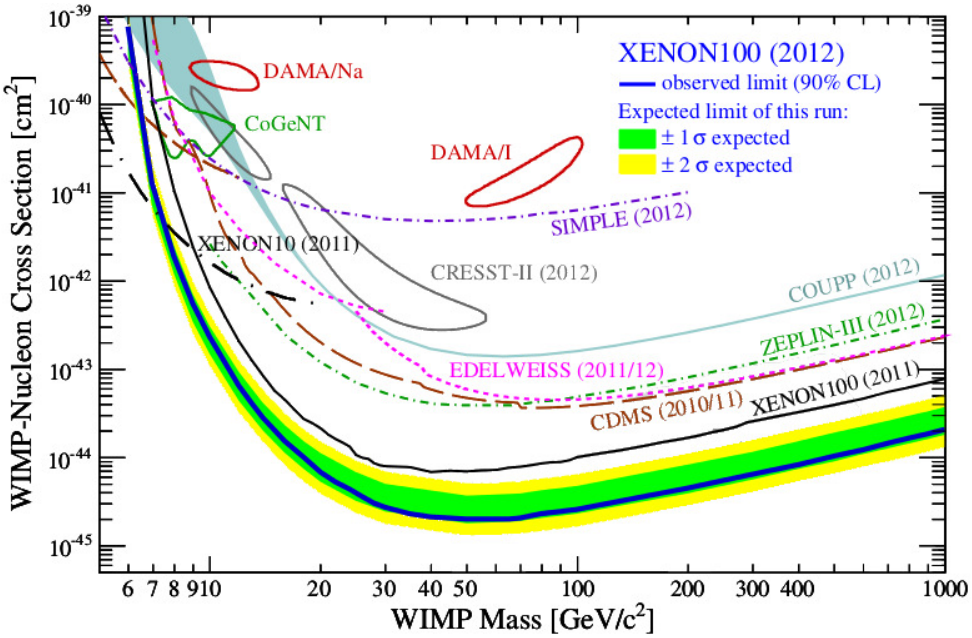

Figure 1.5: The XENON100 exclusion limit (thick blue line), along with the expected sensitivity in green (1σ) and yellow (2σ) band. Other upper bounds are also shown as well as detection claims. From [44].

85.3 live-days of its operation [45]. LUX [53] is a detector containing liquid Xenon, as XENON100, but in larger quantity, with total mass 370 kg. Its operation started on April 2013 with a goal to clearly detect or exclude WIMPs with a spin independent cross section $\sim 2 \cdot 10^{-46}\,\mathrm{cm}^2$.

In Fig. 1.5, except of the XENON100 bounds and other experimental limits on larger WIMP-nucleon cross section, some detection claims also appear. These come from DAMA [48,49], CoGeNT [50] and CRESST-II [51] experiments. The first positive result came from DAMA [52], back in 2000. Since then, the experiment has accumulated 1.17 ton-yr of data over 13 years of operation. DAMA consists of 250 kg of radio pure NaI scintillator and looks for the annual modulation of the WIMP flux in order to reduce the influence of the background.

The annual modulation of the DM flux (see [54] for a recent review) is due to the Earth's orbital motion relative to the rotation of the galactic disk. The galactic disk rotation through an essentially non-rotating DM halo, creates an effective DM wind in the solar frame. During the earth's heliocentric orbit, this wind reaches a maximum when the Earth is moving fastest in the direction of the disk rotation (this happens in the beginning of June) and a minimum when it is moving fastest in the opposite direction (beginning of December).

DAMA claims an 8.9σ annual modulation with a minimum flux on May 26 ± 7 days, consistent with the expectation. Since the detector's target consists of two different nuclei and the experiment cannot distinguish between sodium and iodine recoils, there

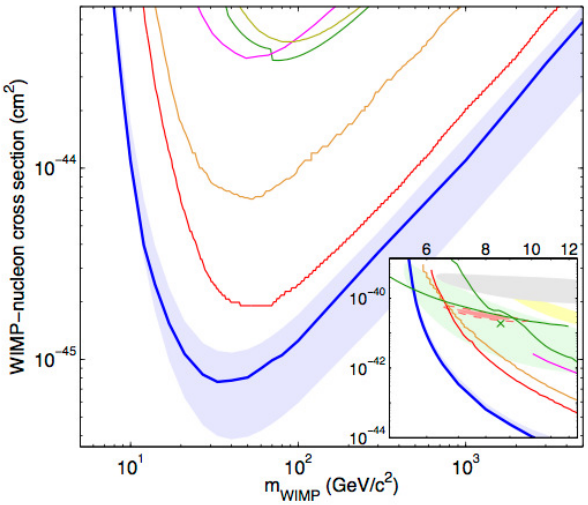

Figure 1.6: The LUX 90% confidence exclusion limit (blue line) with the 1σ range (shaded area). The XENON100 upper bound is represented by the red line. The inset shows also preferred regions by CoGeNT (shaded light red), CDMS II silicon detector (shaded green), CRESST II (shaded yellow) and DAMA (shaded gray). From [45].

is no model independent way to determine the exact region in the cross section versus WIMP mass plane to which the observed modulation corresponds. However, one can assume two cases: one that the WIMP scattering off the sodium nucleus dominates the recoil energy and the other with the iodine recoils dominating. The former corresponds [55] to a light WIMP ($\sim 10\,\text{GeV}$) and quite large scattering cross section and the latter to a heavier WIMP (~ 50 to $100\,\text{GeV}$) with smaller cross section (see Fig. 1.5).

The positive result of DAMA was followed many years later by the ones of CoGeNT and CRESST-II, and more recently by the silicon detector of CDMS [56] (Fig. 1.7). The discrepancy of the results raised a lot of debates among the experiments (for example, [64–67]) and by some the positive results are regarded as controversial. On the other hand, it also raised an effort to find a physical explanation behind this inconsistency (see, for example, [68–71]).

1.6 Indirect Methods for DM Detection

The same annihilation processes that determined the DM relic abundance in the early Universe also occur today in galactic regions where the DM concentration is higher. This fact rises the possibility of detecting potential WIMP pair annihilations indirectly through their imprints on the cosmic rays. Therefore, the indirect DM searches aim at the detection of an excess over the known astrophysical background of charged particles, photons or neutrinos.

Charged particles – electrons, protons and their antiparticles – may originate from direct products (pair of SM particles) of WIMP annihilations, after their decay and

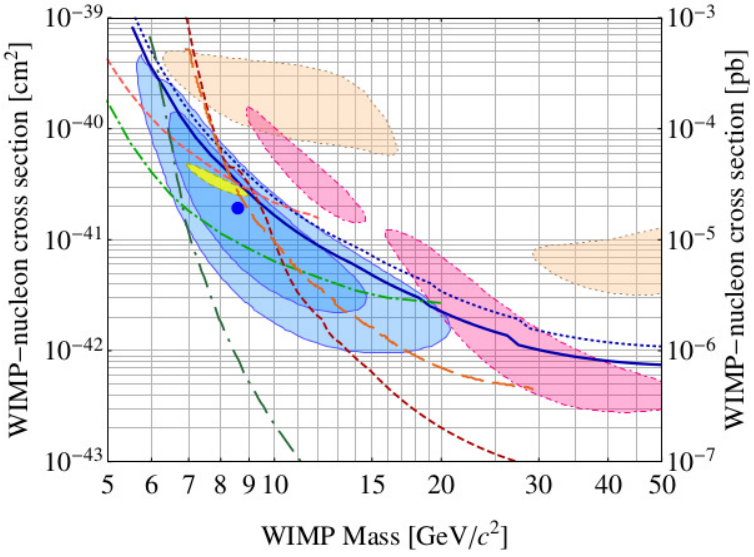

Figure 1.7: The blue contours represent preferred regions for a possible signal at 68% and 90% C.L. using the silicon detector of CMDS [56]. The blue dotted line represents the upper limit obtained by the same analysis and the blue solid line is the combined limit with the silicon CDMS data set reported in [57]. Other limits also appear: from the CMDS standard germanium detector (light and dark red dashed line, for standard [58] and low threshold analysis [59], respectively), EDELWEISS [60] (dashed orange), XENON10 [61] (dash-dotted green) and XENON100 [44] (long-dash-dotted green). The filled regions identify possible signal regions associated with data from CoGeNT [62] (dashed yellow, 90% C.L.), DAMA [49, 55] (dotted tan, 99.7% C.L.) and CRESST-II [51, 63] (dash-dotted pink, 95.45% C.L.) experiments. Taken from [56].

through the process of showering and hadronization. Although the exact shape of the resulting spectrum would depend on the specific process, it is expected to show a steep cutoff at the WIMP mass. Once produced in the DM halo, the charged particles have to travel to the point of detection through the turbulent galactic field, which will cause diffusion. Apart from that, a lot of processes disturb the propagation of the charged particles, such as bremsstrahlung, inverse Compton scattering with CMB photons and many others. Therefore, the uncertainties that enter the propagation of the charged flux until it reaches the telescope are important (contrary to the case of photons and neutrinos that propagate almost unperturbed through the galaxy).

As in the case of direct detection, the experimental status of charged particle detection concerning the DM is confusing. After some hints from HEAT [72] and AMS-01 [73] (the former a far-infrared telescope in Antarctica, the latter a spectrometer, prototype for AMS-02 mounted on the International Space Station [74]), the PAMELA satellite observed [75, 76] a steep increase in the energy spectrum of positron fraction $e^+/(e^+ + e^-)$[8]. Later FERMI satellite [77] and AMS-02 [78] confirmed the results up

[8]The searches for charged particles focus on the antiparticles in order to have a reduced background,

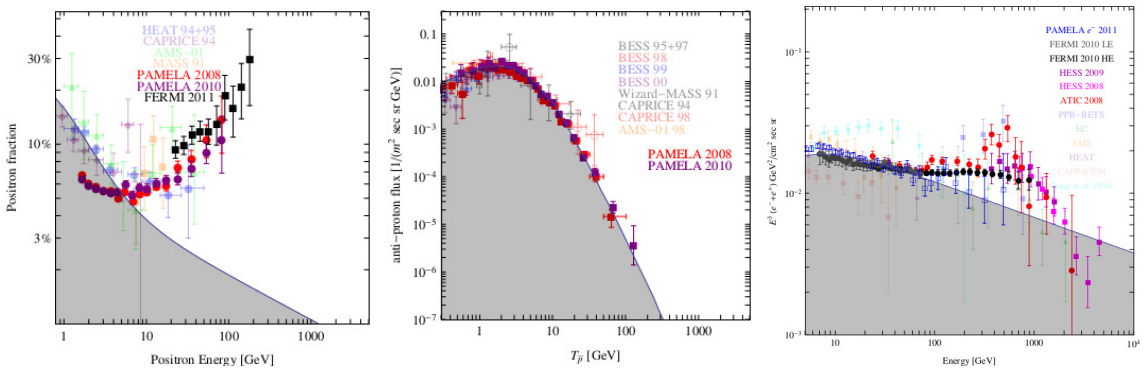

Figure 1.8: A compilation of data of charged cosmic rays, together with plausible but uncertain astrophysical backgrounds, taken from [79]. *Left:* Positron flux. *Center:* Antiproton flux. *Right:* Sum of electrons and positrons.

to energies of $\sim 200\,\mathrm{GeV}$. However, the excess of positrons is not followed by an excess of antiprotons, whose flux seems to coincide with the predicted background [75]. In Fig. 1.8, three plots summarizing the situation are shown [79].

The observed excess is very difficult to explain in terms of DM [79]. To begin with, the annihilation cross section required to reproduce the excess is quite large, many orders of magnitude larger than the thermal cross section. Moreover, an "ordinary" WIMP with large annihilation cross section giving rise to charged leptons is expected to give, additionally, a large number of antiprotons, a fact in contradiction with the observations. Although a lot of work has been done to fit a DM particle to the observed pattern, it is quite possible that the excesses come from a yet unknown astrophysical source. We are not going to discuss further this matter, but we end with a comment. If this excess is due to a source other than DM, then a possible DM positron excess would be lost under this formidable background.

A last hint for DM came from the detection of highly energetic photons. However, we will interrupt this discussion, since this signal and a possible explanation is the subject of Ch. 4. There, we will also see the upper bounds on the annihilation cross section being set due to the absence of excesses in diffuse γ radiation.

since they are much less abundant than the corresponding particles.

CHAPTER 2

PARTICLE PHYSICS

Since the DM comprises of particles, it should be explained by a general particle physics theory. We start in the following section by describing the Standard Model (SM) of particle physics. Although the SM describes so far the fundamental particles and their interactions quite accurately, it cannot provide a DM candidate. Besides, the SM suffers from some theoretical problems, which we discuss in Sec. 2.2. We will see that these problems can be solved if one introduces a new symmetry, the supersymmetry, which we describe in Sec. 2.3. We finish this chapter by briefly describing in Sec. 2.4 a supersymmetric extension of the SM with the minimal additional particle content, the Minimal Supersymmetric Standard Model (MSSM).

2.1 The Standard Model of Particle Physics

The Standard Model (SM) of particle physics[1] consists of two well developed theories, the quantum chromodynamics (QCD) and the electroweak (EW) theory. The former describes the strong interactions among the quarks, whereas the latter describes the electroweak interactions (the weak and electromagnetic interactions in a unified context) between fermions. The EW theory took its final form in the late 1960s by the introduction by S. Weinberg [85] and A. Salam [86] of the Higgs mechanism that gives masses to the SM particles, which followed the unification of electromagnetic and weak interactions [87, 88]. At the same time, the EW model preserves the gauge invariance, making the theory renormalizable, as shown later by 't Hooft [89]. On the other hand, QCD obtained its final form some years later, after the confirmation of the existence of quarks. Of course, the history of the SM is much longer and it can be traced back to 1920s with the formulation of a theoretical basis for a Quantum Field Theory (QFT). Since then, the SM had many successes. The SM particle content was completed with the discovery of the heaviest of the quarks, the top quark [90,91], in 1995 and, recently, with the discovery of the Higgs boson [92, 93].

[1] There are many good textbooks on the SM and Quantum Field Theory, e.g. [80–84].

The key concept within the SM, as in every QFT, is that of symmetries. Each interaction respects a gauge symmetry, based on a Lie algebra. The strong interaction is described by an $SU(3)_c$ symmetry, where the subscript c stands for color, the conserved charge of strong interactions. The EW interactions, on the other hand, are based on a $SU(2)_L \times U(1)_Y$ Lie algebra. Here, as we will subsequently see, L refers to the left-handed fermions and Y is the hypercharge, the conserved charge under the $U(1)$. $SU(2)_L$ conserves a quantity known as weak isospin I. Therefore, the SM contains the internal symmetries of the unitary product group

$$SU(2)_L \times U(1)_Y \times SU(3)_c. \tag{2.1}$$

2.1.1 The particle content of the SM

We mention for completeness that particles are divided into two main classes according to the statistics they follow. The *bosons* are particles with integer spin and follow the Bose-Einstein distribution, whereas *fermions* have half-integer spin and follow the Dirac-Einstein statistics, obeying the Pauli exclusion principle. In the SM, all the fermions have spin 1/2, whereas the bosons have spin 1 with only exception the Higgs boson, which is a scalar (spin zero). We begin the description of the SM particles with the fermions.

Each fermion is classified in irreducible representations of each individual Lie algebra, according to the conserved quantum numbers, i.e. the color C, the weak isospin I and the hypercharge Y. A first classification of fermions can be done into *leptons* and *quarks*, which transform differently under the $SU(3)_c$. Leptons are singlets under this transformation, while quarks act as triplets (the fundamental representation of this group). The EW interactions violate maximally the parity symmetry and $SU(2)_L$ acts only on states with negative chirality (*left-handed*). A Dirac spinor Ψ can be decomposed into left and right chirality components using, respectively, the projection operators $P_L = \frac{1}{2}(1 - \gamma_5)$ and $P_R = \frac{1}{2}(1 + \gamma_5)$:

$$\Psi_L = P_L \Psi \qquad \text{and} \qquad \Psi_R = P_R \Psi. \tag{2.2}$$

Left-handed fermions have $I = 1/2$, with a third component of the isospin $I_3 = \pm 1/2$. Fermions with positive I_3 are called *up-type* fermions and those with negative are called *down-type*. These behave the same way under $SU(2)_L$ and form doublets with one fermion of each type. On the other hand, right-handed fermions have $I = 0$ and form singlets that do not undergo weak interactions. The hypercharge is written in terms of the electric charge Q and the third component of the isospin I_3 through the Gell-Mann–Nishijima relation:

$$Q = I_3 + Y/2. \tag{2.3}$$

Therefore, left- and right-handed components transform differently under the $U(1)_Y$, since they have different hypercharge.

The fermionic sector of the SM comprises three generations of fermions, transforming as spinors under Lorentz transformations. Each generation has the same structure. For leptons, it is an $SU(2)_L$ doublet with components consisting of one left-handed

charged lepton and one neutrino (neutrinos are only left-handed in the SM), along with a gauge singlet right-handed charged lepton. The quark doublet consists of an up- (u) and a down-type (d) (left-handed) quark and the pattern is completed by the two corresponding $SU(2)_L$ singlet right-handed quarks. We write these representations as

$$\text{QUARKS: } Q \equiv \begin{pmatrix} u_L^i \\ d_L^i \end{pmatrix},\ u_R^i,\ d_R^i \qquad \text{LEPTONS: } L \equiv \begin{pmatrix} \nu_L^i \\ e_L^i \end{pmatrix},\ e_R^i, \tag{2.4}$$

with $i = 1, 2, 3$ the generation index.

Having briefly described the fermionic sector, we turn to the bosonic sector of the SM. It consists of the *gauge bosons* that mediate the interactions and the *Higgs boson* that gives masses to the particles through a spontaneous symmetry breaking, the electroweak symmetry breaking (EWSB) [94–98], which we shall describe in Sec. 2.1.3. Before the EWSB, these bosons are

- three W_μ^a $(a = 1, 2, 3)$ weak bosons, associated with the generators of $SU(2)_L$,
- one neutral B_μ boson, associated with the generator of $U(1)_Y$,
- eight gluons G_μ^a $(a = 1, \ldots, 8)$, associated with the generators of $SU(3)_c$, and
- the complex scalar Higgs doublet $\Phi = \begin{pmatrix} \phi^+ \\ \phi^0 \end{pmatrix}$.

After the EWSB, the EW boson states mix and give the two $W^\pm$ bosons, the neutral Z boson and the massless photon γ. From the symmetry breaking, one scalar degree of freedom remains which is the famous (neutral) Higgs boson [97–99]. We will return to the mixed physical states, after describing the Higgs mechanism for symmetry breaking. A complete list of the SM particles (the physical states after EWSB) is shown in Table 2.1.

2.1.2 The SM Lagrangian

The gauge bosons are responsible for the mediation of the interactions and are associated with the generators of the corresponding symmetry. The EW gauge bosons B_μ and W_μ^a are associated, respectively, with the generator Y of the $U(1)_Y$ and the three generators T_2^a of the $SU(2)_L$. The latter are defined as half of the Pauli matrices τ^a ($T_2^a = \frac{1}{2}\tau^a$) and they obey the algebra

$$\left[T_2^a, T_2^b\right] = i\epsilon^{abc} T_2^c, \tag{2.5}$$

where ϵ^{abc} is the fully antisymmetric Levi-Civita tensor. The eight gluons are associated with an equal number of generators T_3^a (Gell-Mann matrices) of $SU(3)_c$ and obey the Lie algebra

$$\left[T_3^a, T_3^b\right] = i f^{abc} T_3^c, \qquad \text{with Tr}\left[T_3^a T_3^b\right] = \frac{1}{2}\delta^{ab}, \tag{2.6}$$

	Name	symbol	mass	charge ($\lvert e\rvert$)	spin
Leptons	electron	e	0.511 MeV	-1	1/2
	electron neutrino	ν_e	0 (<2 eV)	0	1/2
	muon	μ	105.7 MeV	-1	1/2
	muon neutrino	ν_μ	0 (<2 eV)	0	1/2
	tau	τ	1.777 GeV	-1	1/2
	tau neutrino	ν_τ	0 (<2 eV)	0	1/2
Quarks	up	u	$2.7^{+0.7}_{-0.5}$ MeV	2/3	1/2
	down	d	$4.8^{+0.7}_{-0.3}$ MeV	$-1/3$	1/2
	strange	s	(95 ± 5) MeV	$-1/3$	1/2
	charm	c	(1.275 ± 0.025) GeV	2/3	1/2
	bottom	b	(4.18 ± 0.03) GeV	$-1/3$	1/2
	top	t	$(173.5 \pm 0.6 \pm 0.8)$ GeV	2/3	1/2
Bosons	photon	γ	0 ($<10^{-18}$ eV)	0 ($<10^{-35}$)	1
	W boson	$W^\pm$	(80.385 ± 0.015) GeV	± 1	1
	Z boson	Z	(91.1876 ± 0.0021) GeV	0	1
	gluon	g	0 ($\lesssim \mathcal{O}(1)$ MeV)	0	1
	Higgs	H	$(125.3 \pm 0.4 \pm 0.5)$ GeV $(126.0 \pm 0.4 \pm 0.4)$ GeV	0	0

Table 2.1: The particle content of the SM. All values are those given in [100], except of the Higgs mass that is taken from [92, 93] (up and down row, respectively), assuming that the observed excess corresponds to the SM Higgs. The u, d and s quark masses are estimates of so-called "current-quark masses" in a mass-independent subtraction scheme as $\overline{\text{MS}}$ at a scale $\sim 2\,\text{GeV}$. The c and b quark masses are the running masses in the $\overline{\text{MS}}$ scheme. The values in the parenthesis are the current experimental limits.

with f^{abc} the structure constants of the group.

Using the structure constants of the corresponding groups, we define the field strengths for the gauge bosons as

$$B_{\mu\nu} \equiv \partial_\mu B_\nu - \partial_\nu B_\mu, \tag{2.7a}$$

$$W_{\mu\nu} \equiv \partial_\mu W^a_\nu - \partial_\nu W^a_\mu + g_2 \epsilon^{abc} W^b_\mu W^c_\nu \tag{2.7b}$$

and

$$G^a_{\mu\nu} \equiv \partial_\mu G^a_\nu - \partial_\nu G^a_\mu + g_3 f^{abc} G^b_\mu G^c_\nu. \tag{2.7c}$$

We use the notation g_1, g_2 and g_3 for the coupling constants of $U(1)_Y$, $SU(2)_L$ and $SU(3)_c$, respectively. As in any Yang-Mills theory, the non-abelian gauge groups lead to self-interactions, which is not the case for the abelian $U(1)_Y$ group.

Before we finally write the full Lagrangian, we have to introduce the covariant derivative for fermions, which in a general form can be written as

$$\mathcal{D}_\mu \Psi = \left(\partial_\mu - i g_1 \frac{1}{2} Y B_\mu - i g_2 T_2^a W_\mu^a - i g_3 T_3^a G_\mu^a \right) \Psi. \tag{2.8}$$

This form has to be understood as that, depending on Ψ, only the relevant terms apply, hence for $SU(2)_L$ singlet leptons only the two first terms inside the parenthesis are relevant, for doublet leptons the three first terms and for the corresponding quark singlets and doublets the last term also participates. We also have to notice that in order to retain the gauge symmetry, mass terms are forbidden in the Lagrangian. For example, the mass term $m\bar{\psi}\psi = m\left(\bar{\psi}_L \psi_R + \bar{\psi}_R \psi_L\right)$ (with $\bar{\psi} \equiv \psi^\dagger \gamma^0$) is not invariant under $SU(2)_L$. This paradox is solved by the introduction of the Higgs scalar field (see next subsection). The SM Lagrangian can be now written[2], split for simplicity in three parts, each describing the gauge bosons, the fermions and the scalar sector,

$$\mathcal{L}_{SM} = \mathcal{L}_{gauge} + \mathcal{L}_{fermion} + \mathcal{L}_{scalar}, \tag{2.9}$$

with

$$\mathcal{L}_{gauge} = -\frac{1}{4} G_{\mu\nu}^a G_a^{\mu\nu} - \frac{1}{4} W_{\mu\nu}^a W_a^{\mu\nu} - \frac{1}{4} B_{\mu\nu} B^{\mu\nu}, \tag{2.10a}$$

$$\begin{aligned} \mathcal{L}_{fermion} = {} & i\bar{L}\mathcal{D}_\mu \gamma^\mu L + i\bar{e}_R \mathcal{D}_\mu \gamma_\mu e_R \\ & + i\bar{Q}\mathcal{D}_\mu \gamma^\mu Q + i\bar{u}_R \mathcal{D}_\mu \gamma^\mu u_R + i\bar{d}_R \mathcal{D}_\mu \gamma^\mu d_R \\ & - \left(h_e \bar{L} \Phi e_R + h_d \bar{Q} \Phi d_R + h_u \bar{Q} \widetilde{\Phi} u_R + \text{h.c.} \right) \end{aligned} \tag{2.10b}$$

and

$$\mathcal{L}_{scalar} = \left(\mathcal{D}_\mu \Phi\right)^\dagger \left(\mathcal{D}_\mu \Phi\right) - V(\Phi^\dagger \Phi), \tag{2.10c}$$

where

$$V(\Phi^\dagger \Phi) = \mu^2 \Phi^\dagger \Phi + \lambda \left(\Phi^\dagger \Phi\right)^2 \tag{2.11}$$

is the scalar Higgs potential. $\widetilde{\Phi}$ is the conjugate of Φ, related to the charge conjugate by $\widetilde{\Phi} = i\tau_2 \Phi^\star$, with τ_i the Pauli matrices. The covariant derivative acting on the Higgs scalar field gives

$$\mathcal{D}_\mu \Phi = \left[\partial_\mu - i g_1 \frac{1}{2} Y B_\mu - i g_2 T_2^a W_\mu^a \right] \Phi. \tag{2.12}$$

Before we proceed to the description of the Higgs mechanism, a last comment concerning the SM Lagrangian is in order. If we restore the generation indices, we see that

[2]For simplicity, from now on we are going to omit the generations indices.

the Yukawa couplings h are 3×3, in general complex, matrices. As any complex matrix, they can be diagonalized with the help of two unitary matrices V_L and V_R, which are related by $V_R = U^\dagger V_L$ with U again a unitary matrix. The diagonalization in the quark sector to the mass eigenstates induces a mixing among the flavors (generations), described by the Cabibbo–Kobayashi–Maskawa (CKM) matrix [101, 102]. The CKM matrix is defined by

$$V_{CKM} \equiv V_L^{u\dagger} V_L^{d\dagger}, \tag{2.13}$$

where V_L^u, V_L^d are the unitary matrices that diagonalize the Yukawa couplings H^u, H^d, respectively. This product of the two matrices appears in the charged current when it is expressed in terms of the observable mass eigenstates.

2.1.3 Mass generation through the Higgs mechanism

We will start by examining the scalar potential (2.11). The vacuum expectation value (vev) of the Higgs field $\langle\Phi\rangle \equiv \langle 0|\Phi|0\rangle$ is given by the minimum of the potential. For $\mu^2 > 0$, the potential is always non-negative and Φ has a zero vev. The hypothesis of the Higgs mechanism is that $\mu^2 < 0$. In this case, the field Φ will acquire a vev

$$\langle\Phi\rangle = \frac{1}{2}\begin{pmatrix} 0 \\ v \end{pmatrix} \qquad \text{with} \qquad v = \sqrt{-\frac{\mu^2}{\lambda}}. \tag{2.14}$$

Since the charged component of Φ still has a zero vev, the $U(1)_Q$ symmetry of quantum electrodynamics (QED) remains unbroken.

We expand the field Φ around the minima v in terms of real fields, and at leading order we have

$$\Phi(x) = \begin{pmatrix} \theta_2(x) + i\theta_1(x) \\ \frac{1}{\sqrt{2}}(v + H(x)) - i\theta_3(x) \end{pmatrix} = \frac{1}{\sqrt{2}} \mathrm{e}^{i\theta_a(x)\tau^a} \begin{pmatrix} 0 \\ v + H(x) \end{pmatrix}. \tag{2.15}$$

We can eliminate the unphysical degrees of freedom θ_a, using the fact that the theory remains gauge invariant. Therefore, we perform the following $SU(2)_L$ gauge transformation on Φ (unitary gauge)

$$\Phi(x) \to \mathrm{e}^{-i\theta_a(x)\tau^a}\Phi(x), \tag{2.16}$$

so that

$$\Phi(x) = \frac{1}{\sqrt{2}}\begin{pmatrix} 0 \\ v + H(x) \end{pmatrix}. \tag{2.17}$$

We are going to use the following definitions for the gauge fields

$$W_\mu^\pm \equiv \frac{1}{2}\left(W_\mu^1 \mp iW_\mu^2\right), \tag{2.18a}$$

$$Z_\mu \equiv \frac{1}{\sqrt{g_1^2 + g_2^2}}\left(g_2 W_\mu^3 - g_1 B_\mu\right), \tag{2.18b}$$

$$A_\mu \equiv \frac{1}{\sqrt{g_1^2 + g_2^2}}\left(g_1 W_\mu^3 + g_2 B_\mu\right), \tag{2.18c}$$

Then, the kinetic term for Φ (see Eq. (2.10c)) can be written in the unitary gauge as

$$(\mathcal{D}_\mu \Phi)^\dagger (\mathcal{D}^\mu \Phi) = \frac{1}{2}(\partial_\mu H)^2 + M_W^2 W_\mu^+ W^{-\mu} + \frac{1}{2} M_Z^2 Z_\mu Z^\mu, \tag{2.19}$$

with

$$M_W \equiv \frac{1}{2} g_2 v \qquad \text{and} \qquad M_Z \equiv \frac{1}{2}\sqrt{g_1^2 + g_2^2}\, v. \tag{2.20}$$

We see that the definitions (2.18) correspond to the physical states of the gauge bosons that have acquired masses due to the non-zero Higgs vev, given by (2.20). The photon has remained massless, which reflects the fact that after the spontaneous breakdown of $SU(2)_L \times U(1)_Y$ the $U(1)_Q$ remained unbroken. Among the initial degrees of freedom of the complex scalar field Φ, three were absorbed by $W^\pm$ and Z and one remained as the neutral Higgs particle with squared mass

$$m_H^2 = 2\lambda v^2. \tag{2.21}$$

We note that λ should be positive so that the scalar potential (2.11) is bounded from below.

Fermions also acquire masses due to the Higgs mechanism. The Yukawa terms in the fermionic part (2.10b) of the SM Lagrangian are written, after expanding around the vev in the unitary gauge,

$$\mathcal{L}_Y = -\frac{1}{\sqrt{2}} h_e \bar{e}_L (v + H) e_R - \frac{1}{\sqrt{2}} h_d \bar{d}_L (v + H) d_R - \frac{1}{\sqrt{2}} h_u \bar{u}_L (v + H) u_R + \text{h.c.}\,. \tag{2.22}$$

Therefore, we can identify the masses of the fermions as

$$m_{e^i} = \frac{h_e^i v}{\sqrt{2}}, \qquad m_{d^i} = \frac{h_d^i v}{\sqrt{2}}, \qquad m_{u^i} = \frac{h_u^i v}{\sqrt{2}}, \tag{2.23}$$

where we have written explicitly the generation indices.

2.2 Limits of the SM and the emergence of supersymmetry

2.2.1 General discussion of the SM problems

The SM has been proven extremely successful and has been tested in high precision in many different experiments. It has predicted many new particles before their final discovery and also explained how the particles gain their masses. Its last triumph was of course the discovery of a boson that seems to be very similar to the Higgs boson of the SM. However, it is generally accepted that the SM cannot be the ultimate theory. It is not only observed phenomena that the SM does not explain; SM also faces important theoretical issues.

The most prominent among the inconsistencies of the SM with observations is the oscillations among neutrinos of different generations. In order for the oscillations to

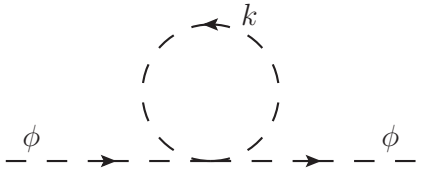

Figure 2.1: The scalar one-loop diagram giving rise to quadratic divergences.

occur, neutrinos should have non-zero masses. However, minimal modifications of the SM are able to fit with the data of neutrino physics. Another issue that a more complete theory has to face is the matter asymmetry, the observed dominance of matter over antimatter in the Universe. In addition, in order to comply with the standard cosmological model, it has to provide the appropriate particle(s) that drove the inflation. Last, but not least, we saw that in order to explain the DM that dominates the Universe, a massive, stable weakly interacting particle must exist. Such a particle is not present in the SM.

On the other hand, the SM also suffers from a theoretical perspective. For example, the SM counts 19 free parameters; one expects that a fundamental theory would have a much smaller number of free parameters. Simple modifications of the SM have been proposed relating some of these parameters. Grand unified theories (GUTs) unify the gauge couplings at a high scale $\sim 10^{16}\,\mathrm{GeV}$. However, this unification is only approximate unless the GUT is embedded in a supersymmetric framework. Another serious problem of the SM is that of naturalness. This will be the topic of the following subsection.

2.2.2 The naturalness problem of the SM

The presence of fundamental scalar fields, like the Higgs, gives rise to quadratic divergences. The diagram of Fig. 2.1 contributes to the squared mass of the scalar

$$\delta m^2 = \lambda \int^{\Lambda} \frac{\mathrm{d}^4 k}{(2\pi)^4}\, k^{-2}. \tag{2.24}$$

This contribution is approximated by $\delta m^2 \sim \lambda\Lambda^2/(16\pi^2)$, quadratic in a cut-off Λ, which should be finite. For the case of the Higgs scalar field, one has to include its couplings to the gauge fields and the top quark[3]. Therefore,

$$\delta m_H^2 = \frac{3\Lambda^2}{8\pi^2 v^2}\left[\left(4m_t^2 - 2M_W^2 - M_Z^2 - m_H^2\right) + \mathcal{O}(\ln\frac{\Lambda}{\mu})\right], \tag{2.25}$$

where we have used Eq. (2.21) and $m_H^2 \equiv m_0^2 + \delta m_H^2$.

[3]Since the contribution to the squared mass correction are quadratic in the Yukawa couplings (or quark masses), the lighter quarks can be neglected.

Taking Λ as a fundamental scale $\Lambda \sim M_{Pl} \sim 10^{19}\,\mathrm{GeV}$ we have

$$m_0^2 = m_H^2 - \frac{3\Lambda^2}{8\pi^2 v^2}\left(4m_t^2 - 2M_W^2 - M_Z^2 - m_H^2\right) \tag{2.26}$$

and we can see that m_0^2 has to be adjusted to a precision of about 30 orders of magnitude in order to achieve an EW scale Higgs mass. This is considered as an intolerable fine-tuning, which is against the general belief that the observable properties of a theory have to be stable under small variations of the fundamental (bare) parameters. It is exactly the above behavior that is considered as unnatural. Although the SM could be self-consistent without imposing a large scale, grand unification of the parameters introduce a hierarchy problem between the different scales.

A more strict definition of naturalness comes from 't Hooft [103], which we rewrite here:

> *At an energy scale μ, a physical parameter or set of physical parameters $\alpha_i(\mu)$ is allowed to be very small only if the replacement $\alpha_i(\mu) = 0$ would increase the symmetry of the system.*

Clearly, this is not the case here. Although m_H is small compared to the fundamental scale Λ, it is not protected by any symmetry and a fine-tuning is necessary.

2.2.3 A way out

The naturalness in the 't Hooft sense is inspired by quantum electrodynamics, which is the archetype for a natural theory. For example, the corrections to the electron mass m_e are themselves proportional to m_e, with a dimensionless proportionality factor that behaves like $\sim \ln\Lambda$. In general, fermion masses are protected by the chiral symmetry; small values (compared to the fundamental scale) of these masses enhances the symmetry.

If a new symmetry exists in nature, relating fermion fields to scalar fields, then each scalar mass would be related somehow to the corresponding fermion mass. Therefore, the scalar mass itself can be naturally small compared to Λ, since this would mean that the fermion mass is small, which enhances the chiral symmetry. Such a symmetry, relating bosons to fermions and vice versa, is known as supersymmetry [104, 105]. Actually, as we will see later, if this new symmetry remains unbroken, the masses of the conjugate bosons and fermions would have to be equal.

In order to make the above statement more concrete, we consider a toy model with two additional complex scalar fields $\widetilde{f}_L$ and $\widetilde{f}_R$. We will discuss only the quadratic divergences that come from corrections to the Higgs mass due to a fermion. The generalization for the contributions from the gauge bosons or the self-interaction is straightforward. The interactions in this toy model of the new scalar fields with the Higgs are described by the Lagrangian

$$\mathcal{L}_{\widetilde{f}\widetilde{f}\phi} = \lambda_{\widetilde{f}}|\phi|^2\left(|\widetilde{f}_L|^2 + |\widetilde{f}_R|^2\right). \tag{2.27}$$

It can be easily checked that the quadratic divergence coming from a fermion at one loop is exactly canceled, as long as the new quartic coupling $\lambda_{\tilde{f}}$ obeys the relation $\lambda_{\tilde{f}} = -\lambda_f^2$ (λ_f is the Yukawa coupling for the fermion f).

2.3 A brief summary of Supersymmetry

Supersymmetry (SUSY) is a symmetry relating fermions and bosons. The supersymmetry transformation should turn a boson state into a fermion state and vice versa. If Q is the operator that generates such transformations, then

$$Q\,|\text{boson}\rangle = |\text{fermion}\rangle \qquad\qquad Q\,|\text{fermion}\rangle = |\text{boson}\rangle\,. \tag{2.28}$$

Due to commutation and anticommutation rules of bosons and fermions, Q has to be an anticommuting spinor operator, carrying spin angular momentum 1/2. Since spinors are complex objects, the hermitian conjugate $Q^\dagger$ is also a symmetry operator[4].

There is a no-go theorem, the Coleman-Mandula theorem [106], that restricts the conserved charges which transform as tensors under the Lorentz group to the generators of translations P_μ and the generators of Lorentz transformations $M_{\mu\nu}$. Although this theorem can be evaded in the case of supersymmetry due to the anticommutation properties of Q, $Q^\dagger$ [107], it restricts the underlying algebra of supersymmetry [108]. Therefore, the basic supersymmetric algebra can be written as[5]

$$\{Q, Q^\dagger\} = P^\mu, \tag{2.29a}$$

$$\{Q, Q\} = \{Q^\dagger, Q^\dagger\} = 0, \tag{2.29b}$$

$$[P^\mu, Q] = [P^\mu, Q] = 0. \tag{2.29c}$$

In the following, we summarize the basic conclusions derived from this algebra.

- The single-particle states of a supersymmetric theory fall into irreducible representations of the SUSY algebra, called *supermultiplets*. A supermultiplet contains both fermion and boson states, called *superpartners*.

- *Superpartners must have equal masses*: Consider $|\Omega\rangle$ and $|\Omega'\rangle$ as the superpartners, $|\Omega'\rangle$ should be proportional to some combination of the Q and $Q^\dagger$ operators acting on $|\Omega\rangle$, up to a space-time translation or rotation. Since $-P^2$ commutes with Q, $Q^\dagger$ and all space-time translation and rotation operators, $|\Omega\rangle$, $|\Omega'\rangle$ will have equal eigenvalues of $-P^2$ and thus equal masses.

- *Superpartners must be in the same representation of gauge groups*, since Q, $Q^\dagger$ commute with the generators of gauge transformations. This means that they have equal charges, weak isospin and color degrees of freedom.

[4] We will confine ourselves to the phenomenologically more interesting case of $N = 1$ supersymmetry, with N referring to the number of distinct copies of Q, $Q^\dagger$.

[5] We present a simplified version, omitting spinor indices in Q and $Q^\dagger$.

- *Each supermultiplet contains an equal number of fermion and boson degrees of freedom* (n_F and n_B, respectively): Consider the operator $(-1)^{2s}$, with s the spin angular momentum, and the states $|i\rangle$ that have the same eigenvalue p^μ of P^μ. Then, using the SUSY algebra (2.29) and the completeness relation $\sum_i |i\rangle \langle i| = 1$, we have $\sum_i \langle i| (-1)^{2s} P^\mu |i\rangle = 0$. On the other hand, $\sum_i \langle i| (-1)^{2s} P^\mu |i\rangle = p^\mu \mathrm{Tr}\left[(-1)^{2s}\right] \propto n_B - n_F$. Therefore, $n_F = n_B$.

As addendum to the last point, we see that two kind of supermultiplets are possible (neglecting gravity):

- A *chiral* (or *matter* or *scalar*) *supermultiplet*, which consists of a single Weyl fermion (with two spin helicity states, $n_F = 2$) and two real scalars (each with $n_B = 1$), which can be replaced by a single complex scalar field.

- A *gauge* (or *vector*) *supermultiplet*, which consists of a massless spin 1 boson (two helicity states, $n_B = 2$) and a massless spin 1/2 fermion ($n_F = 2$).

Other combinations either are reduced to combinations of the above supermultiplets or lead to non-renormalizable interactions.

It is possible to study supersymmetry in a geometric approach, using a space-time manifold extended by four fermionic (Grassmann) coordinates. This manifold is called *superspace*. The fields, in turn, expressed in terms of the extended set of coordinates are called *superfields*. We are not going to discuss the technical details of this topic (the interested reader may refer to the rich bibliography, for example [109–111]).

However, it is important to mention a very useful function of the superfields, the *superpotential*. A generic form of a (renormalizable) superpotential in terms of the superfields $\widehat{\Phi}$ is the following

$$W = \frac{1}{2} M^{ij} \widehat{\Phi}_i \widehat{\Phi}_j + \frac{1}{6} y^{ijk} \widehat{\Phi}_i \widehat{\Phi}_j \widehat{\Phi}_k. \tag{2.30}$$

The Lagrangian density can always be written according to the superpotential. The superpotential has also to fulfill some requirements. In order for the Lagrangian to be supersymmetric invariant, W has to be holomorphic in the complex scalar fields (it does not involve hermitian conjugates $\widehat{\Phi}^\dagger$ of the superfields). Conventionally, W involves only left chiral superfields. Instead of the $SU(2)_L$ singlet right chiral fermion fields, one can use their left chiral charge conjugates.

As we mentioned before, the members of a supermultiplet have equal masses. This contradicts our experience, since the partners of the light SM particles would have been detected long time ago. Hence, the supersymmetry should be broken at a large energy scale. The common approach is that SUSY is broken in a hidden sector, very weakly coupled to the visible sector. Then, one has to explain how the SUSY breaking mediated to the visible sector. The two most popular scenarios are the gravity mediation scenario [112–114] and the Gauge-Mediated SUSY Breaking (GSMB) [113, 115–117], where the mediation occurs through gauge interactions.

There are two approaches with which one can address the SUSY breaking. In the first approach, one refers to a GUT unification and determines the supersymmetric

breaking parameters at low energies through the renormalization group equations. This approach results in a small number of free parameters. In the second approach, the starting point is the low energy scale. In this case, the SUSY breaking has to be parametrized by the addition of breaking terms to the low energy Lagrangian. This results in a larger set of free parameters. These terms should not reintroduce quadratic divergences to the scalar masses, since the cancellation of these divergences was the main motivation for SUSY. Then, one talks about *soft breaking terms*.

2.4 The Minimal Supersymmetric Standard Model

One can construct a supersymmetric version of the standard model with a minimal content of particles. This model is known as the Minimal Supersymmetric Standard Model (MSSM). In a SUSY extension of the SM, each of the SM particles is either in a chiral or in a gauge supermultiplet, and should have a superpartner with spin differing by 1/2.

The spin-0 partners of quarks and leptons are called squarks and sleptons, respectively (or collectively sfermions), and they have to reside in chiral supermultiplets. The left- and right-handed components of fermions are distinct 2-component Weyl fermions with different gauge transformations in the SM, so that each must have its own complex scalar superpartner. The gauge bosons of the SM reside in gauge supermultiplets, along with their spin-1/2 superpartners, which are called gauginos. Every gaugino field, like its gauge boson partner, transforms as the adjoint representation of the corresponding gauge group. They have left- and right-handed components which are charge conjugates of each other: $(\widetilde{\lambda}_L)^c = \widetilde{\lambda}_R$.

The Higgs boson, since it is a spin-0 particle, should reside in a chiral supermultiplet. However, we saw (in the fermionic part of the SM Lagrangian, Eq. (2.10b)) that the $Y = 1/2$ Higgs in the SM can give mass to both up- and down-type quarks, only if the conjugate Higgs field with $Y = -1/2$ is involved. Since in the superpotential there are no conjugate fields, two Higgs doublets have to be introduced. Each Higgs supermultiplet would have hypercharge $Y = +1/2$ or $Y = -1/2$. The Higgs with the negative hypercharge gives mass to the down-type fermions and it is called down-type Higgs (H_d, or H_1 in the SLHA convention [118]) and the other one gives mass to up-type fermions and it is called up-type Higgs (H_u, or H_2).

The MSSM respects a discrete $\mathbb{Z}_2$ symmetry, the R-parity. If one writes the most general terms in the supersymmetric Lagrangian (still gauge-invariant and holomorphic), some of them would lead to non-observed processes. The most obvious constraint comes from the non-observed proton decay, which arises from a term that violates both lepton and baryon numbers (L and B, respectively) by one unit. In order to avoid these terms, R-parity, a multiplicative conserved quantum number, is introduced, defined as

$$\mathcal{P}_R = (-1)^{3(B-L)+2s}, \tag{2.31}$$

with s the spin of the particle.

The R even particles are the SM particles, whereas the R odd are the new particles introduced by the MSSM and are called *supersymmetric particles*. Due to R-parity,

if it is exactly conserved, there can be no mixing among odd and even particles and, additionally, each interaction vertex in the theory can only involve an even number of supersymmetric particles. The phenomenological consequences are quite important. First, the lightest among the odd-parity particles is stable. This particle is known as the *lightest supersymmetric particle* (LSP). Second, in collider experiments, supersymmetric particles can only be produced in pairs. The first of these consequences was a breakthrough for the incorporation of DM into a general theory. If the LSP is electrically neutral, it interacts only weakly and it consists an attractive candidate for DM.

We are not going to enter further into the details of the MSSM[6]. Although MSSM offers a possible DM candidate, there is a strong theoretical reason to move from the minimal model. This reason is the so-called μ-problem of the MSSM, with which we begin the discussion of the next chapter, where we shall describe more thoroughly the Next-to-Minimal Supersymmetric Standard Model.

[6]We refer to [110] for an excellent and detailed description of MSSM.

Part II

Dark Matter in the Next-to-Minimal Supersymmetric Standard Model

CHAPTER 3

THE NEXT-TO-MINIMAL SUPERSYMMETRIC STANDARD MODEL

The Next-to-Minimal Supersymmetric Standard Model (NMSSM) is an extension of the MSSM by a chiral, $SU(2)_L$ singlet superfield $\widehat{S}$ (see [119, 120] for reviews). The introduction of this field solves the μ-problem[1] from which the MSSM suffers, but also leads to a different phenomenology from that of the minimal model. The scalar component of the additional field mixes with the scalar Higgs doublets, leading to three CP-even mass eigenstates and two CP-odd eigenstates (as in the MSSM a doublet-like pair of charged Higgs also exists). On the other hand, the fermionic component of the singlet (*singlino*) mixes with gauginos and higgsinos, forming five neutral states, the *neutralinos*.

Concerning the CP-even sector, a new possibility opens. The lightest Higgs mass eigenstate may have evaded the detection due to a sizeable singlet component. Besides, the SM-like Higgs is naturally heavier than in the MSSM [123–126]. Therefore, a SM-like Higgs mass $\sim 125\,\text{GeV}$ is much easier to explain [127–141]. The singlet component of the CP-odd Higgs also allows for a potentially very light pseudoscalar with suppressed couplings to SM particles, with various consequences, especially on low energy observables (for example, [142–145]). The singlino component of the neutralino may also play an important role for both collider phenomenology and DM. This is the case when the neutralino is the LSP and the lightest neutralino has a significant singlino component.

We start the discussion about the NMSSM by describing the μ-problem and how this is solved in the context of the NMSSM. In Sec. 3.2 we introduce the NMSSM Lagrangian and we write the mass matrices of the Higgs sector particles and the su-

[1] However, historically, the introduction of a singlet field preceded the μ-problem, e.g. [104, 105, 121, 122].

persymmetric particles, at tree level. We continue by examining, in Sec. 3.3, the DM candidates in the NMSSM and particularly the neutralino. The processes which determine the neutralino relic density are described in Sec. 3.4. The detection possibilities of a potential NMSSM neutralino as DM are discussed in (Sec. 3.5). We close this chapter (Sec. 3.6) by examining possible ways to include non-zero neutrino masses and the additional DM candidates that are introduced.

3.1 Motivation – The μ-problem of the MSSM

As we saw, the minimal extension of the SM, the MSSM, contains two Higgs $SU(2)_L$ doublets H_u and H_d. The Lagrangian of the MSSM should contain a supersymmetric mass term, $\mu H_u H_d$, for these two doublets. There are several reasons, which we will subsequently review, that require the existence of such a term. On the other hand, the fact that $|\mu|$ cannot be very large, actually it should be of the order of the EW scale, brings back the problem of naturalness. A parameter of the model should be much smaller than the "natural" scale (the GUT or the Planck scale) before the EW symmetry breaking. This leads to the so-called μ-problem of the MSSM [146].

The reasons that such a term should exist in the Lagrangian of the MSSM are mainly phenomenological. The doublets H_u and H_d are components of chiral superfields that also contain fermionic $SU(2)_L$ doublets. Their electrically charged components mix with the superpartners of the $W^{\pm}$ bosons, forming two charged Dirac fermions, the charginos. The unsuccessful searches for charginos in LEP have excluded charginos with masses almost up to its kinetic limit ($\sim 104\,\text{GeV}$) [147]. Since the μ term determines the mass of the charginos, μ cannot be zero and actually $|\mu| \gtrsim 100\,\text{GeV}$, independently of the other free parameters of the model. Moreover, $\mu = 0$ would result in a Peccei-Quinn symmetry of the Higgs sector and an undesirable massless axion. Finally, there is one more reason for $\mu \neq 0$ related to the mass generation by the Higgs mechanism. The term $\mu H_u H_d$ will be accompanied by a soft SUSY breaking term $B\mu H_u H_d$. This term is necessary so that both neutral components of H_u and H_d are non-vanishing at the minimum of the potential.

The Higgs mechanism also requires that μ is not too large. In order to generate the EW symmetry breaking, the Higgs potential has to be unstable at its origin $H_u = H_d = 0$. Soft SUSY breaking terms for H_u and H_d of the order of the SUSY breaking scale generate such an instability. However, the μ induced squared masses for H_u, H_d are always positive and would destroy the instability in case they dominate the negative soft mass terms.

The NMSSM is able to solve the μ-problem by dynamically generating the mass μ. This is achieved by the introduction of an $SU(2)_L$ singlet scalar field S. When S acquires a vev, a mass term for the H_u and H_d emerges with an effective mass μ_{eff} of the correct order, as long as the vev is of the order of the SUSY breaking scale. This can be obtained in a more "natural" way through the soft SUSY breaking terms.

3.2 The NMSSM Lagrangian

All the necessary information for the Lagrangian of the NMSSM can be extracted from the superpotential and the soft SUSY breaking Lagrangian, containing the soft gaugino and scalar masses, and the trilinear couplings. We begin with the superpotential, writing all the interactions of the NMSSM superfields, which include the MSSM superfields and the additional gauge singlet chiral superfield[2] $\widehat{S}$. Hence, the superpotential reads

$$\begin{aligned} W = {} & \lambda \widehat{S} \widehat{H}_u \cdot \widehat{H}_d + \frac{1}{3}\kappa \widehat{S}^3 \\ & + h_u \widehat{Q} \cdot \widehat{H}_u \widehat{U}^c_R + h_d \widehat{H}_d \cdot \widehat{Q} \widehat{D}^c_R + h_e \widehat{H}_d \cdot \widehat{L} \widehat{E}^c_R. \end{aligned} \tag{3.1}$$

The couplings to quarks and leptons have to be understood as 3×3 matrices and the quark and lepton fields as vectors in the flavor space. The $SU(2)_L$ doublet superfields are given (as in the MSSM) by

$$\widehat{Q} = \begin{pmatrix} \widehat{U}_L \\ \widehat{D}_L \end{pmatrix}, \qquad \widehat{L} = \begin{pmatrix} \widehat{\nu} \\ \widehat{E}_L \end{pmatrix}, \qquad \widehat{H}_u = \begin{pmatrix} \widehat{H}^+_u \\ \widehat{H}^0_u \end{pmatrix}, \qquad \widehat{H}_d = \begin{pmatrix} \widehat{H}^0_d \\ \widehat{H}^-_d \end{pmatrix} \tag{3.2}$$

and the product of two doublets is given by, for example, $\widehat{Q} \cdot \widehat{H}_u = \widehat{U}_L \widehat{H}^0_u - \widehat{H}^+_u \widehat{D}_L$.

An important fact to note is that the superpotential given by (3.1) does not include all possible renormalizable couplings (which respect R-parity). The most general superpotential would also include the terms

$$W \supset \mu \widehat{H}_u \cdot \widehat{H}_d + \frac{1}{2}\mu' \widehat{S}^2 + \xi_F \widehat{s}, \tag{3.3}$$

with the first two terms corresponding to supersymmetric masses and the third one, with ξ_F of dimension $mass^2$, to a tadpole term. However, the above dimensionful parameters μ, μ' and ξ_F should be of the order of the SUSY breaking scale, a fact that contradicts the motivation behind the NMSSM. Here, we omit these terms and we will work with the scale invariant superpotential (3.1). The Lagrangian of a scale invariant superpotential possesses an accidental $\mathbb{Z}_3$ symmetry, which corresponds to a multiplication of all the components of all chiral fields by a phase $e^{i2\pi/3}$.

The corresponding soft SUSY breaking masses and couplings are

$$\begin{aligned} -\mathcal{L}_{soft} = {} & m^2_{H_u}|H_u|^2 + m^2_{H_d}|H_d|^2 + m^2_S|S|^2 \\ & + m^2_Q|Q|^2 + m^2_D|D_R|^2 + m^2_U|U_R|^2 + m^2_L|L|^2 + m^2_E|E_R|^2 \\ & + \Big(h_u A_u Q \cdot H_u U^c_R - h_d A_d Q \cdot H_d D^c_R - h_e A_e L \cdot H_d E^c_R \\ & \qquad + \lambda A_\lambda H_u \cdot H_d S + \frac{1}{3}\kappa A_\kappa S^3 + \text{h.c.} \Big) \\ & + \frac{1}{2} M_1 \lambda_1 \lambda_1 + \frac{1}{2} M_2 \lambda^i_2 \lambda^i_2 + \frac{1}{2} M_3 \lambda^a_3 \lambda^a_3, \end{aligned} \tag{3.4}$$

[2]Here, the hatted capital letters denote chiral superfields, whereas the corresponding unhatted ones indicate their complex scalar components.

where we have also included the soft breaking masses for the gauginos. λ_1 is the $U(1)_Y$ gaugino (*bino*), λ_2^i with $i = 1, 2, 3$ is the $SU(2)_L$ gaugino (*winos*) and, finally, the λ_3^a with $a = 1, \ldots, 8$ denotes the $SU(3)_c$ gaugino (*gluinos*).

The scalar potential, expressed by the so-called D and F terms, can be written explicitly using the general formula

$$V = \frac{1}{2}\left(D^a D^a + D'^2\right) + F_i^\star F_i, \tag{3.5}$$

where

$$D^a = g_2 \Phi_i^* T_{ij}^a \Phi_j \tag{3.6a}$$

$$D' = \frac{1}{2} g_1 Y_i \Phi_i^* \Phi_i \tag{3.6b}$$

$$F_i = \frac{\partial W}{\partial \Phi_i}. \tag{3.6c}$$

We remind that T^a are the $SU(2)_L$ generators and Y_i the hypercharge of the scalar field Φ_i. The Yukawa interactions and fermion mass terms are given by the general Lagrangian

$$\mathcal{L}_{Yukawa} = -\frac{1}{2}\left[\left(\frac{\partial^2 W}{\partial \Phi_i \partial \Phi_j}\psi_i \psi_j + \text{h.c.}\right)\right], \tag{3.7}$$

using the superpotential (3.1). The two-component spinor ψ_i is the superpartner of the scalar Φ_i.

3.2.1 Higgs sector

Using the general form of the scalar potential, the following Higgs potential is derived

$$\begin{aligned} V_{Higgs} = & \left|\lambda\left(H_u^+ H_d^- - H_u^0 H_d^0\right) + \kappa S^2\right|^2 \\ & + \left(m_{H_u}^2 + |\lambda S|^2\right)\left(\left|H_u^0\right|^2 + \left|H_u^+\right|^2\right) \\ & + \left(m_{H_d}^2 + |\lambda S|^2\right)\left(\left|H_d^0\right|^2 + \left|H_d^-\right|^2\right) \\ & + \frac{1}{8}\left(g_1^2 + g_2^2\right)\left(\left|H_u^0\right|^2 + \left|H_u^+\right|^2 - \left|H_d^0\right|^2 - \left|H_d^-\right|^2\right)^2 \\ & + \frac{1}{2} g_2^2 \left|H_u^+ H_d^{0\star} + H_u^0 H_d^{-\star}\right|^2 \\ & + m_S^2 |S|^2 + \left[\lambda A_\lambda\left(H_u^+ H_d^- - H_u^0 H_d^0\right) S + \frac{1}{3}\kappa A_\kappa S^3 + \text{h.c.}\right]. \end{aligned} \tag{3.8}$$

The neutral physical Higgs states are defined through the relations

$$H_u^0 = v_u + \frac{1}{\sqrt{2}}\left(H_{uR} + i H_{uI}\right), \qquad H_d^0 = v_d + \frac{1}{\sqrt{2}}\left(H_{dR} + i H_{dI}\right),$$

$$S = s + \frac{1}{\sqrt{2}}\left(S_R + i S_I\right), \tag{3.9}$$

where v_u, v_d and s are, respectively, the real vevs of H_u, H_d and S, which have to be obtained from the minima of the scalar potential (3.8), after expanding the fields using Eq. (3.9). We notice that when S acquires a vev, a term $\mu_{\rm eff}\widehat{H}_u \cdot \widehat{H}_d$ appears in the superpotential, with

$$\mu_{\rm eff} = \lambda s, \tag{3.10}$$

solving the μ-problem.

Therefore, the Higgs sector of the NMSSM is characterized by the seven parameters λ, κ, $m^2_{H_u}$, $m^2_{H_d}$, m^2_S, A_λ and A_κ. One can express the three soft masses by the three vevs using the minimization equations of the Higgs potential (3.8), which are given by

$$\begin{aligned} v_u\left[m^2_{H_u} + \mu^2_{\rm eff} + \lambda^2 v_d^2 + \frac{1}{2}g^2\left(v_u^2 - v_d^2\right)\right] - v_d\mu_{\rm eff}(A_\lambda + \kappa s) = 0 \\ v_d\left[m^2_{H_d} + \mu^2_{\rm eff} + \lambda^2 v_u^2 + \frac{1}{2}g^2\left(v_d^2 - v_u^2\right)\right] - v_u\mu_{\rm eff}(A_\lambda + \kappa s) = 0 \\ s\left[m^2_S + \kappa A_\kappa s + 2\kappa^2\sigma^2 + \lambda^2\left(v_u^2 + v_d^2\right) - 2\lambda\kappa v_u v_d\right] - \lambda A_\lambda v_u v_d = 0, \end{aligned} \tag{3.11}$$

where we have defined

$$g^2 \equiv \frac{1}{2}\left(g_1^2 + g_2^2\right). \tag{3.12}$$

One can also define the β angle by

$$\tan\beta = \frac{v_u}{v_d}. \tag{3.13}$$

The Z boson mass is given by $M_Z = gv$ with $v^2 = v_u^2 + v_d^2 \simeq (174\,\text{GeV})^2$. Hence, with M_Z given, the set of parameters that describes the Higgs sector of the NMSSM can be chosen to be the following

$$\lambda, \quad \kappa, \quad A_\lambda, \quad A_\kappa, \quad \tan b \quad \text{and} \quad \mu_{\rm eff}. \tag{3.14}$$

CP-even Higgs masses

One can obtain the Higgs mass matrices at tree level by expanding the Higgs potential (3.8) around the vevs, using Eq. (3.9). We begin by writing[3] the squared mass matrix $\mathcal{M}_S^2$ of the scalar Higgses in the basis (H_{dR}, H_{uR}, S_R):

$$\mathcal{M}_S^2 = \begin{pmatrix} g^2 v_d^2 + \mu\tan\beta B_{\rm eff} & (2\lambda^2 - g^2)\, v_u v_d - \mu B_{\rm eff} & 2\lambda\mu v_d - \lambda\left(A_\lambda + 2\kappa s\right) v_u \\ & g^2 v_u^2 + \frac{\mu}{\tan\beta} B_{\rm eff} & 2\lambda\mu v_u - \lambda\left(A_\lambda + 2\kappa s\right) v_d \\ & & \lambda A_\lambda \frac{v_u v_d}{s} + \kappa A_\kappa s + (2\kappa s)^2 \end{pmatrix}, \tag{3.15}$$

where we have defined $B_{\rm eff} \equiv A_\lambda + \kappa s$ (it plays the role of the B parameter of the MSSM).

[3]For economy of space, we omit in this expression the subscript from $\mu_{\rm eff}$.

Although an analytical diagonalization of the above 3×3 mass matrix is lengthy, there is a crucial conclusion that comes from the approximate diagonalization of the upper 2×2 submatrix. If it is rotated by an angle β, one of its diagonal elements is $M_Z^2(\cos^2 2\beta + \frac{\lambda^2}{g^2}\sin^2 2\beta)$ which is an upper bound for its lightest eigenvalue. The first term is the same one as in the MSSM. The conclusion is that in the NMSSM the lightest CP-even Higgs can be heavier than the corresponding of the MSSM, as long as λ is large and $\tan\beta$ relatively small. Therefore, it is much easier to explain the observed mass of the SM-like Higgs. However, λ is bounded from above in order to avoid the appearance of the Landau pole below the GUT scale. Depending on the other free parameters, λ should obey $\lambda \lesssim 0.7$.

CP-odd Higgs masses

For the pseudoscalar case, the squared mass matrix in the basis (H_{dI}, H_{uI}, S_I) is

$$\mathcal{M}_P^2 = \begin{pmatrix} \mu_{\text{eff}}\,(A_\lambda + \kappa s)\tan\beta & \mu_{\text{eff}}\,(A_\lambda + \kappa s) & \lambda v_u\,(A_\lambda - 2\kappa s) \\ & \frac{\mu_{\text{eff}}}{\tan\beta}\,(A_\lambda + \kappa s) & \lambda v_d\,(A_\lambda - 2\kappa s) \\ & & \lambda\,(A_\lambda + 4\kappa s)\,\frac{v_u v_d}{s} - 3\kappa A_\kappa s \end{pmatrix}. \quad (3.16)$$

One eigenstate of this matrix corresponds to an unphysical massless Goldstone boson G. In order to drop the Goldstone boson, we write the matrix in the basis (A, G, S_I) by rotating the upper 2×2 submatrix by an angle β. After dropping the massless mode, the 2×2 squared mass matrix turns out to be

$$\mathcal{M}_P^2 = \begin{pmatrix} \frac{2\mu_{\text{eff}}}{\sin 2\beta}\,(A_\lambda + \kappa s) & \lambda\,(A_\lambda - 2\kappa s)\,v \\ & \lambda\,(A_\lambda + 4\kappa s)\,\frac{v_u v_d}{s} - 3A_\kappa s \end{pmatrix}. \quad (3.17)$$

Charged Higgs mass

The charged Higgs squared mass matrix is given, in the basis $(H_u^+, H_d^{-\star})$, by

$$\mathcal{M}_\pm^2 = \left[\mu_{\text{eff}}\,(A_\lambda + \kappa s) + v_u v_d\left(\frac{1}{2}g_2^2 - \lambda\right)\right]\begin{pmatrix} \cot\beta & 1 \\ 1 & \tan\beta \end{pmatrix}, \quad (3.18)$$

which contains one Goldstone boson and one physical mass eigenstate $H^\pm$ with eigenvalue

$$m_\pm^2 = \frac{2\mu_{\text{eff}}}{\sin 2\beta}\,(A_\lambda + \kappa s) + v^2\left(\frac{1}{2}g_2^2 - \lambda\right). \quad (3.19)$$

3.2.2 Sfermion sector

The mass matrix for the up-type squarks is given in the basis $(\widetilde{u}_R, \widetilde{u}_L)$ by

$$\mathcal{M}_u = \begin{pmatrix} m_u^2 + h_u^2 v_u^2 - \frac{1}{3}\,(v_u^2 - v_d^2)\,g_1^2 & h_u\,(A_u v_u - \mu_{\text{eff}} v_d) \\ h_u\,(A_u v_u - \mu_{\text{eff}} v_d) & m_Q^2 + h_u^2 v_u^2 + \frac{1}{12}\,(v_u^2 - v_d^2)\,(g_1^2 - 3g_2^2) \end{pmatrix}, \quad (3.20)$$

whereas for down-type squarks the mass matrix reads in the basis $(\widetilde{d}_R, \widetilde{d}_L)$

$$\mathcal{M}_d = \begin{pmatrix} m_d^2 + h_d^2 v_d^2 - \frac{1}{6}\left(v_u^2 - v_d^2\right) g_1^2 & h_d\left(A_d v_d - \mu_{\text{eff}} v_u\right) \\ h_d\left(A_d v_d - \mu_{\text{eff}} v_u\right) & m_Q^2 + h_d^2 v_d^2 + \frac{1}{12}\left(v_u^2 - v_d^2\right)\left(g_1^2 - 3g_2^2\right) \end{pmatrix}. \quad (3.21)$$

The off-diagonal terms are proportional to the Yukawa coupling h_u for the up-type squarks and h_d for the down-type ones. Therefore, the two lightest generations remain approximately unmixed. For the third generation, the mass matrices are diagonalized by a rotation by an angle θ_T and θ_B, respectively, for the stop and sbottom. The mass eigenstates are, then, given by

$$\widetilde{t}_1 = \cos\theta_T \widetilde{t}_L + \sin\theta_T \widetilde{t}_R, \qquad \widetilde{t}_2 = \cos\theta_T \widetilde{t}_L - \sin\theta_T \widetilde{t}_R, \quad (3.22)$$

$$\widetilde{b}_1 = \cos\theta_B \widetilde{b}_L + \sin\theta_B \widetilde{b}_R, \qquad \widetilde{b}_2 = \cos\theta_B \widetilde{b}_L - \sin\theta_B \widetilde{b}_R. \quad (3.23)$$

In the slepton sector, for a similar reason, only the left- and right-handed staus are mixed and their mass matrix

$$\mathcal{M}_\tau = \begin{pmatrix} m_{E_3}^2 + h_\tau^2 v_d^2 - \frac{1}{2}\left(v_u^2 - v_d^2\right) g_1^2 & h_\tau\left(A_\tau v_d - \mu_{\text{eff}} v_u\right) \\ h_\tau\left(A_\tau v_d - \mu_{\text{eff}} v_u\right) & m_{L_3}^2 + h_\tau^2 v_d^2 - \frac{1}{4}\left(v_u^2 - v_d^2\right)\left(g_1^2 - g_2^2\right) \end{pmatrix} \quad (3.24)$$

is diagonalized after a rotation by an angle θ_τ. Their mass eigenstates are given by

$$\widetilde{\tau}_1 = \cos\theta_\tau \widetilde{\tau}_L + \sin\theta_\tau \widetilde{\tau}_R, \qquad \widetilde{\tau}_2 = \cos\theta_\tau \widetilde{\tau}_L - \sin\theta_\tau \widetilde{\tau}_R. \quad (3.25)$$

Finally, the sneutrino masses are

$$m_{\widetilde{\nu}} = m_L^2 - \frac{1}{4}\left(v_u^2 - v_d^2\right)\left(g_1^2 + g_2^2\right). \quad (3.26)$$

3.2.3 Gaugino and higgsino sector

The gauginos λ_1 and λ_2^3 mix with the neutral higgsinos ψ_d^0, ψ_u^0 and ψ_S to form neutral particles, the *neutralinos*. The 5×5 mass matrix of the neutralinos is written in the basis

$$(-i\lambda_1, -i\lambda_2^3, \psi_d^0, \psi_u^0, \psi_S) \equiv (\widetilde{B}, \widetilde{W}, \widetilde{H}_d^0, \widetilde{H}_u^0, \widetilde{S}) \quad (3.27)$$

as

$$\mathcal{M}^0 = \begin{pmatrix} M_1 & 0 & -\frac{1}{\sqrt{2}} g_1 v_d & \frac{1}{\sqrt{2}} g_1 v_u & 0 \\ & M_2 & \frac{1}{\sqrt{2}} g_2 v_d & -\frac{1}{\sqrt{2}} g_2 v_u & 0 \\ & & 0 & -\mu_{\text{eff}} & -\lambda v_u \\ & & & 0 & -\lambda v_d \\ & & & & 2\kappa s \end{pmatrix}. \quad (3.28)$$

The mass matrix (3.28) is diagonalized by an orthogonal matrix N_{ij}. The mass eigenstates of the neutralinos are usually denoted by χ_i^0, with $i = 1, \ldots, 5$, with increasing masses ($i = 1$ corresponds to the lightest neutralino). These are given by

$$\chi_i^0 = N_{i1}\widetilde{B} + N_{i2}\widetilde{W} + N_{i3}\widetilde{H}_d^0 + N_{i4}\widetilde{H}_u^0 + N_{i5}\widetilde{S}. \quad (3.29)$$

We use the convention of a real matrix N_{ij}, so that the physical masses $m_{\chi_i^0}$ are real, but not necessarily positive.

In the charged sector, the $SU(2)_L$ charged gauginos $\lambda^- = \frac{1}{\sqrt{2}}(\lambda_2^1 + i\lambda_2^2)$, $\lambda^+ = \frac{1}{\sqrt{2}}(\lambda_2^1 - i\lambda_2^2)$ mix with the charged higgsinos ψ_d^- and ψ_u^+, forming the charginos $\psi^\pm$:

$$\psi^\pm = \begin{pmatrix} -i\lambda^\pm \\ \psi_u^\pm \end{pmatrix}. \tag{3.30}$$

The chargino mass matrix in the basis (ψ^-, ψ^+) is

$$\mathcal{M}^\pm = \begin{pmatrix} M_2 & g_2 v_u \\ g_2 v_d & \mu_{\text{eff}} \end{pmatrix}. \tag{3.31}$$

Since it is not symmetric, the diagonalization requires different rotations of ψ^- and ψ^+. We denote these rotations by U and V, respectively, so that the mass eigenstates are obtained by

$$\chi^- = U\psi^-, \qquad \chi^+ = V\psi^+. \tag{3.32}$$

3.3 DM Candidates in the NMSSM

Let us first review the characteristics that a DM candidate particle should have. First, it should be massive in order to account for the missing mass in the galaxies. Second, it must be electrically and color neutral. Otherwise, it would have condensed with baryonic matter, forming anomalous heavy isotopes. Such isotopes are absent in nature. Finally, it should be stable and interact only weakly, in order to fit the observed relic density.

In the NMSSM there are two possible candidates. Both can be stable particles if they are the LSPs of the supersymmetric spectrum. The first one is the sneutrino (see [148,149] for early discussions on MSSM sneutrino LSP). However, although sneutrinos are WIMPs, their large coupling to the Z bosons result in a too large annihilation cross section. Hence, if they were the DM particles, their relic density would have been very small compared to the observed value. Exceptions are very massive sneutrinos, heavier than about 5 TeV [150]. Furthermore, the same coupling result in a large scattering cross section off the nuclei of the detectors. Therefore, sneutrinos are also excluded by direct detection experiments.

The other possibility is the lightest neutralino. Neutralinos fulfill successfully, at least in principle, all the requirements for a DM candidate. However, the resulting relic density, although weakly interacting, may vary over many orders of magnitude as a function of the free parameters of the theory. In the next sections we will investigate further the properties of the lightest neutralino as the DM particle. We begin by studying its annihilation that determines the DM relic density.

3.4 Neutralino relic density

We remind that the neutralinos are mixed states composed of bino, wino, higgsinos and the singlino. The exact content of the lightest neutralino determines its pair annihilation channels and, therefore, its relic density (for detailed analyses, we refer to [151–154]). Subsequently, we will briefly describe the neutralino pair annihilation in various scenarios. We classify these scenarios with respect to the lightest neutralino content.

Before we proceed, we should mention another mechanism that affects the neutralino LSP relic density. If there is a supersymmetric particle with mass close to the LSP (but always larger), it would be abundant during the freeze-out and LSP coannihilations with this particle would contribute to the total annihilation cross section. This particle, which is the Next-to-Lightest Supersymmetric Particle (NLSP), is most commonly a stau or a stop. In the above sense, coannihilations refer not only to the LSP–NLSP coannihilations, but also to the NLSP–NLSP annihilations, since the latter reduce the number density of the NLSPs [155].

- Bino-like LSP
  In principle, if the lightest neutralino is mostly bino-like, the total annihilation cross section is expected to be small. Therefore, a bino-like neutralino LSP would have been overabundant. The reason for this is that there is only one available annihilation channel via t-channel sfermion exchange, since all couplings to gauge bosons require a higgsino component. The cross section is even more reduced when the sfermion mass is large.

  However, there are still two ways to achieve the correct relic density. The first one is using the coannihilation effect: if there is a sfermion with a mass slightly larger (some GeV) than the LSP mass, their coannihilations can be proved to reduce efficiently the relic density to the desired value. The second one concerns a bino-like LSP, with a very small but non-negligible higgsino component. In this case, if in addition the lightest CP-odd Higgs A_1 is light enough, the annihilation to a pair A_1A_1 (through an s-channel CP-even Higgs H_i exchange) can be enhanced via H_i resonances. In this scenario a fine-tuning of the masses is necessary.

- Higgsino-like LSP
  A mostly higgsino LSP is as well problematic. The strong couplings of the higgsinos to the gauge bosons lead to very large annihilation cross section. Therefore, a possible higgsino LSP would have a very small relic density.

- Mixed bino–higgsino LSP
  In this case, as it was probably expected, one can easily fit the relic density to the observed value. This kind of LSP annihilates to W^+W^-, ZZ, $W^\pm H^\mp$, ZH_i, H_iA_j, $b\bar{b}$ and $\tau^+\tau^-$ through s-channel Z or Higgs boson exchange or t-channel neutralino or chargino exchange. The last two channels are the dominant ones when the Higgs coupling to down-type fermions is enhanced, which occurs more commonly in the regime of relatively large $\tan\beta$. The annihilation channel to a

pair of top quarks also contributes to the total cross section, if it is kinematically allowed. However, in order to achieve the correct relic density, the higgsino component cannot be very large.

- Singlino-like LSP
  Since a mostly singlino LSP has small couplings to SM particles, the resulting relic density is expected to be large. However, there are some annihilation channels that can be enhanced in order to reduce the relic density. These include the s-channel (scalar or pseudoscalar) Higgs exchange and the t-channel neutralino exchange.

  For the former, any Higgs with sufficient large singlet component gives an important contribution to the cross section, increasing with the parameter κ (since the singlino-singlino-singlet coupling is proportional to κ). Concerning the latter annihilation, in order to enhance it, one needs large values of the parameter λ. In this case, the neutralino-neutralino-singlet coupling, which is proportional to λ, is large and the annihilation proceeds giving a pair of scalar H_sH_s or a pair of pseudoscalar A_sA_s singlet like Higgs.

  As in the case of bino-like LSP, one can also use the effect of s-channel resonances or coannihilations. In the latter case, an efficient NLSP can be the neutralino χ_2^0 or the lightest stau $\widetilde{\tau}_1$. In the case that the neutralino NLSP is higgsino-like, the LSP-NLSP coannihilation through a (doublet-like) Higgs exchange can be proved very efficient. A stau NLSP reduces the relic density through NLSP-NLSP annihilations, which is the only possibility in the case that both parameters κ and λ are small. We refer to [156,157] for further discussion on this possibility.

Assuming universality conditions the wino mass M_2 has to be larger than the bino mass M_1 ($M_2 \sim 2M_1$). This is the reason that we have not considered a wino-like LSP.

3.5 Detection of neutralino DM

3.5.1 Direct detection

Since neutralinos are Majorana fermions, the effective Lagrangian describing their elastic scattering with a quark in a nucleon can be written, in the Dirac fermion notation, as [158]

$$\mathcal{L}_{\text{eff}} = a_i^{SI}\bar{\chi}_1^0\chi_1^0\bar{q}_iq_i + a_i^{SD}\bar{\chi}_1^0\gamma_5\gamma_\mu\chi_1^0\bar{q}_i\gamma_5\gamma^\mu q_i, \tag{3.33}$$

with $i = u, d$ corresponding to up- and down-type quarks, respectively. The Lagrangian has to be understood as summing over the quark generations.

In this expression, we have omitted terms containing the operator $\bar{\psi}\gamma_5\psi$ or a combination of $\bar{\psi}\gamma_5\gamma_\mu\psi$ and $\bar{\psi}\gamma_\mu\psi$ (with $\psi = \chi, q$). This is a well qualified assumption: Due to the small velocity of WIMPs, the momentum transfer $\vec{q}$ is very small compared

to the reduced mass of the WIMP-nucleus system. In the extreme limit of zero momentum transfer, the above operators vanish[4]. Hence, we are left with the Lagrangian (3.33) consisting of two terms, the first one corresponding to spin-independent (SI) interactions and the second to spin-dependent (SD) ones. In the following, we will focus again only to SI scattering, since the detector sensitivity to SD scattering is low, as it has been already mentioned in Sec. 1.5.1.

The SI cross section for the neutralino-nucleus scattering can be written as [158] (see, also, [159])

$$\sigma_{\rm tot}^{SI} = \frac{4m_r^2}{\pi}\left[Zf_p + (A-Z)f_n\right]^2. \tag{3.34}$$

m_r is the neutralino-nucleus reduced mass $m_r = \frac{m_\chi m_N}{m_\chi + m_N}$, and Z, A are the atomic and the nucleon number, respectively. It is more common, however, to use an expression for the cross section normalized to the nucleon. In this case, on has for the neutralino-proton scattering

$$\sigma_p^{SI} = \frac{4}{\pi}\left(\frac{m_p m_{\chi_1^0}}{m_p + m_{\chi_1^0}}\right)^2 f_p^2 \simeq \frac{4m_{\chi_1^0}^2}{\pi} f_p^2, \tag{3.35}$$

with a similar expression for the neutron.

The form factor f_p is related to the couplings a to quarks through the expression (omitting the "SI" superscripts)

$$\frac{f_p}{m_p} = \sum_{q=u,d,s} f_{Tq}^p \frac{a_q}{m_q} + \frac{2}{27} f_{TG} \sum_{q=c,b,t} \frac{a_q}{m_q}. \tag{3.36}$$

A similar expression may be obtained for the neutron form factor f_n, by the replacement $p \to n$ in the previous expression (henceforth, we focus to neutralino-proton scattering). The parameters f_{Tq} are defined by the quark mass matrix elements

$$\langle p|\, m_q \bar{q} q\, |p\rangle = m_p f_{Tq}, \tag{3.37}$$

which corresponds to the contribution of the quark q to the proton mass and the parameter f_{TG} is related to them by

$$f_{TG} = 1 - \sum_{q=u,d,s} f_{Tq}. \tag{3.38}$$

The above parameters can be obtained by the following quantities

$$\sigma_{\pi N} = \frac{1}{2}(m_u + m_d)(B_u + B_d) \qquad \text{and} \qquad \sigma_0 = \frac{1}{2}(m_u + m_d)(B_u + B_d - 2B_s,) \tag{3.39}$$

with $B_q = \langle N|\, \bar{q} q\, |N\rangle$, which are obtained by chiral perturbation theory [160] or by lattice simulations. Unfortunately, the uncertainties on the values of these quantities are large (see [161], for more recent values and error bars).

[4]While there are possible circumstances in which the operators of (3.33) are also suppressed and, therefore, comparable to the operators omitted, they are not phenomenologically interesting.

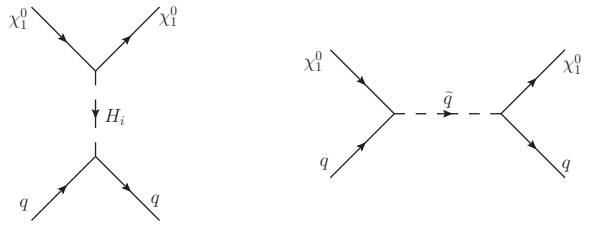

Figure 3.1: Feynman diagrams contributing to the elastic neutralino-quark scalar scattering amplitude at tree level.

The SI neutralino-nucleon interactions arise from t-channel Higgs exchange and s-channel squark exchange at tree level (see Fig. 3.1), with one-loop contributions from neutralino-gluon interactions. In practice, the s-channel Higgs exchange contribution to the scattering amplitude dominates, especially due to the large masses of squarks. In this case, the effective couplings a are given by

$$a_d^{SI} = \sum_{i=1}^{3} \frac{1}{m_{H_i}^2} C_i^1 C_{\chi_1^0\chi_1^0 H_i}, \qquad a_u^{SI} = \sum_{i=1}^{3} \frac{1}{m_{H_i}^2} C_i^2 C_{\chi_1^0\chi_1^0 H_i}. \tag{3.40}$$

C_i^1 and C_i^2 are the Higgs H_i couplings to down- and up-type quarks, respectively, given by

$$C_i^1 = \frac{g_2 m_d}{2 M_W \cos\beta} S_{i1}, \qquad C_i^2 = \frac{g_2 m_u}{2 M_W \sin\beta} S_{i2}, \tag{3.41}$$

with S the mixing matrix of the CP-even Higgs mass eigenstates and m_d, m_u the corresponding quark mass. We see from Eqs. (3.36) and (3.41) that the final cross section (3.35) is independent of each quark mass. We write for completeness the neutralino-neutralino-Higgs coupling $C_{\chi_1^0\chi_1^0 H_i}$:

$$\begin{aligned} C_{\chi_1^0\chi_1^0 H_i} = {} & \sqrt{2}\lambda \left(S_{i1}N_{14}N_{15} + S_{i2}N_{13}N_{15} + S_{i3}N_{13}N_{14}\right) - \sqrt{2}\kappa S_{i3}N_{15}^2 \\ & + g_1 \left(S_{i1}N_{11}N_{13} - S_{i2}N_{11}N_{14}\right) - g_2 \left(S_{i1}N_{12}N_{13} - S_{i2}N_{12}N_{14}\right), \end{aligned} \tag{3.42}$$

with N the neutralino mixing matrix given in (3.29).

The resulting cross section is proportional to $m_{H_i}^{-4}$. In the NMSSM, it is possible for the lightest scalar Higgs eigenstate to be quite light, evading detection due to its singlet nature. This scenario can give rise to large values of SI scattering cross section, provided that the doublet components of the lightest Higgs are not negligible. These scenarios have been examined in the context of explaining the CoGeNT signal [162,163]. For general discussions about NMSSM neutralino direct detection, see [164–167].

3.5.2 Indirect detection

The indirect signals of the NMSSM neutralino come from its pair annihilation via the processes described in Sec. 3.4 for the various scenarios of the neutralino content.

However, since the DM particles move today very slowly, the average of cross section times velocity is expected to differ from this in the early Universe. For example, annihilations through an s-channel CP-even Higgs exchange are generally p-wave, and their contribution to indirect signals is expected to be suppressed.

Neutralino DM in the NMSSM has been used to explain the PAMELA excess on positrons (see Sec. 1.6 and Fig. 1.8), with an anti-proton flux consistent with the astrophysical background [168–170]: If the CP-odd Higgs A_1 is very light, a neutralino (with, e.g., a mass of $\sim 160\,\mathrm{GeV}$) can annihilate to pairs of A_1 and H_1 through A_2 exchange. Due to the very low mass of A_1, it can only decay into a pair of leptons, while H_1 dominantly decays into a pair of A_1.

Another characteristic process in the NMSSM is the neutralino annihilation through an s-channel CP-odd Higgs exchange, giving rise at one loop level to monochromatic photons. In the NMSSM, the exchanged pseudoscalar can be dominantly singlet-like, so that, even though the annihilation at one loop level may proceed with large cross section, the tree-level annihilation is suppressed leading to neutralino relic density that can still fit the observed value. More details will be given in the following chapter.

3.6 Neutrino masses and more DM candidates

Although the NMSSM is a quite complete particle physics theory and, at least, so far, no phenomenological inconsistency appeared, in its vanilla form it does not provide masses for neutrinos. However, the observed neutrino oscillations imply that neutrinos have non-zero, although very small, masses. It is not difficult to incorporate neutrino masses in the NMSSM, nonetheless the possible mechanisms are numerous and many of them equally well motivated; hence, more experimental results are required in order to choose one of them. In the following, we review basic neutrino physics and the experimental status. Subsequently, we will see some of the mechanisms that can provide the predicted masses and the new DM possibilities that arise from them.

Since the end of 1990s, neutrino oscillations [171] – transitions between the different flavors of neutrinos or antineutrinos – have been verified through many experiments. First, LSND indicated $\nu_\mu \leftrightarrow \nu_e$ and $\bar{\nu}_\mu \leftrightarrow \bar{\nu}_e$ oscillations from their accelerator neutrino experiment [172], confirming the preexisting evidence of oscillations from solar neutrino experiments [173–176]. Super-Kamiokande followed, reporting a strong evidence for neutrino oscillations in their atmospheric neutrino data [177]. Nowadays, the existence of oscillations of the solar electron neutrinos, ν_e, atmospheric muon neutrinos and antineutrinos, ν_μ and $\bar{\nu}_\mu$, accelerator ν_μ and reactor $\bar{\nu}_e$ has been firmly established (for some recent results, see [178–182]).

Neutrino oscillations suggest that the neutrino weak (flavor) eigenstates (which are produced in the reactor experiments, the Sun and so on) do not coincide with the mass eigenstates. This fact implies that neutrinos should have non-zero masses. The transition probability from one state i to one other j depends on the mass squared difference $\Delta m^2_{ij} \equiv m^2_i - m^2_j$ of the two states and it is zero for degenerate states.

The neutrino mass eigenstates ν_i (with $i = 1, 2, 3$) are related to the flavor eigen-

states ν_l (with $l = e,\, \mu,\, \tau$) through the neutrino mixing matrix U:

$$|\nu_l\rangle = \sum_{i=1}^{3} U_{li}^{\star}\, |\nu_i\rangle\,, \tag{3.43}$$

in an analogous way to the quark mixing via the CKM matrix (see Sec. 2.1.2, Eq. (2.13)). This relation implies that individual lepton charges L_e, L_μ and L_τ are not conserved. The unitary mixing matrix U is called *Pontecorvo-Maki-Nakagawa-Sakata* (PMNS) *matrix* and, in general, can be parametrized by three Euler angles θ_{12}, θ_{23} and θ_{13} and 6 phases. In the case neutrinos are Dirac particles, only one phase is physical, which can induce CP violation in the lepton sector, in a similar way to CP-violation in the quark sector. In the case of Majorana neutrinos, two more phases are physical. The mixing matrix for the Majorana case is usually written in terms of the Dirac mixing matrix as $U_{Maj} = U_{Dir} \cdot P$, with $P = \mathrm{diag}(1,\, \mathrm{e}^{i\delta_1/2},\, \mathrm{e}^{i\delta_2/2})$, with δ_1 and δ_2 the Majorana phases. (For the standard parametrization of the PMNS matrix, see [100].)

The unitarity of the PMNS matrix implies that $\sum_{l'=e,\mu,\tau} P(\nu_l \leftrightarrow \nu_{l'}) = 1$, with $P(\nu_l \leftrightarrow \nu_{l'})$ the transition probability and $l' = e,\, \mu,\, \tau$. Since the transition probability is directly related to the mass squared differences Δm_{ij}^2, only two out of the three of Δm_{ij}^2 are independent, usually taken to be Δm_{21}^2 and Δm_{31}^2. It follows from the neutrino oscillation data that the absolute value of one of them is much smaller than the absolute value of the other:

$$\begin{aligned} \left|\Delta m_{21}^2\right| &\simeq 7.6 \cdot 10^{-5}\,\mathrm{eV}^2, \\ \left|\Delta m_{31}^2\right| &\simeq 2.4 \cdot 10^{-3}\,\mathrm{eV}^2. \end{aligned} \tag{3.44}$$

We see that the two first mass eigenstates have similar masses, whereas the third one might have either much larger mass, a case which is referred as *normal hierarchy*, or much smaller, corresponding to *inverted hierarchy*. One can identify Δm_{21}^2 and θ_{12} as the mass squared difference and mixing angle, respectively, responsible for the solar ν_e oscillations (with the corresponding notation $\Delta m_{21}^2 \equiv \Delta m_{\odot}^2$ and $\theta_{12} \equiv \theta_{\odot}$) and Δm_{31}^2 and θ_{23} as those associated with the atmospheric oscillations ($\Delta m_{31}^2 \equiv \Delta m_{atm}^2$ and $\theta_{23} \equiv \theta_{atm}$). The solar and atmospheric angles are relatively large, whereas the third angle θ_{13} is small but not zero.

Many mechanisms can provide masses to neutrinos (see, e.g., [183,184] for reviews). The simplest way is the introduction of a right chiral state whose Yukawa coupling with the neutrino doublet and the Higgs generates a Dirac mass term through the Higgs mechanism. However, the Yukawa coupling constant should be extremely small to explain the smallness of the neutrino masses, of the order of 10^{-12}. Such a small value is often regarded as unnatural.

The very small values for the Yukawa couplings may be avoided if neutrinos have Majorana masses. Although a Majorana mass term cannot be introduced in a gauge invariant way, it is possible to be induced by higher order non-renormalizable operators. For example, the operator [185]

$$\lambda L \cdot H_u L \cdot H_u \tag{3.45}$$

would give rise to a Majorana mass for neutrinos of the order $\sim \lambda\langle\Phi\rangle^2$.

In case the strength λ of the operator (3.45) is suppressed by a large scale M, the induced Majorana mass $\frac{\lambda_0}{M}\langle\Phi\rangle^2$ (with λ_0 a dimensionless parameter) can be sufficiently small, for large enough scale M. This is the case of the seesaw mechanisms, which generate the operator (3.45) through the exchange of heavy states. The heavy states can be singlet fermions [186, 187] (Type-I seesaw), triplet scalars [188, 189] (Type-II seesaw) or triplet fermions [190] (Type-III seesaw). The seesaw mechanisms have an attractive feature: the decays of the heavy states (heavy sterile neutrinos) in the early Universe could, in principle, generate a lepton asymmetry which subsequently led to the baryon asymmetry observed in the Universe. This scenario is called *leptogenesis* (see [191] for a review).

Instead of suppressing the strength λ by a large scale, it is possible to introduce new physics, accessible at the TeV scale, that suppresses the strength by small lepton number violating parameters. These are "naturally" small in the 't Hooft sense, since their small values enhance the lepton symmetry. An example of this mechanism is the *inverse seesaw mechanism* [192]. In this model, two additional singlet leptons with opposite lepton numbers are introduced for each generation. One of them is usually identified as the charge conjugate of the right-handed neutrino. The small (Majorana) mass term of the other one violates the lepton number conservation and is responsible for the smallness of the neutrino masses.

Many other mechanisms are possible. For example, one may have a linear seesaw mechanism [193] where the lepton number violation comes from a mass term induced by the Yukawa coupling of the right-handed neutrino and the extra singlet lepton, or radiative models [194, 195] where the neutrino masses are induced by radiative corrections. One more possibility in a supersymmetric framework is that neutrino masses are induced by higher order operators responsible for the SUSY breaking [196]. Neutrino masses are also present in supersymmetric models with lepton number violation through terms that do not respect the R-parity. However, these models do not provide a stable particle that can account for the DM (for a long-lived DM candidate in an R-parity violating version of the NMSSM, see [197]).

So far, there is no well motivated reason to prefer a specific model in favor of others. The observation of a neutrinoless double beta decay could provide evidence for Majorana neutrinos, since in case of neutrinos with only Dirac masses the double beta decay always gives neutrinos among the final states. Unfortunately, current experiments are not yet able to conclude about the nature of neutrinos.

Although the exact mechanism of neutrino mass generation is unknown, most of them incorporate additional singlet fields. Let us consider the inverse seesaw scenario. The additional terms in the NMSSM superpotential, required to give masses to neutrinos through this mechanism, would be

$$W_{ISS} \supset h_\nu \widehat{L}\cdot\widehat{H}_u\widehat{\nu}^c_R + \lambda_\nu \widehat{S}\widehat{N}\widehat{\nu}^c_R + \frac{1}{2}\kappa_N \widehat{S}\widehat{N}^2, \tag{3.46}$$

where two new chiral superfields (vectors in family space) have been introduced: the right-handed neutrino superfield $\widehat{\nu}^c_R$ (with lepton number -1) and one additional singlet

superfield $\widehat{N}$ (with lepton number +1). The smallness of the neutrino masses is due to the small value of the coupling κ_N of the last term, which violates explicitly the lepton number. The bosonic components of these fields mix with left-handed sneutrinos, forming sneutrino states with smaller couplings to gauge bosons. If the lightest of these states is the LSP, it is possible to be a viable DM candidate. The initial abundance of the lightest sneutrino may be reduced to the observed value through annihilation processes induced by a (in principle, small) doublet component. In the same way, the direct detection cross section is suppressed by the singlet component. Various mechanisms lead to different DM phenomenology. For a comparative study, see [198]. The sneutrino DM of NMSSM-like models has been studied in [199–204], whereas some important analyses of sneutrino DM in MSSM extensions include [205–209].

In Ch. 6 we will motivate another neutrino mass generation mechanism by the requirement of a DM whose density was determined by its asymmetry. However, until then, we leave aside the sneutrino DM and we focus on the NMSSM neutralino DM.

CHAPTER 4

A POSSIBLE INDIRECT INDICATION FOR DARK MATTER

Recent analyses of the publicly available data from Fermi-LAT [210–213] have discovered hints for a gamma (γ) line, at energy $E_\gamma \sim 130\,\mathrm{GeV}$, in the form of an excess of about $3-4$ standard deviations, assuming that the background flux can be approximated by a single power law. An interpretation of this excess as DM pair annihilation into a pair of photons would require a partial annihilation cross section of about $10^{-27}\,\mathrm{cm}^3\,\mathrm{s}^{-1}$ [211, 212]. However, more general parametrizations of the background flux [214,215] reduce the significance of the excess, making it compatible with a diffuse background possibly of instrumental or astrophysical origin.

Following the publication [211], different types of models trying to explain this excess have been proposed: models with an extra $U(1)'$ gauge symmetry where the DM couples only to the extra Z' gauge boson, and the Z' to photons via a Chern-Simons term [216]; models with an extra singlet and extra charged fields allowing for an enhanced branching ratio of the SM-like Higgs boson into two photons [217]; extensions of the MSSM by right-handed neutrinos and extra Higgs doublets (with a right-handed sneutrino as DM) [218]; decaying DM in the MSSM extended by additional fields and couplings [219]; extensions of the SM or the MSSM by singlets with Peccei-Quinn symmetry where DM can annihilate into a photon pair via an axion in the s-channel [220]; a string/M-theory motivated version of the MSSM (with an unconventional spectrum involving very heavy scalar superpartners) where wino-like DM can annihilate into a photon plus a Z boson [221]. (In the MSSM with bino- or higgsino-like DM, the annihilation cross section into one or two photons would be too small [222–226].)

Before we discuss the particular monochromatic photon excess, we provide in the following section a general discussion of the photon radiation from DM annihilation and its detection. We continue in Sec. 4.2 by reviewing the propagation of photon flux from a distant point of emission in the DM halo to the point of observation. In Sec. 4.3 we present the characteristics of the 130 GeV photon line as they were established by [210, 211] and subsequent analyses. At the same time, the absence of

an excess in the diffuse photon radiation data leads to upper bounds that constrain the DM candidates. We present these bounds in Sec. 4.4. Sec. 4.5 is the main part of our work, based on [2]. There, we investigate the properties of the NMSSM which allow to describe a phenomenologically viable neutralino DM giving rise to the desired monochromatic line. Details of the Higgs and neutralino sectors are also presented for a typical benchmark point. We finish the chapter in Sec. 4.6, which is devoted to a short summary and conclusions.

4.1 Photon Radiation and Detection

The products of neutralino pair annihilations in the more condensed regions of the dark halo may produce secondary photons that can be detected as diffuse photon radiation. In some cases, if at least one photon is directly produced during the annihilation process, a distinctive line would appear at a specific energy [165, 222–242]. The possible detection of such rays, and additionally the fact that photons travel across the Universe to the location of detection without significantly interacting with the interstellar medium, has motivated the construction and operation of many ground-based or space-based telescopes and photon detectors. Actually, the detection of a monochromatic line is an almost clear evidence for DM, since it is quite unlikely for such a line to originate from an astrophysical source, at least for energies of the order of $\mathcal{O}(100)$ GeV or larger. While the characteristics of the diffuse radiation are essentially model independent, a possible detection of a monochromatic line might lead to the determination of the parameters of specific models. However, as we will see in the following section, a potentially observed signal depends strongly, not only on the free parameters of the particle physics model, but also, on the halo profile, the DM mass distribution across the galaxy.

There are several mechanisms related to DM annihilation that can give rise to photons. Each of them results in a specific photon spectrum. The main source of secondary photons is the neutral pion decay. Pions are produced after fragmentation and hadronization of the gauge bosons and quarks that are produced directly from the WIMP annihilation. This procedure will give a continuum of γ-rays, peaked at energies somewhat smaller than the DM mass. A similar spectrum appears also due to the bremsstrahlung of the charged particles that are produced directly from DM annihilation.

Two other phenomena may also contribute to the diffuse photon radiation. They are both related to charged leptons, which might be directly produced from the WIMP annihilation. The inverse Compton scattering of the charged leptons off the cosmic microwave background photons or off the starlight results in photons scattered to higher energy than the initial ones. This mechanism can lead to a continuum spectrum with energies that range from a fraction of the DM mass up to this mass itself. Moreover, if the charged leptons pass through a galactic region with high magnetic field, there would be a synchrotron emission of photons. The resulting spectrum depends strongly on the magnitude of the magnetic field. However, in most cases, these two mechanisms

are subdominant compared to the spectrum originating from pion decay.

In order that a distinctive line appears, at least one photon has to be produced directly during the DM annihilation. Since WIMPs are neutral particles, this may occur only through loop diagrams or, alternatively, through the emission of a photon from bremsstrahlung of an internal particle of the annihilation process. The latter, even though it is in principle a procedure with very small cross section surmounted by the continuum spectrum, can be enhanced under certain conditions. Concerning the former, the branching ratios of the loop processes are in general expected to be small since the cross sections are suppressed by the fourth power of the electromagnetic coupling constant. Nevertheless, it is possible in specific cases for the loop diagram cross section to be enhanced, as we will examine in detail in Sec. 4.5 for the NMSSM neutralino.

Since the possibility of photon detection related to DM was realized, many telescopes have been used for this purpose. Space-based telescopes on board of satellites are widely used for the indirect DM detection. The fact that they are located outside the atmosphere gives them the obvious advantage, among others, of the lack of distortion and diffusion of the radiation that occurs in the atmosphere. The most important telescopes among them are EGRET [243], which was able to detect photons in an energy range of 30 MeV to 30 GeV, and its successor, the Large Area Telescope (LAT) [244] on board of the Fermi satellite, with an extended range that reaches to about 300 GeV. The upper cutoff in the energy range comes from the limited photon collection area of the space-borne detectors. However, the energy range can be extended to higher energies using ground-based telescopes. Specifically, the Cherenkov telescopes essentially use the earth's atmosphere as detection medium, implying a photon collection area of hundreds of square meters. For example, H.E.S.S. can observe photons with energies up to tens of TeV (~ 50 TeV) and is completing Fermi-LAT to higher energies [245]. Other important current Cherenkov telescopes are VERITAS and MAGIC.

The targets of the telescopes aiming at DM searches are galactic regions where DM is more concentrated and/or regions where the photon background is low. The most DM rich area in our galaxy is the galactic center (GC) of the Milky Way [246], where there is also a strong evidence for a super-massive black hole. However, areas around the GC, such as the Galactic Ridge or the Galactic Center Halo, have additionally a reduced background and, as a consequence, they exhibit a better signal-to-noise ratio (SNR). Promising targets are also some satellite galaxies of the Milky Way that are believed to be DM dominated. These are dwarf spheroidal (dSph) galaxies, such as Carina, Draco, Segue 1, just to name a few. Even though the signal is much weaker than the signal from the aforementioned targets, the SNR is even more improved.

4.2 Photon Flux

In this section we are going to discuss the photon flux that arrives at a space- or ground-based telescope from DM annihilations in the galactic halo. Even though we

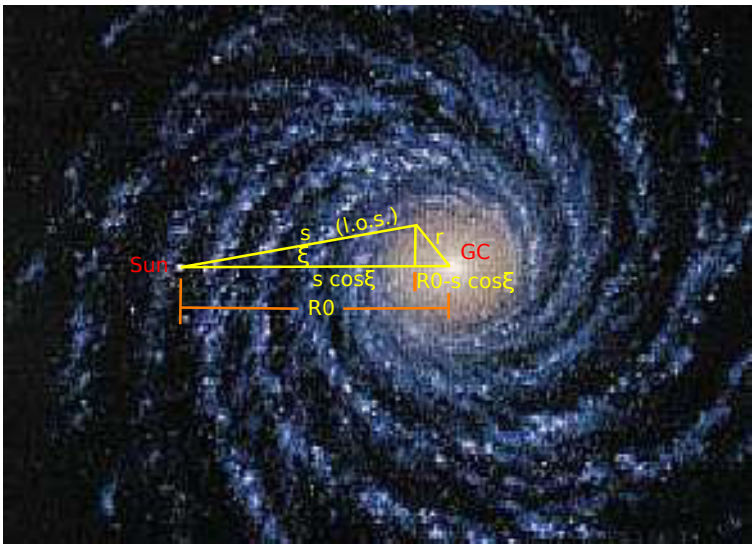

Figure 4.1: The Sun location in the Milky Way and a graphical representation of the photon flux.

will focus on the Milky Way GC, the same analysis applies essentially also to signals coming from other targets. We will, additionally, examine the way the DM distribution in the galactic halo affects the photon signals and we will calculate the flux for various halo profiles.

We assume that the line-of-sight ($l.o.s.$) of a telescope forms an angle ξ with the direction of the GC. The differential photon flux that arrives at the telescope from an annihilation occurring in the galactic halo at a distance r from the GC can be written as

$$\frac{\mathrm{d}\Phi_\gamma}{\mathrm{d}E_\gamma}(\xi) = \frac{N_\chi \langle\sigma v\rangle}{4\pi m_\chi^2} \frac{1}{\Delta\Omega} \int_{\Delta\Omega} \mathrm{d}\Omega \int_{l.o.s.} \mathrm{d}s\, \rho^2(r(s,\xi)), \tag{4.1}$$

where m_χ is the DM mass and the factor $N_\chi = 1$ for Majorana DM or $N_\chi = 1/2$ in case of Dirac DM. The last integral is calculated along the $l.o.s.$ and $\rho_{DM}(r)$ is the DM density at the location r. The distance r depends on the heliocentric distance s and the angle ξ. Specifically (see also Fig. 4.1),

$$r(s,\xi) = \sqrt{(R_0 - s\cos\xi)^2 + (s\sin\xi)^2}, \tag{4.2}$$

with $R_0 \simeq 8.5$ kpc the distance between the Sun and the GC. The exact dependence of the DM density on r is determined by the DM halo profile. Various numerical simulations favor different profiles. The flux is also averaged over the solid angle $\Delta\Omega$ of the detector.

The expression (4.1) can be separated into two distinct parts: one related to the particle physics model and one dependent only on astrophysics. The particle physics contribution to the flux is encoded in the fraction $\frac{N_\chi \langle\sigma v\rangle}{4\pi m_\chi^2}$. As usual, $\langle\sigma v\rangle$ is the average cross section of the DM annihilation times the relative velocity v of the DM particles.

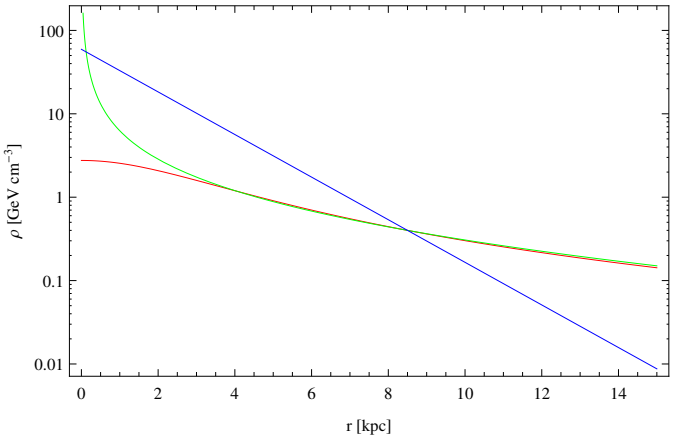

Figure 4.2: The DM density dependence on the distance from the GC for three halo profiles. The *red* curve corresponds to the cored isothermal profile, the *green* to NFW and the *blue* to the Einasto profile.

In the case of a monochromatic line this is the cross section of the loop induced annihilation to photons. For the continuum spectrum, it is the total cross section for the γ-rays production from all DM annihilations. The thermal average has to be calculated in the limit $v \to 0$, since the relative velocity of the DM particles at the present temperature of the Universe is low.

It is frequent in the literature to define the integral along the *l.o.s.* as [225]

$$J(\xi) \equiv \int_{l.o.s.} \mathrm{d}s \rho^2_{DM}(r). \tag{4.3}$$

Using Eq. (4.2), we can write this integral as

$$J(\xi) = \int_{s_-}^{s_+} \mathrm{d}s\, \rho^2_{DM}\left(\sqrt{s^2 + R_0^2 - 2sR_0\cos\xi}\right), \tag{4.4}$$

where the limits of integration are $s_\pm = R_0\cos\xi \pm \sqrt{r_t^2 - R_0^2\sin\xi}$ and r_t is the galactic tidal radius. Therefore, the astrophysical part of Eq. (4.1) can be written as

$$\langle J\rangle_{\Delta\Omega} \equiv \frac{1}{\Delta\Omega}\int_{\Delta\Omega} J(\xi)\mathrm{d}\Omega = \frac{2\pi}{\Delta\Omega}\int_0^{\theta_{max}} \mathrm{d}\theta\, \sin\theta J(\xi). \tag{4.5}$$

θ_{max} is the angle over which the average flux is calculated around the GC. The expression (4.5) is often denoted as J *factor*. Since the J factor is independent of the specific particle physics model, it is a quantity which can be used to characterize the various targets. In general, larger J factor means a better target.

In order to calculate the J factor, one has to choose a specific DM halo profile. Unfortunately, the current numerical simulations do not allow to discriminate the various halo profiles proposed in the literature, although, as we will see below, it seems

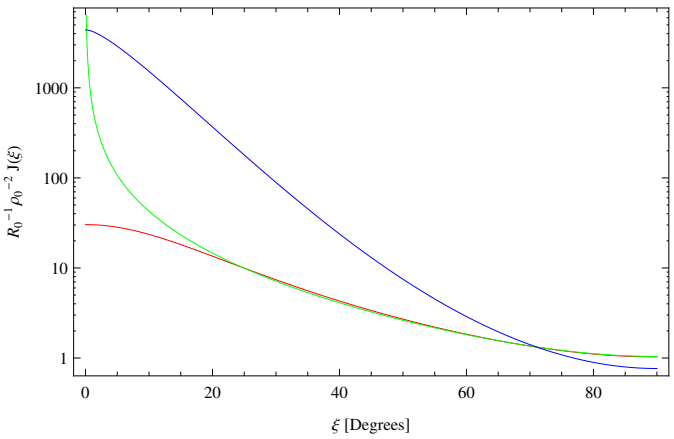

Figure 4.3: The dimensionless quantity $\frac{1}{R_0\rho_0^2}J(\xi)$ as a function of the angle ξ between the *l.o.s.* and the GC. The color code is the same as in Fig. 4.2.

that some of them exhibit a preference for specific profiles. Here, we will consider a number of different profiles before we examine the angular dependence of $J(\xi)$ on them.

A general radial halo profile can be parametrized as (*Hernquist profile*)

$$\rho(r) \propto \frac{1}{\left(\frac{r}{r_s}\right)^{\gamma}\left[1+\left(\frac{r}{r_s}\right)^{\alpha}\right]^{(\beta-\gamma)/\alpha}}. \tag{4.6}$$

The core radius r_s and, additionally, the free parameters α, β, γ define each specific profile. Specifically, the parameter α controls the sharpness of the transition from the inner slope. Profiles with small values of γ, which parametrize the profile's inner slope, are cored profiles, while cusped profiles are characterized by large values of γ. All the profiles have to be normalized to the local (at the position of the Sun) DM density $\rho_{DM}(R_0)$, which, as we have already seen, is usually assumed to take the value $\rho_0 \equiv \rho_{DM}(R_0) = 0.3\,\mathrm{GeV\,cm^{-3}} - 0.4\,\mathrm{GeV\ cm^{-3}}$.

There are many specific parametrizations of the general radial profile [247]. Here, we will show the most common examples. First, we consider for reference the cored isothermal profile. This is defined by $r_s = 3.5\,\mathrm{kpc}$ and $(\alpha, \beta, \gamma) = (2, 2, 0)$. The general Navarro-Frenk-White (henceforth NFW) profile [248] is defined by $r_s = 20\,\mathrm{kpc}$ and $\alpha = 1$, $\beta = 3$. The parameter γ remains free (it takes the value $\gamma = 1$ for the common NFW profile). The findings of Via Lactea II simulation [249] seem to confirm the general tendencies appearing in the NFW profile. However, the Aquarius Project simulation [250] seem to favor a profile that does not belong to the general profile class (4.6), but it is based on the general Einasto profile. The DM Einasto profile is defined by

$$\rho_{DM}(r) \propto \exp\left(-\frac{2}{\alpha_E}\frac{r}{r_s}\right), \tag{4.7}$$

with $\alpha_E = 0.17$ and $r_s = 20\,\mathrm{kpc}$.

In Fig. 4.2 we show the dependence of the three aforementioned profiles on the distance r from the galactic center. Fig. 4.3 shows the angular dependence of the integral J, specifically the dependence of the dimensionless quantity $\frac{1}{R_0\rho_0^2}J(\xi)$ with $R_0 = 8.5\,\mathrm{kpc}$ and $\rho_0 = 0.4\,\mathrm{GeV\,cm^{-3}}$. As it was expected, the photon flux is much more enhanced in the GC, with the NFW profile being more steep than the others.

4.3 The 130 GeV Fermi line

A monochromatic signal is often characterized as a "smoking gun" signature for DM, since there is no other known astrophysical source that might give rise to a photon line. Up to now, there is no clear and confirmed evidence for such a signal. However, in an independent analysis of the Fermi-LAT data [210, 211], an evidence for a monochromatic line at $\sim 130\,\mathrm{GeV}$ is revealed with a significance of $\sim 4.6\sigma$ (reduced to 3.2σ taking into account the look-elsewhere effect). The signal is based on about 50 photons; although more data are needed in order to confirm its existence, it is interesting to check if this signal could be explained by WIMP DM annihilation. In this section we will briefly review the analysis and the main results of [211], as well as the present situation after the publication of this work.

The novelty of the analysis under discussion compared to the official Fermi-LAT collaboration analysis, is a new data-driven algorithm for the target selection, essential for such faint signals. 43 months of data (4th of August 2008 to 8th of March 2012) have been analyzed, with photon energies between 1 and 300 GeV. The first cut applied to them was a zenith-angle cut $\theta < 100^\circ$, in order to avoid contamination with the earth albedo. We recall that an optimal target region is one that maximizes the SNR, depending on both the morphology of the DM signal and the morphology of the the background flux, with the former given by the Eq. (4.1) for a specific DM profile. The latter was approximated for energies above 20 GeV by the spatial distribution of γ-rays measured between 1 and 20 GeV. In this way, the authors of [211] determined the optimal targets for each DM profile. In case of a cored isothermal profile, the target region (henceforth Reg1) was the largest and reached up to latitudes of $\sim 84^\circ$. The smallest region (Reg5) corresponded to a compressed profile with inner slope $\alpha = 1.3$, and contained the central $2^\circ \times 2^\circ$ area of the GC only.

After the target regions have been determined, they proceed to a shape analysis of the energy spectra. This is done, for a given γ-ray line energy E_γ, in a small energy window that contains E_γ. The boundaries were parametrized as $E_0 = E_\gamma/\epsilon$ and $E_1 = \min(E_\gamma\sqrt{\epsilon}, 300\,\mathrm{GeV})$. The parameter ϵ varied between $\epsilon \simeq 1.6$ at low energies (few times wider than the LAT energy resolution) and $\epsilon \simeq 3$ at higher energies, in order to compensate for the lower number of events. Within the adopted windows, the spectra were fitted with a simple 3-parameter (S, β, γ) model

$$\frac{\mathrm{d}\Phi}{\mathrm{d}E} = S\delta(E - E_\gamma) + \beta\left(\frac{E}{E_\gamma}\right)^{-\gamma}. \tag{4.8}$$

In this context, background fluxes are approximated by a single power law with a free spectral index γ and normalization β, whereas the monochromatic DM signal has a

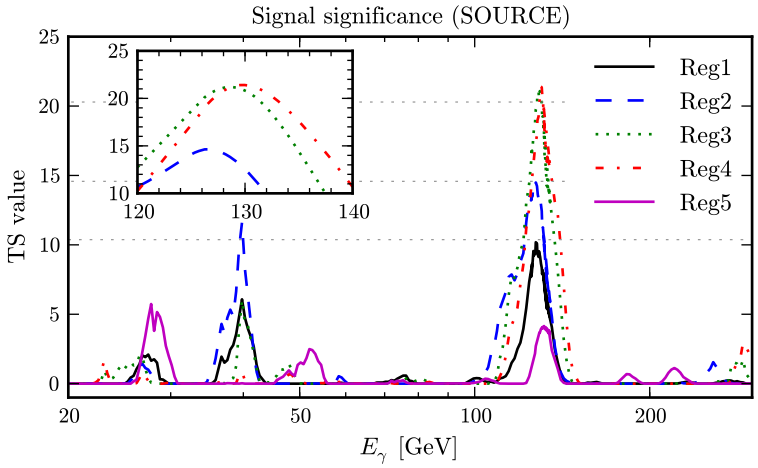

Figure 4.4: The significance versus the line energy E_γ for 5 different target regions, from [211]. The horizontal gray lines correspond from bottom to top to 1σ, 2σ and 3σ after the look-elsewhere effect correction. The inset is a zoom on the energy range of interest. Reg1 corresponds to the cored isothermal profile, Reg2 to NFW, Reg3 to Einasto and Reg4 and Reg5 to a general NFW profile with $\alpha = 1.15$ and $\alpha = 1.3$, respectively (see also text).

free normalization parameter $S \geq 0$. After fixing the experimental conditions and the profile, the annihilation cross section was related to S by a straightforward rescaling.

The best fit model parameters $(S_{bf}, \beta_{bf}, \gamma_{bf})$ were obtained by maximizing the likelihood function $\mathcal{L}(S, \beta, \gamma) \equiv \prod_i P(s_i|\nu_i)$, where $P(s|\nu) = \nu^s \mathrm{e}^{-\nu}/s!$ is the Poisson probability distribution function. s_i, ν_i denote the number of measured and expected events, respectively, in an energy bin i, whereas ν_i is a function of the model parameters (we are not going to reproduce the calculation here, see [211] for details). The significance of a line signal for a given value of E_γ is derived from the test statistic function

$$TS \equiv -2 \ln \frac{\mathcal{L}_{null}}{\mathcal{L}_{best}}, \tag{4.9}$$

where $\mathcal{L}_{best} = \mathcal{L}(S_{bf}, \beta_{bf}, \gamma_{bf})$ and $\mathcal{L}_{null}$ is the likelihood function of a fit without signal.

The final results of [211] are shown in Fig. 4.4. This plot presents the values of the TS significance versus the energy E_γ for five reference target regions. In this figure, we can distinguish a clear peak around $E_\gamma \simeq 130\,\mathrm{GeV}$, with a significance somewhat larger than 3σ (the look-elsewhere effect has already been taken into account) for the target regions Reg3 and Reg4. These regions correspond, respectively, to Einasto and a NFW profile with $\alpha = 1.15$.

In general, a monochromatic line in supersymmetric models may come either from a DM annihilation to a pair of photons $\gamma\gamma$ either from an annihilation to $Z\gamma$ or $h\gamma$, with h a Higgs boson. The annihilation is through a loop with charged particles. For the annihilation $\chi\chi \to \gamma X$ with χ the DM particle and $X = \gamma$, Z, h, the rest frame

energy of the photon is

$$E_\gamma = m_\chi \left(1 - \frac{m_X^2}{4m_\chi^2}\right). \tag{4.10}$$

Since the WIMPs are non-relativistic in the DM halo, the photons are approximately monochromatic in the lab frame. For the case of the photon pair, the energy of the photons is equal to the DM mass m_χ.

If the excess on the Fermi data is interpreted as an annihilation to a pair of photons, it corresponds to DM mass $m_\chi \simeq 130\,\mathrm{GeV}$ and an annihilation cross section $\langle\sigma v\rangle_{\chi\chi\to\gamma\gamma} = \mathcal{O}(10^{-27})\,\mathrm{cm}^3\,\mathrm{s}^{-1}$, with the exact value depending on the specific DM halo profile. Specifically, for the two profiles with the largest significance (Reg3 and Reg4, see above), Weniger [211] obtained $\langle\sigma v\rangle^{Ein}_{\chi\chi\to\gamma\gamma} = (1.27\pm0.32^{+0.18}_{-0.28})\times10^{-27}\,\mathrm{cm}^3\,\mathrm{s}^{-1}$ (Einasto) and $\langle\sigma v\rangle^{NFW}_{\chi\chi\to\gamma\gamma} = (2.27\pm0.57^{+0.32}_{-0.51})\times10^{-27}\,\mathrm{cm}^3\,\mathrm{s}^{-1}$ (NFW). For the cored isothermal profile, there was some tension among the cross sections obtained from different target regions.

After the publication of [211], many other analyses followed [210–213], using independent methods and trying to confirm or reject the announced results. Some of them attempted simultaneously to address one more issue that arose. In the majority of the particle physics models, the primary photon line is always accompanied by one more line at an energy close to the first one. The loop of charged particles, which couple to the photon, also couple to the Z boson. Hence, in case that the 130 GeV line corresponds to an annihilation to a pair of photons, another excess at $\sim 114\,\mathrm{GeV}$ should appear. In [251], it was claimed that the two lines provide a marginally better fit than one line, with a DM particle with mass $m_\chi = 127.3\pm2.7\,\mathrm{GeV}$ annihilating to $\gamma\gamma$ and $Z\gamma$. However, *Hektor et al* [252] concluded that the Fermi-LAT energy resolution and the low statistics do not allow to distinguish one from two lines with any meaningful statistical significance. In any case, a second monochromatic line at lower energy and with a somewhat smaller cross section, if not welcome, is at least not disallowed by the data.

The Fermi-LAT collaboration preferred in the beginning to interpret the same data only in terms of upper bounds on the partial annihilation cross section [253]. However, in a subsequent paper [254], new selection tools were employed and the most significant fit occurred at $E_\gamma = 133\,\mathrm{GeV}$, but with a reduced local significance of 3.3σ, corresponding to a 1.6σ global significance. The large decrease in the global value is due to the line feature which is narrower than the instrument resolution and due to its absence in areas around the GC with angles larger than 50°. Interestingly, the same line appeared also in data from photons coming from the Earth limb with about equal local significance, leading to the suspicion that the line feature may be due to an unknown systematic effect. However, the uncertainties related to this significance are in some cases very large, as pointed out in [255]. Specifically, systematic 2σ differences in the Earth limb spectra among γ-rays with small and large incidence angles were observed, leading to the conclusion that the spectral features are likely statistical fluctuations.

Still, future additional data could confirm the present hints for a possible excess; hence it is of interest to study whether it could be explained within concrete models

for DM which are compatible with bounds on its relic density from WMAP [22] and Planck [9] and bounds on its direct detection cross section (in the relevant mass range) from XENON100 [44, 47] and LUX [45]. Furthermore, we have to mention that a concrete model with an enhanced DM annihilation cross section to photons is very likely to also give large annihilation cross sections to SM particles that would produce diffuse γ-rays. Hence, before we proceed to a possible explanation of DM, it is of great importance to review in the next section the current experimental upper limits on the diffuse radiation.

4.4 Upper bounds from diffuse γ-rays

Since no excess on diffuse γ-rays has been observed, upper limits on the annihilation cross section can be derived. As it has been already mentioned, dSph satellites of the Milky Way lead to a large signal-to-noise ratio and are potentially good targets for DM searches. Furthermore, the final limits from these targets are quite insensitive to the assumed DM distribution profile.

The Fermi-LAT collaboration has performed a combined analysis on 10 dwarf satellites [256]. In this analysis, they combine all the dSph observations into a single joint likelihood function, taking into account the uncertainties in estimates of the J factors. Including these uncertainties in the fit results in stronger upper limits compared to a common method that uses nominal J factors. However, the combination of the dSph satellites yields a much milder increase (by about a factor of 1.3). The J factors are calculated using the l.o.s. velocities of the stars in dSph and the Jeans equation via a Bayesian method, commonly used in the literature (see [257] and references therein). They assume an inner DM density profile scaling as $1/r$, in order to be consistent with DM-only (initially cold particles) numerical simulations. The DM mass distribution is modeled by the NFW profile. The final results are shown in Fig. 4.5. Even if the limits are recalculated using J factors that allow for shallower profiles than NFW, the final constraint would agree with the previous limit within about 10%, confirming the insensitivity on the DM distribution profile.

If DM annihilation processes are purely s-wave, the cross section in the early Universe, which determined the DM relic abundance, would have essentially the same value today. However, the thermal cross section ($\sim 3 \cdot 10^{-26}\,\mathrm{cm}^3\,\mathrm{s}^{-1}$), required to conform with the observed relic density, exceeds the upper limits in the low mass range. Hence, Fermi-LAT has excluded DM lighter than about 30 GeV with purely s-wave annihilation to $b\bar{b}$, W^+W^- and $\tau^+\tau^-$, almost independently of the assumed profile. For specific DM distribution profiles, the exclusion can be extended to larger DM mass using other targets, such as clusters of galaxies [258, 259] or the Milky Way galactic center [260].

As we have seen, the 130 GeV line feature is best fitted if one assumes the NFW or the Einasto profile. In this case, stringent limits have been derived with the galactic center as the target [261], using the analysis performed in [260]. The results for DM mass 130 GeV and NFW profile with $\gamma = 1.15$ are shown in Table 4.1. These values have

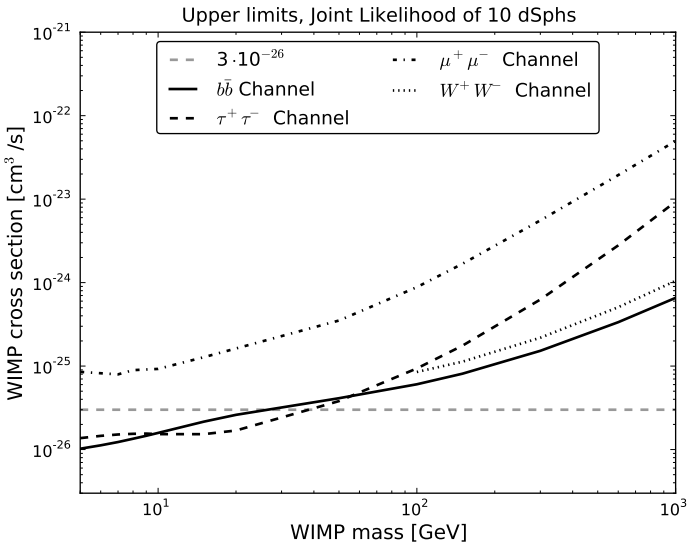

Figure 4.5: Upper limits on the DM annihilation cross section for the individual channels $b\bar{b}$, $\tau^+\tau^-$, $\mu^+\mu^-$ and W^+W^- using the joint likelihood of the 10 dSphs. The dashed gray line represents the thermal cross section ($3 \cdot 10^{-26}\,\mathrm{cm}^3\,\mathrm{s}^{-1}$) for a purely s-wave annihilation. Taken from [256].

been calculated in [261] using the Fermi data from the Inner Galaxy, after subtracting known point sources and emission tracing the Galactic Disk. The Einasto profile would yield similar (about 10% less stringent) results.

Annihilation Channel	Upper limits on cross section ($\mathrm{cm}^3\,\mathrm{s}^{-1}$)	
	Galactic Center [261]	dSph [256]
$b\bar{b}$	$8 \cdot 10^{-27}$	$2 \cdot 10^{-25}$
$\tau^+\tau^-$	$7 \cdot 10^{-27}$	$1.2 \cdot 10^{-24}$
$\mu^+\mu^-$	$7.0 \cdot 10^{-26}$	$9.4 \cdot 10^{-24}$
W^+W^-	$1.0 \cdot 10^{-26}$	$3 \cdot 10^{-25}$

Table 4.1: The upper limits on the annihilation cross section for four individual channels using the Galactic Center target [261] with NFW profile and the combined analysis of the dSph satellites [256]. The DM mass has been fixed to 130 GeV.

4.5 A 130 GeV photon line in the NMSSM

In this section, we will show that the NMSSM is able to provide a viable DM candidate, which annihilates to photons, giving rise to the desired line features. At the same time, constraints from collider and B-physics are respected and a Standard Model-like Higgs with mass $\sim 125\,\text{GeV}$ emerges, as observed by ATLAS [93] and CMS [92] collaborations. We will also check the consistency of our candidate with the other direct and indirect DM searches. The following analysis is based on the work we performed in [2], which preceded the most updated direct detection results from 225 live-days of XENON100 [44] and LUX [45]. As a consequence, the previous bounds from the 100-live days of the XENON100 experiment [47] will be used instead, but an update will be provided in the last section, supplemented with a discussion on the possibility of a small nucleon scattering cross section.

4.5.1 General aspects

The DM particle in this context is the lightest neutralino χ_1^0 of the NMSSM. Its decomposition in the mass basis (3.27) is written as

$$\chi_1^0 = N_{11}\widetilde{B} + N_{12}\widetilde{W}^3 + N_{13}\widetilde{H}_d^0 + N_{14}\widetilde{H}_u^0 + N_{15}\widetilde{S}. \tag{4.11}$$

We remind that $\widetilde{B}$, $\widetilde{W}^3$, $\widetilde{H}_d^0$, $\widetilde{H}_u^0$ and $\widetilde{S}$ are, respectively, the bino, wino, down-type higgsino, up-type higgsino and singlino components. Its relic density should fit the observed value ($\Omega h^2 \simeq 0.11$) through annihilations occurred in the early Universe. However, as we have seen in the previous section, since we would like to explain the photon line features that arise in the NFW or Einasto DM profile, its relic density should have been reduced to the observed value through mainly p-wave annihilations.

The neutralino χ_1^0 would give rise to photons through loop diagrams, a well-studied feature in the MSSM. A complete list of these processes in the case of MSSM can be found, for example, in [222]. Although the cross section of these processes is loop suppressed, a relatively large value is possible if a resonance occurs. When the annihilation proceeds through an s-channel exchange and the exchanged particle mass approaches the pole (twice the mass of the neutralino), the process amplitude increases rapidly. As can be seen in [222], the only case with a particle exchange in s-channel, with additionally a mass determined by free parameters (i.e., we exclude diagrams with an s-channel Z boson exchange), is the CP-odd Higgs exchange [165, 240, 241]. However, the resonance would also occur at tree level, giving SM particles with much larger cross sections. In this way, the relic density is difficult to be kept fixed at the desired value and, additionally, the SM products would give rise to diffuse γ-ray radiation exceeding the current bounds.

Turning now to the NMSSM, there are two CP-odd Higgs states instead of the one unique state in the MSSM. The additional state will give two more classes of loop diagrams, which are shown in Fig. 4.6. The cross sections of these diagrams can be found in the App. B. It is possible, one of the two states A_1, A_2 to be almost completely singlet-like, avoiding in this manner SM annihilation products at tree level.

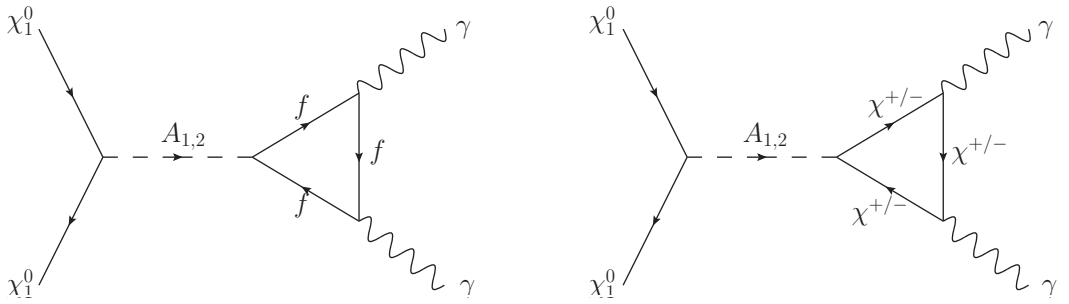

Figure 4.6: The NMSSM specific loop diagrams of neutralino pair annihilation that give rise to a pair of photons through an s-channel CP-odd Higgs exchange. The one on the left contains sfermions or fermions in the loop, while the one on the right proceeds with charginos $\chi^{+/-}$ in the loop.

Henceforth, we will denote this state as A_S. The dominant diagram of neutralino pair annihilation in case the mass of A_S (m_{A_S}) is about twice the neutralino mass is the one shown on the right of Fig. 4.6. The singlet nature of A_S suppresses the couplings to fermions (and sfermions) and, subsequently, the cross section of the other diagram (on the left panel of Fig. 4.6).

We recall here some features of the foregoing analysis of the NMSSM Higgs sector. First we remind that, after using the minimization equations of the Higgs potential, the Higgs sector can be described (at tree level) by the six parameters

$$\lambda\,, \quad \kappa\,, \quad A_\lambda\,, \quad A_\kappa\,, \quad \mu_{\rm eff}\,, \quad \tan\beta \equiv \frac{v_u}{v_d}\,. \tag{4.12}$$

The neutral CP-even Higgs sector contains 3 states H_i, which are mixtures of the CP-even components of the superfields $\widehat{H}_u$, $\widehat{H}_d$ and $\widehat{S}$. Their masses are described by a 3×3 mass matrix $\mathcal{M}^2_{H\,ij}$ given by (3.15), where the dominant contribution to the singlet-like component $\mathcal{M}^2_{H\,33}$ reads [119, 120]

$$\mathcal{M}^2_{H\,33} \sim \kappa s\,(A_\kappa + 4\kappa s)\ . \tag{4.13}$$

The neutral CP-odd Higgs sector contains 2 physical states A_i, whose masses are described by a 2×2 mass matrix $\mathcal{M}^2_{A\,ij}$ (3.17), where $\mathcal{M}^2_{A\,11}$ corresponds to the MSSM-like CP-odd Higgs mass squared. The dominant contributions to the singlet-like component $\mathcal{M}^2_{A\,22}$ and the singlet-doublet mixing term $\mathcal{M}^2_{A\,12}$ are given by

$$\mathcal{M}^2_{A\,22} \sim -3\kappa s A_\kappa\,, \quad \mathcal{M}^2_{A\,12} \sim \lambda(A_\lambda - 2\kappa s)\sqrt{v_u^2 + v_d^2}\,, \tag{4.14}$$

respectively [119, 120].

4.5.2 Implementation for the Fermi Line

Now we turn to the masses and couplings of the particles and the corresponding regions in the NMSSM parameter space, which have all the desired phenomenological properties. First we consider the dominantly singlet-like CP-odd Higgs state

A_S. For a sufficiently large χ_1^0 pair annihilation cross section into two photons (and $E_\gamma = M_{\chi_1^0} \sim 130\,\text{GeV}$), we need

$$M_{A_S} \sim 2M_{\chi_1^0} \sim 260\,\text{GeV}\ , \tag{4.15}$$

which can be achieved by appropriate values of $-3\kappa s A_\kappa$. As it has been already pointed out, the $SU(2)_L$ doublet admixture of A_S must be small. From the second of Eqs. (4.14) the mixing of A_S with the MSSM-like doublet is small for

$$A_\lambda \approx 2\kappa s\ . \tag{4.16}$$

Next we consider the DM particle χ_1^0. It would have a large singlino component for small $2\kappa s$. However, from Eq. (4.13) and the first of Eqs. (4.14) one can derive

$$(2\kappa s)^2 \sim \mathcal{M}^2_{H\,33} + \frac{1}{3}M^2_{A_S}\ ; \tag{4.17}$$

from $M_{A_S} \sim 260\,\text{GeV}$ and $\mathcal{M}^2_{H\,33} > 0$ it follows that $2\kappa s$ cannot be small. Hence, assuming $M_1 \lesssim M_2/2$ (assuming universal gaugino masses at the GUT scale), it follows that χ_1^0 has dominant bino and higgsino components. A priori large higgsino components seem desirable, given the required coupling of χ_1^0 to A_S in Fig. 4.6: This coupling is induced by the first term $\lambda \widehat{S}\widehat{H}_u \cdot \widehat{H}_d$ in the superpotential (3.1), which leads to a Yukawa coupling $\lambda A_S \widetilde{H}_u^0 \widetilde{H}_d^0$. Likewise, the coupling of A_S to the charginos $\chi^\pm$ originates from the higgsino components $\widetilde{H}_u^+$, $\widetilde{H}_d^-$ of $\chi^\pm$ and the Yukawa coupling $\lambda A_S \widetilde{H}_u^+ \widetilde{H}_d^-$.

However, too large higgsino components of χ_1^0 imply again a too small relic density; diagrams with charginos and neutralinos in the t-channel (and W^+W^- or ZZ in the final state), CP-even Higgs bosons in the s-channel etc. would lead to a too large pair annihilation cross section of χ_1^0. Hence we end up with a dominantly bino-like χ_1^0, but with non-zero (non-negligible) higgsino components. Its mass of 130 GeV has to follow from appropriate values of M_1 and μ_{eff}, with $M_1 < \mu_{\text{eff}}$.

Finally, we require a SM-like CP-even Higgs boson H_{SM} with a mass $M_{H_{SM}}$ near 125 GeV. It has been known since a long time that the SM-like CP-even Higgs boson can be heavier in the NMSSM compared to the MSSM due to the NMSSM-specific coupling $\lambda S H_u H_d$ [119, 120, 123–126], provided λ is large and $\tan\beta$ is relatively small. Subsequently we choose corresponding values of λ and $\tan\beta$ such that $M_{H_{SM}} \sim 125\,\text{GeV}$ [127–137]. We find that the above properties in the neutralino and CP-odd Higgs sector imply that H_{SM} is the lightest CP-even Higgs state; the singlet-like CP-even Higgs state has a mass $\gtrsim 200\,\text{GeV}$. The scenario with a lightest singlet-like Higgs state and a next-to-lightest SM-like Higgs state (allowing for an enhanced branching ratio into $\gamma\gamma$ [129, 131, 133, 134]) seems difficult to realize. Herewith we have sketched the interesting regions in the parameter space in (4.12).

4.5.3 Constraints from direct DM searches

An open question remains whether the DM particle can comply with the constraints from XENON100 on its spin-independent detection cross section: χ_1^0-nucleon scattering

is induced dominantly by H_{SM}-exchange in the t-channel [262], and the H_{SM}-χ_1^0-χ_1^0 vertex is proportional to the product of the bino- and higgsino-components of χ_1^0 (from $g_1\times$ bino $\times$ Higgs $\times$ higgsino terms in the Lagrangian, where g_1 is the $\mathrm{U}(1)_B$ gauge coupling). This issue will be studied below.

We have scanned the parameter space of the general NMSSM with help of the NMSSMTools package [263, 264], supplemented with suitably modified formulas for the cross sections for $\chi_1^0\chi_1^0 \to \gamma\gamma$ (and for $\chi_1^0\chi_1^0 \to Z\gamma$) from [222, 224] (see App. B). MicrOmegas [151, 159, 265] is used for the calculation of the DM relic density and direct detection cross sections. For the latter we have to specify the strange quark content of the nucleons, i.e. the relevant sigma terms. We use the most recent values from [161] with, to be conservative, a value for $\sigma_{\pi N}$ near the lower end of the 1σ error bars: $\sigma_{\pi N} = 40\,\mathrm{MeV}$, $\sigma_0 = 39\,\mathrm{MeV}$.

For the soft SUSY breaking terms we made the following choices:

- Squark masses of 1.5 TeV, except for the left-handed squarks of the 3rd generation (1 TeV) and the right-handed top squark (300 GeV). The latter values are motivated by universal soft scalar masses at the GUT scale [135], and alleviate LHC constraints from direct SUSY searches due to the more complicated squark and gluino decay cascades involving the light stops.
- Trilinear soft susy breaking terms $A_t = A_b = -1.1\,\mathrm{TeV}$.
- Slepton masses in the $140 - 500\,\mathrm{GeV}$ range such that the SUSY contributions to the anomalous muon magnetic moment are sufficiently large (inspite of low values of $\tan\beta$), while slepton exchange in the t-channel of the pair annihilation cross section of χ_1^0 does not imply a too small relic density.
- Whereas we vary M_1 in the $140 - 160\,\mathrm{GeV}$ range (see below), M_2 and the gluino mass M_3 are kept fixed at $M_2 = 300\,\mathrm{GeV}$, $M_3 = 800\,\mathrm{GeV}$ for simplicity.
- Finally we use 173.1 GeV for the top quark pole mass.

Subsequently we impose the following phenomenological constraints:

- $M_{\chi_1^0} = 129 - 131\,\mathrm{GeV}$ and $\langle\sigma v\rangle(\chi_1^0\chi_1^0 \to \gamma\gamma) \gtrsim 10^{-27}\ \mathrm{cm}^3\ \mathrm{s}^{-1}$ in order to obtain a photon line in agreement with the excess found in [211, 212].
- Upper bounds on annihilation cross sections into W^+W^-, ZZ, $b\bar{b}$ and $\tau\bar{\tau}$ channels from the Fermi-LAT collaboration [253,256] (see also [260,261]), as well as bounds from PAMELA on the antiproton flux [266]. For the determination of these cross sections/fluxes we use micrOMEGAs2.4 [267].
- A relic density complying with the WMAP / Planck bound $\Omega h^2 = 0.1120 \pm 0.011$ [21] (with 2σ error bars).
- A SM-like Higgs boson with $M_{H_{SM}} = 124 - 127$ GeV, as it was confirmed recently by the ATLAS and CMS collaborations [92, 93].

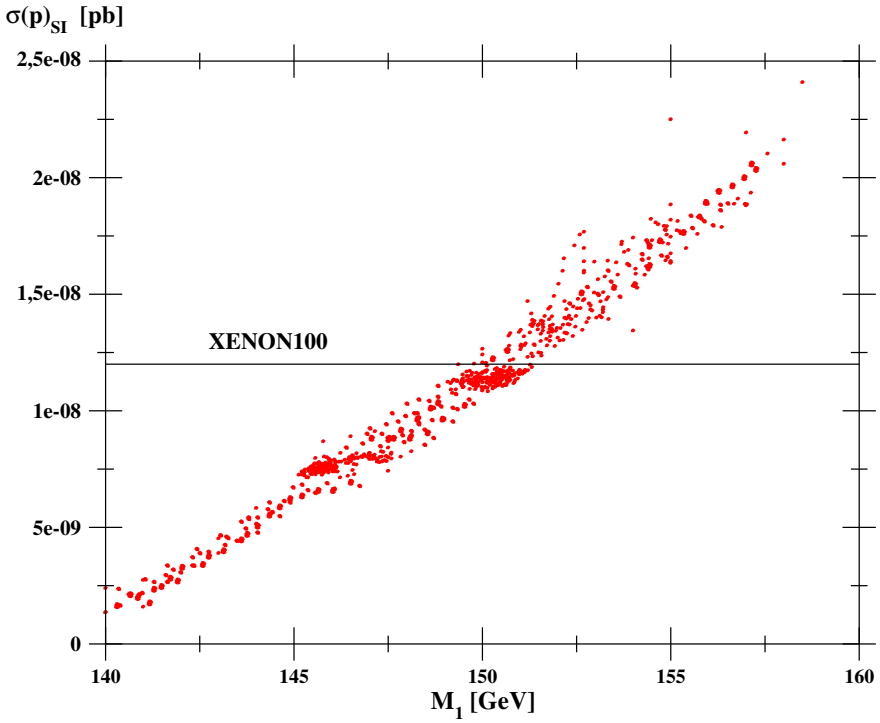

Figure 4.7: $\sigma(p)_{SI}$ as function of M_1 for a sample of points satisfying all other phenomenological constraints as indicated in the text. The horizontal line indicates the previous bound from XENON100 [47] for a 130 GeV DM particle, which holds for all points shown.

- Constraints from B-physics as implemented in NMSSMTools (which have actually no impact for the low values of $\tan\beta$ considered here).
- A sufficiently large SUSY contribution Δa_μ to the muon anomalous magnetic moment as implemented in NMSSMTools.
- Constraints from the absence of Landau singularities of the running Yukawa couplings below the GUT scale, and the absence of unphysical global minima of the Higgs potential.

We have found corresponding points in the NMSSM parameter space, both below and slightly above the previous XENON100 bound [47] on the spin-independent DM – proton cross section of $\sigma(p)_{SI} \lesssim 1.2 \times 10^{-8}$ pb for $M_{\chi_1^0} \sim 130\,\text{GeV}$ [47]. In Fig. 4.7 we show $\sigma(p)_{SI}$ as function of M_1 for a sample of such points, where we varied the parameters in (4.12) in the range $\lambda = 0.6 - 0.615$, $\kappa = 0.326 - 0.329$, $A_\lambda = 240 - 400\,\text{GeV}$, $A_\kappa = -130 - (-60)\,\text{GeV}$, $\mu_{\text{eff}} = 230 - 445\,\text{GeV}$, $\tan\beta = 1.68 - 1.82$.

4.5.4 Final Remarks

In Table 4.2 we show the details (parameters, masses and relevant observables) for a sample point with $M_1 = 150\,\text{GeV}$. The couplings of $H_1 \equiv H_{SM}$ to quarks, leptons,

Parameters	
λ	0.61
κ	0.328
A_λ	267
A_κ	-114.1
$\tan\beta$	1.8
$\mu_{\rm eff}$	269
M_1	150
left-h. slepton masses	150
right-h. slepton masses	160
$A_e = A_\mu = A_\tau$	500

Sparticle masses	
$m_{\tilde{g}}$	971
$\langle m_{\tilde{q}} \rangle$	1530
$m_{\tilde{t}_1}$	204
$m_{\tilde{t}_2}$	1034
$m_{\tilde{b}_1}$	1005
$m_{\tilde{\mu}_L}$	154
$M_{\chi_1^0}$	129.6
$M_{\chi_2^0}$	217
$M_{\chi_3^0}$	287
$M_{\chi_4^0}$	309
$M_{\chi_5^0}$	376
$M_{\chi_1^\pm}$	210
$M_{\chi_2^\pm}$	370

Higgs masses	
$M_{H_1}(= M_{H_{SM}})$	124.3
M_{H_2}	256
M_{H_3}	519
$M_{A_1}(= M_{A_S})$	258.9
$R^{bb}_{A_S}$	3×10^{-3}
M_{A_2}	515
$M_{H^\pm}$	511

Components of χ_1^0	
N_{11}^2	0.826
N_{12}^2	0.026
N_{13}^2	0.077
N_{14}^2	0.065
N_{15}^2	0.009

Observables	
Ωh^2	0.11
$\sigma(p)_{SI}$ [10^{-8} pb]	1.21
$\langle\sigma v\rangle(\chi_1^0\chi_1^0 \to \gamma\gamma)$ [10^{-27}cm^3 s^{-1}]	1.1
$\langle\sigma v\rangle(\chi_1^0\chi_1^0 \to Z\gamma)$ [10^{-27}cm^3 s^{-1}]	0.8
$\langle\sigma v\rangle(\chi_1^0\chi_1^0 \to WW)$ [10^{-27}cm^3 s^{-1}]	3.46
$\langle\sigma v\rangle(\chi_1^0\chi_1^0 \to ZZ)$ [10^{-27}cm^3 s^{-1}]	0.26
$\langle\sigma v\rangle(\chi_1^0\chi_1^0 \to b\bar{b})$ [10^{-27}cm^3 s^{-1}]	0.60
$\langle\sigma v\rangle(\chi_1^0\chi_1^0 \to \tau\bar{\tau})$ [10^{-27}cm^3 s^{-1}]	0.09
Δa_μ [10^{-10}]	6.5 ± 3.0

Table 4.2: Properties of a sample point with $M_1 = 150\,\text{GeV}$. Dimensionful parameters are given in GeV. $R^{bb}_{A_S}$ denotes the coupling of A_S to b-quarks normalized to the one of a SM-like Higgs boson. The components of χ_1^0 are defined in Eq. (4.11). The value of Δa_μ includes theoretical error bars.

electroweak gauge bosons, gluons and photons are SM-like within $\sim 5\%$. $R^{bb}_{A_S}$ denotes the coupling of A_S to b-quarks normalized to the one of a SM-like Higgs boson; its small value underlines its singlet-like nature.

We begin with a comment concerning the relic density. As we have already discussed, the relic density should be determined by p-wave annihilations, in order to comply with the diffuse γ-ray bounds. We remind (see, e.g., [268]) that annihilations through a CP-odd Higgs exchange is both s- and p-wave. The contribution of the neutralino annihilation to photons to the total relic density is small (smaller than about 10%), since the cross section is about one order of magnitude smaller that the thermal cross section, while the singlet-like nature of the lightest pseudoscalar suppresses the tree level annihilation through s-channel exchange. However, the s-channel CP-even Higgs exchange is exclusively p-wave. As a consequence, in the majority of the points in Fig. 4.7, the correct relic density is obtained through a resonance of the H_2. However, this resonance does not have to be narrow and it can be easily present.

The following remarks are also in order: The larger M_1, the smaller one has to choose $\mu_{\rm eff}$ in order to maintain $M_{\chi_1^0} \sim 130\,{\rm GeV}$. It follows that, for larger M_1, the higgsino component of χ_1^0 increases leading to a larger $\chi_1^0\chi_1^0$ annihilation cross section. Hence, for too large M_1, the relic density falls below the WMAP bound.

On the other hand, for smaller M_1 one has to choose larger values for $\mu_{\rm eff}$ implying a smaller higgsino component of χ_1^0, which explains the decrease of $\sigma(p)_{SI}$ in Fig. 4.7. However, simultaneously, the coupling of A_S to χ_1^0 decreases as well. As a consequence, the mass M_{A_S} of A_S has to be closer and closer to the pole $2M_{\chi_1^0}$ in order to obtain $\sigma(\chi_1^0\chi_1^0 \to \gamma\gamma) > 10^{-27}{\rm cm}^3\ {\rm s}^{-1}$. In order to clarify the required tuning, we show $\sigma(\chi_1^0\chi_1^0 \to \gamma\gamma)$ in Fig. 4.8 as function of M_{A_S} for the point listed in Table 4.2. (Note that the finite width $\Gamma(A_S) \sim 1.6\,{\rm keV}$, dominated by $A_S \to \gamma\gamma$, is not visible in Fig. 4.8. Due to the small couplings of A_S to quarks and leptons, the contributions of A_S in the s-channel to the annihilation cross sections into $b\bar{b}$ and $\tau\bar{\tau}$ final states are well below the Fermi-LAT bounds. The annihilation cross sections into W^+W^- and ZZ originate from the second CP-even Higgs boson in the s-channel. The antiproton flux has a maximum of $\sim 2.47 \times 10^{-4}(\,{\rm GeV\,m^2\,s\,sr})^{-1}$ for an energy of ~ 2 GeV, which is well below the PAMELA bound.)

We see that $\sigma(\chi_1^0\chi_1^0 \to \gamma\gamma)$ is larger than 10^{-27} cm^3 s^{-1} only within a $\sim 0.7\,{\rm GeV}$ wide window of M_{A_S}. This required tuning becomes worse for lower values of M_1, and it is the price to pay (in this region of the parameter space) for the stronger latest constraint on $\sigma(p)_{SI}$ from LUX. (On the other hand, modifications of the present best estimates for the Higgs-nucleon coupling and/or the local DM density could alleviate the present constraints from direct detection.)

Finally we should add that diagrams similar to Fig. 4.6, but with one photon replaced by a Z boson, contribute to $\sigma(\chi_1^0\chi_1^0 \to Z\gamma)$ leading to an additional photon line with, for $M_{\chi_1^0} \sim 130\,{\rm GeV}$, $E_\gamma \sim 114\,{\rm GeV}$. For the present scenario we find $\sigma(\chi_1^0\chi_1^0 \to Z\gamma) \sim 75\% \times \sigma(\chi_1^0\chi_1^0 \to \gamma\gamma)$. Such an additional line would be compatible with the structure observed in [213]. In any case, additional lines—also from $\sigma(\chi_1^0\chi_1^0 \to H\gamma)$ or interpreting the 130 GeV line as due to $\chi_1^0\chi_1^0 \to Z\gamma$—can be interesting checks of such scenarios in the future [251].

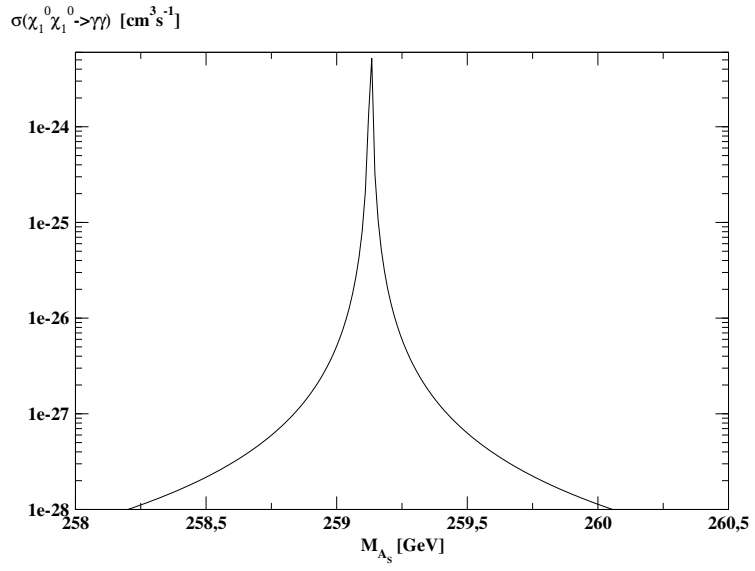

Figure 4.8: $\sigma(\chi_1^0\chi_1^0 \to \gamma\gamma)$ as function of M_{A_S} for the point listed in Table 4.2.

4.5.5 Update for the latest direct detection constraints

The negative DM search results from the LUX detector resulted in much stringent upper bounds on the WIMP–nucleon scalar scattering cross section [44], almost one order of magnitude lower than the constraint [47] used in the above analysis. For a WIMP mass of $\sim 130\,\text{GeV}$, the new upper limit is $\sigma^{SI} \lesssim 2\cdot 10^{-9}\,\text{pb}$ [45]. Applying this limit to the points of Fig. 4.7, we can check that only few points survive, near the lower end of the bino mass M_1 ($\sim 140\,\text{GeV}$). As we have already explained, such small values of M_1 lead to a mostly bino LSP with a reduced coupling to the singlet pseudoscalar A_s. Hence, although these few points respect the direct detection constraints, a strong fine-tuning is necessary in order that the annihilation cross section to photons is sufficiently large. In this section, we are going to check whether the NMSSM is able to provide a neutralino LSP with a much smaller scattering cross section with nucleons and also with the desired annihilation cross section to photons applying a "reasonable" fine-tuning (respecting, at the same time, all the phenomenological constraints set in the previous sections).

In order to reduce the spin-independent scattering cross section σ_p^{SI}, we will use a MSSM approximation. We will see that this approximation is working in this context, since the lightest neutralino has a very small singlino component, as it was explained previously, and additionally we can approximate two of the three CP-even Higgs mass eigenstates as MSSM-like. In the configuration of the parameter space that we are going to establish, the second eigenstate is mostly singlet-like (this is also true for the point of Table 4.2).

As it has been pointed out in [269] (see also [270, 271]) for the MSSM case, small values of σ_p^{SI} can be obtained when μ and $M_1 + \mu \sin 2\beta$ have opposite signs.[1] Below

[1]This fact has been already used in [272] in order to explain the Fermi line in the NMSSM, using negative values for μ_{eff}. However, in this paper, non-perturbativity at the GUT scale was not an issue,

we explain why this happens.

We recall that the spin-independent cross section depends on the effective couplings a_d^{SI} and a_u^{SI} to down- and up-type quarks, respectively, given by Eqs. (3.40), which we rewrite here:

$$a_d^{SI} = \sum_{i=1}^{3} \frac{1}{m_{H_i}^2} C_i^d C_{\chi_1^0\chi_1^0 H_i}, \qquad a_u^{SI} = \sum_{i=1}^{3} \frac{1}{m_{H_i}^2} C_i^u C_{\chi_1^0\chi_1^0 H_i}. \tag{4.18}$$

We will express these couplings in the MSSM limit; i.e. we have to calculate the couplings $C_i^{d,u}$ and $C_{\chi_1^0\chi_1^0 H_i}$, given, respectively, by Eqs. (3.41) and (3.42), in the limit $N_{15} \to 0$ and for two dominantly doublet-like Higgs scalars. We denote these scalars by h and H (with h the lightest one), assuming to correspond to H_1 and H_2, respectively. Then, these two mass eigenstates can be obtained by a rotation by an angle α. Therefore, the MSSM limit implies $S_{11} \to -\sin\alpha$, $S_{22} \to \sin\alpha$ and $S_{12} = S_{21} \to \cos\alpha$. Moreover, one can prove a relation between the angles α and β [110, 274]:

$$\cos^2(\beta - \alpha) = \frac{m_h^2}{m_A^2} \frac{m_Z^2 - m_h^2}{m_H^2 - m_h^2}, \tag{4.19}$$

with A the doublet-like pseudoscalar. Since the doublet pseudoscalar is expected to be much heavier than the SM-like Higgs h and, also, the difference between the masses of h and H is much larger than the mass difference of the Z boson and h, we are allowed to assume $\cos^2(\beta - \alpha) \ll 1$. Hence,

$$\sin\alpha \simeq \cos\beta, \qquad \cos\alpha \simeq -\sin\beta. \tag{4.20}$$

Then, Eqs. (3.41) become[2]

$$C_h^d = -\frac{g_2 \sin\alpha}{2M_W \cos\beta} \simeq -\frac{g_2}{2M_W}, \qquad C_h^u = \frac{g_2 \cos\alpha}{2M_W \sin\beta} \simeq -\frac{g_2}{2M_W}, \tag{4.21a}$$

$$C_H^d = -\frac{g_2 \cos\alpha}{2M_W \cos\beta} \simeq -\frac{g_2}{2M_W} \tan\beta, \qquad C_H^u = \frac{g_2 \sin\alpha}{2M_W \sin\beta} \simeq \frac{g_2}{2M_W} \cot\beta. \tag{4.21b}$$

We see that all of them but one are negative. However, we are going to neglect the positive coupling C_H^u for a couple of reasons: since $\tan\beta > 1$, the coupling to down-type quarks is expected larger (in absolute value) and moreover the up quark form factors are much smaller than the ones of the down-type quarks (notably, the strange quark). We turn now to Eqs. (3.42), which give

$$C_{\chi_1^0\chi_1^0 h} = -(g_1 N_{11} - g_2 N_{12})(N_{13}\cos\beta - N_{14}\sin\beta) \tag{4.22a}$$

$$C_{\chi_1^0\chi_1^0 H} = -(g_1 N_{11} - g_2 N_{12})(N_{13}\sin\beta + N_{14}\cos\beta) \tag{4.22b}$$

since this paper refers to what has been denoted in the literature as λ-SUSY scenarios [127,273]. Here, we will not allow for the appearance of Landau pole below the GUT scale.

[2]We write, instead, the reduced couplings to the quark masses, since the final result would be independent of them.

We will use, subsequently, an approximate diagonalization of the (MSSM) neutralino mass matrix, obtained in [275] for the limits $|M_2 \pm \mu| \gg M_Z$ and $|M' \pm \mu| \gg M_Z$, with $M' = \frac{5}{3}\tan^2\theta_w M_2$ (θ_w is the weak mixing angle). The two expressions that we need read

$$N_{13} \simeq -\frac{g_1}{\sqrt{2}}\frac{v}{M'^2 - \mu^2}(M_1 \cos\beta + \mu \sin\beta), \tag{4.23a}$$

$$N_{14} \simeq \frac{g_1}{\sqrt{2}}\frac{v}{M'^2 - \mu^2}(M_1 \sin\beta + \mu \cos\beta). \tag{4.23b}$$

Plugging them into Eqs. (4.22), we obtain

$$C_{\chi_1^0\chi_1^0 h} \propto M_1 + \mu \sin 2\beta, \qquad C_{\chi_1^0\chi_1^0 H} \propto -\mu \cos 2\beta = \mu|\cos 2\beta|, \tag{4.24}$$

sharing the same positive proportionality factor. Substituting Eqs. (4.24) and (4.21) into (4.18), we can see that the effective couplings a^{SI} are proportional to the expression $A(M_1 + \mu \sin 2\beta) + B\mu$, with A and B some negative coefficients (due to the negative signs in (4.21)) of comparable order of magnitude. If $M_1 + \mu \sin 2\beta$ and μ have opposite signs, a cancellation would occur and the resulting scattering cross section would be suppressed.

After this interlude, we continue with the parameter space of NMSSM, searching for the required properties for a viable DM with small direct detection cross section and large annihilation cross section to two photons. We will assume positive values for μ_{eff}, and negative for the expression $M_1 + \mu_{\text{eff}} \sin 2\beta$, i.e. $M_1 < 0$ and $|M_1| < \mu_{\text{eff}} \sin 2\beta$ ($\sin 2\beta > 0$ for $\tan\beta > 1$). We note that similar results can be obtained using $\mu_{\text{eff}} < 0$ and $M_1 > 0$, flipping also the signs of A_λ and A_κ to avoid negative squared sfermion masses. In the following, we are going to describe how one can obtain valid points of the parameter space obeying the requirements mentioned in Sec. 4.5.3, using a negative bino mass.

Compared to the case of a positive bino mass, the flip of its sign will lead to an LSP with a much larger bino component. In order to increase its higgsino components, the value of μ_{eff} has to be closer to $|M_1|$, but still with μ_{eff} somewhat larger, in order to avoid a very small relic density. Even then, the LSP mass is still close to M_1 for relatively small values of $\tan\beta$, hence $|M_1| \gtrsim 130\,\text{GeV}$. Such small values for M_1 in the previous configuration led to a very strong "fine-tuning". However, now we are going to further increase the higgsino components in order to relax it. The correct relic density will be obtained by the larger higgsino component of the LSP and not by a resonance with a CP-even Higgs or co-annihilations with sleptons. The larger higgsino component will also lead to a larger σ^{SI} compared to a mostly bino LSP, however the cancellation that occurs with the negative bino mass will keep, as we will see, its value well below the LUX bound.

We give a sample point in Table 4.3 to make the description more concrete. We fix for simplicity both the left- and right-handed sleptons mass to 250 GeV and all the soft squark masses to 1.5 TeV. We have to note that using negative M_1, the theory becomes easily non-perturbative. In order to avoid a Landau pole below the GUT scale, we have to use even lower values for the parameters λ and κ. This fact, along with the small value of μ_{eff}, reduces the mass of the lightest Higgs. In order to obtain a

SM-like Higgs with mass $\sim 125\,\text{GeV}$, a large value of the trilinear soft SUSY breaking term A_t has to be used. The rest of the parameters will be fixed in order to satisfy the phenomenological constraints.

Parameters			
λ	0.539	M_1	-136
κ	0.492	M_2	-300
A_λ	270	M_3	-800
A_κ	-130.6	A_t	-2500
$\tan\beta$	3.35	A_b	-1000
μ_{eff}	150.5	A_e, A_μ, A_τ	500

Higgs masses	
$m_{H_1}(=m_{H_{SM}})$	124.3
m_{H_2}	220.4
m_{H_3}	479.9
$m_{A_1}(=m_{A_S})$	257.9
m_{A_2}	468.8
$m_{H^\pm}$	466.9

Sparticle masses			
$M_{\chi_1^0}$	-129.2	$m_{\tilde{g}}$	-951
$M_{\chi_2^0}$	157.6	$M_{\chi_1^\pm}$	-155.7
$M_{\chi_3^0}$	-170.1	$M_{\chi_2^\pm}$	328.5
$M_{\chi_4^0}$	309.2		
$M_{\chi_5^0}$	-328.5		

Components of χ_1^0	
N_{11}^2	0.777
N_{12}^2	0.001
N_{13}^2	0.168
N_{14}^2	0.043
N_{15}^2	0.011

Observables					
		$(\times 10^{-27}\,\text{cm}^3\,\text{s}^{-1})$			
Ωh^2	0.12	$\langle\sigma v\rangle_{WW}$	6.52	$\langle\sigma v\rangle_{\gamma\gamma}$	1.1
σ_p^{SI} [pb]	$4.57\cdot 10^{-10}$	$\langle\sigma v\rangle_{ZZ}$	3.72	$\langle\sigma v\rangle_{Z\gamma}$	0.8
σ_p^{SD} [pb]	$6.2\cdot 10^{-4}$	$\langle\sigma v\rangle_{b\bar{b}}$	0.02		
σ_n^{SD} [pb]	$4.8\cdot 10^{-4}$	$\langle\sigma v\rangle_{\tau\bar{\tau}}$	0.11		

Table 4.3: A sample point that satisfies all the phenomenological constraints, along with the latest LUX [45] upper limis. Dimensionful parameters are given in GeV, unless otherwise stated. All the soft slepton masses has been taken equal to 250 GeV and the squark masses to 1.5 TeV. The components of χ_1^0 are defined in Eq. (4.11).

Some remarks are in order. First, the scalar scattering cross section is indeed low, about 1 order of magnitude below the LUX bound, even with relatively large higgsino components. The smaller bino component improves the fine-tuning; the desired annihilation cross section to photons is achieved with m_{A_S} slightly further from the pole compared to the sample point of Table 4.2. The relic density is fitted to the observed value by the correct amount of the LSP higgsino component, thus the main annihilation channels are those with gauge bosons as final states. As a consequence, the cross section of the present-day neutralino annihilation to W^+W^- and ZZ is also large, but below the experimental limits, as it can be checked comparing the values of the

Tables 4.1 and 4.3. This comes from the fact that the neutralino annihilation to gauge bosons that determined the relic density was partly p-wave, through an s-channel CP-even Higgs exchange. The lightest pseudoscalar is again almost totally singlet-like, with reduced coupling to b quarks for the sample point $R^{bb}_{A_1} \simeq -4 \cdot 10^{-3}$. A last thing we have to notice is the larger value of the spin-dependent scattering cross section to nucleons, however still well below the current limits [276, 277].

4.6 Discussion

We have shown that the simplest version of the NMSSM (with a scale invariant superpotential) could explain a 130 GeV photon line from DM annihilation with $\sigma(\chi_1^0\chi_1^0 \to \gamma\gamma) > 10^{-27}$ cm^3 s^{-1} and, simultaneously, a 125 GeV SM-like Higgs boson. No additional fields or couplings need to be introduced. All constraints from WMAP on the relic density, from XENON100 and LUX on the direct detection cross section, from colliders and from precision observables can be satisfied.

However, the mass M_{A_S} of the singlet-like CP-odd Higgs scalar A_S has to satisfy accidentally $M_{A_S} \approx 2M_{\chi_1^0} \sim 260$ GeV to a precision $\lesssim 1$ GeV. We have shown that this fine-tuning can be relaxed using negative gaugino masses, following [269, 272], reducing at the same time the direct detection cross section.

Unfortunately a direct verification of this scenario at colliders through searches for a 130 GeV photon line seems hopeless: Due to the singlet-like nature of A_S, production cross sections for this state (as well as decay widths of sparticles or other Higgs bosons into this state) are too small. Only the mass of 130 GeV of the LSP χ_1^0 should fit the data, once searches for supersymmetry turn out to be successful. Of course, first of all the present hints for a 130 GeV photon line [210–213] need to be confirmed.

Part III

Asymmetric Dark Matter

CHAPTER 5

ASYMMETRIC DM AND UPPER BOUNDS ON ITS SELF-ANNIHILATION

So far, we have assumed that the present day density of DM is a relic of WIMP self-annihilation processes which occurred in the early Universe, through the thermal mechanism described in Sec. 1.4. Although this mechanism predicts that a WIMP would have "miraculously" a relic density with roughly the correct order of magnitude, its value is very sensitive to the WIMP self-annihilation cross section and the WIMP mass, and varies over many orders of magnitude as function of the unknown parameters in the models beyond the SM (BSM) attempting to explain the present DM relic density. Moreover, this mechanism is not able to address another important fact. In the cosmological Standard Model, the present day baryon density Ω_B and the DM relic density Ω_{DM} are of similar order of magnitude, $\Omega_{DM}/\Omega_B \approx 5.4$ (see Sec. 1.2.3). According to the thermal mechanism, the origin of Ω_{DM} would be completely disconnected from Ω_B, which is conventionally attributed to a baryon asymmetry η_B originating from CP violating processes in the early Universe. Their similar sizes result, then, from a numerical coincidence.

Asymmetric DM (ADM) (see [278–282] for some early discussions, and [283, 284] for reviews) is an attempt to explain the proximity of Ω_{DM} and Ω_B. The particles X forming the DM are assumed to be distinct from their antiparticles $\bar{X}$, and to carry a certain quantum number. The corresponding charge density of the Universe is assumed to be related to baryon number through equilibrium processes in the early hot Universe, such that the asymmetries η_B and η_X become related. If the $X - \bar{X}$ annihilation rate $\sigma_{X\bar{X}}$ is sufficiently large, the resulting X relic density will be determined exclusively by the asymmetry η_X. Then one obtains $\Omega_{DM} \simeq \frac{m_X \eta_X}{m_p \eta_B}\Omega_B$ (where m_p is the proton mass, and m_X the mass of the DM X particles), which gives the correct order if $\eta_X \approx \eta_B$.

In this chapter we aim at the calculation of the current DM density in the case that this is not determined by the thermal mechanism, but it is due to an asymmetry. In the next section we discuss the role of the chemical potential for the number densities of

particles and antiparticles and we will see that a particle may carry an asymmetry only when it is characterized by a conserved quantum number. Subsequently, we discuss the importance of the DM particle or antiparticle self-annihilation (XX or $\bar{X}\bar{X}$) for the determination of the final density. This analysis is based on [1]. A general discussion on this subject is presented on Sec. 5.2. In Sec. 5.3, we establish the Boltzmann equation for the $X-\bar{X}$ asymmetry for non-vanishing self-annihilation cross section σ_{XX}, and clarify the assumptions allowing for its model-independent integration. Our main results are upper bounds on this cross section, depending on the tolerated dilution of the initial $X-\bar{X}$ asymmetry. In Sec. 5.4, we study the consequences of this result for sneutrino and higgsino ADM scenarios and, subsequently, we consider the model with a term X^2LH/Λ in the superpotential introduced in [285], where the expression for σ_{XX} is different from the previous scenarios. A summary and conclusions are given in Sec. 5.5.

5.1 Chemical potential and number densities

We begin by reminding the thermal equilibrium distributions of a particle species i

$$f_i = \left[\exp\left(\frac{E_i-\mu_i}{T}\right)\pm 1\right]^{-1}. \tag{5.1}$$

The "plus" sign corresponds to fermions (*Fermi-Dirac statistics*) and the "minus" to bosons (*Bose-Einstein statistics*). The chemical potential is denoted by μ. We shall see its significance in the following.

We consider a process $12 \leftrightarrow 34$ in equilibrium. As always, the evolution of the phase-space densities of the species involved in the process is governed by the Boltzmann equation (1.25). If we neglect, for the moment, the expansion of the Universe, the equilibrium of this process requires that the densities should remain constant. Therefore, the collision term (1.29) should vanish. By examining (1.29), we see that this requires $f_1f_2(1\pm f_3)(1\pm f_4) - f_3f_4(1\pm f_1)(1\pm f_2) = 0$ or

$$\frac{f_1}{1\pm f_1}\frac{f_2}{1\pm f_2} = \frac{f_3}{1\pm f_3}\frac{f_4}{1\pm f_4}. \tag{5.2}$$

This condition is satisfied for both Bose-Einstein and Fermi-Dirac distributions (5.1), if the following relation among the chemical potentials holds

$$\mu_1+\mu_2 = \mu_3+\mu_4. \tag{5.3}$$

The above conclusion can be generalized in an obvious way for reactions involving more than two particles.

The existence of the chemical potential is always related to the conservation of a quantum number. For example, consider the bremsstrahlung reaction $e^-p \leftrightarrow e^-p\gamma$. The condition (5.3) (in a generalized form) implies that the chemical potential of the photons vanishes, $\mu_\gamma = 0$. In general, the chemical potential of any species whose

production is not constrained by the conservation of a quantum number must vanish in thermal equilibrium.

Another important fact is the relation between the chemical potentials of particle and antiparticles. The particle-antiparticle annihilation in equilibrium implies opposite chemical potentials for the two species. For example, this fact becomes obvious in an equilibrium lepton–antilepton annihilation to two photons. Therefore, in general

$$\mu_X = -\mu_{\bar{X}}. \tag{5.4}$$

The particle density for a species i can be obtained from the distribution functions (5.1) through integration over momenta as $n_i^{eq} = \frac{g_i}{(2\pi)^3}\int \mathrm{d}^3p f_i(\vec{p})$ – with g_i the internal degrees of freedom –, which can be transformed using $E/T \to y$ to (omitting the indices i)

$$n^{eq} = \frac{gT^3}{2\pi^2}\int_x^\infty \mathrm{d}y\, \frac{y\sqrt{y^2-x^2}}{\mathrm{e}^y\,\mathrm{e}^{-\mu/T} \pm 1}. \tag{5.5}$$

(As usual, $x \equiv m/T$.) This integral can be performed analytically only under some assumptions. First, we note that, in principle, the quantity μ/T has to be extremely small[1] ($\mu/T \sim 10^{-9}$). Additionally, in the current context, we are mainly interested in non-relativistic particles. In this case $\mathrm{e}^{(E-\mu)/T} \gg 1$, and both Fermi-Dirac and Bose-Einstein statistics (5.1) are degenerate to Maxwell-Boltzmann statistics, a justified approximation for $x \gtrsim 3$. In this case, the integration can be performed by means of the modified Bessel function of the second kind, K_2. Assuming a particle X with chemical potential μ and its antiparticle $\bar{X}$ (which has, as we mentioned, opposite chemical potential $-\mu$), their number densities, using Maxwell-Boltzmann statistics, are

$$n_X^{eq} = \frac{T}{2\pi^2}gm^2\mathrm{K}_2(m/T)\mathrm{e}^{\mu/T}\,, \qquad n_{\bar{X}}^{eq} = \frac{T}{2\pi^2}gm^2\mathrm{K}_2(m/T)\mathrm{e}^{-\mu/T}\,. \tag{5.6}$$

Concerning now the asymmetry – or, in other words, the (conserved) charge density – defined by $a^{eq} \equiv n_X^{eq} - n_{\bar{X}}^{eq}$, it will be given, still for Maxwell-Boltzmann statistics, just by the difference of Eqs. (5.6),

$$a^{eq} = \frac{T}{\pi^2}gm^2\mathrm{K}_2(m/T)\sinh\left(\frac{\mu}{T}\right) \simeq \frac{T}{\pi^2}gm^2\mathrm{K}_2(m/T)\left(\frac{\mu}{T}\right). \tag{5.7}$$

In the general case of Fermi-Dirac or Bose-Einstein statistics, this quantity would be given, using Eq. (5.5), by[2]

$$a^{eq} = \frac{gT^3}{6}\left(\frac{\mu}{T}\right)k(x), \tag{5.8}$$

where $k(x)$ is the integral

$$k(x) = \frac{6}{\pi^2}\int_x^\infty \mathrm{d}y\, \frac{y\sqrt{y^2-x^2}\mathrm{e}^y}{\left(\mathrm{e}^y \pm 1\right)^2}. \tag{5.9}$$

[1] Since, as we shall see below, the particle asymmetry is proportional to this quantity.

[2] It is useful to keep explicitly the term μ/T instead of μ, since this quantity is conserved during an adiabatic procedure [286].

Again, the "plus" sign holds for fermions and the "minus" for bosons. This integral has been defined in such a way that, in the ultrarelativistic limit $x \ll 1$, it takes the value 1 for fermions and 2 for bosons, while in the opposite limit $x \gg 1$ it vanishes in both cases[3].

5.2 Asymmetric DM self-annihilation

In supersymmetric scenarios, the discrete $\mathbb{Z}_N$ symmetry responsible for the stability of the particles X is equal to or related to R-parity. For instance, sneutrinos (left-handed or right-handed, mixtures thereof or mixtures with singlets) have been proposed as ADM [287–292]. Singlet extensions of the MSSM have been considered in [285, 293]. Recently, higgsinos have been suggested in [294], since they possess a conserved quantum number before the electroweak phase transition. In all these cases, the dark matter asymmetry can be related to the baryon and/or lepton asymmetry through sphaleron, gauge and Yukawa induced processes (see [295] and references therein). As long as the baryon/lepton asymmetry is generated at temperatures above the freeze out of the processes which transfer it to the ADM, this mechanism is independent from the precise CP and baryon/lepton number violating origin of the baryon asymmetry.

However, typically the discrete $\mathbb{Z}_N$ symmetry responsible for the stability of the particles X does not forbid $X - X$ self-annihilation processes, through the same couplings which transfer the baryon or lepton asymmetry to the X particles. Once $X - X$ self-annihilation processes are allowed, these processes can wash out the asymmetry η_X.

A rough condition for the absence of a wash-out is to require that, at temperatures of the order of the DM mass, the rate of these processes is below the Hubble expansion rate. Subsequently we study this phenomenon quantitatively in the form of the coupled set of Boltzmann equations for the symmetric and antisymmetric dark matter number densities. We find that the upper bounds on the self-annihilation cross section σ_{XX} are extremely strong if one wishes to obtain a final X number density which is dominated by its asymmetry η_X such that Ω_{DM} is related to Ω_B as described in the introduction of the current chapter.

Interestingly it turns out that, under typical assumptions as a large $X - \bar{X}$ annihilation rate, a fairly model independent upper bound on σ_{XX} (depending in a simple way on M_X and the s-wave or p-wave nature of the $X - X$ annihilation process) can be derived from the only condition that the X asymmetry is *not* reduced by a large amount. The determination of this upper bound is the main result of the current chapter. Subsequently, we apply it to sneutrino and higgsino ADM scenarios, and to the singlet extension of the MSSM proposed in [285] (in an approach similar to, but slightly different from [296]).

Our approach is based on the Boltzmann equations for the X and $\bar{X}$ number densities in the presence of an $X - \bar{X}$ asymmetry. Boltzmann equations in the presence

[3]The non-relativistic limit is also described by (5.7), where it is obvious that for $m \gg T$ the asymmetry vanishes due to the behavior of the Bessel function K_2.

of asymmetries have been considered previously e.g. in [296–299] where, however, the $X-X$ annihilation rate σ_{XX} was assumed to vanish. We find that even a small $X-X$ annihilation rate σ_{XX} can have a strong (negative) impact on the resulting $X-\bar{X}$ asymmetry.

5.3 Boltzmann equations for asymmetric DM

We consider a DM particle X and its antiparticle $\bar{X}$, with a common mass m and equilibrium number densities differing by a chemical potential μ. Assuming Maxwell-Boltzmann statistics, the equilibrium number densities are given by Eqs. (5.6). We assume that the $X-\bar{X}$ asymmetry has been generated during periods before the one considered here, through processes (such as sphaleron processes) which have frozen out. Since we assume that the $X-\bar{X}$ asymmetry is related to the baryon asymmetry, μ/T should be very small: $\mu/T \lesssim 10^{-9}$.

As usual, it is convenient to introduce number densities per comoving volume, $Y = n/s$, with s the entropy density (see Eq. (1.21)). Following the same procedure as in Sec. 1.4, the Boltzmann equations for Y_X and $Y_{\bar{X}}$ as functions of $x \equiv m/T$ become

$$\frac{\mathrm{d}Y_X}{\mathrm{d}x} = -\sqrt{\frac{\pi}{45G}}\frac{g_*^{1/2}m}{x^2}\left[\langle\sigma_{XX}v\rangle\left(Y_X^2 - Y_X^{eq\ 2}\right) + \langle\sigma_{X\bar{X}}v\rangle\left(Y_XY_{\bar{X}} - Y_X^{eq}Y_{\bar{X}}^{eq}\right)\right] , \quad (5.10a)$$

$$\frac{\mathrm{d}Y_{\bar{X}}}{\mathrm{d}x} = -\sqrt{\frac{\pi}{45G}}\frac{g_*^{1/2}m}{x^2}\left[\langle\sigma_{XX}v\rangle\left(Y_{\bar{X}}^2 - Y_{\bar{X}}^{eq\ 2}\right) + \langle\sigma_{X\bar{X}}v\rangle\left(Y_XY_{\bar{X}} - Y_X^{eq}Y_{\bar{X}}^{eq}\right)\right] \quad (5.10b)$$

where the effective number of degrees of freedom g_* is given by Eq. (1.39) and we have assumed that the self-annihilation cross sections satisfy $\sigma_{\bar{X}\bar{X}} = \sigma_{XX}$. We remind that the thermal average of the cross section times velocity $\langle\sigma v\rangle$ is given by Eq. (1.45), which we rewrite here

$$\langle\sigma v_{M\o l}\rangle = \frac{1}{8m^4T\mathrm{K}_2^2(x)}\int_{4m^2}^{\infty}\mathrm{d}s\,\sigma(s)(s-4m^2)\sqrt{s}\,\mathrm{K}_1(\sqrt{s}/T), \quad (5.11)$$

with K_1, K_2 the modified Bessel functions of the first and the second kind, respectively. In most cases $\langle\sigma v\rangle$ can be expanded in powers of the relative velocity of the incoming particles. Then, the thermal average is approximated by an expansion in powers of $1/x$:

$$\langle\sigma v\rangle \simeq a + bx^{-1} + \mathcal{O}\left(x^{-2}\right) , \quad (5.12)$$

with a and b given by Eq. (1.48).

5.3.1 Qualitative analysis

Before we proceed to the numerical solution of the coupled set of Eqs. (5.10a,5.10b), we will try to understand the features of these equations intuitively. To this end, it is useful to consider the difference and the sum of Y_X and $Y_{\bar{X}}$ defined by A and Z, respectively:

$$A = Y_X - Y_{\bar{X}}, \qquad Z = Y_X + Y_{\bar{X}} . \quad (5.13)$$

Their equilibrium expressions can be obtained from Eqs. (5.6) and (1.21) and are given by

$$Z^{eq} = \frac{45g}{2\pi^4}\frac{x^2K_2(x)}{h_{\rm eff}(m/x)}\cosh\left(\frac{\mu}{T}\right) , \qquad A^{eq} = \frac{45g}{2\pi^4}\frac{x^2K_2(x)}{h_{\rm eff}(m/x)}\sinh\left(\frac{\mu}{T}\right) . \tag{5.14}$$

Neglecting terms of $\mathcal{O}(\mu/T)^2$, these expressions read

$$Z^{eq} = \frac{45g}{2\pi^4}\frac{x^2K_2(x)}{h_{\rm eff}(m/x)} , \qquad A^{eq} = \frac{\mu}{T}Z^{eq} . \tag{5.15}$$

Then the Boltzmann equation for A becomes

$$\frac{{\rm d}A}{{\rm d}x} = -\sqrt{\frac{\pi}{45G}}\frac{g_*^{1/2}m}{x^2}\langle\sigma_{XX}v\rangle\left(ZA - Z^{eq}A^{eq}\right) . \tag{5.16}$$

Concerning the Boltzmann equation for the sum of densities Z, we assume that the self-annihilation cross section is much smaller than the particle–antiparticle annihilation, $\sigma_{XX} \ll \sigma_{X\bar{X}}$. Then, we can write

$$\frac{{\rm d}Z}{{\rm d}x} = -\sqrt{\frac{\pi}{45G}}\frac{g_*^{1/2}m}{x^2}\langle\sigma_{X\bar{X}}v\rangle\frac{1}{2}\left(Z^2 - A^2 - Z^{eq\ 2} + A^{eq\ 2}\right) . \tag{5.17}$$

Previously these Boltzmann equations were investigated in [296–299] under the assumption that A remains constant, i.e. that the right hand side of (5.16) vanishes.

If $\sigma_{X\bar{X}}$ is large enough, the freeze-out temperature is low, and $Z \sim Z^{eq}$ to a very good approximation over a long period, and finally $Z_{t\to\infty} \sim A$ up to corrections studied in [296, 299]. This is the desired result leading to a DM relic density determined by A which, in turn, is supposed to be related to the baryon asymmetry. During the period where $Z \sim Z^{eq}$, (5.16) simplifies to

$$\frac{{\rm d}A}{{\rm d}x} = -\sqrt{\frac{\pi}{45G}}\frac{g_*^{1/2}m}{x^2}\langle\sigma_{XX}v\rangle Z^{eq}\left(A - A^{eq}\right) , \tag{5.18}$$

which can be integrated with the usual initial condition $A_{in} \sim A^{eq}$ for $T \sim m$ or $x \sim 1$, and a given expression for $m\langle\sigma_{XX}v\rangle$. Note that it is A_{in} which is assumed to be related to the baryon asymmetry.

Eq. (5.18) may be written in the more intuitional form

$$\frac{{\rm d}A}{{\rm d}x} = -\sqrt{\frac{\pi}{45G}}\frac{g_*^{1/2}m}{x^2}\langle\sigma_{XX}v\rangle\left(\frac{\mu}{T}\right)^{-1}\left(AA^{eq} - A^{eq2}\right) . \tag{5.19}$$

Although Eq. (5.19) does not have the same form as the Boltzmann equation (1.38), which describes the density evolution of species without asymmetry, it exhibits a similar behavior. When the asymmetry A differs from its equilibrium value A^{eq}, the overall minus sign attracts its value to A^{eq}. The large factor $(\mu/T)^{-1}$ compensates for the small values of A and A^{eq}, and one expects that A freezes out at a freeze-out temperature

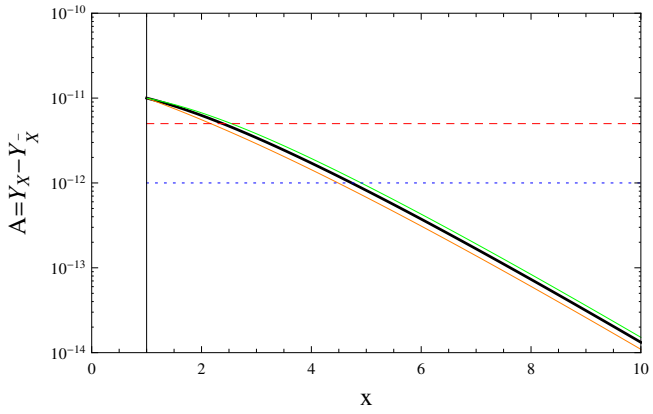

Figure 5.1: The evolution of the equilibrium asymmetry with the variable $x = m/T$, in the approximation of constant entropy degrees of freedom. The black line is the equilibrium asymmetry using Maxwell-Boltzmann statistics. Fermi-Dirac (green line) and Bose-Einstein (orange line) asymmetries per comoving volume are also presented, evaluated using the expression (5.8) divided by the entropy density. The chemical potential has been chosen in each case so that the initial asymmetry is fixed to 10^{-11} (in all cases $\mu/T \sim 10^{-9}$). The horizontal lines indicate $R = 0.5$ (dashed red) and $R = 0.1$ (dotted blue).

$T_f = m/x_f^A$ determined by the self-annihilation cross section $\langle\sigma_{XX}v\rangle$ in a similar way as the number density of species without asymmetry does.

The final asymmetry $A_\infty \equiv A_{t\to\infty}$ can be approximated by the equilibrium value of the asymmetry during its freeze-out, $A_\infty \sim A^{eq}(x_f^A)$. However, since Eq. (5.18) is linear in A, the ratio $R \equiv A_\infty/A_{in}$ is independent from A_{in} and hence independent from μ/T. The ADM paradigm requires that R is not too small; otherwise A_∞ is sensitive to $\langle\sigma_{XX}v\rangle$ as in usual DM scenarios, and $\Omega_{DM} \approx \Omega_B$ remains a numerical coincidence.

As we can see in Fig. 5.1, the equilibrium asymmetry falls rapidly. In order that a sizeable amount of the initial asymmetry survives, the freeze-out of the asymmetry has to occur rapidly after the particles X, $\bar{X}$ become non-relativistic. If we require that at least 10% of the initial asymmetry is maintained, the asymmetry freeze-out point has to be $x_f^A \lesssim 4.7$, whereas if this percentage is increased to at least half of the initial asymmetry, $x_f^A \lesssim 2.3$. In order to achieve a so early freeze-out, a very small value of the self-annihilation cross section is required. We will investigate this further by solving numerically the Boltzmann equations.

5.3.2 Numerical solution

Boltzmann equations belong to the general family of Riccati ordinary differential equations, quadratic in the unknown function. It is well known that Riccati equations exhibit a stiff behavior and special solving algorithms have to be used. One can use

an implicit solver, by means that the solution at each step will depend not only on x and the value of the unknown function of the previous step, but also on the solution of the current step itself. Therefore, at each step an algebraic equation has to be solved. However, since Riccati equations are, additionally, not linear, the convergence is not guaranteed. In the case of one single Boltzmann equation implicit methods might work (for example the implicit Adams-Moulton method used in DarkSUSY [300]). However, for a coupled set of Boltzmann equations, another method has to be applied.

The Rosenbrock method (see, for example, [301]) addresses the problem of convergence by the approximate linearization of the non-linear systems using derivatives. Actually, we found that the most appropriate algorithm for the solution of (5.10a,5.10b) is a 4-stage Rosenbrock method with an adaptive step-size. The step-size is fixed at each step according to the difference of the order 4 and order 3 solutions[4]. In practice, in order to control the tolerance, it is better to consider one of Eqs.(5.10) and their difference.

The dominant dependence on the parameters of the model originates from the combination $m\langle\sigma_{XX}v\rangle$ in (5.10), an additional weak dependence on m arises from the effective number of degrees of freedom in $h_{\rm eff}(m/x)$ in (5.15) and in g_*. For these we use the parametrization given in [302]. Now, R can be computed for any given expression for $m\langle\sigma_{XX}v\rangle$. We presume that $\sigma_{XX} \lesssim 10^{-5}\sigma_{X\bar{X}}$, so that we have $Z \simeq Z^{eq}$ for the relevant range of x, and the result for R is independent from $\sigma_{X\bar{X}}$ as it is obvious from (5.18). Assuming Eq. (5.12), we will consider the two cases

(a) purely s-wave annihilation: $\langle\sigma_{XX}v\rangle \simeq a$ and

(b) purely p-wave annihilation: $\langle\sigma_{XX}v\rangle \simeq b/x$,

although in practice one may find a combination of both. The results for R as function of $\log(ma)$ and $\log(mb)$ are shown in Fig. 5.2.

We see that within the cases (a) or (b) the dependence on m beyond the one in $m\langle\sigma_{XX}v\rangle$ is negligibly small, and we can deduce upper bounds on $m\langle\sigma_{XX}v\rangle$ as function of the tolerated reduction R of the asymmetry:

$$\begin{aligned} R>0.5: &\quad ma \lesssim 5\times10^{-17}\,\mathrm{GeV}^{-1}\ \text{(case (a))}, \quad mb \lesssim 1\times10^{-16}\,\mathrm{GeV}^{-1}\ \text{(case (b))}\,, \\ R>0.1: &\quad ma \lesssim 1\times10^{-15}\,\mathrm{GeV}^{-1}\ \text{(case (a))}, \quad mb \lesssim 5\times10^{-15}\,\mathrm{GeV}^{-1}\ \text{(case (b))}\,. \end{aligned} \tag{5.20}$$

Clearly, if we require only a moderate reduction of the asymmetry A, the freeze-out temperature $T_f^A = m/x_f^A$ must not be far below m, or x_f^A must not be too large. (Here we define x_f^A as the temperature where the expansion rate of the Universe becomes larger than the rate of self-annihilation, i.e. $H(x_f^A) = (n_X^{eq} - n_{\bar{X}}^{eq})\langle\sigma_{XX}v\rangle(x_f^A)$ which is solved numerically.) In Fig. 5.3 we show x_f^A as function of $\log(ma)$ and $\log(mb)$ and, indeed, x_f^A is well below 5 if the first of the conditions (5.20) is satisfied.

[4] A solution y_p is defined as order p if the Taylor series for the exact solution $y(x_0+h)$ and for y_p coincide up to (and including) the term h^p.

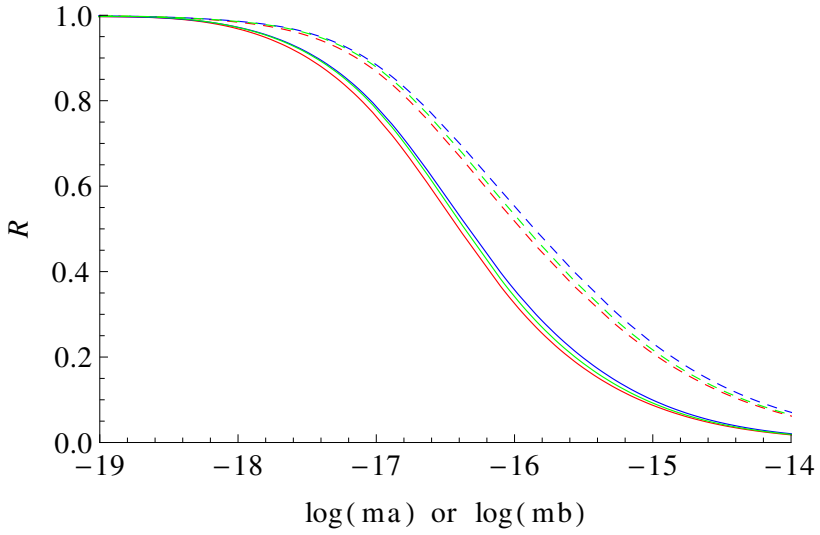

Figure 5.2: The ratio $R \equiv A_\infty/A_{in}$ of the final asymmetry over the initial asymmetry as a function of $\log(ma)$ or $\log(ma)$, with ma or mb in GeV. The solid lines represents the values of R if $\langle\sigma_{XX}v\rangle = a$, and the dashed lines the values of R if $\langle\sigma_{XX}v\rangle = b/x$. The color corresponds to the mass of the DM particle, red for $m = 10\,\text{GeV}$, green for $m = 100\,\text{GeV}$ and blue for $m = 1\,\text{TeV}$.

The requirement for a not too large value of x_f^A and the fact that $\langle\sigma_{XX}v\rangle(x_f^A) \sim \mathrm{e}^{x_f^A}$ explains why we obtain $\langle\sigma_{XX}v\rangle \ll \langle\sigma_{X\bar{X}}v\rangle$; the desired value of x_f in case of $X - \bar{X}$ annihilation is rather of $\mathcal{O}(20)$.

5.4 Implications for specific models

In this section we study the implications of the upper bounds on σ_{XX} that we have obtained in the previous section for various models for supersymmetric ADM.

5.4.1 Sneutrino ADM

Left-handed sneutrinos or mixtures of left- and right-handed sneutrinos (or singlets) have been proposed as ADM in [287–292]. Clearly, left-handed sneutrinos $\tilde{\nu}_L$ can self-annihilate through processes of the form $\tilde{\nu}_L + \tilde{\nu}_L \to \nu_L + \nu_L$ by the exchange of electroweak gauginos in the t-channel. Electroweak gauginos are the binos with mass M_1, and winos with mass M_2. The corresponding expression for $\langle\sigma_{\tilde{\nu}_L\tilde{\nu}_L}v\rangle$ can be obtained from [303], and reads in the limit $M_1,\ M_2 \gg m$

$$\langle\sigma_{\tilde{\nu}_L\tilde{\nu}_L}v\rangle \simeq \frac{g_2^4}{16\pi}\left(1 - \frac{3}{2x}\right)\left(\frac{\tan^2\theta_w}{M_1} + \frac{1}{M_2}\right)^2 \tag{5.21}$$

where g_2 is the $SU(2)_L$ gauge coupling and θ_w the weak mixing angle. If one assumes universal gaugino masses at the GUT scale, M_1 and M_2 are related by $M_1 \simeq M_2/2$

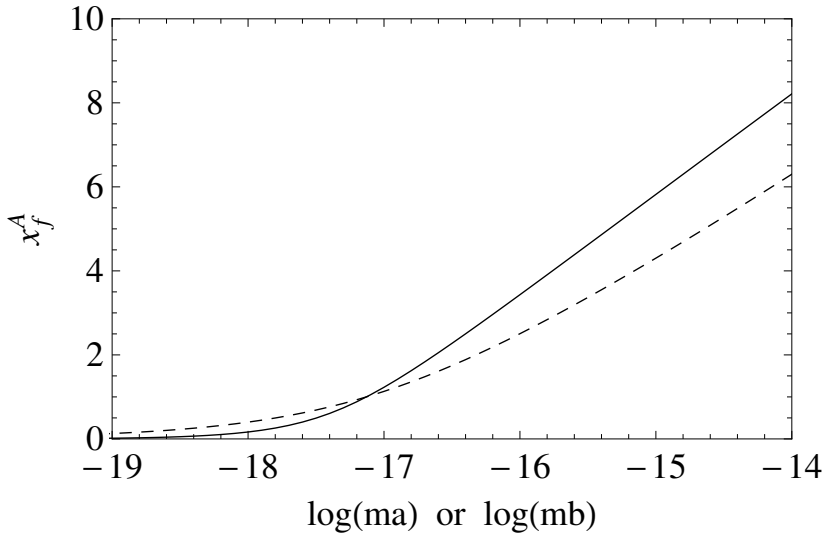

Figure 5.3: The freeze-out point $x_f^A = \frac{m}{T_f^A}$ as a function of $\log(ma)$ (solid line) and $\log(mb)$ (dotted line).

and, with $\tan^2\theta_w \approx 0.3$, (5.21) simplifies to

$$\langle \sigma_{\tilde{\nu}_L \tilde{\nu}_L} v \rangle \simeq \frac{g_2^4}{8\pi} \left(1 - \frac{3}{2x}\right) \frac{1}{M_2^2} \,. \tag{5.22}$$

From Fig. 5.2, the first term leads to stronger constraints, and applying the conservative bound $R > 0.1$ (case (a)) from (5.20) leads to

$$M_2 \gtrsim 3 \times 10^7 \text{ GeV} \times \left(\frac{m}{100 \text{ GeV}}\right)^{1/2} \tag{5.23}$$

which excludes gaugino masses of the order of the electroweak scale. (Even for such large gaugino masses the sneutrino-antisneutrino annihilation rate would remain large due to processes with slepton exchange in the t-channel.)

If the ADM X consists in a mixture of left-handed sneutrinos $\tilde{\nu}_L$ and right-handed sneutrinos or other electroweak singlets, the result depends on the $\tilde{\nu}_L$ component of X or the mixing angle $\sin\delta$ where $X = \tilde{\nu}_L \sin\delta + \ldots$:

$$\langle \sigma_{XX} v \rangle \simeq \frac{g_2^4 \sin^4\delta}{8\pi} \left(1 - \frac{3}{2x}\right) \frac{1}{M_2^2} \,. \tag{5.24}$$

Now the same argument leads to

$$\sin^2\delta \lesssim 3.3 \times 10^{-6} \times \frac{M_2}{\sqrt{m \cdot 100 \text{ GeV}}} \,. \tag{5.25}$$

Hence, for $M_2 \approx m \approx 100$ GeV, $\sin\delta$ has to be very small independently from constraints from direct DM detection experiments – or, for mixing angles $\sin\delta \approx 1$, one is lead back to (5.23).

5.4.2 Higgsino ADM

Higgsinos $\tilde{h}_u$, $\tilde{h}_d$ with masses $m \sim 200 - 1000$ GeV as ADM were proposed recently in [294]. Before the electroweak phase transition (where the Higgs vevs develop), higgsinos can be considered as mass eigenstates. Through sphaleron, gauge and Yukawa interactions at high temperature, a higgsino asymmetry $A_{\tilde{h}_u} \sim A_{\tilde{h}_d}$ proportional to the baryon asymmetry is generated [294, 295]. If the higgsinos are the LSPs (lightest supersymmetric particles) and other sparticles are sufficiently heavy, this asymmetry could survive until today [294] provided the $\tilde{h}_u\tilde{h}_u$ (and $\tilde{h}_d\tilde{h}_d$) self-annihilation rates are sufficiently small.

However, higgsinos have the same couplings to electroweak gauginos as sneutrinos, and can again self-annihilate into H_u, H_d (to be considered as eigenstates before the electroweak phase transition) through t-channel exchange of binos and winos. This time the scattering process is a p-wave process (case (b) in (5.20)) and we obtain from [268] (again for $M_1,\ M_2 \gg m$)

$$\langle \sigma_{\tilde{h}_u\tilde{h}_u} v\rangle = \langle \sigma_{\tilde{h}_d\tilde{h}_d} v\rangle \simeq \frac{3g_2^4}{x8\pi}\left(\frac{\tan^2\theta_w}{M_1}+\frac{1}{M_2}\right)^2 . \tag{5.26}$$

Applying again the conservative bound $R > 0.1$ (case (b)) from (5.20) leads to the same constraint on M_2 as in (5.23), which is close to the estimated bound on gaugino masses given in [294] from the same argument.

5.4.3 The $\Delta W \sim XXHL/\Lambda$ model

Left-handed sneutrinos and higgsinos as ADM tend to violate bounds on direct DM detection cross sections (unless mass splittings are introduced leading to inelastic scattering [292, 294]). Moreover, as we have seen in the previous section, constraints from sufficiently small self-annihilation cross sections are very strong. These constraints would be alleviated, if the asymmetry is transferred to lighter essentially inert particles. A simple model of that kind has been proposed in [285], where a gauge singlet scalar superfield X and a superpotential

$$\Delta W = \frac{1}{\Lambda} X X H_u L_i \tag{5.27}$$

are introduced. (Here H_u denotes a Higgs superfield, and L_i any left-handed lepton superfield.) This non-renormalizable interaction can originate from integrating out heavy vector-like sterile neutrinos or electroweak doublets [285] with mass $\sim \Lambda$, typically $\gtrsim 1\,\text{TeV}$. Another singlet chiral superfield $\bar{X}$ should be introduced to allow for a supersymmetric Dirac mass term M_X for the fermionic components $\psi_X\psi_{\bar{X}}$, e.g. via a NMSSM-like singlet S with $\langle S\rangle \neq 0$ and a coupling $\lambda' S X \bar{X}$ in the superpotential.

$\psi_{\bar{X}}$, ψ_X would carry lepton number ± 1, respectively. The superpotential (5.27) breaks the usual R parity, but preserves a $\mathbb{Z}_4$ symmetry which allows for the decay of the usual LSP into $\psi_X\psi_X$ [285]. At high temperature where the processes induced by (5.27) are in equilibrium together with sphaleron, gauge and Yukawa interactions,

these imply an asymmetry A_X of $\sim 35\%$ of the baryon asymmetry [285,296], the precise value depending on whether top quarks and squarks are still in equilibrium when the interactions from (5.27) decouple. Assuming a sufficiently rapid $\psi_X - \bar{\psi}_X$ annihilation rate and $M_X \sim 11 - 13$ GeV, the relic density is then automatically of the correct order.

After electroweak symmetry breaking, the superpotential (5.27) gives rise to an interaction of the form

$$\frac{v_u}{\Lambda}\psi_X\psi_X\tilde{\nu}_i \ . \tag{5.28}$$

(Subsequently we omit the neutrino/sneutrino index i.) The sneutrino $\tilde{\nu}$ does not have to be the LSP; the LSP can be the lightest neutralino $\tilde{\chi}$. Then an on-shell sneutrino $\tilde{\nu}$ would decay via the usual vertex $g\tilde{\nu}\tilde{\chi}\nu$ – where g is of the order of electroweak gauge couplings, if $\tilde{\chi}$ is dominantly bino-like – into $\tilde{\chi}$ plus a neutrino ν. At energies below the sneutrino mass $m_{\tilde{\nu}}$, integrating out the sneutrino leads to an effective four Fermi interaction

$$\frac{g v_u}{m_{\tilde{\nu}}^2\Lambda}\psi_X\psi_X\tilde{\chi}\nu \ . \tag{5.29}$$

At energies above $M_{\tilde{\chi}}$, (5.29) allows for the scattering process $\psi_X\psi_X \to \tilde{\chi}\nu$. However, assuming $M_{\tilde{\chi}} > 2M_X$, the lightest neutralino $\tilde{\chi}$ is not stable. Since $\tilde{\chi}$ is a Majorana fermion, (5.29) leads to its decay into $\psi_X\psi_X\nu$ and $\bar{\psi}_X\bar{\psi}_X\bar{\nu}$ with corresponding branching ratios of 50%. The latter case leads to the scattering process

$$\psi_X\psi_X \to \bar{\psi}_X\bar{\psi}_X\bar{\nu}\bar{\nu} \ . \tag{5.30}$$

As in the case of sneutrinos and higgsinos, this ADM self-annihilation process can have potentially disastrous consequences for the remaining asymmetry. In [285], the rate for this process has been estimated by integrating out both the sneutrino $\tilde{\nu}$ and the lightest neutralino $\tilde{\chi}$ with the result that, for $m_{\tilde{\nu}} \sim M_{\tilde{\chi}} \sim 100\,\text{GeV}$ and $\Lambda \gtrsim 1\,\text{TeV}$, it would go out of equilibrium (drop below the Hubble expansion rate) for decoupling temperatures T_D somewhat above M_X, in which case the asymmetry would hardly be washed out.

A more detailed analysis of the ADM self-annihilation processes has been performed in [296]. There it was pointed out that, for $m_{\tilde{\nu}} \sim M_{\tilde{\chi}} \sim 100$ GeV and $\Lambda \gtrsim 1$ TeV, the dominant ADM self-annihilation process is *real* $\tilde{\chi}$ production through the interaction (5.29), and the corresponding cross section was given.

Subsequently, in [296], T_D was estimated by equating the ADM self-annihilation rate with the Hubble expansion rate. They tolerated a considerable wash-out of the asymmetry and/or a Boltzmann suppression for $T_D < M_X$, and studied the necessary relations between the final values for A_∞ and Z_∞ defined in (5.13) (or $r_\infty = (Z_\infty - A_\infty)/(Z_\infty + A_\infty)$), the DM mass M_X and the lightest neutralino mass $M_{\tilde{\chi}}$ required for a desired DM relic density. Clearly, in most of the parameter space (after a considerable wash-out of the asymmetry and/or Boltzmann suppression), the desired DM relic density is no longer simply related to the baryon asymmetry in contrast to ADM paradigm.

Here we ask the question under which conditions this does *not* happen, i.e. under which conditions the initial asymmetry A_X determines essentially the DM relic density.

As before we assume that the $\psi_X - \bar{\psi}_X$ annihilation rate is sufficiently large, such that we can assume $Z \sim Z^{eq}$ in (5.16) leading to (5.18).

If the threshold for the process (5.30) would be $s > 4M_X^2$, we could apply our previous formulas. However, for the (dominant) annihilation process via *real* $\tilde{\chi}$ (plus neutrino) production, the threshold is $s > M_{\tilde{\chi}}^2 > 4M_X^2$. As a consequence the thermal average of the cross section times velocity in (5.18) depends in a more complicated way on M_X, $M_{\tilde{\chi}}$ and notably on the temperature or $x = M_X/T$ such that the expansion (5.12) is no longer applicable. First, we use the cross section $\sigma_{XX}(s)$ for the process $\psi_X \psi_X \to \tilde{\chi}\bar{\nu}$ from [296]:

$$\sigma_{XX}(s) = \frac{\kappa^2 M_{\tilde{\chi}}^4}{256\pi} \frac{1}{s} \left(\frac{s}{M_{\tilde{\chi}}^2} - 1 \right)^2 \tag{5.31}$$

where $\kappa = \frac{g v_u}{\Lambda m_{\tilde{\nu}}^2}$. Then, using (5.11) with $M_{\tilde{\chi}}^2$ as lower threshold of the integral (without expanding in $M_X/M_{\tilde{\chi}}$ as in [296]), we obtain

$$\langle \sigma_{XX} v \rangle = \frac{\kappa^2}{16\pi} \left(\frac{M_{\tilde{\chi}}}{M_X} \right)^2 \frac{(M_{\tilde{\chi}}^2 - 4M_X^2) \mathrm{K}_2(\frac{M_{\tilde{\chi}}}{M_X} x) + \frac{6 M_{\tilde{\chi}} M_X}{x} \mathrm{K}_3(\frac{M_{\tilde{\chi}}}{M_X} x)}{x^2 \mathrm{K}_2^2(x)} \,. \tag{5.32}$$

For $M_X \ll M_{\tilde{\chi}}$, $\langle \sigma_{XX} v \rangle$ is proportional to $M_{\tilde{\chi}}^{7/2} \mathrm{e}^{-M_{\tilde{\chi}}/T}$ like the collision term evaluated in [296]. The Boltzmann suppression $\sim \mathrm{e}^{-M_{\tilde{\chi}}/T}$ is an obvious consequence of the threshold $s > M_{\tilde{\chi}}^2$ required for real $\tilde{\chi}$ production. Subsequently we integrate the Boltzmann equation (5.18) numerically employing (5.32) for $\langle \sigma_{XX} v \rangle$, which allows us to study $R \equiv A_\infty / A_{in}$ as before. Now, however, R depends in a more complicated way on the parameters κ, $M_{\tilde{\chi}}$ and M_X of the model. On the other hand, the initial asymmetry is quite well known in this class of models, $A_{in} \sim 0.35\, B$ (where B is the baryon asymmetry), and finally we must obtain

$$\frac{\Omega_{DM}}{\Omega_B} = \frac{A_\infty M_X}{B m_p} \sim 5.4 \tag{5.33}$$

which determines M_X in terms of A_∞ or R:

$$M_X \sim (12.5\,\mathrm{GeV})/R \,. \tag{5.34}$$

Hence, once the correct ADM relic density is imposed, the free parameters of the model are $\kappa = \frac{g v_u}{\Lambda m_{\tilde{\nu}}^2}$, $M_{\tilde{\chi}}$ and M_X or R. In order to clarify the correlations between these parameters, we show R in the range $R = 1 \ldots 0.1$ ($M_X = 12.5 \ldots 125\,\mathrm{GeV}$) as function of $M_{\tilde{\chi}}$ for various values of $\kappa \leq 10^{-5}\,\mathrm{GeV}^{-2}$ in Fig. 5.4. (Note that all curves continue horizontally along $R = 1$ beyond their upper end.)

The shape of these curves can be understood as follows: Near the upper end, $R \sim 1$, $M_X \sim 12.5$ GeV and practically no wash-out takes place by construction, since $\langle \sigma_{XX} v \rangle$ is too small. For fixed κ, $\langle \sigma_{XX} v \rangle$ increases for decreasing $M_{\tilde{\chi}}$ due to $\langle \sigma_{XX} v \rangle \sim \mathrm{e}^{-M_{\tilde{\chi}}/T}$, and below some critical value of $M_{\tilde{\chi}}$, $\langle \sigma_{XX} v \rangle$ is large enough such that R starts to decrease.

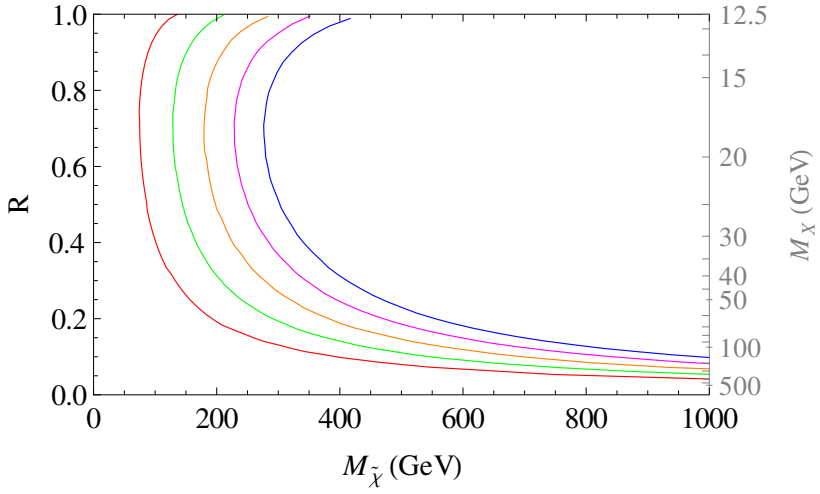

Figure 5.4: R as function of $M_{\tilde{\chi}}$ for different values of κ: red $\kappa = 10^{-9}\,\mathrm{GeV}^{-2}$, green: $\kappa = 10^{-8}\,\mathrm{GeV}^{-2}$, orange: $\kappa = 10^{-7}\,\mathrm{GeV}^{-2}$, magenta: $\kappa = 10^{-6}\,\mathrm{GeV}^{-2}$, blue: $\kappa = 10^{-5}\,\mathrm{GeV}^{-2}$. The mass M_X of the dark matter, related to R as in (5.34), is indicated on the right vertical axis.

If a sizeable wash-out takes place ($R \lesssim 0.5$), it stops when the annihilation rate falls below the Hubble expansion rate, i.e. for a given value of $\langle\sigma_{XX}v\rangle$. For fixed κ, this implies a certain fixed value for $\mathrm{e}^{-M_{\tilde{\chi}}/T_D}$ or $M_{\tilde{\chi}}/T_D$. Using $x_D = M_X/T_D$ and (5.34) one easily derives $R \sim 1/(x_D M_{\tilde{\chi}})$, which explains the decrease of R for increasing $M_{\tilde{\chi}}$ in this range.

Fig. 5.4 allows to identify the regions in parameter space in which R is not too small ($R \gtrsim 0.5$), i.e. where Ω_{DM} follows naturally from Ω_B as in the ADM paradigm. If the coefficient κ is relatively large, $\kappa \sim 10^{-5}\,\mathrm{GeV}^{-2}$ or $m_{\tilde{\nu}} \sim 100\,\mathrm{GeV}$ and $\Lambda \sim 1\,\mathrm{TeV}$, one needs $M_{\tilde{\chi}} \gtrsim 300\,\mathrm{GeV}$. If $\tilde{\chi}$ is lighter, $M_{\tilde{\chi}} \sim 100\,\mathrm{GeV}$, one needs a very small value of $\kappa \lesssim 10^{-9}\,\mathrm{GeV}^{-2}$, hence correspondingly large values of $m_{\tilde{\nu}}$ and/or Λ.

5.5 Discussion

If the dark matter asymmetry is related to the baryon (or lepton) asymmetry, some couplings must necessarily relate these sectors. The same couplings can lead to dark matter self-annihilation processes, which can wash out the corresponding asymmetry A. A rough condition for the absence of a wash-out is to require that, at temperatures of the order of the DM mass, the rate of these processes is below the Hubble expansion rate. In Sec. 5.3 we have studied the corresponding set of Boltzmann equations quantitatively (assuming a two-body final state). Requiring a modest wash-out ($A_\infty/A_{in} \gtrsim 0.1$), the upper bounds on $m\langle\sigma_{XX}v\rangle$ are very strong, and can be deduced from Fig. 5.2 if $\langle\sigma_{XX}v\rangle \sim a$ or $\langle\sigma_{XX}v\rangle \sim b/x$.

If the ADM consists in sparticles with couplings to electroweak gauginos (left-

handed sneutrinos or higgsinos), it follows that the electroweak gauginos must be extremely heavy such that supersymmetry does not solve the hierarchy problem. If the ADM consists in particles like right-handed sneutrinos which mix weakly with left-handed sneutrinos, the mixing angle must be very small, see Eq. (5.25).

In different models for ADM, the dominant ADM self-annihilation process may be kinematically possible only for s above a threshold larger than $(2M_X)^2$, in which case it becomes Boltzmann suppressed and Eq. (5.12) is no longer valid. An example is the popular $\Delta W \sim XXHL/\Lambda$ model of [285]. Also in this case, the numerical integration of the Boltzmann equation for the asymmetry allowed us to specify the range of parameters where the wash-out of the asymmetry remains modest.

In the past, the constraints following from the absence of a wash-out of the asymmetry have sometimes been neglected or underestimated (notably in the case of sneutrinos); we hope that the present work helps to clarify the relevance of ADM self-annihilation processes and the resulting conditions on corresponding models.

Of course, in the case of sizeable ADM couplings to Higgs or Z bosons, the direct detection rate must be studied and must not exceed present bounds [47]. (See [304] for a discussion of the potential conflict between a sufficiently large $X - \bar{X}$ annihilation rate and a too large direct detection rate.) A too large direct detection rate can be avoided through mass splittings leading to inelastic scattering [292, 294]. Alternatively, one may consider that the X particles – after their density has frozen out to a value related to the baryon density – decay later into other essentially inert particles with very small couplings, which have not been in thermal equilibrium. In the present treatment, we left aside the problem of direct detection rates.

CHAPTER 6

A SPECIFIC MODEL FOR ASYMMETRIC DM

We have seen so far that although a symmetry implying stable WIMPs may arise due to independent phenomenological reasons, in principle there is no such symmetry forbidding the self-annihilation of weakly interacting massive particles or antiparticles. In the context of asymmetric DM, we derived in the previous chapter quite severe upper bounds on the cross section of these self-annihilation processes. In some cases, the symmetry forbidding self-annihilation is imposed ad hoc (see, for example, [299]). In this chapter, we try to build a model that provides an asymmetric DM, without any assumptions imposed "by hand".

Since the existence of an asymmetry is closely connected with the conservation of a quantum number, the sneutrino could, in principle, be a suitable ADM candidate. A general discussion will follow in Sec. 6.1. We will see that in order to obtain ADM with the desired characteristics, Dirac masses for the neutrinos have to be imposed. The additional degrees of freedom of the Dirac neutrinos may affect the relativistic degrees of freedom during Big Bang Nucleosynthesis (BBN). We discuss this issue in Sec. 6.2. Eventually, we proceed to the main part of our work based on [3]. Details of the model will be presented in Sec. 6.3, where we also discuss possible constraints from particle physics and cosmology. An analysis of the ADM in this model will follow in Sec. 6.4. Finally, in Sec. 6.5 we summarize our results.

6.1 Sneutrinos as asymmetric DM

At first sight, sneutrinos are promising candidates for asymmetric DM [287–292][1]. They carry a conserved quantum number, lepton number, such that they can share the asymmetry of charged leptons through processes which were in equilibrium in the

[1] Higgsinos could also be ADM, but only if a number of strong constraints is satisfied, see [294] and Sec. 5.4.2.

early hot Universe. Then, their asymmetry can have become related to the baryon asymmetry through sphaleron processes [295, 305]. However, although the large annihilation cross section between sneutrinos and anti-sneutrinos is a good feature allowing for ADM, their self-annihilation cross sections are also typically large, destroying the asymmetry (see Sec. 5.4.1).

However, non-zero neutrino masses suggest the existence of right-handed neutrinos (and sneutrinos). In the past years, a variety of models aiming at the explanation of neutrino masses have been proposed, some of them described very briefly in Sec. 3.6. We can classify them into two main categories, those which employ Majorana mass terms for right-handed neutrinos and those employing Dirac mass terms only. The former allow for various versions of seesaw mechanisms, amongst others the inverse seesaw which allows for electroweak scale right-handed neutrinos. The common characteristic of these models is the violation of lepton number by a Majorana mass term. Dirac neutrino masses are less well studied, though not less motivated. We recall that the simplest way to obtain Dirac masses for neutrinos is the introduction of Yukawa couplings to Higgs bosons, but with unnatural small Yukawa coupling constants. A more elegant way is the introduction of an additional Higgs field which couples only to right-handed neutrinos. Then, the smallness of neutrino masses is no longer due to small values of coupling constants, but can be due to a small vacuum expectation value (vev) of the new Higgs field.

The presence of right-handed sneutrinos opens new possibilities for sneutrino DM: right-handed sneutrinos with a small left-handed component may have at the same time a large pair annihilation cross section, but a negligible self-annihilation cross section. However, in scenarios such as seesaw models which do not conserve lepton number, an asymmetry of sneutrinos is difficult to maintain due to oscillations between sneutrinos and anti-sneutrinos [306–308] (see also [309]). In the Dirac case with small Yukawa couplings, asymmetric DM faces the following difficulties: First, the annihilation cross section, proportional to the small couplings, is not adequate to eliminate the symmetric part of the DM, resulting in a large relic density unrelated to the asymmetry. Second, such small Yukawa couplings keep the right-handed neutrinos and sneutrinos out of equilibrium in the early Universe and, as a result, the asymmetry of the sneutrinos was never related to the baryonic asymmetry. However, if the small neutrino masses originate from the small vev of an additional Higgs field (but with large Yukawa couplings), these difficulties are solved.

Such scenarios, often denoted as *neutrinophilic Higgs doublet models*, appeared first in [310,311] (for an earlier approach, but with Majorana neutrinos, see [312]). In these models, a $\mathbb{Z}_2$ symmetry is spontaneously broken generating a small vev of the new Higgs scalar. This mechanism results also in a very light scalar with mass of the order of eV. Such light scalars have been ruled out [313, 314] by astrophysical arguments. However, the $\mathbb{Z}_2$ symmetry can be replaced by a global $U(1)$ symmetry in order to forbid Majorana masses, but which is broken explicitly so that a very light scalar is avoided [315]. The $U(1)$ symmetry makes very small explicit breaking terms (see below) more natural. The LHC phenomenology of this model is studied in [316], while in [317] a supersymmetric variant based on the MSSM and its phenomenology are

examined. The additional Higgs doublets still allow the SUSY version to be embedded into a grand unified symmetry as verified in [318]. Furthermore, the additional Higgs doublets do not spoil proton stability since they couple only to leptons. In [319], the Higgs potential is studied for both SUSY and non-SUSY models. Scenarios for leptogenesis with neutrinophilic Higgs are discussed in [320–322]. Finally, the sneutrino of the SUSY model of [317] has been used as DM candidate in [218,323]. In particular, the possibility of ADM is also considered in [323], but with a trilinear soft coupling of the order of several TeV and a (related) very large annihilation cross section into monochromatic photons.

Subsequently, we will consider the NMSSM extended by a pair of neutrinophilic Higgs doublets and three generations of right-handed neutrino superfields. Although the NMSSM singlet superfield $\widehat{S}$ plays no particular role in our model (the vev of its bosonic component could be replaced by a constant dimensionful parameter), it is chosen for the reasons explained in Ch. 3. Namely, the solution of the μ-problem of the MSSM through the introduction of the singlet S and the naturally heavier, compared to the MSSM, SM-like Higgs due to the additional coupling λ, making the observed 125 GeV mass easier to explain.

We are going to explore whether and under which circumstances this model can accommodate right-handed sneutrinos as ADM. We find that this is indeed possible under certain conditions. First, we note that the ordinary Higgs sector of the NMSSM is not affected by the introduction of the neutrophilic Higgses (henceforth ν-Higgses). The scalar ν-Higgses, however, have to be relatively heavy of the order of $\mathcal{O}(1)$ TeV such that the additional degrees of freedom of the Dirac neutrinos do not lead to ^{4}He overabundance through their contribution to the expansion rate of the Universe during big bang nucleosynthesis (BBN). On the other hand, light ν-higgsinos are required for a large sneutrino–anti-sneutrino pair annihilation cross section which is necessary for the sneutrino relic density to be determined by its asymmetry.

6.2 Big Bang Nucleosynthesis and neutrinos

In the Dirac notation, a spin-1/2 fermion that is different from its antiparticle is described by a complex spinor and has four degrees of freedom (two for the spin states of the particle and two for the antiparticle). Majorana particles have only the half number of degrees of freedom, since particles and antiparticles coincide. In case neutrinos are Dirac particles, their additional degrees of freedom may affect the Big Bang Nucleosynthesis (BBN) by increasing the energy density of the Universe during this epoch and, therefore, accelerate its expansion.

We recall that the expansion rate of the Universe at a given moment (temperature) of its history is determined by its energy density ρ; in a radiation dominated era $H = \left(\frac{8\pi}{3} G_N \rho\right)^{1/2}$, where G_N is the gravitational constant. If a particle species A went out of the equilibrium from the thermal bath while still relativistic, it continues to contribute to the energy density with its own temperature T_A that is redshifting ($T_A R^3 = \text{const.}$, with R the scale factor). On the other hand, even though the temperature of the

thermal bath T_γ is also decreasing due to the expansion, the decrease rate falls off each time the temperature falls below the mass of one of the particle species that constitute the thermal bath. Thereafter, the annihilation of these particles is heating the bath, transferring finally all of their entropy to it.

The abundance of ^{4}He emerging from BBN depends on the Hubble expansion rate of the Universe when processes like $e^- p \leftrightarrow n \nu_e$ and $e^+ n \leftrightarrow p \bar{\nu}_e$ were in equilibrium, since practically all the remaining neutrons after these processes went out of equilibrium have been incorporated to the helium nuclei. The larger the Hubble rate was, the faster (at higher temperature) neutrons went out of equilibrium, resulting in their larger abundance (the equilibrium density of neutrons falls as $n_n^{eq} \sim \exp(-\frac{\Delta m}{T}) n_p^{eq}$ with $\Delta m \equiv m_n - m_p$ the mass difference between neutron and proton).

In the epoch just before nucleosynthesis photons, electrons and left-handed neutrinos were in equilibrium[2] at a common temperature $T_{\gamma,n}$ (henceforth, the subscript n on temperatures will denote the epoch just before nucleosynthesis). Right-handed neutrinos remained in equilibrium as long as processes $\nu_R \bar{\nu}_R \leftrightarrow l \bar{l}$ (with l a charged lepton) were fast enough. However, even after right-handed neutrinos went out of equilibrium at a temperature $T_{R,d}$ (where the subscript d stands for decoupling), they continue to contribute to the total energy density of the Universe with their own temperature T_R that is redshifting.

The energy density at this time is the sum of the energy density of species in equilibrium plus the energy density of the relativistic particles that have already decoupled:

$$\begin{aligned} \rho_n &= \rho_{eq} + \rho_R \\ &= \frac{\pi^2}{30}\left[g_\gamma + \frac{7}{8}(g_e + N_L g_\nu)\right] T_{\gamma,n}^4 + \frac{\pi^2}{30} N_R g_\nu T_{R,n}^4, \end{aligned} \tag{6.1}$$

with N_L,N_R the number of left- and right-handed neutrino generations, respectively. Writing the above energy density in the form

$$\rho_n = \frac{\pi^2}{30}\left[g_\gamma + \frac{7}{8}\left(g_e + \mathcal{N}_{\text{eff}}\, g_\nu\right)\right] T_{\gamma,n}^4, \tag{6.2}$$

$\mathcal{N}_{\text{eff}}$ is defined as $\mathcal{N}_{\text{eff}} = N_L + N_R \left(\frac{T_{R,n}}{T_{\gamma,n}}\right)^4$. Taking $N_L = N_R = 3$ we write $\mathcal{N}_{\text{eff}} = 3 + \Delta N_\nu$ with

$$\Delta N_\nu \equiv 3 \left(\frac{T_{R,n}}{T_{\gamma,n}}\right)^4. \tag{6.3}$$

We are going to relate, eventually, the ratio of the temperatures during nucleosynthesis that appears in the expression above to the temperature when the right-handed neutrinos decoupled (see also [324]). We begin by considering a general case with particle species A that decoupled from the thermal bath while relativistic ($T_{A,d} > m_A$)

[2]The neutrinos decouple from the thermal plasma at a temperature $T_d \gtrsim 1\,\text{MeV}$, when H becomes larger than the rate of the processes $\nu\bar{\nu} \to e^+e^-$. Nevertheless, even after their decoupling but before the decoupling of the electrons, their temperature is the same as the one of photons since both are decreasing with the same rate.

and since then they have their own temperature T_A. We will consider two instants of the history of the Universe: the first is when the photons had a temperature $T_{\gamma,i}$ with $T_{\gamma,i} < T_{A,d}$ and the second much after the decoupling (it can be the present time) with temperature $T_{\gamma,f} \ll T_{A,d}$ (notice that both are after the decoupling of A). The temperatures of the particles A at these moments are $T_{A,i}$ and $T_{A,f}$, respectively. During this period, the entropy is conserved separately for the particles A and for the thermal bath. Therefore, with s_A, s_t denoting the entropy density of the particles A and the total entropy density of the thermal bath, respectively, we have

$$s_A(T_{A,i})R^3(T_{\gamma,i}) = s_A(T_{A,f})R^3(T_{\gamma,f}) \qquad \text{and} \tag{6.4}$$

$$s_t(T_{\gamma,i})R^3(T_{\gamma,i}) = s_t(T_{\gamma,f})R^3(T_{\gamma,f}), \tag{6.5}$$

with R the scale factor. Using the expression[3] $s_i(T) = \frac{2\pi^2}{45} g_i T_i^3$ for the entropy density, the above equations combined are leading to the formula

$$\left(\frac{T_{A,i}}{T_{\gamma,i}}\right)^3 = \frac{g(T_{\gamma,i})}{\sum_{d,rel} g_d \left(\frac{T_{d,f}}{T_{\gamma,f}}\right)^3 + g_\gamma} \left(\frac{T_{A,f}}{T_{\gamma,f}}\right)^3, \tag{6.6}$$

where the sum is running over all particles decoupled after $T_{\gamma,i}$ while being relativistic.

We apply the above formula for the case of left-handed neutrinos. As initial temperature we take $T_{\gamma,i} = m_e$, i.e. just before the thermal bath is starting to be heated by the annihilation of the electrons. Until then, $T_L = T_\gamma$, so that (6.6) will give

$$\left(\frac{T_{L,f}}{T_{\gamma,f}}\right)^3 = \frac{4}{11}. \tag{6.7}$$

In this case, there were no relativistic species decoupled in between. Applying Eq. (6.6) to the right-handed neutrinos, we have to use Eq. (6.7), since left-handed neutrinos, which decoupled at a later time while relativistic, continue to contribute to the total entropy. As initial temperature we choose again the temperature at which one species started to heat the bath for the first time after the decoupling of right-handed neutrinos, so that $T_{A,i} = T_{\gamma,i}$ and

$$\left(\frac{T_{R,f}}{T_{\gamma,f}}\right)^3 = \frac{43}{11 g(T_{R,d})}. \tag{6.8}$$

$g(T_{R,d})$ is the number of the degrees of freedom that the thermal bath possesses just after the decoupling of the right-handed neutrinos. Last, we will apply for a third time the Eq. (6.6) concerning again the decoupling of right-handed neutrinos but taking as initial moment the nucleosynthesis (actually just before the nucleosynthesis as discussed above). Then

$$\frac{T_{R,n}}{T_{\gamma,n}} = \left(\frac{11}{4}\right)^{1/3} \frac{T_{R,f}}{T_{\gamma,f}}, \tag{6.9}$$

[3]Henceforth, we assume for simplicity that g_i include the factor $\frac{7}{8}$ in the case that i is a fermion.

which combined with (6.8) gives the desired relation among the ratio $T_{R,n}/T_{\gamma,n}$ and the temperature $T_{R,d}$.

Finally, using (6.3),(6.8) and (6.9) we derive the final result

$$g(T_{R,d}) = \frac{43}{4}\left(\frac{3}{\Delta N_\nu}\right)^{3/4}. \tag{6.10}$$

This expression allows to calculate the number of relativistic degrees of freedom $g(T_{R,d})$ during the decoupling of the right-handed neutrinos for a specific contribution ΔN_ν to the effective degrees of freedom $\mathcal{N}_{\text{eff}}$ during BBN. From $g(T_{R,d})$ one can extract the temperature when the decoupling occurred.

6.3 The model

In the following, we present the model we propose in order to provide a viable candidate for ADM. We extend the NMSSM by three right-handed neutrino superfields $\widehat{\nu}_R^c$ and a pair of new Higgs doublets $\widehat{H}_u^\nu$ and $\widehat{H}_d^\nu$. These fields are charged under a new global $U(1)$ symmetry with charges -1, $+1$ and -1, respectively, while the usual NMSSM superfields remain uncharged. The superpotential is written as

$$W = W^{\text{NMSSM}} + y_\nu \widehat{L}\cdot\widehat{H}_u^\nu\widehat{\nu}_R^c + \lambda_\nu \widehat{S}\widehat{H}_u^\nu\cdot\widehat{H}_d^\nu, \tag{6.11}$$

where the Yukawa coupling y_ν and the superfields $\widehat{L}$ and $\widehat{\nu}_R^c$ should be understood as matrix and vectors, respectively, in flavor space. The corresponding soft SUSY breaking masses and couplings are

$$\begin{aligned} -\mathcal{L}_{\text{soft}} = -\mathcal{L}_{\text{soft}}^{\text{NMSSM}} + m_{H_u^\nu}^2|H_u^\nu|^2 + m_{H_d^\nu}^2|H_d^\nu|^2 + m_{\nu_R}^2|\nu_R|^2 \\ + y_\nu A_\nu L\cdot H_u^\nu\nu_R^c + \lambda_\nu A_{\lambda_\nu} S H_u^\nu\cdot H_d^\nu. \end{aligned} \tag{6.12}$$

W^{NMSSM} and $\mathcal{L}_{\text{soft}}^{\text{NMSSM}}$ are the superpotential and the soft terms of the $\mathbb{Z}_3$-invariant NMSSM, given in Sec. 3.2 by Eqs. (3.1) and (3.4), respectively.

The new $U(1)$ symmetry needs to be broken by the vev of the ν-Higgs in order to give masses to the neutrinos. To this end we include to the Lagrangian (6.12) the following additional soft terms

$$A_{\lambda_1} S H_u\cdot H_d^\nu + A_{\lambda_2} S H_u^\nu\cdot H_d.$$

It is important to note that these two terms do not correspond to terms in the superpotential. Since they break the $U(1)$ explicitly, it is natural in the 't Hooft sense for the trilinear couplings A_{λ_i} to assume small values. Such small values can be obtained through higher dimensional operators involving SUSY and $U(1)$ symmetry breaking spurion fields [317]. For instance, introducing a superfield $\widehat{X}$ with charge $-1/2$ under $U(1)$ and with $\langle X\rangle = \theta^2 F + \sqrt{F}$ (see, e.g., [196] for similar mechanisms), a trilinear soft term can originate from the operator $\frac{1}{M_{Pl}^2}\left|\widehat{X}^2\widehat{S}\widehat{H}_u^\nu\cdot\widehat{H}_d\right|_F \sim \frac{F^{3/2}}{M_{Pl}^2} S H_u^\nu\cdot H_d$. If

$F = m_I^2$ with $m_I \simeq \sqrt{vM_{Pl}}$ an intermediate scale where supersymmetry is broken, then $\frac{F^{3/2}}{M_{Pl}^2} \sim 10^{-7}\,\text{GeV}$, while the corresponding term in the superpotential is suppressed by several orders of magnitude.

The resulting vevs for the H_u^ν, H_d^ν fields have the form [312]

$$v_u^\nu \simeq \frac{A_{\lambda_2} s}{m^2_{H_u^\nu}}\, v_d \quad \text{and} \quad v_d^\nu \simeq \frac{A_{\lambda_1} s}{m^2_{H_d^\nu}}\, v_u, \tag{6.13}$$

respectively. Taking $A_{\lambda_1} s \simeq A_{\lambda_2} s \sim 10^{-5}\,\text{GeV}^2$ and assuming soft masses $m_{H_d^\nu} \sim m_{H_u^\nu} \sim \mathcal{O}(1)\,\text{TeV}$ (see below), then $v_u^\nu \simeq v_d^\nu \sim$ eV. Hence, the first extra term in the superpotential (6.11) will generate Dirac neutrino masses of the correct order for $y_\nu \sim \mathcal{O}(1)$ [310, 315].

The sneutrino mass squared symmetric matrix, neglecting flavor indices, reads in the basis $(\widetilde{\nu}_L, \widetilde{\nu}_R)$

$$\mathcal{M}^2_{\widetilde{\nu}} = \begin{pmatrix} y_\nu^2 v_u^{\nu 2} + \frac{1}{2} g^2 (v_d^2 - v_u^2) + m^2_{\nu_L} & y_\nu v_u^\nu (\lambda_\nu s + A_\nu) \\ & y_\nu^2 v_u^{\nu 2} + m^2_{\nu_R} \end{pmatrix}. \tag{6.14}$$

Taking into account the small value of v_u^ν, this matrix can be approximated by the diagonal form

$$\mathcal{M}^2_{\widetilde{\nu}} \simeq \text{diag}\left[\frac{1}{2} g^2 (v_d^2 - v_u^2) + m^2_{\nu_L},\, m^2_{\nu_R}\right]. \tag{6.15}$$

We note that the mixing between the various sneutrino flavors in the right-handed sector is small, since it is proportional to the vev of the ν-Higgs provided that $m_{\nu_R^i} \gg v_u^\nu$ and flavour diagonal.

The ν-Higgses form two nearly degenerate SU(2) doublets. (Since $U(1)$ is not spontaneously broken, there are no Goldstone bosons.) These additional fields mix very weakly with the standard Higgs fields due to their small vevs; in the following we will consider the new Higgs fields completely unmixed.

The mass matrices in the neutral sector are in the basis (H_u^ν, H_d^ν) [325]

$$\mathcal{M}^2_{H^\nu} = \begin{pmatrix} \lambda_\nu^2 s^2 - \frac{1}{2} g^2 (v_d^2 - v_u^2) + m^2_{H_u^\nu} & \pm\lambda_\nu (\lambda v_u v_d - \kappa s^2 + A_{\lambda_\nu} s) \\ & \lambda_\nu^2 s^2 + \frac{1}{2} g^2 (v_d^2 - v_u^2) + m^2_{H_d^\nu} \end{pmatrix} \tag{6.16}$$

with plus (minus) signs in the off-diagonal elements for the scalar (pseudoscalar), and

$$\mathcal{M}^2_{H^{\nu +}} = \begin{pmatrix} \lambda_\nu^2 s^2 + \frac{1}{2} g^2 (v_d^2 - v_u^2) \cos 2\theta_W + m^2_{H_u^\nu} & \lambda_\nu (\lambda v_u v_d - \kappa s^2 + A_{\lambda_\nu} s) \\ & \lambda_\nu^2 s^2 - \frac{1}{2} g^2 (v_d^2 - v_u^2) \cos 2\theta_W + m^2_{H_d^\nu} \end{pmatrix} \tag{6.17}$$

in the charged ν-Higgs sector. The neutral and charged ν-higgsinos, forming Dirac fermions with masses $\mu' = \lambda_\nu s$, are also practically unmixed with the neutralinos and the charginos of the NMSSM.

6.3.1 Constraints from lepton flavour violation and BBN

A first constraint on the model originates from the muon decay to an electron and a photon. The charged Higgs $H^{\nu+}$ mediates the decay of the muon at one loop with a branching ratio [326]

$$\mathrm{BR}\,(\mu \to e\gamma) = \frac{\alpha_{EM}}{24\pi}\left(\frac{v}{v_\nu m_{H^{\nu+}}}\right)^4 \left|\sum_j m_j^2 U_{ej}^* U_{\mu j}\right|^2 , \tag{6.18}$$

where U is the Pontecorvo–Maki–Nakagawa–Sakata (PMNS) matrix defined by $|\nu_l\rangle = \sum_{j=1}^3 U_{lj}^\star\,|\nu_j\rangle$, with $l = e,\ \mu,\ \tau$ and $j = 1,\ 2,\ 3$ corresponding to the three mass eigenstates (see Sec. 3.6). The unitarity of the PMNS matrix allows to replace the sum in Eq. (6.18) by $\sum_j m_j^2 U_{ej}^* U_{\mu j} = -\Delta m_{21}^2 U_{e1}^* U_{\mu 1} + \Delta m_{32}^2 U_{e3}^* U_{\mu 3}$, where the mass squared differences are defined by $\Delta m_{ij}^2 \equiv m_i^2 - m_j^2$ and m_i are the neutrino mass eigenvalues. Using the upper 90% C.L. limit

$$\mathrm{BR}\,(\mu \to e\gamma) < 5.7 \cdot 10^{-13} \tag{6.19}$$

from the MEG experiment [327], we obtain a lower bound on the charged ν-Higgs mass,

$$m_{H^{\nu+}} \gtrsim \left(\frac{1\,\mathrm{eV}}{v_\nu}\right) 300\,\mathrm{GeV}, \tag{6.20}$$

where we have used the standard values for Δm_{21}^2, Δm_{32}^2 given in [100] and the elements of the PMNS matrix.

A second constraint comes from the Helium abundance that is determined by the relativistic degrees of freedom during BBN, as explained in the previous section. Recently, Planck constrained this quantity to $\mathcal{N}_{\mathrm{eff}} = 3.30 \pm 0.27$ at 68% C.L. [9]. In the following we determine the lowest temperature $T_{R,d}$ at which the right-handed neutrinos can decouple without $\mathcal{N}_{\mathrm{eff}}$ exceeding the above limit, and subsequently we derive the necessary condition on the $\nu_R\,\bar{\nu}_R \leftrightarrow l\,\bar{l}$ rate for this to occur.

As we saw, applying entropy conservation separately for the decoupled species and the thermal bath, one obtains the relation (6.10) between the maximally allowed value of ΔN_ν^{max} and the temperature at which the right-handed neutrinos went out of equilibrium. For $\Delta N_\nu^{max} \lesssim 0.57$ at 1σ, $g(T_{R,d}) \geq 37.35$. This means that decoupling should have occurred before the quark-hadron phase transition when $g = 51.25$ (just after the transition the number of degrees of freedom was $g = 17.25$, see Table A.1 in App. A). Assuming that the QCD confinement temperature is roughly $T_c \simeq 200\,\mathrm{MeV}$ [328], we are led to the inequality $T_{R,d} \gtrsim 200\,\mathrm{MeV}$.

Taking into account the approximate decoupling condition $n(T_d)\langle\sigma v\rangle(T_d) = H(T_d)$, one finds that the ratio of the decoupling temperatures of right- and left-handed neutrinos is

$$\left(\frac{T_{R,d}}{T_{L,d}}\right)^3 = \sqrt{\frac{g(T_{L,d})}{g(T_{R,d})}}\frac{\sigma_L}{\sigma_R}, \tag{6.21}$$

with σ_L and σ_R the cross sections of the processes that were keeping left- and right-handed neutrinos, respectively, in equilibrium. In the current model, the process

$\nu_R \bar{\nu}_R \leftrightarrow l \bar{l}$, which keeps right-handed neutrinos in equilibrium, is mediated by the charged ν-Higgses. Using $\frac{\sigma_L}{\sigma_R} = \left(\frac{2\sqrt{2} m_{H^{\nu+}}}{y_\nu^{li} v_u |U_{li}|}\right)^4$ [315], where U_{li} are again the elements of the PMNS mixing matrix, leads to the following bound on the charged Higgs mass and the couplings y_ν^{li}

$$\frac{m_{H^{\nu+}}}{y_\nu^{li}} \gtrsim 3\,\text{TeV}. \tag{6.22}$$

As we will explain later, the couplings y_ν^{li} cannot be very small, and as a consequence $m_{H^{\nu+}}$ has to be relatively large.

6.4 Right-handed sneutrinos as ADM

In the following we study more closely the role of right-handed neutrinos as ADM. We will use the notation $N \equiv \widetilde{\nu}_{R1}^c$ with the index 1 denoting the lightest among the three right-handed neutrinos. Its mass m_N is essentially its soft SUSY breaking mass, and we safely assume that it is a pure state since its left-handed component is negligibly small.

6.4.1 Asymmetry from sphaleron processes and the ADM mass

Since the sneutrinos carry a conserved charge (lepton number), it is possible that their relic density is not determined by the thermal mechanism but by their asymmetry. The asymmetry was related to the baryon asymmetry through equilibrium processes in the early Universe. These allow to estimate the relation between the two asymmetries and, ultimately, to determine the mass range of the (right-handed sneutrino) DM that will provide the correct abundance.

If the N, N^* annihilation is strong enough such that the less frequent species has been completely eliminated, the remaining abundance is the product of the charge density $\eta_N \equiv |n_N - n_{N^*}|$ times its mass m_N (n denotes the number density). The relation between the DM relic density Ω_N and the baryonic relic density Ω_b is

$$\Omega_N = \frac{\eta_N}{B} \frac{m_N}{m_p} \Omega_b, \tag{6.23}$$

where m_p is the proton mass, which gives the desired result if η_N is of same order of magnitude as the baryon charge density B.

The charge density of a particle X in kinetic equilibrium as a function of the temperature can be written as (see Sec. 5.1)

$$\eta_X(T) = \frac{T^3}{6} g_X k(x) \frac{\mu_X}{T}, \tag{6.24}$$

where we have assumed that $\mu_X/T \ll 1$, and μ_X is the chemical potential of the species X. g_X is the number of internal degrees of freedom of the particle X, we defined $x \equiv \frac{m_X}{T}$,

and

$$k(x) = \frac{6}{\pi^2}\int_x^\infty \mathrm{d}y\, y\sqrt{y^2-x^2}\frac{\mathrm{e}^y}{(\mathrm{e}^y \pm 1)^2}. \tag{6.25}$$

In the above integral, the plus (minus) sign holds for fermions (bosons). In the ultra-relativistic limit $x \ll 1$, k takes the values 1 for fermions and 2 for bosons, while in the opposite limit $x \gg 1$ it vanishes in both cases.

A sneutrino asymmetry can originate from primordial asymmetries in the baryonic or leptonic sectors. Although we will be agnostic about the exact mechanism that created these primordial asymmetries, the fact that certain processes were in equilibrium in the early Universe can be used to relate η_N to the baryon asymmetry B. We note that common mechanisms for thermal leptogenesis would not work in the present framework since the violation of lepton number is far too small (see the next section). However, other known mechanisms are possible, such as the Affleck-Dine mechanism [329].

In the absence of lepton number violating processes other than electroweak sphalerons, $\sum_{i=1}^3 (B/3 - L_i)$ is conserved. The relatively large Yukawa coupling constants of the neutrinos assure not only the equilibrium of the right-handed neutrinos with the thermal bath in the early Universe, but also rapid flavor changing processes. As a result, lepton flavor equilibrium had been established and $B-L = \sum_{i=1}^3 (B/3 - L_i)$ is conserved. However, the sphaleron processes were still violating $B+L$. We are going to consider two cases [305]. In the first case we will assume that sphaleron processes were rapid only above the electroweak phase transition (EWPT), e.g. if the EWPT was strongly first order. In the second case, we will allow the sphaleron processes to violate $B+L$ also below the transition, until they went out of equilibrium because of the expansion of the Universe.

In the first case we proceed along the lines of [295], where one can find a complete list of the equilibrium reactions in the MSSM and the relations between the chemical potentials. The reactions specific to the present model lead to the following equilibrium relations which have to be added to this list:

$$\begin{aligned} &\mu_{L^i} + \mu_H = \mu_{\nu^i}, \quad \mu_H = \mu_{H_u^\nu} = \mu_{H_d^\nu}, \\ &\mu_{\widetilde{L}^i} + \mu_H = \mu_{\widetilde{\nu}_i}, \quad \mu_{\widetilde{L}^i} + \mu_{\widetilde{H}} = \mu_{\nu_i}, \quad \mu_{L^i} + \mu_{\widetilde{H}} = \mu_{\widetilde{\nu}_i}, \end{aligned} \tag{6.26}$$

where we have used the notation of [295], i.e. μ_{L^i} is the chemical potential of the left-handed leptons, i is the flavor index, μ_ν is the chemical potential of the right-handed neutrinos and *tilde* stands for the supersymmetric particles. The sneutrinos share the chemical potential with the neutrinos through the equilibrium of processes such as those of Fig. 6.1.

Eliminating the chemical potentials using the sphaleron equilibrium relation

$$\sum_{i=1}^3 (3\mu_{Q_i} + \mu_{L_i}) = 0 \tag{6.27}$$

and the fact that the total hypercharge Y of the Universe vanishes, we can calculate the baryon charge B and the DM leptonic charge η_N densities as functions of the

Figure 6.1: Annihilation diagrams of right-handed sneutrinos N, N^* into neutrinos and charged leptons.

conserved difference $B - L$. We assume all the masses of supersymmetric particles except these of sleptons much larger than the EWPT critical temperature T_c, and we also consider SM particles as massless. First, assuming light right-handed sneutrinos and masses $\sim 2T_c$ for the other sleptons, we find, using Eqs. (6.24), (6.25), that the charge densities B and η_N are related by

$$B \simeq 0.14\,(B-L) \quad \text{and} \quad \eta_N \simeq 0.10\,(B-L), \quad \text{(light sleptons)} \tag{6.28a}$$

while for large slepton masses

$$B \simeq 0.18\,(B-L) \quad \text{and} \quad \eta_N \simeq 0.12\,(B-L). \quad \text{(heavy sleptons)} \tag{6.28b}$$

The DM mass, using (6.23) and $\Omega_N/\Omega_b \simeq 5.44$ [9], has to be $m_N \sim 7.1 - 7.6\,\text{GeV}$ (the smaller value corresponding to light sleptons).

In case the process induced by electroweak sphalerons were rapid also below the EWPT, the relations between the chemical potential are altered. First, due to the vacuum condensate of the neutral Higgs bosons, their chemical potentials have to vanish. However, the total hypercharge has no longer to be zero since $SU(2)_L$ has been broken, resulting in a non-zero chemical potential for the W bosons. Generalizing the SM equilibrium processes of [305] we find, considering all the supersymmetric particles (except for the right-handed sneutrinos) as heavy, again using Eqs. (6.24) and (6.25),

$$B \simeq 0.18\,(B-L) \quad \text{and} \quad \eta_N \simeq 0.10\,(B-L). \quad \text{(heavy SUSY paricles)} \tag{6.29a}$$

The resulting DM mass in this case has to be $m_N \simeq 9.2\,\text{GeV}$. However, allowing the left-handed sneutrinos to be light (with mass around the temperature at which the sphaleron processes went out of equilibrium), the value for the ratio B/η_N becomes maximal:

$$B \simeq 0.31\,(B-L) \quad \text{and} \quad \eta_N \simeq 0.07\,(B-L). \quad \text{(light LH sneutrinos)} \tag{6.29b}$$

In this case the DM mass has to be larger, $m_N \simeq 23\,\text{GeV}$.

Summarizing, depending on the sparticle spectrum and the nature of the EWPT, the DM mass can be roughly in the range

$$m_N \sim 7\,\text{GeV} \; - \; 23\,\text{GeV}. \tag{6.30}$$

The lowest value corresponds to light sleptons and a first order EWPT that terminated the sphaleron processes, while for the highest value the sphaleron processes have to continue to be in equilibrium for a short time after the EWPT and the left-handed sneutrinos have to be relatively light.

6.4.2 Constraints from oscillations, self and pair annihilation

In order that the current DM density is determined by its asymmetry, a number of conditions have to be fulfilled. First, the annihilation of DM particles with antiparticles has to be strong enough so that one of them is completely depleted. However, in many cases, it is possible for a particle to oscillate into its antiparticle and vice versa. These oscillations, if rapid enough, might lead to a continuous repopulation of the depleted particles. As a result, however strong the pair annihilation cross section is, the antiparticles (or the particles) are never exhausted and, finally, the thermal mechanism is responsible for the relic density. Furthermore, if self-annihilation[4] of DM particles occurs before the DM particles become non-relativistic, their asymmetry decreases rapidly due to this annihilation. If the self-annihilation does not freeze-out sufficiently fast, the thermal mechanism takes over again since there is no asymmetry left after the particle–antiparticle annihilation freeze-out. We will show that the sneutrino DM considered here can fulfill all these criteria for a successful asymmetric DM candidate.

Quantum mechanical oscillations would occur between N and N^* if these are not coincide with the mass eigenstates. Then the rate of N – N^* conversion is approximately given by the mass difference δm of the two eigenstates. The conversion starts to be significant only at times larger than δm^{-1} or, expressed in terms of the temperature T of the Universe, for $T \lesssim T(\delta m)$ given by [307]

$$T(\delta m) \sim \left(\frac{g_*^{1/2}}{h_{\rm eff}} \sqrt{\frac{45}{4\pi^3}} M_{Pl}\, \delta m \right)^{1/2}, \tag{6.31}$$

where M_{Pl} is the Planck mass and g_* and $h_{\rm eff}$ are effective degrees of freedom (see App. A for exact definitions).

A mass split appears if there exists a lepton number violating Majorana mass term m_M; if $m_M \ll m_D$ (m_D is the Dirac mass), the mass split can be written as $\delta m \simeq \frac{m_M^2}{m_D}$. The operator $\frac{1}{M_{Pl}^4} |X^4 S N^2|_F$, with X the superfield spurion whose vev brakes the $U(1)$ symmetry, induces a tiny Majorana mass squared of the order $m_M^2 \simeq 10^{-32}\,\mathrm{GeV}^2$, which corresponds to a mass difference $\delta m \sim 10^{-33}\,\mathrm{GeV}$ for $m_D \sim 10\,\mathrm{GeV}$. With such a small value for the Majorana mass, the oscillations start very late in the history of the Universe (see (6.31)), much later than the DM freeze-out (at $T \sim 1\,\mathrm{GeV}$), and do not affect the final DM density.

We recall that if the self-annihilation cross section does not obey the bounds (5.20) derived in the previous chapter, the asymmetry falls rapidly. In order that at least 90% of the asymmetry survives, the decoupling of self-annihilation should happen before

[4] the particle–particle or the antiparticle–antiparticle annihilation.

$x \equiv m_N/T \sim 5$ (we recall that the decoupling for WIMPs occurs at $x \sim 20$ – 30). However, in our case the possible annihilation of right-handed sneutrinos into two neutrinos through t- or u-channel exchange of neutral ν-higgsinos is impossible due to the Dirac nature of the ν-higgsinos. Furthermore, the left-handed components in N and N^* are sufficiently small, since they are induced only by the off-diagonal element of the mass matrix (6.14) and hence many orders of magnitude below the bound (5.20). Consequently, the self-annihilation cross sections of N or N^* are sufficiently small.

Having shown that the asymmetry does not get destroyed by oscillations or self annihilations, the condition that remains to be satisfied is a sufficiently strong N, N^* pair annihilation. This is required so that only the DM asymmetry survives as relic density. The dominant annihilation channels of right-handed sneutrinos are the annihilation into neutrinos and charged leptons (Fig. 6.1). The former proceeds through a t-channel neutral ν-higgsino exchange, the latter by charged ν-higgsino exchange. The thermal average of the cross section of these processes times velocity can be written as (to leading order in x^{-1})

$$\langle \sigma v \rangle \simeq f \, \frac{y_\nu^4}{8\pi} \frac{m_N^2}{(m_N^2 + \mu'^2)^2} x^{-1}, \tag{6.32}$$

where the factor $f = 18$ counts the number of final states (9 neutrinos and 9 charged leptons) and we have assumed a common value y_ν for the coupling constants y_ν^{li}. The s-wave contribution is helicity suppressed and can be neglected (see also [330]).

In the usual symmetric DM case, the thermally averaged cross section during freeze out has to be of the order of the thermal cross section, roughly given by (see section Sec. 1.4.1)

$$\langle \sigma v \rangle_{th} \simeq \frac{3 \cdot 10^{-27}}{\Omega_{DM} h^2} \, \mathrm{cm^3 s^{-1}} \simeq 3 \cdot 10^{-26} \, \mathrm{cm^3 \, s^{-1}}. \tag{6.33}$$

In the asymmetric DM scenarios, the pair annihilation cross section must be equal to or larger than the thermal cross section; even if the cross section is much larger than its thermal value, the final density remains constant since annihilations become impossible due to the lack of N or N^*. Examining eq. (6.32) at fixed m_N, the cross section decreases with increasing mass μ' of the ν-higgsino.

Fig. 6.2 shows the maximal value of the ν-higgsino mass as function of the coupling constant y_ν for a sufficiently large annihilation cross section. The corresponding minimal allowed mass of the lightest scalar charged ν-Higgs (from the condition that $\mathcal{N}_{\mathrm{eff}}$ is within the 1σ region determined by Planck) is shown along the upper axis. For a light right-handed sneutrino mass (7 GeV) the coupling constant has to be relatively large, $y_\nu \gtrsim 0.6$, which requires $m_{H_1^\nu} \gtrsim 1.8\,\mathrm{TeV}$. Smaller values of y_ν (and lower bounds on the scalar ν-Higgs mass) are allowed for heavier DM. For $m_N = 23\,\mathrm{GeV}$, the smallest allowed value for the ν-Higgs mass is $\sim 1\,\mathrm{TeV}$.

We see that the right-handed sneutrino can have a relic density determined by its asymmetry if the ν-higgsino is relatively light, while the scalar ν-Higgs should be heavy. The ν-higgsino mass is given, in terms of the coupling λ_ν in the NMSSM Lagrangian and the singlet vev s, by $\mu' = \lambda_\nu \, s$ and hence it is small for small λ_ν, whereas a heavy charged ν-Higgs requires a large soft SUSY breaking mass.

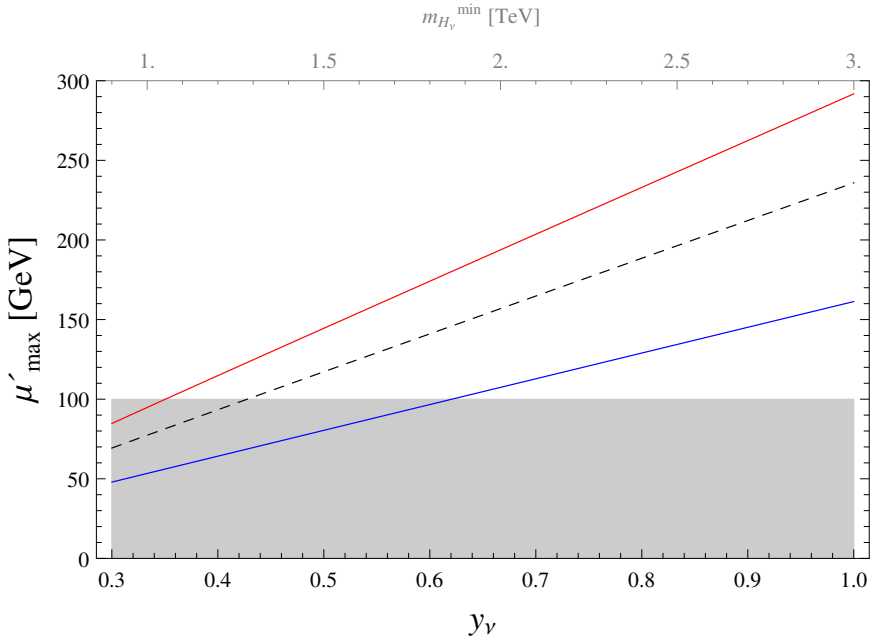

Figure 6.2: The largest allowed ν-higgsino mass as function of the coupling y_ν such that right-handed sneutrinos with mass 7 GeV (blue –lower– line), 15 GeV (dashed line) or 23 GeV (red –upper– line) have a large enough pair annihilation cross section such that their relic density is determined by their asymmetry. The corresponding lower limit on the lightest ν-Higgs mass, derived from Eq. (6.22), is indicated along the upper axis. The shaded area is excluded by chargino searches at LEP (e.g. [147]).

6.4.3 ADM Detection: prospects and constraints

Upper bounds on the (bosonic) ADM-nucleon scattering cross section originate from both the direct detection and observations of old neutron stars. Concerning the latter, if the cross section is too large, the accumulation of asymmetric bosonic DM inside the neutron stars can form a black hole which would potentially destroy the star. This is a specific feature of asymmetric DM, since in the common symmetric case the annihilation of DM with anti-DM prevents the accumulation. For bosonic asymmetric DM in the mass range $5\,\text{GeV} \lesssim m_{DM} \lesssim 16\,\text{GeV}$, nucleon–DM cross sections $\sigma \gtrsim 10^{-50}\,\text{cm}^3\,\text{s}^{-1}$ are excluded [331, 332]. However, the value of the cross section depends on the parameter space, particularly on the value of A_ν (see [218]), while for DM heavier than $\sim 16\,\text{GeV}$ there is no limit due to Hawking evaporation [331], letting a completely unconstrained mass range ($16\,\text{GeV} \lesssim m_{DM} \lesssim 23\,\text{GeV}$) for the ADM of this scenario.

Concerning direct detection, since right-handed sneutrinos couple only to neutrinophilic Higgses, there are no tree-level contributions to the scattering cross section of N off nuclei. However, as it was pointed out in [218], the contribution of Z exchange induced at one loop (with left-handed sneutrinos and ν-Higgses running on the loop) may be significant. The value obtained in [218] ($\sim 10^{-45}\,\text{cm}^3\text{s}^{-1}$), assuming a relatively large value for the trilinear soft coupling A_ν, is at the lower bound of the current

experimental direct detection sensitivity for a DM mass around 100 GeV. However, for the mass range considered here ($\mathcal{O}(10)$ GeV), the upper limits on the scalar scattering cross section are much higher.

Concerning indirect detection, pure asymmetric DM does not give rise to detectable signals due to the absence of either DM particles or antiparticles. (The self-annihilation cross section is required to be too small to generate measurable signals.) However, the operators which break the $U(1)$ symmetry might also induce a very small mass difference δm among the sneutrino and anti-sneutrino eigenstates. Even though the induced sneutrino – anti-sneutrino oscillations are slow enough so that they did not affect the relic density, they may have led to the repopulation of the exhausted species in case δm^{-1} is smaller than the current age of the Universe. This would be the case, e.g., for the value $\delta m \sim 10^{-33}$ GeV obtained in the scenario sketched below (6.31).

In case the exhausted species has been regenerated, the same N, N^* annihilation processes (Fig. 6.1) that occurred in the early Universe may happen today in galactic regions of large DM density, giving rise to leptonic charged cosmic rays and γ-rays. However, assuming that the excess of positrons observed amongst others by AMS-02 [78] originates from astrophysical sources, it constitutes an insurmountable background making the distinction of a potential DM signal from charged leptonic rays difficult. Concerning the diffuse photon radiation, we recall that the s-wave annihilation of N, N^* is helicity suppressed. The low present-day velocity of DM particles leads to a low σv, evading the bounds set by the Fermi collaboration [333]. Finally, as pointed out in [323], N, N^* annihilation through a box loop with sleptons and charged ν-Higgs can give rise to a monochromatic photon line with a large cross section proportional to $\left(\frac{y_\nu A_\nu}{M_{H_\nu^+}}\right)^4$. The Fermi bound for a DM mass of ~ 10 GeV is quite severe, $\langle\sigma v\rangle_{\gamma\gamma} \lesssim 5 \cdot 10^{-29}\,\mathrm{cm^3 s^{-1}}$ [253]. However, taking A_ν of the order of the EW scale (~ 100 GeV), this bound is easily satisfied since $\langle\sigma v\rangle_{\gamma\gamma} \lesssim 10^{-29}\,\mathrm{cm^3 s^{-1}}$.

We close this section with a last constraint coming from the CMB. An increased amount of free electrons at redshifts $z \sim 1000$ would had affected the process of recombination, leaving an imprint on the CMB anisotropies. An electron excess may come from the injection of secondary particles produced by DM annihilation, or directly from the annihilation. Strong constraints have been derived for the DM annihilation cross section in [334,335]. For example, in the most stringent case where the dominant annihilation channel leads to electron production, thermal DM with mass smaller than ~ 10 GeV is excluded (assuming purely s-wave annihilation).

Since these constraints are more severe in the low mass range, they are particular interesting for the case of asymmetric DM, where, additionally, the pair annihilation cross section is expected to be larger than the thermal one. However, the current model is not affected, even in the case that late oscillations reopened the way to annihilations, again due to the absence of s-wave DM annihilation. At the period of interest, the temperature of the Universe was $\lesssim 1$ eV; hence, the (p-wave) annihilation cross section during that period is expected to be $\sim 10^{-9}$ times smaller than the cross section that determined the DM density.

6.5 Discussion

In this chapter we have presented an extension of the NMSSM introducing an additional pair of Higgs doublets with small vevs, explaining the smallness of neutrino masses and, at the same time, the present day coincidence of DM and baryon densities. The additional Higgses and the right-handed neutrinos are charged under a new $U(1)$ symmetry which is explicitly broken by soft SUSY breaking terms. This symmetry forces the new Higgses to couple in the superpotential only to right-handed neutrinos (so-called neutrinophilic Higgses). The neutrinos have Dirac masses which are generated dynamically by the neutrinophilic Higgs vev and hence naturally small.

We have shown that the right-handed sneutrinos can carry an asymmetry related to the baryon asymmetry due to their conserved lepton number and equilibrium processes in the early Universe. They can maintain their asymmetry at least until the freeze-out of sneutrino–anti-sneutrino annihilations. Therefore, their relic density is determined by their asymmetry and of the correct value if their mass is $\mathcal{O}(10)\,\mathrm{GeV}$, provided that the coupling constant λ' is small compared to λ. However, the bound on the relativistic degrees of freedom during BBN set by the Planck collaboration requires large soft breaking mass for the neutrinophilic Higgs. At present this scenario satisfies constraints from DM detection experiments. Actually, the scattering cross section is too small in order to explain possible excesses observed in the CDMS, DAMA, CoGeNT and CRESST-II experiments [48, 50, 51, 57] in this mass range, which have been interpreted as possible evidence of DM. Still, direct detection is possible in the future once the sensitivity in the lower mass range is improved. On the other hand, neutrinoless double beta decay is impossible in this model and a future observation of this process would rule out the current scenario.

CONCLUSION

Copious evidence, coming from galactic rotation curves, gravitational lensing observations and many other observations, suggest that DM is present in our Universe in a large amount. Its abundance has been specified quite accurately through the observation of the cosmic microwave background radiation by the satellites WMAP and Planck. However, the exact nature of DM is not yet evident.

In this thesis, we dealt with the particle DM emerging from supersymmetric models and, specifically, the NMSSM. We explained successfully, in this context, a possible monochromatic photon excess on the data of the Fermi-LAT, which comprises an indirect DM signal. This was achieved assuming the lightest neutralino as DM, annihilating to photons through a chargino loop, via an s-channel singlet-like pseudoscalar exchange. However, in order to obtain the large annihilation cross section that the data suggest, a considerable amount of "fine-tuning" on the mass of the pseudoscalar is required.

We showed that NMSSM is able to explain, at the same time, the SM-like Higgs boson discovered at LHC and be consistent with constraints imposed by collider physics. We also investigated under which conditions the neutralino DM, which gives rise to the desired photon line, has the correct relic abundance and satisfies the established bounds from direct and indirect DM detection. Despite the naive expectation that thermal neutralino DM with large annihilation cross section to photons is excluded by the non-observation of diffuse photon radiation, we demonstrated that it is possible in the NMSSM to elude these limits. This is achieved mainly due to the negligible doublet component of the pseudoscalar and the p-wave pair annihilations of the neutralino.

A notable part of the thesis deals with DM with a density which was not determined by the standard thermal mechanism, but it is coming from the asymmetry between DM and anti-DM. However, an initial DM asymmetry may be destroyed by self-annihilations, which, nevertheless, were often neglected in the past when their cross section was small compared to DM particle-antiparticle annihilation cross section. We solved numerically the coupled set of Boltzmann equations that govern the evolution of the two species (DM particles and antiparticles) in a model independent way and we concluded that the final DM density is very sensitive to the self-annihilation cross

section, independently on the DM particle–antiparticle pair annihilation cross section. In order that a sizeable amount of asymmetry survives, self-annihilation cross section has to be (in most cases unnaturally) extremely small. Our main result is an upper bound on this self-annihilation cross section.

Motivated by the severe bounds on the self-annihilation cross section, we proposed a model of asymmetric DM, which respects these limits. This model is an extension of the NMSSM through the introduction of a pair of neutrinophilic doublet Higgs superfields and three generations of right-handed neutrino superfields. The small neutrino Dirac masses are due to a small vev of the additional up Higgs scalar. The DM in this model, a right-handed sneutrino, is proved to be consistent with experimental bounds. In order for the asymmetry to be responsible for the DM present-day density, relatively large Yukawa coupling constants are required. However, a large value for these couplings means late decoupling of the right-handed neutrinos, increasing the relativistic degrees of freedom during BBN. To compensate this effect and be consistent with the Planck results, large values of soft SUSY breaking masses for the additional Higgses have to be present.

Appendices

APPENDIX A

RELATIVISTIC DEGREES OF FREEDOM

A.1 Energy Density

The total energy density ρ of the Universe is dominated by the energy densities of the relativistic particle species:

$$\rho = \sum_i \rho_i \simeq \sum_{\substack{i \\ (relativistic)}} \rho_i. \tag{A.1}$$

The energy density of a particle species i with energy E_i which follow a phase space distribution f_i would be, after summing over the spin degrees of freedom g_i,

$$\rho_i = \frac{g_i}{(2\pi)^3} \int E_i f_i(E_i) \mathrm{d}^3 p_i. \tag{A.2}$$

The phase space density could be Fermi-Dirac for the case of fermion species or Bose-Einstein for bosons, given by

$$f_i(E_i) = \frac{1}{\mathrm{e}^{(E_i - \mu_i)/T_i} \pm 1}, \tag{A.3}$$

with the former corresponding to the "plus" sign and the latter to the "minus". μ_i is the chemical potential of the species i. The chemical potential is always several orders of magnitude smaller than the temperature, hence it can be safely neglected for relativistic particles. Moreover, relativistic particles can be treated as massless ($E \simeq p$), so that the integral in Eq. (A.2) can be easily performed analytically for both fermions and bosons, giving

$$\rho_i = \begin{cases} \frac{7}{8} \frac{\pi^2}{30} g_i T_i^4, & \text{fermions} \\ \frac{\pi^2}{30} g_i T_i^4, & \text{bosons} \end{cases}. \tag{A.4}$$

The total energy density would be just given by the sum of ρ_i, Eq. (A.4), over all relativistic fermion and boson species. However, it is convenient to express it in terms of the common temperature T of the species in equilibrium in the thermal plasma (this temperature is usually considered as the photon temperature, since photons were the last particles that went out of equilibrium). The species temperature T_i would be the same in case of equilibrium, but in principle different if they have gone out of equilibrium. Therefore, the energy density of the Universe is written as

$$\rho = \sum_{bosons} \frac{\pi^2}{30}\, g_i\, T_i^4 \; + \sum_{fermions} \frac{7}{8}\frac{\pi^2}{30}\, g_i\, T_i^4 = \frac{\pi^2}{30}\, g_{\rm eff}(T)\, T^4, \tag{A.5}$$

where, in the last step, we have defined the *effective relativistic degrees of freedom for the energy density* as

$$g_{\rm eff}(T) \equiv \sum_{bosons} g_i \left(\frac{T_i}{T}\right)^4 + \frac{7}{8} \sum_{fermions} g_i \left(\frac{T_i}{T}\right)^4. \tag{A.6}$$

A.2 Pressure

The pressure $\mathtt{p}$ appears in the diagonal spatial elements of the energy-momentum tensor (1.6). The calculation of this tensor yields that the pressure is the density of $p^2/(3E)$, so that the pressure $\mathtt{p}_i$ of the particle species i can be written as

$$\mathtt{p}_i = \frac{g_i}{(2\pi)^3} \int \frac{p_i^2}{3E_i} f_i(E_i) \mathrm{d}^3 p_i. \tag{A.7}$$

Taking the sum of all relativistic particle species, the pressure of the Universe simplifies to

$$\mathtt{p} = \frac{\rho}{3}. \tag{A.8}$$

A.3 Entropy density

Assuming adiabatic expansion for a particle species with entropy S, we have $T\mathrm{d}S = \mathrm{d}E + \mathtt{p}\mathrm{d}V = 0$. Replacing the entropy and energy by their densities times the volume and identifying the coefficients of $\mathrm{d}V$, we obtain the following expression

$$s_i = \frac{1}{T_i}(\rho + \mathtt{p}_i). \tag{A.9}$$

Using Eqs. (A.4) and (A.7), the entropy density is written as

$$s_i = \frac{g_i}{(2\pi)^3} \int \frac{3E_i^2 + p_i^2}{3E_i T_i} f(E_i) \mathrm{d}_i^p. \tag{A.10}$$

Calculating the integral in the relativistic limit, we have $s_i = \frac{1}{T_i}\frac{4\rho}{3}$. Summing over the particle species and expressing the final result in terms of the temperature T of the thermal plasma, as we did for the energy density, we find

$$s = \frac{2\pi^2}{45} h_{\rm eff}(T) T^3, \tag{A.11}$$

where the *effective relativistic degrees of freedom for the entropy density* have been defined as

$$h_{\rm eff} = \sum_{bosons} g_i \left(\frac{T_i}{T}\right)^3 + \frac{7}{8} \sum_{fermions} g_i \left(\frac{T_i}{T}\right)^3. \tag{A.12}$$

A.4 Calculation of the effective degrees of freedom

It is possible to calculate approximately the effective degrees of freedom by counting the relativistic particles that are in equilibrium for a given temperature T. For temperatures below the top quark mass, $T \lesssim m_t$, only SM particles are expected to be in equilibrium. All the SM particles, except the neutrinos, went out of equilibrium while non-relativistic. Therefore, they would stop to contribute to the total energy density once the temperature T falls below their mass. In the massless approximation, the effective degrees of freedom for the energy and the entropy density would be equal,

$$g_{\rm eff}(T) = h_{\rm eff}(T) = \sum_{\rm bosons} g_i \; + \sum_{\rm fermions} g_i \equiv \mathcal{N}(T). \tag{A.13}$$

The values of the relativistic degrees of freedom obtained in this way for various temperature ranges appear in Table A.1.

For the calculation of the DM relic density, a more accurate value for the degrees of freedom is required and one has to drop the ultra-relativistic assumption $m \to 0$ of massless particles. In this case, the expression for the energy and entropy densities for a particle species i read, respectively,

$$\rho_i = \frac{g_i T^4}{2\pi^2} x_i^4 \int_1^\infty {\rm d}y \, \frac{y^2\sqrt{y^2-1}}{{\rm e}^{x_i y} \pm 1}, \tag{A.14}$$

$$\sigma_i = \frac{g_i T^3}{6\pi^2} x_i^4 \int_1^\infty {\rm d}y \, \frac{(4y^2-1)\sqrt{y^2-1}}{{\rm e}^{x_i y} \pm 1}, \tag{A.15}$$

where we have defined $x_i \equiv m_i/T_i$ and we have performed the transformation $y = E/m$ in the integral. Comparing the above expressions with the corresponding expressions (A.5) and (A.11), we can define, respectively,

$$g_i(x_i) = \frac{15 g_i}{\pi^4} x_i^4 \int_1^\infty {\rm d}y \, \frac{y^2\sqrt{y^2-1}}{{\rm e}^{x_i y} \pm 1} \qquad \text{and} \tag{A.16}$$

$$h_i(x_i) = \frac{45 g_i}{12\pi^2} x_i^4 \int_1^\infty {\rm d}y \, \frac{(4y^2-1)\sqrt{y^2-1}}{{\rm e}^{x_i y} \pm 1}, \tag{A.17}$$

Temperature	Relativistic particles in equilibrium	Relativistic degrees of freedom
$\lesssim m_e$	γ, $\nu^{\{e,\mu,\tau\}}$	7.25
$\in (m_e, m_\mu)$	$e^\pm$	10.75
$\in (m_\mu, m_\pi)$	$\mu^\pm$	14.25
$\in (m_\pi, T_c)$	π^0, $\pi^\pm$	17.25
$\in (T_c, m_s)$	u, $\bar{u}$, d, $\bar{d}$, gluons	51.25
$\in (m_s, m_c)$	s, $\bar{s}$	61.75
$\in (m_c, m_\tau)$	c, $\bar{c}$	72.25
$\in (m_\tau, m_b)$	τ, $\bar{\tau}$	75.25
$\in (m_b, m_W)$	b, $\bar{b}$	86.25
$\in (m_W, m_H)$	$W^\pm$, Z	95.25
$\in (m_H, m_t)$	H	96.25
$\gtrsim m_t$	t, $\bar{t}$	106.75

Table A.1: The number of relativistic degrees of freedom for the SM particles. T_c corresponds to the temperature at which the quark-hadron phase transition occurred. The relativistic particles in equilibrium for each temperature range include the particles of all previous rows in the table, with the exception of the pions that appear only for $T > T_c$.

so that the effective number of degrees of freedom can be calculated using these two expressions, as

$$g_{\text{eff}} = \sum_i g_i \left(\frac{T_i}{T}\right)^4, \qquad h_{\text{eff}} = \sum_i h_i \left(\frac{T_i}{T}\right)^3. \tag{A.18}$$

We begin by the calculation of the entropy effective degrees of freedom h_{eff}. We separate the sum (A.18) into two parts, one coming from the contribution of species in equilibrium with common temperature T and the other from the decoupled species. In this way,

$$h_{\text{eff}}(T) = h_c(T) + \sum_{\text{dec}} h_i(T) \left(\frac{T_i}{T}\right)^3. \tag{A.19}$$

After the decoupling of a species i at a temperature T_{di}[1], the total entropy as well as

[1]Although the decoupling is not a momentary process, we make the simplification that it occurs at a specific temperature.

the entropy of the decoupled species are separately conserved:

$$h_{\rm eff}(T)\, T^3 R^3(T) = h_{\rm eff}(T_{di}) T_{di}^3 R^3(T_{di}), \tag{A.20}$$

$$h_i(T) \left(\frac{T_i}{T}\right)^3 T^3 R^3(T) = h_i(T_{di}) T_{di}^3 R^3(T_{di}), \tag{A.21}$$

with R the scale factor. Combining the above equations, we have

$$h_i(T) \left(\frac{T_i}{T}\right)^3 = h_{\rm eff}(T) \frac{h_i(T_{di})}{h_{\rm eff}(T_{di})}. \tag{A.22}$$

Inserting this result into Eq. (A.19), we arrive at the expression

$$h_{\rm eff}(T) = h_c(T) + h_{\rm eff}(T) \sum_{\rm dec} \frac{h_i(T_{di})}{h_{\rm eff}(T_{di})}. \tag{A.23}$$

We follow [38] and introduce the ratios $r_c(T) \equiv \frac{h_c(T)}{h_{\rm eff}(T)}$ and $r_i \equiv \frac{h_i(T_{di})}{h_c(T_{di})}$. Then, Eq. (A.23) becomes

$$r_c(T) = 1 - \sum_{\rm dec} r_i r_c(T_{di}). \tag{A.24}$$

Let us suppose now that at a temperature T_1 just one species has already gone out of equilibrium, at T_2 two species and so on, so that at temperature T_n, n species would have decoupled. Then, for a temperature at which $n+1$ species have decoupled, Eq. (A.24) gives

$$r_c(T_{n+1}) = r_c(T_n) - r_n r_c(T_{dn}), \tag{A.25}$$

which in the limit $T_{n+1} \to T_{dn}$ becomes

$$r_c(T_{dn}) = \frac{r_c(T_n)}{1 + r_n}. \tag{A.26}$$

Substituting (A.26) back into (A.25), we obtain the recurrence formula

$$r_c(T_{n+1}) = \frac{r_c(T_n)}{1 + r_n}. \tag{A.27}$$

Using this recurrence formula, we can finally write

$$r_c(T_{n+1}) = r_c(T_0) \prod_{i=1}^{n} \frac{1}{1 + r_n}, \tag{A.28}$$

where T_0 corresponds to a temperature at which all species were in equilibrium. At this temperature $h_{\rm eff}(T_0) = h_c(T_0)$ and, therefore, $r_c(T_0) = 1$. Switching back from the ratios r to the quantities h on Eq. (A.28), we arrive at the final result

$$h_{\rm eff}(T) = h_c(T) \prod_{\rm dec} \left(1 + \frac{h_i(T_{di})}{h_c(T_{di})}\right), \tag{A.29}$$

which allows to compute the entropy effective degrees of freedom, knowing only the temperature when the various species decoupled. Using this expression, Eq. (A.22) and the first of Eqs. (A.18), it is now straightforward to write the corresponding expression for $g_{\rm eff}$.

In the current analysis, we have assumed that the ensemble of the various species can be regarded as an ideal gas and, additionally, that there is no entropy production during the whole evolution of the Universe. However, this is not always the case. For example, during the QCD quark-hadron phase transition, the interparticle distances become small, the hadrons begin to overlap and the interactions among them become important. The ideal gas assumption is not anymore valid and one has to choose a model for the transition in order to compute the effective degrees of freedom, something that goes beyond our scope.

APPENDIX B

CROSS SECTION FOR THE NEUTRALINO ANNIHILATION TO PHOTONS

B.1 $\chi_1^0\chi_1^0 \to \gamma\gamma$

The cross section times velocity for the lightest neutralino pair annihilation to two photons through loop diagrams is given by

$$\sigma v = \frac{\alpha^2 m_{\chi_1^0}^2}{16\pi^3}|\widetilde{A}|^2, \tag{B.1}$$

where α is the electromagnetic coupling constant and $m_{\chi_1^0}$ the mass of the lightest neutralino. $\widetilde{A}$ is the total amplitude, the sum of the partial amplitudes $\widetilde{A}$ of all possible annihilations. Here, we assume that the annihilation of Fig. B.1 is dominant and we neglect contributions from other diagrams.

The amplitude of the diagram B.1, by suitably modifying the expressions of [222], turns out to be

$$\widetilde{A}_i = -\sum_{k=1}^{2} \frac{m_{\chi_k^+}}{m_{\chi_1^0}} \frac{g_{A_i\chi_1^0\chi_1^0}\, g_{A_i\chi_k^+\chi_k^+}}{4m_{\chi_1^0}^2 - m_{A_i}^2 + im_{A_i}\Gamma_{A_i}} \mathcal{I}\left(\frac{m_{\chi_k^+}}{m_{\chi_1^0}}\right). \tag{B.2}$$

$m_{\chi_k^+}$ is the mass of the k chargino, m_{A_i} and Γ_{A_i} is the mass and the decay width, respectively, of the i mass eigenstate of the pseudoscalar. The function $\mathcal{I}(x)$ is given by

$$\mathcal{I}(x) = \begin{cases} -2\arctan^2 \frac{1}{\sqrt{x^2-1}}, & \text{for } x \geq 1 \\ \frac{1}{2}\ln^2 \frac{1+\sqrt{1-x^2}}{1-\sqrt{1-x^2}}, & \text{for } x \leq 1. \end{cases} \tag{B.3}$$

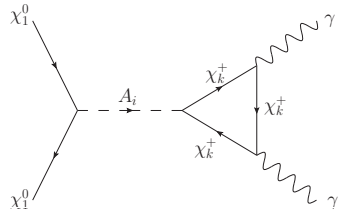

Figure B.1: Neutralino pair annihilation to two through an s-channel CP-odd Higgs exchange and chargino loop.

The coupling $g_{A_i\chi_1^0\chi_1^0}$ of the pseudoscalar to the lightest neutralinos is given by

$$\begin{aligned} g_{A_i\chi_1^0\chi_1^0} = \sqrt{2}\lambda\left[P_{i1}(N_{14}N_{15}\cos\beta + N_{13}N_{15}\sin\beta) + P_{i2}N_{13}N_{14}\right] - \sqrt{2}\kappa P_{i2}N_{15}^2 \\ + g_1 P_{i1}(N_{11}N_{13}\cos\beta - N_{11}N_{14}\sin\beta) \\ - g_2 P_{i1}(N_{12}N_{13}\cos\beta - N_{12}N_{14}\sin\beta), \end{aligned} \quad \text{(B.4)}$$

where P is the 2×2 matrix that diagonalizes the CP-odd Higgs mass squared matrix given by the Eq. (3.17) and N the real 5×5 neutralino mixing matrix defined in Eq. (3.29). We see that for a CP-odd Higgs with negligible doublet component, the above expression reduces to

$$g_{A_s\chi_1^0\chi_1^0} \simeq \sqrt{2}\lambda N_{13}N_{14} - \sqrt{2}\kappa N_{15}^2. \quad \text{(B.5)}$$

As it was expected, the gaugino components of the neutralino do not couple to a singlet pseudoscalar. Finally, the coupling of the pseudoscalar to the charginos is given by

$$g_{A_i\chi_k^+\chi_l^+} = \frac{\lambda}{\sqrt{2}}P_{i2}U_{k2}V_{l2} - \frac{g_2}{\sqrt{2}}P_{i1}\left(U_{k1}V_{l2}\cos\beta + U_{k2}V_{l1}\sin\beta\right), \quad \text{(B.6)}$$

with U and V the matrices that rotate, respectively, the negative and positive charged charginos of the weak basis into the mass eigenstates $\chi^\pm$ (see (3.32)).

B.2 $\chi_1^0\chi_1^0 \to Z\gamma$

For this process, the cross section times velocity is given by

$$\sigma v = \frac{\alpha}{32\pi^4}\frac{(m_{\chi_1^0}^2 - \frac{1}{4}M_Z^2)^3}{m_{\chi_1^0}^4}|\widetilde{A}|^2, \quad \text{(B.7)}$$

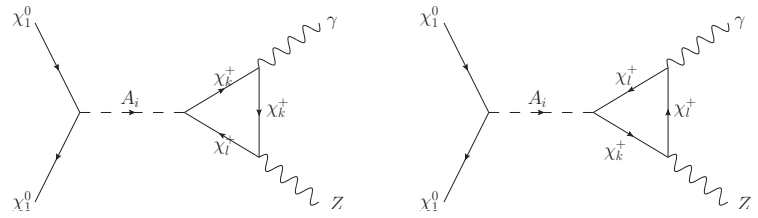

Figure B.2: The diagrams of neutralino pair annihilation through s-channel CP-odd Higgs exchange, contributing to the $Z\gamma$.

in a notation similar to Eq. (B.1) (M_Z is the mass of the Z boson). The amplitude for the diagrams B.2 is given by [224]

$$\begin{aligned}\widetilde{A} = &\frac{1}{m_{\chi_1^0} - \frac{1}{4}M_Z^2} \sum_{k,l=1}^{2} \frac{2m_{\chi_1^0} m_{\chi_j^+}}{4m_{\chi_1^0}^2 - m_{A_i}^2 + i m_{A_i}\Gamma_{A_i}} \\ &\left\{ \left(g_{A_i\chi_k^+\chi_l^+} g^L_{Z\chi_l^+\chi_k^+} + g_{A_i\chi_l^+\chi_k^+} g^R_{Z\chi_l^+\chi_k^+} \right) g_{A_i\chi_1^0\chi_1^0}\, \mathcal{I}' \left(\frac{m_{\chi_1^0}}{m_{\chi_k^+}}, \frac{m_{\chi_l^+}}{m_{\chi_k^+}}, 1, \frac{M_Z}{2m_{\chi_k^+}} \right) \right. \\ &\left. + \left(g_{A_i\chi_k^+\chi_l^+} g^R_{Z\chi_l^+\chi_k^+} + g_{A_i\chi_l^+\chi_k^+} g^L_{Z\chi_l^+\chi_k^+} \right) g_{A_i\chi_1^0\chi_1^0}\, \mathcal{I}' \left(\frac{m_{\chi_1^0}}{m_{\chi_k^+}}, 1, \frac{m_{\chi_l^+}}{m_{\chi_k^+}}, \frac{M_Z}{2m_{\chi_k^+}} \right) \right\}. \end{aligned} \tag{B.8}$$

The couplings of the Z boson to the left and right components of the charginos are

$$g^L_{Z\chi_l^+\chi_k^+} = \frac{g_2}{\cos\theta_w} \left(-V_{k1}V_{l1} - \frac{1}{2}V_{k2}V_{l2} + \delta_{kl}\sin^2\theta_w \right), \tag{B.9a}$$

$$g^R_{Z\chi_l^+\chi_k^+} = \frac{g_2}{\cos\theta_w} \left(-U_{k1}U_{l1} - \frac{1}{2}U_{k2}U_{l2} + \delta_{kl}\sin^2\theta_w \right). \tag{B.9b}$$

Finally, the integral $\mathcal{I}'$ has to calculated numerically by the expression

$$\mathcal{I}'(a,b,c,d) = \int_0^1 \frac{\mathrm{d}x}{x} \ln \left| \frac{4a^2x^2 + (-4a^2 + b^2 - c^2)x + c^2}{4d^2x^2 + (-4d^2 + b^2 - c^2)x + c^2} \right|. \tag{B.10}$$

BIBLIOGRAPHY

[1] U. Ellwanger and P. Mitropoulos, "Upper Bounds on Asymmetric Dark Matter Self Annihilation Cross Sections," *JCAP* **1207** (2012) 024, arXiv:1205.0673 [hep-ph].

[2] D. Das, U. Ellwanger, and P. Mitropoulos, "A 130 GeV photon line from dark matter annihilation in the NMSSM," *JCAP* **1208** (2012) 003, arXiv:1206.2639 [hep-ph].

[3] P. Mitropoulos, "Right-handed sneutrinos as asymmetric DM and neutrino masses from neutrinophilic Higgs bosons," *JCAP* **1311** (2013) 008, arXiv:1307.2823 [hep-ph].

[4] F. Zwicky, "Spectral displacement of extra galactic nebulae," *Helv.Phys.Acta* **6** (1933) 110–127.

[5] F. Zwicky, "On the Masses of Nebulae and of Clusters of Nebulae," *Astrophys.J.* **86** (1937) 217–246.

[6] K. Freeman and G. McNamara, *In Search of Dark Matter*. Springer Praxis Books / Space Exploration. Praxis Publishing Limited, 2006.

[7] J. H. Oort, "The force exerted by the stellar system in the direction perpendicular to the galactic plane and some related problems," *Bulletin of the Astronomical Institutes of the Netherlands* **6** (Aug., 1932) 249.

[8] E. Hubble, "A relation between distance and radial velocity among extra-galactic nebulae," *Proc.Nat.Acad.Sci.* **15** (1929) 168–173.

[9] **Planck** Collaboration, P. Ade *et al.*, "Planck 2013 results. XVI. Cosmological parameters," arXiv:1303.5076 [astro-ph.CO].

[10] J. Yadav, S. Bharadwaj, B. Pandey, and T. Seshadri, "Testing homogeneity on large scales in the Sloan Digital Sky Survey Data Release One,"

Mon.Not.Roy.Astron.Soc. **364** (2005) 601–606, arXiv:astro-ph/0504315 [astro-ph].

[11] S. M. Carroll, "Lecture notes on general relativity," arXiv:gr-qc/9712019 [gr-qc].

[12] V. C. Rubin and J. Ford, W. Kent, "Rotation of the Andromeda Nebula from a Spectroscopic Survey of Emission Regions," *Astrophys.J.* **159** (1970) 379–403.

[13] Y. Sofue and V. Rubin, "Rotation curves of spiral galaxies," *Ann.Rev.Astron.Astrophys.* **39** (2001) 137–174, arXiv:astro-ph/0010594 [astro-ph].

[14] E. Corbelli and P. Salucci, "The extended rotation curve and the dark matter halo of m33," arXiv:astro-ph/9909252 [astro-ph].

[15] D. Roy, "Basic constituents of the visible and invisible matter: A Microscopic view of the universe," arXiv:physics/0007025 [physics].

[16] C. Munoz, "Dark matter detection in the light of recent experimental results," *Int.J.Mod.Phys.* **A19** (2004) 3093–3170, arXiv:hep-ph/0309346 [hep-ph].

[17] E. Battaner and E. Florido, "The Rotation curve of spiral galaxies and its cosmological implications," *Fund.Cosmic Phys.* **21** (2000) 1–154, arXiv:astro-ph/0010475 [astro-ph].

[18] A. Taylor, S. Dye, T. J. Broadhurst, N. Benitez, and E. van Kampen, "Gravitational lens magnification and the mass of abell 1689," arXiv:astro-ph/9801158 [astro-ph].

[19] D. Clowe, A. Gonzalez, and M. Markevitch, "Weak lensing mass reconstruction of the interacting cluster 1E0657-558: Direct evidence for the existence of dark matter," *Astrophys.J.* **604** (2004) 596–603, arXiv:astro-ph/0312273 [astro-ph].

[20] D. Clowe, M. Bradac, A. H. Gonzalez, M. Markevitch, S. W. Randall, *et al.*, "A direct empirical proof of the existence of dark matter," *Astrophys.J.* **648** (2006) L109–L113, arXiv:astro-ph/0608407 [astro-ph].

[21] **WMAP** Collaboration, E. Komatsu *et al.*, "Seven-Year Wilkinson Microwave Anisotropy Probe (WMAP) Observations: Cosmological Interpretation," *Astrophys.J.Suppl.* **192** (2011) 18, arXiv:1001.4538 [astro-ph.CO].

[22] **WMAP** Collaboration, G. Hinshaw *et al.*, "Nine-Year Wilkinson Microwave Anisotropy Probe (WMAP) Observations: Cosmological Parameter Results," *Astrophys.J.Suppl.* **208** (2013) 19, arXiv:1212.5226 [astro-ph.CO].

[23] E. Kolb and M. Turner, *The Early Universe*. Frontiers in Physics. Addison-Wesley Longman, Incorporated, 1990.

[24] S. Weinberg, *Cosmology*. Cosmology. OUP Oxford, 2008.

[25] D. Fixsen, "The Temperature of the Cosmic Microwave Background," *Astrophys.J.* **707** (2009) 916–920, arXiv:0911.1955 [astro-ph.CO].

[26] W. Hu, "CMB anisotropies: A Decadal survey," arXiv:astro-ph/0002520 [astro-ph].

[27] M. Giovannini, "Theoretical tools for the physics of CMB anisotropies," *Int.J.Mod.Phys.* **D14** (2005) 363–510, arXiv:astro-ph/0412601 [astro-ph].

[28] **Planck** Collaboration, P. Ade *et al.*, "Planck 2013 results. XV. CMB power spectra and likelihood," arXiv:1303.5075 [astro-ph.CO].

[29] G. Efstathiou, "Cmb anisotropies and the determination of cosmological parameters," arXiv:astro-ph/0002249 [astro-ph].

[30] W. Hu and M. J. White, "The Damping tail of CMB anisotropies," *Astrophys.J.* **479** (1997) 568, arXiv:astro-ph/9609079 [astro-ph].

[31] M. Milgrom, "A Modification of the Newtonian dynamics as a possible alternative to the hidden mass hypothesis," *Astrophys.J.* **270** (1983) 365–370.

[32] R. H. Sanders and S. S. McGaugh, "Modified Newtonian dynamics as an alternative to dark matter," *Ann.Rev.Astron.Astrophys.* **40** (2002) 263–317, arXiv:astro-ph/0204521 [astro-ph].

[33] **SDSS** Collaboration, K. Glazebrook *et al.*, "The Sloan Digital Sky Survey: The Cosmic spectrum and star - formation history," *Astrophys.J.* **587** (2003) 55–70, arXiv:astro-ph/0301005 [astro-ph].

[34] A. Aguirre, C. Burgess, A. Friedland, and D. Nolte, "Astrophysical constraints on modifying gravity at large distances," *Class.Quant.Grav.* **18** (2001) R223–R232, arXiv:hep-ph/0105083 [hep-ph].

[35] R. Peccei and H. R. Quinn, "Constraints Imposed by CP Conservation in the Presence of Instantons," *Phys.Rev.* **D16** (1977) 1791–1797.

[36] R. Peccei and H. R. Quinn, "CP Conservation in the Presence of Instantons," *Phys.Rev.Lett.* **38** (1977) 1440–1443.

[37] G. Jungman, M. Kamionkowski, and K. Griest, "Supersymmetric dark matter," *Phys.Rept.* **267** (1996) 195–373, arXiv:hep-ph/9506380 [hep-ph].

[38] P. Gondolo and G. Gelmini, "Cosmic abundances of stable particles: Improved analysis," *Nucl.Phys.* **B360** (1991) 145–179.

[39] T. Nihei, L. Roszkowski, and R. Ruiz de Austri, "Towards an accurate calculation of the neutralino relic density," *JHEP* **0105** (2001) 063, arXiv:hep-ph/0102308 [hep-ph].

[40] M. Srednicki, R. Watkins, and K. A. Olive, "Calculations of Relic Densities in the Early Universe," *Nucl.Phys.* **B310** (1988) 693.

[41] M. W. Goodman and E. Witten, "Detectability of Certain Dark Matter Candidates," *Phys.Rev.* **D31** (1985) 3059.

[42] I. Wasserman, "POSSIBILITY OF DETECTING HEAVY NEUTRAL FERMIONS IN THE GALAXY," *Phys.Rev.* **D33** (1986) 2071–2078.

[43] J. Bovy and S. Tremaine, "On the local dark matter density," *Astrophys.J.* **756** (2012) 89, arXiv:1205.4033 [astro-ph.GA].

[44] **XENON100** Collaboration, E. Aprile *et al.*, "Dark Matter Results from 225 Live Days of XENON100 Data," *Phys.Rev.Lett.* **109** (2012) 181301, arXiv:1207.5988 [astro-ph.CO].

[45] **LUX Collaboration** Collaboration, D. Akerib *et al.*, "First results from the LUX dark matter experiment at the Sanford Underground Research Facility," arXiv:1310.8214 [astro-ph.CO].

[46] **XENON100** Collaboration, E. Aprile *et al.*, "The XENON100 Dark Matter Experiment," *Astropart.Phys.* **35** (2012) 573–590, arXiv:1107.2155 [astro-ph.IM].

[47] **XENON100** Collaboration, E. Aprile *et al.*, "Dark Matter Results from 100 Live Days of XENON100 Data," *Phys.Rev.Lett.* **107** (2011) 131302, arXiv:1104.2549 [astro-ph.CO].

[48] **DAMA** Collaboration, R. Bernabei *et al.*, "First results from DAMA/LIBRA and the combined results with DAMA/NaI," *Eur.Phys.J.* **C56** (2008) 333–355, arXiv:0804.2741 [astro-ph].

[49] **DAMA, LIBRA** Collaboration, R. Bernabei *et al.*, "New results from DAMA/LIBRA," *Eur.Phys.J.* **C67** (2010) 39–49, arXiv:1002.1028 [astro-ph.GA].

[50] **CoGeNT** Collaboration, C. Aalseth *et al.*, "Results from a Search for Light-Mass Dark Matter with a P-type Point Contact Germanium Detector," *Phys.Rev.Lett.* **106** (2011) 131301, arXiv:1002.4703 [astro-ph.CO].

[51] G. Angloher, M. Bauer, I. Bavykina, A. Bento, C. Bucci, *et al.*, "Results from 730 kg days of the CRESST-II Dark Matter Search," *Eur.Phys.J.* **C72** (2012) 1971, arXiv:1109.0702 [astro-ph.CO].

[52] **DAMA** Collaboration, R. Bernabei *et al.*, "Search for WIMP annual modulation signature: Results from DAMA / NaI-3 and DAMA / NaI-4 and the global combined analysis," *Phys.Lett.* **B480** (2000) 23–31.

[53] **LUX** Collaboration, D. Akerib *et al.*, "The Large Underground Xenon (LUX) Experiment," *Nucl.Instrum.Meth.* **A704** (2013) 111–126, arXiv:1211.3788 [physics.ins-det].

[54] K. Freese, M. Lisanti, and C. Savage, "Annual Modulation of Dark Matter: A Review," arXiv:1209.3339 [astro-ph.CO].

[55] C. Savage, G. Gelmini, P. Gondolo, and K. Freese, "Compatibility of DAMA/LIBRA dark matter detection with other searches," *JCAP* **0904** (2009) 010, arXiv:0808.3607 [astro-ph].

[56] **CDMS** Collaboration, R. Agnese *et al.*, "Dark Matter Search Results Using the Silicon Detectors of CDMS II," *Phys.Rev.Lett.* (2013) , arXiv:1304.4279 [hep-ex].

[57] **CDMS** Collaboration, R. Agnese *et al.*, "Silicon Detector Results from the First Five-Tower Run of CDMS II," *Phys.Rev.D* (2013) , arXiv:1304.3706 [astro-ph.CO].

[58] **CDMS-II** Collaboration, Z. Ahmed *et al.*, "Dark Matter Search Results from the CDMS II Experiment," *Science* **327** (2010) 1619–1621, arXiv:0912.3592 [astro-ph.CO].

[59] **CDMS-II** Collaboration, Z. Ahmed *et al.*, "Results from a Low-Energy Analysis of the CDMS II Germanium Data," *Phys.Rev.Lett.* **106** (2011) 131302, arXiv:1011.2482 [astro-ph.CO].

[60] **EDELWEISS** Collaboration, E. Armengaud *et al.*, "A search for low-mass WIMPs with EDELWEISS-II heat-and-ionization detectors," *Phys.Rev.* **D86** (2012) 051701, arXiv:1207.1815 [astro-ph.CO].

[61] **XENON10** Collaboration, J. Angle *et al.*, "A search for light dark matter in XENON10 data," *Phys.Rev.Lett.* **107** (2011) 051301, arXiv:1104.3088 [astro-ph.CO].

[62] **CoGeNT** Collaboration, C. Aalseth *et al.*, "CoGeNT: A Search for Low-Mass Dark Matter using p-type Point Contact Germanium Detectors," *Phys.Rev.* **D88** (2013) 012002, arXiv:1208.5737 [astro-ph.CO].

[63] A. Brown, S. Henry, H. Kraus, and C. McCabe, "Extending the CRESST-II commissioning run limits to lower masses," *Phys.Rev.* **D85** (2012) 021301, arXiv:1109.2589 [astro-ph.CO].

[64] J. Collar and D. McKinsey, "Comments on 'First Dark Matter Results from the XENON100 Experiment'," arXiv:1005.0838 [astro-ph.CO].

[65] **XENON100** Collaboration, "Reply to the Comments on the XENON100 First Dark Matter Results," arXiv:1005.2615 [astro-ph.CO].

[66] J. Collar and D. McKinsey, "Response to arXiv:1005.2615," arXiv:1005.3723 [astro-ph.CO].

[67] C. Savage, G. Gelmini, P. Gondolo, and K. Freese, "XENON10/100 dark matter constraints in comparison with CoGeNT and DAMA: examining the Leff dependence," *Phys.Rev.* **D83** (2011) 055002, arXiv:1006.0972 [astro-ph.CO].

[68] J. L. Feng, J. Kumar, and D. Sanford, "Xenophobic Dark Matter," *Phys.Rev.* **D88** (2013) 015021, arXiv:1306.2315 [hep-ph].

[69] M. R. Buckley and W. H. Lippincott, "A Spin-Dependent Interpretation for Possible Signals of Light Dark Matter," *Phys.Rev.* **D88** (2013) 056003, arXiv:1306.2349 [hep-ph].

[70] D. Hooper, "Revisiting XENON100's Constraints (and Signals?) For Low-Mass Dark Matter," *JCAP* **1309** (2013) 035, arXiv:1306.1790 [hep-ph].

[71] L.-B. Jia and X.-Q. Li, "Study on WIMP dark matter model with the updated results of CDMS II," arXiv:1309.6029 [hep-ph].

[72] **HEAT** Collaboration, S. Barwick *et al.*, "Measurements of the cosmic ray positron fraction from 1-GeV to 50-GeV," *Astrophys.J.* **482** (1997) L191–L194, arXiv:astro-ph/9703192 [astro-ph].

[73] **AMS-01** Collaboration, M. Aguilar *et al.*, "Cosmic-ray positron fraction measurement from 1 to 30-GeV with AMS-01," *Phys.Lett.* **B646** (2007) 145–154, arXiv:astro-ph/0703154 [ASTRO-PH].

[74] M. Pohl, "The AMS experiment: Results from AMS-01 and prospects for AMS-02," *Nucl.Phys.Proc.Suppl.* **122** (2003) 151–160.

[75] **PAMELA** Collaboration, O. Adriani *et al.*, "An anomalous positron abundance in cosmic rays with energies 1.5-100 GeV," *Nature* **458** (2009) 607–609, arXiv:0810.4995 [astro-ph].

[76] O. Adriani, G. Barbarino, G. Bazilevskaya, R. Bellotti, M. Boezio, *et al.*, "A statistical procedure for the identification of positrons in the PAMELA experiment," *Astropart.Phys.* **34** (2010) 1–11, arXiv:1001.3522 [astro-ph.HE].

[77] **Fermi-LAT** Collaboration, M. Ackermann *et al.*, "Measurement of separate cosmic-ray electron and positron spectra with the Fermi Large Area Telescope," *Phys.Rev.Lett.* **108** (2012) 011103, arXiv:1109.0521 [astro-ph.HE].

[78] **AMS** Collaboration, M. Aguilar *et al.*, "First Result from the Alpha Magnetic Spectrometer on the International Space Station: Precision Measurement of the Positron Fraction in Primary Cosmic Rays of 0.5–350 GeV," *Phys.Rev.Lett.* **110** no. 14, (2013) 141102.

[79] M. Cirelli, "Indirect Searches for Dark Matter: a status review," *Pramana* **79** (2012) 1021–1043, arXiv:1202.1454 [hep-ph].

[80] Q. Ho-Kim and X. Pham, *Elementary Particles and Their Interactions: Concepts and Phenomena*. Springer, 1998.

[81] K. Huang, *Quarks, Leptons & Gauge Fields*. World Scientific, 1992.

[82] M. Peskin and D. Schroeder, *An Introduction to Quantum Field Theory*. Advanced book classics. Addison-Wesley Publishing Company, 1995.

[83] L. Ryder, *Quantum Field Theory*. Cambridge University Press, 1996.

[84] M. Srednicki, *Quantum Field Theory*. Cambridge University Press, 2007.

[85] S. Weinberg, "A Model of Leptons," *Phys.Rev.Lett.* **19** (1967) 1264–1266.

[86] A. Salam, "Weak and Electromagnetic Interactions," *Conf.Proc.* **C680519** (1968) 367–377.

[87] S. Glashow, "Partial Symmetries of Weak Interactions," *Nucl.Phys.* **22** (1961) 579–588.

[88] A. Salam and J. C. Ward, "Electromagnetic and weak interactions," *Phys.Lett.* **13** (1964) 168–171.

[89] G. 't Hooft, "Renormalization of Massless Yang-Mills Fields," *Nucl.Phys.* **B33** (1971) 173–199.

[90] **D0** Collaboration, S. Abachi *et al.*, "Search for high mass top quark production in $p\bar{p}$ collisions at $\sqrt{s} = 1.8$ TeV," *Phys.Rev.Lett.* **74** (1995) 2422–2426, arXiv:hep-ex/9411001 [hep-ex].

[91] **CDF** Collaboration, F. Abe *et al.*, "Observation of top quark production in $\bar{p}p$ collisions," *Phys.Rev.Lett.* **74** (1995) 2626–2631, arXiv:hep-ex/9503002 [hep-ex].

[92] **CMS** Collaboration, S. Chatrchyan *et al.*, "Observation of a new boson at a mass of 125 GeV with the CMS experiment at the LHC," *Phys.Lett.* **B716** (2012) 30–61, arXiv:1207.7235 [hep-ex].

[93] **ATLAS** Collaboration, G. Aad *et al.*, "Observation of a new particle in the search for the Standard Model Higgs boson with the ATLAS detector at the LHC," *Phys.Lett.* **B716** (2012) 1–29, arXiv:1207.7214 [hep-ex].

[94] Y. Nambu, "Quasiparticles and Gauge Invariance in the Theory of Superconductivity," *Phys.Rev.* **117** (1960) 648–663.

[95] P. W. Anderson, "Plasmons, Gauge Invariance, and Mass," *Phys.Rev.* **130** (1963) 439–442.

[96] F. Englert and R. Brout, "Broken Symmetry and the Mass of Gauge Vector Mesons," *Phys.Rev.Lett.* **13** (1964) 321–323.

[97] P. W. Higgs, "Broken Symmetries and the Masses of Gauge Bosons," *Phys.Rev.Lett.* **13** (1964) 508–509.

[98] P. W. Higgs, "Broken symmetries, massless particles and gauge fields," *Phys.Lett.* **12** (1964) 132–133.

[99] P. W. Higgs, "Spontaneous Symmetry Breakdown without Massless Bosons," *Phys.Rev.* **145** (1966) 1156–1163.

[100] **Particle Data Group** Collaboration, J. Beringer *et al.*, "Review of Particle Physics (RPP)," *Phys.Rev.* **D86** (2012) 010001.

[101] M. Kobayashi and T. Maskawa, "CP Violation in the Renormalizable Theory of Weak Interaction," *Prog.Theor.Phys.* **49** (1973) 652–657.

[102] N. Cabibbo, "Unitary Symmetry and Leptonic Decays," *Phys.Rev.Lett.* **10** (1963) 531–533.

[103] G. 't Hooft, "Naturalness, chiral symmetry, and spontaneous chiral symmetry breaking," *NATO Adv.Study Inst.Ser.B Phys.* **59** (1980) 135.

[104] P. Fayet and S. Ferrara, "Supersymmetry," *Phys.Rept.* **32** (1977) 249–334.

[105] P. Fayet, "Supergauge Invariant Extension of the Higgs Mechanism and a Model for the electron and Its Neutrino," *Nucl.Phys.* **B90** (1975) 104–124.

[106] S. R. Coleman and J. Mandula, "All Possible Symmetries of the S Matrix," *Phys.Rev.* **159** (1967) 1251–1256.

[107] R. Haag, J. T. Lopuszanski, and M. Sohnius, "All Possible Generators of Supersymmetries of the s Matrix," *Nucl.Phys.* **B88** (1975) 257.

[108] M. Sohnius, "Introducing Supersymmetry," *Phys.Rept.* **128** (1985) 39–204.

[109] S. P. Martin, "A Supersymmetry primer," `arXiv:hep-ph/9709356 [hep-ph]`.

[110] M. Drees, P. Roy, and R. Godbole, *Theory And Phenomenology of Sparticles: An Account of Four-dimensional N=1 Supersymmetry in High Energy Physics.* World Scientific Publishing Company, Incorporated, 2004.

[111] P. Binetruy, *Supersymmetry: Theory, Experiment, and Cosmology.* Oxford Graduate Texts. OUP Oxford, 2012.

[112] L. J. Hall, J. D. Lykken, and S. Weinberg, "Supergravity as the Messenger of Supersymmetry Breaking," *Phys.Rev.* **D27** (1983) 2359–2378.

[113] R. Barbieri, S. Ferrara, and C. A. Savoy, "Gauge Models with Spontaneously Broken Local Supersymmetry," *Phys.Lett.* **B119** (1982) 343.

[114] L. O'Raifeartaigh, "Spontaneous Symmetry Breaking for Chiral Scalar Superfields," *Nucl.Phys.* **B96** (1975) 331.

[115] M. Dine and W. Fischler, "A Phenomenological Model of Particle Physics Based on Supersymmetry," *Phys.Lett.* **B110** (1982) 227.

[116] M. Dine and A. E. Nelson, "Dynamical supersymmetry breaking at low-energies," *Phys.Rev.* **D48** (1993) 1277–1287, arXiv:hep-ph/9303230 [hep-ph].

[117] M. Dine, A. E. Nelson, Y. Nir, and Y. Shirman, "New tools for low-energy dynamical supersymmetry breaking," *Phys.Rev.* **D53** (1996) 2658–2669, arXiv:hep-ph/9507378 [hep-ph].

[118] P. Z. Skands, B. Allanach, H. Baer, C. Balazs, G. Belanger, *et al.*, "SUSY Les Houches accord: Interfacing SUSY spectrum calculators, decay packages, and event generators," *JHEP* **0407** (2004) 036, arXiv:hep-ph/0311123 [hep-ph].

[119] M. Maniatis, "The Next-to-Minimal Supersymmetric extension of the Standard Model reviewed," *Int.J.Mod.Phys.* **A25** (2010) 3505–3602, arXiv:0906.0777 [hep-ph].

[120] U. Ellwanger, C. Hugonie, and A. M. Teixeira, "The Next-to-Minimal Supersymmetric Standard Model," *Phys.Rept.* **496** (2010) 1–77, arXiv:0910.1785 [hep-ph].

[121] P. Fayet, "Spontaneously Broken Supersymmetric Theories of Weak, Electromagnetic and Strong Interactions," *Phys.Lett.* **B69** (1977) 489.

[122] N. Sakai, "Naturalness in Supersymmetric Guts," *Z.Phys.* **C11** (1981) 153.

[123] J. R. Ellis, J. Gunion, H. E. Haber, L. Roszkowski, and F. Zwirner, "Higgs Bosons in a Nonminimal Supersymmetric Model," *Phys.Rev.* **D39** (1989) 844.

[124] M. Drees, "Supersymmetric Models with Extended Higgs Sector," *Int.J.Mod.Phys.* **A4** (1989) 3635.

[125] U. Ellwanger, "Radiative corrections to the neutral Higgs spectrum in supersymmetry with a gauge singlet," *Phys.Lett.* **B303** (1993) 271–276, arXiv:hep-ph/9302224 [hep-ph].

[126] U. Ellwanger and C. Hugonie, "The Upper bound on the lightest Higgs mass in the NMSSM revisited," *Mod.Phys.Lett.* **A22** (2007) 1581–1590, arXiv:hep-ph/0612133 [hep-ph].

[127] L. J. Hall, D. Pinner, and J. T. Ruderman, "A Natural SUSY Higgs Near 126 GeV," *JHEP* **1204** (2012) 131, arXiv:1112.2703 [hep-ph].

[128] A. Arvanitaki and G. Villadoro, "A Non Standard Model Higgs at the LHC as a Sign of Naturalness," *JHEP* **1202** (2012) 144, arXiv:1112.4835 [hep-ph].

[129] U. Ellwanger, "A Higgs boson near 125 GeV with enhanced di-photon signal in the NMSSM," *JHEP* **1203** (2012) 044, arXiv:1112.3548 [hep-ph].

[130] J. F. Gunion, Y. Jiang, and S. Kraml, "The Constrained NMSSM and Higgs near 125 GeV," *Phys.Lett.* **B710** (2012) 454–459, arXiv:1201.0982 [hep-ph].

[131] S. King, M. Muhlleitner, and R. Nevzorov, "NMSSM Higgs Benchmarks Near 125 GeV," *Nucl.Phys.* **B860** (2012) 207–244, arXiv:1201.2671 [hep-ph].

[132] Z. Kang, J. Li, and T. Li, "On Naturalness of the MSSM and NMSSM," *JHEP* **1211** (2012) 024, arXiv:1201.5305 [hep-ph].

[133] J.-J. Cao, Z.-X. Heng, J. M. Yang, Y.-M. Zhang, and J.-Y. Zhu, "A SM-like Higgs near 125 GeV in low energy SUSY: a comparative study for MSSM and NMSSM," *JHEP* **1203** (2012) 086, arXiv:1202.5821 [hep-ph].

[134] D. A. Vasquez, G. Belanger, C. Boehm, J. Da Silva, P. Richardson, *et al.*, "The 125 GeV Higgs in the NMSSM in light of LHC results and astrophysics constraints," *Phys.Rev.* **D86** (2012) 035023, arXiv:1203.3446 [hep-ph].

[135] U. Ellwanger and C. Hugonie, "Higgs bosons near 125 GeV in the NMSSM with constraints at the GUT scale," *Adv.High Energy Phys.* **2012** (2012) 625389, arXiv:1203.5048 [hep-ph].

[136] P. Lodone, "Supersymmetry phenomenology beyond the MSSM after 5/fb of LHC data," *Int.J.Mod.Phys.* **A27** (2012) 1230010, arXiv:1203.6227 [hep-ph].

[137] K. S. Jeong, Y. Shoji, and M. Yamaguchi, "Singlet-Doublet Higgs Mixing and Its Implications on the Higgs mass in the PQ-NMSSM," *JHEP* **1209** (2012) 007, arXiv:1205.2486 [hep-ph].

[138] E. Hardy, J. March-Russell, and J. Unwin, "Precision Unification in λSUSY with a 125 GeV Higgs," *JHEP* **1210** (2012) 072, arXiv:1207.1435 [hep-ph].

[139] K. Agashe, Y. Cui, and R. Franceschini, "Natural Islands for a 125 GeV Higgs in the scale-invariant NMSSM," *JHEP* **1302** (2013) 031, arXiv:1209.2115 [hep-ph].

[140] N. D. Christensen, T. Han, Z. Liu, and S. Su, "Low-Mass Higgs Bosons in the NMSSM and Their LHC Implications," arXiv:1303.2113 [hep-ph].

[141] M. Badziak, M. Olechowski, and S. Pokorski, "New Regions in the NMSSM with a 125 GeV Higgs," arXiv:1304.5437 [hep-ph].

[142] A. Arhrib, K. Cheung, T.-J. Hou, and K.-W. Song, "The Light pseudoscalar Higgs boson in NMSSM," *AIP Conf.Proc.* **903** (2007) 193–196, arXiv:hep-ph/0611211 [hep-ph].

[143] F. Domingo, U. Ellwanger, E. Fullana, C. Hugonie, and M.-A. Sanchis-Lozano, "Radiative Upsilon decays and a light pseudoscalar Higgs in the NMSSM," *JHEP* **0901** (2009) 061, arXiv:0810.4736 [hep-ph].

[144] A. Abada, G. Bhattacharyya, D. Das, and C. Weiland, "A possible connection between neutrino mass generation and the lightness of a NMSSM pseudoscalar," *Phys.Lett.* **B700** (2011) 351–355, arXiv:1011.5037 [hep-ph].

[145] D. G. Cerdeno, P. Ghosh, C. B. Park, and M. Peiro, "Collider signatures of a light NMSSM pseudoscalar in neutralino decays in the light of LHC results," arXiv:1307.7601 [hep-ph].

[146] J. E. Kim and H. P. Nilles, "The mu Problem and the Strong CP Problem," *Phys.Lett.* **B138** (1984) 150.

[147] **OPAL** Collaboration, G. Abbiendi *et al.*, "Search for anomalous production of dilepton events with missing transverse momentum in e+ e- collisions at s**(1/2) = 183-Gev to 209-GeV," *Eur.Phys.J.* **C32** (2004) 453–473, arXiv:hep-ex/0309014 [hep-ex].

[148] L. E. Ibanez, "The Scalar Neutrinos as the Lightest Supersymmetric Particles and Cosmology," *Phys.Lett.* **B137** (1984) 160.

[149] J. S. Hagelin, G. L. Kane, and S. Raby, "Perhaps Scalar Neutrinos Are the Lightest Supersymmetric Partners," *Nucl.Phys.* **B241** (1984) 638.

[150] T. Falk, K. A. Olive, and M. Srednicki, "Heavy sneutrinos as dark matter," *Phys.Lett.* **B339** (1994) 248–251, arXiv:hep-ph/9409270 [hep-ph].

[151] G. Belanger, F. Boudjema, C. Hugonie, A. Pukhov, and A. Semenov, "Relic density of dark matter in the NMSSM," *JCAP* **0509** (2005) 001, arXiv:hep-ph/0505142 [hep-ph].

[152] D. Cerdeno, E. Gabrielli, D. Lopez-Fogliani, C. Munoz, and A. Teixeira, "Phenomenological viability of neutralino dark matter in the NMSSM," *JCAP* **0706** (2007) 008, arXiv:hep-ph/0701271 [HEP-PH].

[153] C. Hugonie, G. Belanger, and A. Pukhov, "Dark matter in the constrained NMSSM," *JCAP* **0711** (2007) 009, arXiv:0707.0628 [hep-ph].

[154] D. A. Vasquez, G. Belanger, C. Boehm, A. Pukhov, and J. Silk, "Can neutralinos in the MSSM and NMSSM scenarios still be light?," *Phys.Rev.* **D82** (2010) 115027, arXiv:1009.4380 [hep-ph].

[155] K. Griest and D. Seckel, "Three exceptions in the calculation of relic abundances," *Phys.Rev.* **D43** (1991) 3191–3203.

[156] A. Djouadi, U. Ellwanger, and A. Teixeira, "Phenomenology of the constrained NMSSM," *JHEP* **0904** (2009) 031, arXiv:0811.2699 [hep-ph].

[157] A. Djouadi, U. Ellwanger, and A. Teixeira, "The Constrained next-to-minimal supersymmetric standard model," *Phys.Rev.Lett.* **101** (2008) 101802, arXiv:0803.0253 [hep-ph].

[158] T. Falk, A. Ferstl, and K. A. Olive, "Variations of the neutralino elastic cross-section with CP violating phases," *Astropart.Phys.* **13** (2000) 301–316, arXiv:hep-ph/9908311 [hep-ph].

[159] G. Belanger, F. Boudjema, A. Pukhov, and A. Semenov, "Dark matter direct detection rate in a generic model with micrOMEGAs 2.2," *Comput.Phys.Commun.* **180** (2009) 747–767, arXiv:0803.2360 [hep-ph].

[160] J. Gasser and H. Leutwyler, "Quark Masses," *Phys.Rept.* **87** (1982) 77–169.

[161] A. Thomas, P. Shanahan, and R. Young, "Strangeness in the nucleon: what have we learned?," *Nuovo Cim.* **C035N04** (2012) 3–10, arXiv:1202.6407 [nucl-th].

[162] D. Das and U. Ellwanger, "Light dark matter in the NMSSM: upper bounds on direct detection cross sections," *JHEP* **1009** (2010) 085, arXiv:1007.1151 [hep-ph].

[163] J. F. Gunion, A. V. Belikov, and D. Hooper, "CoGeNT, DAMA, and Neutralino Dark Matter in the Next-To-Minimal Supersymmetric Standard Model," arXiv:1009.2555 [hep-ph].

[164] D. Cerdeno, C. Hugonie, D. Lopez-Fogliani, C. Munoz, and A. Teixeira, "Theoretical predictions for the direct detection of neutralino dark matter in the NMSSM," *JHEP* **0412** (2004) 048, arXiv:hep-ph/0408102 [hep-ph].

[165] F. Ferrer, L. M. Krauss, and S. Profumo, "Indirect detection of light neutralino dark matter in the NMSSM," *Phys.Rev.* **D74** (2006) 115007, arXiv:hep-ph/0609257 [hep-ph].

[166] D. Albornoz Vasquez, G. Belanger, and C. Boehm, "Astrophysical limits on light NMSSM neutralinos," *Phys.Rev.* **D84** (2011) 095008, arXiv:1107.1614 [hep-ph].

[167] D. Albornoz Vasquez, G. Belanger, J. Billard, and F. Mayet, "Probing neutralino dark matter in the MSSM & the NMSSM with directional detection," *Phys.Rev.* **D85** (2012) 055023, arXiv:1201.6150 [hep-ph].

[168] W. Wang, Z. Xiong, J. M. Yang, and L.-X. Yu, "Dark Matter in the Singlet Extension of MSSM: Explanation of Pamela and Implication on Higgs Phenomenology," *JHEP* **0911** (2009) 053, arXiv:0908.0486 [hep-ph].

[169] Y. Bai, M. Carena, and J. Lykken, "The PAMELA excess from neutralino annihilation in the NMSSM," *Phys.Rev.* **D80** (2009) 055004, arXiv:0905.2964 [hep-ph].

[170] D. Hooper and T. M. Tait, "Neutralinos in an extension of the minimal supersymmetric standard model as the source of the PAMELA positron excess," *Phys.Rev.* **D80** (2009) 055028, arXiv:0906.0362 [hep-ph].

[171] Z. Maki, M. Nakagawa, and S. Sakata, "Remarks on the unified model of elementary particles," *Prog.Theor.Phys.* **28** (1962) 870–880.

[172] **LSND** Collaboration, C. Athanassopoulos *et al.*, "Evidence for $\nu_\mu \to \nu_e$ neutrino oscillations from LSND," *Phys.Rev.Lett.* **81** (1998) 1774–1777, arXiv:nucl-ex/9709006 [nucl-ex].

[173] **GALLEX** Collaboration, P. Anselmann *et al.*, "Solar neutrinos observed by GALLEX at Gran Sasso.," *Phys.Lett.* **B285** (1992) 376–389.

[174] **Kamiokande** Collaboration, Y. Fukuda *et al.*, "Solar neutrino data covering solar cycle 22," *Phys.Rev.Lett.* **77** (1996) 1683–1686.

[175] **GALLEX** Collaboration, W. Hampel *et al.*, "GALLEX solar neutrino observations: Results for GALLEX IV," *Phys.Lett.* **B447** (1999) 127–133.

[176] B. Cleveland, T. Daily, J. Davis, Raymond, J. R. Distel, K. Lande, *et al.*, "Measurement of the solar electron neutrino flux with the Homestake chlorine detector," *Astrophys.J.* **496** (1998) 505–526.

[177] **Super-Kamiokande** Collaboration, Y. Fukuda *et al.*, "Neutrino induced upward stopping muons in Super-Kamiokande," *Phys.Lett.* **B467** (1999) 185–193, arXiv:hep-ex/9908049 [hep-ex].

[178] **DOUBLE-CHOOZ** Collaboration, Y. Abe *et al.*, "Indication for the disappearance of reactor electron antineutrinos in the Double Chooz experiment," *Phys.Rev.Lett.* **108** (2012) 131801, arXiv:1112.6353 [hep-ex].

[179] **MINOS** Collaboration, P. Adamson *et al.*, "Improved search for muon-neutrino to electron-neutrino oscillations in MINOS," *Phys.Rev.Lett.* **107** (2011) 181802, arXiv:1108.0015 [hep-ex].

[180] **RENO** Collaboration, J. Ahn *et al.*, "Observation of Reactor Electron Antineutrino Disappearance in the RENO Experiment," *Phys.Rev.Lett.* **108** (2012) 191802, arXiv:1204.0626 [hep-ex].

[181] **DAYA-BAY** Collaboration, F. An *et al.*, "Observation of electron-antineutrino disappearance at Daya Bay," *Phys.Rev.Lett.* **108** (2012) 171803, arXiv:1203.1669 [hep-ex].

[182] **T2K** Collaboration, K. Abe *et al.*, "Indication of Electron Neutrino Appearance from an Accelerator-produced Off-axis Muon Neutrino Beam," *Phys.Rev.Lett.* **107** (2011) 041801, arXiv:1106.2822 [hep-ex].

[183] J. Valle, "Neutrino physics overview," *J.Phys.Conf.Ser.* **53** (2006) 473–505, arXiv:hep-ph/0608101 [hep-ph].

[184] S. Morisi and J. Valle, "Neutrino masses and mixing: a flavour symmetry roadmap," arXiv:1206.6678 [hep-ph].

[185] S. Weinberg, "Varieties of Baryon and Lepton Nonconservation," *Phys.Rev.* **D22** (1980) 1694.

[186] T. Yanagida, "Horizontal symmetry and masses of neutrinos," *Conf.Proc.* **C7902131** (1979) 95–99.

[187] R. N. Mohapatra and G. Senjanovic, "Neutrino Masses and Mixings in Gauge Models with Spontaneous Parity Violation," *Phys.Rev.* **D23** (1981) 165.

[188] J. Schechter and J. Valle, "Neutrino Masses in SU(2) x U(1) Theories," *Phys.Rev.* **D22** (1980) 2227.

[189] M. Magg and C. Wetterich, "Neutrino Mass Problem and Gauge Hierarchy," *Phys.Lett.* **B94** (1980) 61.

[190] E. Ma, "Pathways to naturally small neutrino masses," *Phys.Rev.Lett.* **81** (1998) 1171–1174, arXiv:hep-ph/9805219 [hep-ph].

[191] S. Davidson, E. Nardi, and Y. Nir, "Leptogenesis," *Phys.Rept.* **466** (2008) 105–177, arXiv:0802.2962 [hep-ph].

[192] R. Mohapatra and J. Valle, "Neutrino Mass and Baryon Number Nonconservation in Superstring Models," *Phys.Rev.* **D34** (1986) 1642.

[193] M. Malinsky, J. Romao, and J. Valle, "Novel supersymmetric SO(10) seesaw mechanism," *Phys.Rev.Lett.* **95** (2005) 161801, arXiv:hep-ph/0506296 [hep-ph].

[194] A. Zee, "A Theory of Lepton Number Violation, Neutrino Majorana Mass, and Oscillation," *Phys.Lett.* **B93** (1980) 389.

[195] K. Babu, "Model of 'Calculable' Majorana Neutrino Masses," *Phys.Lett.* **B203** (1988) 132.

[196] N. Arkani-Hamed, L. J. Hall, H. Murayama, D. Tucker-Smith, and N. Weiner, "Small neutrino masses from supersymmetry breaking," *Phys.Rev.* **D64** (2001) 115011, arXiv:hep-ph/0006312 [hep-ph].

[197] C.-C. Jean-Louis and G. Moreau, "Dark matter and neutrino masses in the R-parity violating NMSSM," *J.Phys.* **G37** (2010) 105015, arXiv:0911.3640 [hep-ph].

[198] V. De Romeri and M. Hirsch, "Sneutrino Dark Matter in Low-scale Seesaw Scenarios," *JHEP* **1212** (2012) 106, arXiv:1209.3891 [hep-ph].

[199] D. G. Cerdeno, C. Munoz, and O. Seto, "Right-handed sneutrino as thermal dark matter," *Phys.Rev.* **D79** (2009) 023510, arXiv:0807.3029 [hep-ph].

[200] D. G. Cerdeno and O. Seto, "Right-handed sneutrino dark matter in the NMSSM," *JCAP* **0908** (2009) 032, arXiv:0903.4677 [hep-ph].

[201] F. Bazzocchi, D. Cerdeno, C. Munoz, and J. Valle, "Calculable inverse-seesaw neutrino masses in supersymmetry," *Phys.Rev.* **D81** (2010) 051701, arXiv:0907.1262 [hep-ph].

[202] D. G. Cerdeno, J.-H. Huh, M. Peiro, and O. Seto, "Very light right-handed sneutrino dark matter in the NMSSM," *JCAP* **1111** (2011) 027, arXiv:1108.0978 [hep-ph].

[203] G. Belanger, J. Da Silva, and A. Pukhov, "The Right-handed sneutrino as thermal dark matter in U(1) extensions of the MSSM," *JCAP* **1112** (2011) 014, arXiv:1110.2414 [hep-ph].

[204] K. Huitu, J. Laamanen, L. Leinonen, S. K. Rai, and T. Ruppell, "Comparison of neutralino and sneutrino dark matter in a model with spontaneous CP violation," *JHEP* **1211** (2012) 129, arXiv:1209.6302 [hep-ph].

[205] C. Arina and N. Fornengo, "Sneutrino cold dark matter, a new analysis: Relic abundance and detection rates," *JHEP* **0711** (2007) 029, arXiv:0709.4477 [hep-ph].

[206] H.-S. Lee, K. T. Matchev, and S. Nasri, "Revival of the thermal sneutrino dark matter," *Phys.Rev.* **D76** (2007) 041302, arXiv:hep-ph/0702223 [HEP-PH].

[207] C. Arina, F. Bazzocchi, N. Fornengo, J. Romao, and J. Valle, "Minimal supergravity sneutrino dark matter and inverse seesaw neutrino masses," *Phys.Rev.Lett.* **101** (2008) 161802, arXiv:0806.3225 [hep-ph].

[208] G. Belanger, M. Kakizaki, E. Park, S. Kraml, and A. Pukhov, "Light mixed sneutrinos as thermal dark matter," *JCAP* **1011** (2010) 017, arXiv:1008.0580 [hep-ph].

[209] B. Dumont, G. Belanger, S. Fichet, S. Kraml, and T. Schwetz, "Mixed sneutrino dark matter in light of the 2011 XENON and LHC results," *JCAP* **1209** (2012) 013, arXiv:1206.1521 [hep-ph].

[210] T. Bringmann, X. Huang, A. Ibarra, S. Vogl, and C. Weniger, "Fermi LAT Search for Internal Bremsstrahlung Signatures from Dark Matter Annihilation," *JCAP* **1207** (2012) 054, arXiv:1203.1312 [hep-ph].

[211] C. Weniger, "A Tentative Gamma-Ray Line from Dark Matter Annihilation at the Fermi Large Area Telescope," *JCAP* **1208** (2012) 007, arXiv:1204.2797 [hep-ph].

[212] E. Tempel, A. Hektor, and M. Raidal, "Fermi 130 GeV gamma-ray excess and dark matter annihilation in sub-haloes and in the Galactic centre," *JCAP* **1209** (2012) 032, arXiv:1205.1045 [hep-ph].

[213] M. Su and D. P. Finkbeiner, "Strong Evidence for Gamma-ray Line Emission from the Inner Galaxy," arXiv:1206.1616 [astro-ph.HE].

[214] S. Profumo and T. Linden, "Gamma-ray Lines in the Fermi Data: is it a Bubble?," *JCAP* **1207** (2012) 011, arXiv:1204.6047 [astro-ph.HE].

[215] A. Boyarsky, D. Malyshev, and O. Ruchayskiy, "Spectral and spatial variations of the diffuse gamma-ray background in the vicinity of the Galactic plane and possible nature of the feature at 130 GeV," *Phys.Dark Univ.* **2** (2013) 90–96, arXiv:1205.4700 [astro-ph.HE].

[216] E. Dudas, Y. Mambrini, S. Pokorski, and A. Romagnoni, "Extra U(1) as natural source of a monochromatic gamma ray line," *JHEP* **1210** (2012) 123, arXiv:1205.1520 [hep-ph].

[217] J. M. Cline, "130 GeV dark matter and the Fermi gamma-ray line," *Phys.Rev.* **D86** (2012) 015016, arXiv:1205.2688 [hep-ph].

[218] K.-Y. Choi and O. Seto, "A Dirac right-handed sneutrino dark matter and its signature in the gamma-ray lines," *Phys.Rev.* **D86** (2012) 043515, arXiv:1205.3276 [hep-ph].

[219] B. Kyae and J.-C. Park, "130 GeV Fermi gamma-ray line from dark matter decay," *Phys.Lett.* **B718** (2013) 1425–1429, arXiv:1205.4151 [hep-ph].

[220] H. M. Lee, M. Park, and W.-I. Park, "Fermi Gamma Ray Line at 130 GeV from Axion-Mediated Dark Matter," *Phys.Rev.* **D86** (2012) 103502, arXiv:1205.4675 [hep-ph].

[221] B. S. Acharya, G. Kane, P. Kumar, R. Lu, and B. Zheng, "Mixed Wino-Axion Dark Matter in String/M Theory and the 130 GeV Gamma-line 'Signal'," arXiv:1205.5789 [hep-ph].

[222] L. Bergstrom and P. Ullio, "Full one loop calculation of neutralino annihilation into two photons," *Nucl.Phys.* **B504** (1997) 27–44, arXiv:hep-ph/9706232 [hep-ph].

[223] Z. Bern, P. Gondolo, and M. Perelstein, "Neutralino annihilation into two photons," *Phys.Lett.* **B411** (1997) 86–96, arXiv:hep-ph/9706538 [hep-ph].

[224] P. Ullio and L. Bergstrom, "Neutralino annihilation into a photon and a Z boson," *Phys.Rev.* **D57** (1998) 1962–1971, arXiv:hep-ph/9707333 [hep-ph].

[225] L. Bergstrom, P. Ullio, and J. H. Buckley, "Observability of gamma-rays from dark matter neutralino annihilations in the Milky Way halo," *Astropart.Phys.* **9** (1998) 137–162, arXiv:astro-ph/9712318 [astro-ph].

[226] F. Boudjema, A. Semenov, and D. Temes, "Self-annihilation of the neutralino dark matter into two photons or a Z and a photon in the MSSM," *Phys.Rev.* **D72** (2005) 055024, arXiv:hep-ph/0507127 [hep-ph].

[227] L. Bergstrom and H. Snellman, "Observable monochromatic photons from cosmic photino annihilation," *Phys.Rev.* **D37** (1988) 3737–3741.

[228] L. Bergstrom, T. Bringmann, M. Eriksson, and M. Gustafsson, "Two photon annihilation of Kaluza-Klein dark matter," *JCAP* **0504** (2005) 004, arXiv:hep-ph/0412001 [hep-ph].

[229] A. Birkedal, A. Noble, M. Perelstein, and A. Spray, "Little Higgs dark matter," *Phys.Rev.* **D74** (2006) 035002, arXiv:hep-ph/0603077 [hep-ph].

[230] M. Perelstein and A. Spray, "Indirect Detection of Little Higgs Dark Matter," *Phys.Rev.* **D75** (2007) 083519, arXiv:hep-ph/0610357 [hep-ph].

[231] M. Gustafsson, E. Lundstrom, L. Bergstrom, and J. Edsjo, "Significant Gamma Lines from Inert Higgs Dark Matter," *Phys.Rev.Lett.* **99** (2007) 041301, arXiv:astro-ph/0703512 [ASTRO-PH].

[232] G. Bertone, C. Jackson, G. Shaughnessy, T. M. Tait, and A. Vallinotto, "The WIMP Forest: Indirect Detection of a Chiral Square," *Phys.Rev.* **D80** (2009) 023512, arXiv:0904.1442 [astro-ph.HE].

[233] E. Dudas, Y. Mambrini, S. Pokorski, and A. Romagnoni, "(In)visible Z-prime and dark matter," *JHEP* **0908** (2009) 014, arXiv:0904.1745 [hep-ph].

[234] Y. Mambrini, "A Clear Dark Matter gamma ray line generated by the Green-Schwarz mechanism," *JCAP* **0912** (2009) 005, arXiv:0907.2918 [hep-ph].

[235] C. Jackson, G. Servant, G. Shaughnessy, T. M. Tait, and M. Taoso, "Higgs in Space!," *JCAP* **1004** (2010) 004, arXiv:0912.0004 [hep-ph].

[236] J. Goodman, M. Ibe, A. Rajaraman, W. Shepherd, T. M. Tait, *et al.*, "Gamma Ray Line Constraints on Effective Theories of Dark Matter," *Nucl.Phys.* **B844** (2011) 55–68, arXiv:1009.0008 [hep-ph].

[237] G. Bertone, C. Jackson, G. Shaughnessy, T. M. Tait, and A. Vallinotto, "Gamma Ray Lines from a Universal Extra Dimension," *JCAP* **1203** (2012) 020, arXiv:1009.5107 [astro-ph.HE].

[238] S. Profumo, L. Ubaldi, and C. Wainwright, "Singlet Scalar Dark Matter: monochromatic gamma rays and metastable vacua," *Phys.Rev.* **D82** (2010) 123514, arXiv:1009.5377 [hep-ph].

[239] T. Bringmann, F. Calore, G. Vertongen, and C. Weniger, "On the Relevance of Sharp Gamma-Ray Features for Indirect Dark Matter Searches," *Phys.Rev.* **D84** (2011) 103525, arXiv:1106.1874 [hep-ph].

[240] G. Chalons and A. Semenov, "Loop-induced photon spectral lines from neutralino annihilation in the NMSSM," *JHEP* **1112** (2011) 055, arXiv:1110.2064 [hep-ph].

[241] G. Chalons, "Gamma-ray lines constraints in the NMSSM," arXiv:1204.4591 [hep-ph].

[242] L. Bergstrom, "Dark Matter Evidence, Particle Physics Candidates and Detection Methods," *Annalen Phys.* **524** (2012) 479–496, arXiv:1205.4882 [astro-ph.HE].

[243] G. Kanbach *et al.*, "The project EGRET (energetic gamma-ray experiment telescope) on NASA's Gamma-Ray Observatory GRO," *Space Science Reviews* **49** no. 1-2, (1989) 69–84.

[244] **LAT** Collaboration, W. Atwood *et al.*, "The Large Area Telescope on the Fermi Gamma-ray Space Telescope Mission," *Astrophys.J.* **697** (2009) 1071–1102, arXiv:0902.1089 [astro-ph.IM].

[245] **H.E.S.S.** Collaboration, A. Abramowski *et al.*, "Search for photon line-like signatures from Dark Matter annihilations with H.E.S.S," *Phys.Rev.Lett.* **110** (2013) 041301, arXiv:1301.1173 [astro-ph.HE].

[246] A. Cesarini, F. Fucito, A. Lionetto, A. Morselli, and P. Ullio, "The Galactic center as a dark matter gamma-ray source," *Astropart.Phys.* **21** (2004) 267–285, arXiv:astro-ph/0305075 [astro-ph].

[247] A. W. Graham, D. Merritt, B. Moore, J. Diemand, and B. Terzic, "Empirical models for Dark Matter Halos. I. Nonparametric Construction of Density Profiles and Comparison with Parametric Models," *Astron.J.* **132** (2006) 2685–2700, arXiv:astro-ph/0509417 [astro-ph].

[248] J. F. Navarro, C. S. Frenk, and S. D. White, "A Universal density profile from hierarchical clustering," *Astrophys.J.* **490** (1997) 493–508, arXiv:astro-ph/9611107 [astro-ph].

[249] J. Diemand, M. Kuhlen, P. Madau, M. Zemp, B. Moore, *et al.*, "Clumps and streams in the local dark matter distribution," *Nature* **454** (2008) 735–738, arXiv:0805.1244 [astro-ph].

[250] V. Springel, J. Wang, M. Vogelsberger, A. Ludlow, A. Jenkins, *et al.*, "The Aquarius Project: the subhalos of galactic halos," *Mon.Not.Roy.Astron.Soc.* **391** (2008) 1685–1711, arXiv:0809.0898 [astro-ph].

[251] A. Rajaraman, T. M. Tait, and D. Whiteson, "Two Lines or Not Two Lines? That is the Question of Gamma Ray Spectra," *JCAP* **1209** (2012) 003, arXiv:1205.4723 [hep-ph].

[252] A. Hektor, M. Raidal, and E. Tempel, "Double gamma-ray lines from unassociated Fermi-LAT sources revisited," arXiv:1208.1996 [astro-ph.HE].

[253] **LAT** Collaboration, M. Ackermann *et al.*, "Fermi LAT Search for Dark Matter in Gamma-ray Lines and the Inclusive Photon Spectrum," *Phys.Rev.* **D86** (2012) 022002, arXiv:1205.2739 [astro-ph.HE].

[254] **Fermi-LAT** Collaboration, "Search for Gamma-ray Spectral Lines with the Fermi Large Area Telescope and Dark Matter Implications," arXiv:1305.5597 [astro-ph.HE].

[255] A. Hektor, M. Raidal, and E. Tempel, "Fermi-LAT gamma-ray signal from Earth Limb, systematic detector effects and their implications for the 130 GeV gamma-ray excess," arXiv:1209.4548 [astro-ph.HE].

[256] **Fermi-LAT** Collaboration, M. Ackermann *et al.*, "Constraining Dark Matter Models from a Combined Analysis of Milky Way Satellites with the Fermi Large Area Telescope," *Phys.Rev.Lett.* **107** (2011) 241302, arXiv:1108.3546 [astro-ph.HE].

[257] G. D. Martinez, J. S. Bullock, M. Kaplinghat, L. E. Strigari, and R. Trotta, "Indirect Dark Matter Detection from Dwarf Satellites: Joint Expectations from Astrophysics and Supersymmetry," *JCAP* **0906** (2009) 014, arXiv:0902.4715 [astro-ph.HE].

[258] L. Feng, Q. Yuan, P.-F. Yin, X.-J. Bi, and M. Li, "Search for dark matter signals with Fermi-LAT observation of globular clusters NGC 6388 and M 15," *JCAP* **1204** (2012) 030, arXiv:1112.2438 [astro-ph.HE].

[259] J. Han, C. S. Frenk, V. R. Eke, L. Gao, S. D. White, *et al.*, "Constraining Extended Gamma-ray Emission from Galaxy Clusters," *Mon.Not.Roy.Astron.Soc.* **427** (2012) 1651–1665, arXiv:1207.6749 [astro-ph.CO].

[260] D. Hooper and T. Linden, "On The Origin Of The Gamma Rays From The Galactic Center," *Phys.Rev.* **D84** (2011) 123005, arXiv:1110.0006 [astro-ph.HE].

[261] M. R. Buckley and D. Hooper, "Implications of a 130 GeV Gamma-Ray Line for Dark Matter," *Phys.Rev.* **D86** (2012) 043524, arXiv:1205.6811 [hep-ph].

[262] S. J. Underwood, J. Giedt, A. W. Thomas, and R. D. Young, "Neutralino-hadron scattering in the NMSSM," *Phys.Rev.* **D86** (2012) 035009, arXiv:1203.1092 [hep-ph].

[263] U. Ellwanger, J. F. Gunion, and C. Hugonie, "NMHDECAY: A Fortran code for the Higgs masses, couplings and decay widths in the NMSSM," *JHEP* **0502** (2005) 066, arXiv:hep-ph/0406215 [hep-ph].

[264] U. Ellwanger and C. Hugonie, "NMHDECAY 2.0: An Updated program for sparticle masses, Higgs masses, couplings and decay widths in the NMSSM," *Comput.Phys.Commun.* **175** (2006) 290–303, arXiv:hep-ph/0508022 [hep-ph].

[265] G. Belanger, F. Boudjema, A. Pukhov, and A. Semenov, "MicrOMEGAs 2.0: A Program to calculate the relic density of dark matter in a generic model," *Comput.Phys.Commun.* **176** (2007) 367–382, arXiv:hep-ph/0607059 [hep-ph].

[266] **PAMELA** Collaboration, O. Adriani *et al.*, "PAMELA results on the cosmic-ray antiproton flux from 60 MeV to 180 GeV in kinetic energy," *Phys.Rev.Lett.* **105** (2010) 121101, arXiv:1007.0821 [astro-ph.HE].

[267] G. Belanger, F. Boudjema, P. Brun, A. Pukhov, S. Rosier-Lees, *et al.*, "Indirect search for dark matter with micrOMEGAs2.4," *Comput.Phys.Commun.* **182** (2011) 842–856, arXiv:1004.1092 [hep-ph].

[268] T. Nihei, L. Roszkowski, and R. Ruiz de Austri, "Exact cross-sections for the neutralino WIMP pair annihilation," *JHEP* **0203** (2002) 031, arXiv:hep-ph/0202009 [hep-ph].

[269] P. Grothaus, M. Lindner, and Y. Takanishi, "Naturalness of Neutralino Dark Matter," *JHEP* **1307** (2013) 094, arXiv:1207.4434 [hep-ph].

[270] J. R. Ellis, A. Ferstl, and K. A. Olive, "Reevaluation of the elastic scattering of supersymmetric dark matter," *Phys.Lett.* **B481** (2000) 304–314, arXiv:hep-ph/0001005 [hep-ph].

[271] T. Cohen, D. J. Phalen, and A. Pierce, "On the Correlation Between the Spin-Independent and Spin-Dependent Direct Detection of Dark Matter," *Phys.Rev.* **D81** (2010) 116001, arXiv:1001.3408 [hep-ph].

[272] G. Chalons, M. J. Dolan, and C. McCabe, "Neutralino dark matter and the Fermi gamma-ray lines," *JCAP* **1302** (2013) 016, arXiv:1211.5154 [hep-ph].

[273] R. Barbieri, L. J. Hall, and V. S. Rychkov, "Improved naturalness with a heavy Higgs: An Alternative road to LHC physics," *Phys.Rev.* **D74** (2006) 015007, arXiv:hep-ph/0603188 [hep-ph].

[274] J. Gunion and H. E. Haber, "Higgs Bosons in Supersymmetric Models. 2. Implications for Phenomenology," *Nucl.Phys.* **B278** (1986) 449.

[275] J. F. Gunion and H. E. Haber, "Two-body Decays of Neutralinos and Charginos," *Phys.Rev.* **D37** (1988) 2515.

[276] J. Angle, E. Aprile, F. Arneodo, L. Baudis, A. Bernstein, *et al.*, "Limits on spin-dependent WIMP-nucleon cross-sections from the XENON10 experiment," *Phys.Rev.Lett.* **101** (2008) 091301, arXiv:0805.2939 [astro-ph].

[277] **ICECUBE** Collaboration, R. Abbasi *et al.*, "Limits on a muon flux from neutralino annihilations in the Sun with the IceCube 22-string detector," *Phys.Rev.Lett.* **102** (2009) 201302, arXiv:0902.2460 [astro-ph.CO].

[278] S. Nussinov, "Technocosmology: Could a technibaryon excess provide a 'natural' missing mass candidate?," *Phys.Lett.* **B165** (1985) 55.

[279] S. M. Barr, R. S. Chivukula, and E. Farhi, "Electroweak fermion number violation and the production of stable particles in the early universe," *Phys.Lett.* **B241** (1990) 387–391.

[280] S. M. Barr, "Baryogenesis, sphalerons and the cogeneration of dark matter," *Phys.Rev.* **D44** (1991) 3062–3066.

[281] S. Dodelson, B. R. Greene, and L. M. Widrow, "Baryogenesis, dark matter and the width of the Z," *Nucl.Phys.* **B372** (1992) 467–493.

[282] D. B. Kaplan, "A Single explanation for both the baryon and dark matter densities," *Phys.Rev.Lett.* **68** (1992) 741–743.

[283] H. Davoudiasl and R. N. Mohapatra, "On Relating the Genesis of Cosmic Baryons and Dark Matter," *New J.Phys.* **14** (2012) 095011, arXiv:1203.1247 [hep-ph].

[284] K. Petraki and R. R. Volkas, "Review of asymmetric dark matter," arXiv:1305.4939 [hep-ph].

[285] D. E. Kaplan, M. A. Luty, and K. M. Zurek, "Asymmetric Dark Matter," *Phys.Rev.* **D79** (2009) 115016, arXiv:0901.4117 [hep-ph].

[286] L. Landau, E. Lifshitz, and L. Pitaevskii, *Statistical physics*. Pergamon international library of science, technology, engineering, and social studies. Pergamon Press, 1980.

[287] D. Hooper, J. March-Russell, and S. M. West, "Asymmetric sneutrino dark matter and the Omega(b) / Omega(DM) puzzle," *Phys.Lett.* **B605** (2005) 228–236, arXiv:hep-ph/0410114 [hep-ph].

[288] J. McDonald, "Right-handed sneutrino condensate cold dark matter and the baryon-to-dark matter ratio," *JCAP* **0701** (2007) 001, arXiv:hep-ph/0609126 [hep-ph].

[289] S. Abel and V. Page, "(Pseudo)-Dirac neutrinos and leptogenesis," *AIP Conf.Proc.* **878** (2006) 341–346, arXiv:hep-ph/0609140 [hep-ph].

[290] V. Page, "Non-thermal right-handed sneutrino dark matter and the Omega(DM)/Omega(b) problem," *JHEP* **0704** (2007) 021, arXiv:hep-ph/0701266 [hep-ph].

[291] Z. Kang, J. Li, T. Li, T. Liu, and J. Yang, "Asymmetric Sneutrino Dark Matter in the NMSSM with Minimal Inverse Seesaw," arXiv:1102.5644 [hep-ph].

[292] E. Ma and U. Sarkar, "Scalar Neutrino as Asymmetric Dark Matter: Radiative Neutrino Mass and Leptogenesis," *Phys.Rev.* **D85** (2012) 075015, arXiv:1111.5350 [hep-ph].

[293] D. Suematsu, "Dark world and baryon asymmetry from a common source," *JCAP* **0601** (2006) 026, arXiv:astro-ph/0511742 [astro-ph].

[294] K. Blum, A. Efrati, Y. Grossman, Y. Nir, and A. Riotto, "Asymmetric Higgsino Dark Matter," *Phys.Rev.Lett.* **109** (2012) 051302, arXiv:1201.2699 [hep-ph].

[295] D. J. Chung, B. Garbrecht, and S. Tulin, "The Effect of the Sparticle Mass Spectrum on the Conversion of B-L to B," *JCAP* **0903** (2009) 008, arXiv:0807.2283 [hep-ph].

[296] M. L. Graesser, I. M. Shoemaker, and L. Vecchi, "Asymmetric WIMP dark matter," *JHEP* **1110** (2011) 110, arXiv:1103.2771 [hep-ph].

[297] K. Griest and D. Seckel, "Cosmic Asymmetry, Neutrinos and the Sun," *Nucl.Phys.* **B283** (1987) 681.

[298] A. Belyaev, M. T. Frandsen, S. Sarkar, and F. Sannino, "Mixed dark matter from technicolor," *Phys.Rev.* **D83** (2011) 015007, arXiv:1007.4839 [hep-ph].

[299] H. Iminniyaz, M. Drees, and X. Chen, "Relic Abundance of Asymmetric Dark Matter," *JCAP* **1107** (2011) 003, arXiv:1104.5548 [hep-ph].

[300] P. Gondolo, J. Edsjo, P. Ullio, L. Bergstrom, M. Schelke, *et al.*, "DarkSUSY: Computing supersymmetric dark matter properties numerically," *JCAP* **0407** (2004) 008, arXiv:astro-ph/0406204 [astro-ph].

[301] E. Hairer and G. Wanner, *Solving Ordinary Differential Equations II: Stiff and Differential-Algebraic Problems*. Solving ordinary differential equations. Springer, 2010.

[302] M. Hindmarsh and O. Philipsen, "WIMP dark matter and the QCD equation of state," *Phys.Rev.* **D71** (2005) 087302, arXiv:hep-ph/0501232 [hep-ph].

[303] T. Nihei, L. Roszkowski, and R. Ruiz de Austri, "Exact cross-sections for the neutralino slepton coannihilation," *JHEP* **0207** (2002) 024, arXiv:hep-ph/0206266 [hep-ph].

[304] J. March-Russell, J. Unwin, and S. M. West, "Closing in on Asymmetric Dark Matter I: Model independent limits for interactions with quarks," *JHEP* **1208** (2012) 029, arXiv:1203.4854 [hep-ph].

[305] J. A. Harvey and M. S. Turner, "Cosmological baryon and lepton number in the presence of electroweak fermion number violation," *Phys.Rev.* **D42** (1990) 3344–3349.

[306] M. Cirelli, P. Panci, G. Servant, and G. Zaharijas, "Consequences of DM/antiDM Oscillations for Asymmetric WIMP Dark Matter," *JCAP* **1203** (2012) 015, arXiv:1110.3809 [hep-ph].

[307] M. R. Buckley and S. Profumo, "Regenerating a Symmetry in Asymmetric Dark Matter," *Phys.Rev.Lett.* **108** (2012) 011301, arXiv:1109.2164 [hep-ph].

[308] S. Tulin, H.-B. Yu, and K. M. Zurek, "Oscillating Asymmetric Dark Matter," *JCAP* **1205** (2012) 013, arXiv:1202.0283 [hep-ph].

[309] C. Arina and N. Sahu, "Asymmetric Inelastic Inert Doublet Dark Matter from Triplet Scalar Leptogenesis," *Nucl.Phys.* **B854** (2012) 666–699, arXiv:1108.3967 [hep-ph].

[310] S. Gabriel and S. Nandi, "A New two Higgs doublet model," *Phys.Lett.* **B655** (2007) 141–147, arXiv:hep-ph/0610253 [hep-ph].

[311] F. Wang, W. Wang, and J. M. Yang, "Split two-Higgs-doublet model and neutrino condensation," *Europhys.Lett.* **76** (2006) 388–394, arXiv:hep-ph/0601018 [hep-ph].

[312] E. Ma, "Naturally small seesaw neutrino mass with no new physics beyond the TeV scale," *Phys.Rev.Lett.* **86** (2001) 2502–2504, arXiv:hep-ph/0011121 [hep-ph].

[313] S. Zhou, "Comment on astrophysical consequences of a neutrinophilic 2HDM," *Phys.Rev.* **D84** (2011) 038701, arXiv:1106.3880 [hep-ph].

[314] M. Sher and C. Triola, "Astrophysical Consequences of a Neutrinophilic Two-Higgs-Doublet Model," *Phys.Rev.* **D83** (2011) 117702, arXiv:1105.4844 [hep-ph].

[315] S. M. Davidson and H. E. Logan, "Dirac neutrinos from a second Higgs doublet," *Phys.Rev.* **D80** (2009) 095008, arXiv:0906.3335 [hep-ph].

[316] S. M. Davidson and H. E. Logan, "LHC phenomenology of a two-Higgs-doublet neutrino mass model," *Phys.Rev.* **D82** (2010) 115031, arXiv:1009.4413 [hep-ph].

[317] G. Marshall, M. McCaskey, and M. Sher, "A Supersymmetric Model with Dirac Neutrino Masses," *Phys.Rev.* **D81** (2010) 053006, arXiv:0912.1599 [hep-ph].

[318] N. Haba, K. Kaneta, and Y. Shimizu, "Phenomenology of supersymmetry SU(5) GUT with neutrinophilic Higgs boson," *Phys.Rev.* **D86** (2012) 015019, arXiv:1204.4254 [hep-ph].

[319] N. Haba and T. Horita, "Vacuum stability in neutrinophilic Higgs doublet model," *Phys.Lett.* **B705** (2011) 98–105, arXiv:1107.3203 [hep-ph].

[320] W. Chao and M. J. Ramsey-Musolf, "Hidden from View: Neutrino Masses, Dark Matter and TeV-Scale Leptogenesis in a Neutrinophilic 2HDM," arXiv:1212.5709 [hep-ph].

[321] N. Haba and O. Seto, "Thermal leptogenesis in a supersymmetric neutrinophilic Higgs model," *Phys.Rev.* **D84** (2011) 103524, arXiv:1106.5354 [hep-ph].

[322] N. Haba, O. Seto, and O. Seto, "Low scale thermal leptogenesis in neutrinophilic Higgs doublet models," *Prog.Theor.Phys.* **125** (2011) 1155–1169, arXiv:1102.2889 [hep-ph].

[323] K.-Y. Choi and O. Seto, "Light Dirac right-handed sneutrino dark matter," arXiv:1305.4322 [hep-ph].

[324] G. Steigman, K. A. Olive, and D. Schramm, "Cosmological Constraints on Superweak Particles," *Phys.Rev.Lett.* **43** (1979) 239–242.

[325] A. Aranda and M. Sher, "Generations of Higgs bosons in supersymmetric models," *Phys.Rev.* **D62** (2000) 092002, arXiv:hep-ph/0005113 [hep-ph].

[326] T. Fukuyama and K. Tsumura, "Detecting Majorana nature of neutrinos in muon decay," arXiv:0809.5221 [hep-ph].

[327] **MEG** Collaboration, J. Adam *et al.*, "New constraint on the existence of the $\mu^+ \to e^+\gamma$Yan decay," arXiv:1303.0754 [hep-ex].

[328] F. Karsch, E. Laermann, and A. Peikert, "The Pressure in two flavor, (2+1)-flavor and three flavor QCD," *Phys.Lett.* **B478** (2000) 447–455, arXiv:hep-lat/0002003 [hep-lat].

[329] I. Affleck and M. Dine, "A New Mechanism for Baryogenesis," *Nucl.Phys.* **B249** (1985) 361.

[330] M. Lindner, A. Merle, and V. Niro, "Enhancing Dark Matter Annihilation into Neutrinos," *Phys.Rev.* **D82** (2010) 123529, arXiv:1005.3116 [hep-ph].

[331] C. Kouvaris and P. Tinyakov, "Excluding Light Asymmetric Bosonic Dark Matter," *Phys.Rev.Lett.* **107** (2011) 091301, arXiv:1104.0382 [astro-ph.CO].

[332] S. D. McDermott, H.-B. Yu, and K. M. Zurek, "Constraints on Scalar Asymmetric Dark Matter from Black Hole Formation in Neutron Stars," *Phys.Rev.* **D85** (2012) 023519, arXiv:1103.5472 [hep-ph].

[333] M. Mazziotta, F. Loparco, F. de Palma, and N. Giglietto, "A model-independent analysis of the Fermi Large Area Telescope gamma-ray data from the Milky Way dwarf galaxies and halo to constrain dark matter scenarios," arXiv:1203.6731 [astro-ph.IM].

[334] G. Hutsi, J. Chluba, A. Hektor, and M. Raidal, "WMAP7 and future CMB constraints on annihilating dark matter: implications on GeV-scale WIMPs," *Astron.Astrophys.* **535** (2011) A26, arXiv:1103.2766 [astro-ph.CO].

[335] S. Galli, F. Iocco, G. Bertone, and A. Melchiorri, "Updated CMB constraints on Dark Matter annihilation cross-sections," *Phys.Rev.* **D84** (2011) 027302, arXiv:1106.1528 [astro-ph.CO].